CHAPTER 1

INTRODUCTION TO THESIS

This chapter describes the development from liquid electrolytes to solid polymer electrolytes (SPEs). Next section reveals the advantages of SPEs over the conventional liquid electrolytes and hence explains the applications of SPEs in the electrochemical devices. The difficulties faced in the polymer electrolytes research, the objectives and the novelty of this current work are thus enlightened. Last section discusses the scope of the thesis.

1.1 Liquid Electrolytes

Liquid electrolytes have been widely employed in electrochemical devices, especially lithium batteries. However, these conventional liquid electrolytes possess several disadvantages such as leakages of corrosive solvent and harmful gas, electrolytic degradation of electrolyte, formation of lithium dendrite growth and poor long–term stability due to the evaporation of the liquid electrolyte as well as low safety performance because of using the flammable organic solvent (Ramesh *et al.*, 2011a and Yang *et al.*, 2008). Other drawbacks are low operating temperature range, difficulty in handling and manufacturing due to the presence of liquid phase in the electrolytes and short shelf–life with high possibility of internal circuit shorting (Gray, 1997; Stephan, 2006). Therefore, the researchers came up with a brilliant idea to replace the conventional liquid electrolytes that is solid state electrolytes.

1.2 Solid Electrolytes

Solid electrolytes are non–aqueous based ionic conductive materials with negligible electrical conductivity. Sometimes, these electrolytes are known as fast ion conductors, superionic conductors or optimized ionic conductors (Takahashi, 1989).

These electrolytes are generally sub–divided into four classes: crystalline solid electrolytes, glass electrolytes, molten electrolytes and polymer electrolytes. Crystalline solid electrolytes are the electrolytes involve numerous divalent or/and trivalent cations for ionic hopping mechanism in the crystal structures. Some of the common crystalline electrolytes are β–alumina, γ–Li_2ZnGeO_4 and $RbAg_4I_5$ (Gray, 1997). On the other hand, glassy electrolytes are amorphous solid conductors that form when the liquids containing ions cool rapidly below its glass transition temperature (T_g) without any crystallization process. These vitreous materials are made up from three basic elements, namely network formers, network modifiers and ionic salts (Gray, 1997). Molten electrolytes are the conductors containing molten single salt or molten eutectic mixtures. These electrolytes are usually exhibit relatively high ionic conductivity (> 1 S cm^{-1}). The common molten electrolytes used are LiCl–KCl eutectic mixture and chloroaluminates ($AlCl_3$–MCl, where M represents alkali metal). However, several technical requirements are needed in the molten electrolytes to prevent corrosion and eutectic mixture leakage of the cell (Gray, 1997). Although crystalline and glassy electrolytes exhibit high ionic conductivity, these materials are brittle. Therefore, polymeric materials which can accommodate volume changes are used to improve the mechanical properties of materials. This makes solid polymer electrolyte (SPE) a suitable candidate for electrochemical applications together with intercalation materials such as anode and cathode in lithium rechargeable battery.

1.3 Solid Polymer Electrolytes (SPEs)

Conductive solid polymer electrolytes (SPEs) were firstly prepared by Wright (1975), a polymer chemist from Sheffield in year 1975 to overcome the shortcomings of conventional liquid electrolytes. SPEs are truly interdisciplinary materials as flexible ion transporting medium in vital applications such as energy storage and electrochemical displays (Wright, 1998). Solid polymer electrolytes (SPEs) are solvent–free systems whereby the ionically conducting pathway is generated by dissolving the low lattice energy metal salts in ion–coordinating macromolecules (Bruce and Vincent, 1993). Armand (1986) used graphite intercalation compounds as electrodes and polymer–salt complexes as electrolyte in lithium battery fabrication. This idea opened up new perspectives in the international solid–state ionics community as the conductive SPE worked well with the intercalation electrodes (Armand, 1986).

Apart from high safety performances, these electrolytes possess some other advantages. These advantages are negligible vapor pressure, high automation potential, low volatility, high energy density and excellent electrochemical, structural, thermal, photochemical and chemical stabilities as well as low electronic conductivity (Adebahr *et al*., 2003; Armand, 1986; Gray, 1991; Gray, 1997; Nicotera *et al*., 2002; Ramesh and Liew, 2013; Stephan, 2006). Other superior features are inherent viscoelastic, suppression of lithium dendrite growth, high mechanical properties, light in weight, ease of handling and manufacturing, wide operating temperature range, low cost and no new technology requirement (Baskaran *et al*., 2007; Imrie and Ingram, 2000; Rajendran *et al*., 2004a; Ramesh *et al*., 2011a). Moreover, these SPEs can be configured in any shape due to high flexibility of polymer membranes (Gray, 1991).

The development in SPEs has drawn the great attention from the researchers in recent years due to the wide range of applications of SPEs in the technology field, especially in electrochemical devices. The application range is from small scale production of commercial secondary lithium ion batteries (also known as the rechargeable batteries) to advanced high energy electrochemical devices, such as chemical sensors, fuel cells, electrochromic windows (ECWs), solid state reference electrode systems, supercapacitors, thermoelectric generators, analogue memory devices and solar cells (Armand, 1986; Gray, 1991; Rajendran *et al*., 2004a). These electrochemical devices also exhibit a wide range of applications, ranging from portable electronic and personal communication devices such as laptop, mobile phone, MP3 player, PDA to hybrid electrical vehicle (EV) and start–light–ignition (SLI) which serves as traction power source for electricity (Ahmad *et al.*, 2005; Gray, 1997).

1.4 Problem Statements

Waste disposal problem and depletion of non–renewable fossil fuel catalyzes the development of environmental friendly alternative energy sources (Liew *et al.*, 2014a). In addition, the dilemma of pollution from the plastic waste becomes a main concern in the environmental trepidation because of the lack of degradation after being discarded. Therefore, a force has been driven to the development of biodegradable polymer to replace those non–biodegradable polymers. Synthetic biodegradable polymer, poly(vinyl alcohol) (PVA) is employed in this work. Low ionic mobility and low ion diffusion are main difficulties of ionic transportation in polymer electrolytes. Polymer–salt electrolytes exhibit low ionic conductivity due to their high degree of crystallinity as the mobility in crystalline region is extremely low. Therefore, this shortcoming becomes the main concern in the development of polymer electrolytes. Several attempts have been made to improve the ionic conductivity of polymer electrolytes. Addition of environmental friendly ionic liquid is the method used to increase the ionic conductivity of polymer electrolytes. Several intensive researches have been done to reach the target of ionic conductivity of polymer electrolytes above 10^{-3} S cm^{-1} at ambient temperature. However, the successful case to get high ionic conductivity which is above 10^{-3} S cm^{-1} at room temperature is quite rare. Thus, there is a need to consider the cause of this problem. The first thought that comes to mind could be the ion transport mechanism in the polymer electrolytes. Therefore, the ion transport mechanism in the polymer electrolytes must be studied. The anions are free to move in the polymer electrolytes as the cations are solvated in the polymer backbone. So, the counteranion of ionic liquids could assist in increasing the diffusivity of the charge carriers. Therefore, different counteranion of ionic liquids in the polymer matrix is employed to investigate the effect of anion of ionic liquid in the ion diffusion in the polymer electrolytes.

1.5 Objectives of Research

- to develop environmental friendly ionic liquid–added polymer electrolytes with high conductivity feature
- to explore the effect of addition of ionic liquid onto polymer electrolytes
- to envisage the effect of counteranion of ionic liquid in the ionic transportation
- to investigate the mechanism pertaining to ion transport in the polymer electrolytes
- to characterize the electrical, structural and thermal properties of ionic liquid–added polymer electrolytes using various instruments
- to test the ability of the prepared ionically conducting polymer electrolytes in the fabricated EDLCs
- to examine the electrochemical properties and its cyclability performances of assembled EDLCs

1.6 Novelty

PVA–ammonium acetate (CH_3COONH_4) polymeric conductors have been widely prepared and investigated (Hirankumar *et al.*, 2004; Hirankumar *et al.*, 2005; Selvasekarapandian *et al.*, 2005). However, the ionic conductivity of the polymer electrolytes is relatively low that is $\sim 10^{5}$ S cm^{-1}. These low conductive polymer electrolytes are not applicable in any electrochemical devices. Up to date, there is no report on the ionic liquid–added polymer electrolytes based on PVA and CH_3COONH_4, except our previous published work (Liew *et al.*, 2014a; Liew *et al.*, 2014b). The effect of addition of ionic liquids is investigated throughout this research. Three different ionic liquid counteranions are added into PVA–CH_3COONH_4 polymer electrolytes in this work to study the effect of the counteranions on ion diffusion in the polymer electrolytes. Apart from that, these ionic liquid–added polymer electrolytes are applied in the electric double layer capacitors (EDLCs) cell fabrication.

1.7 Scope of the thesis

Chapter 1 describes the development of solid polymer electrolytes, problem statements, the objectives and novelty in this work. Chapter 2 reviews the literatures on polymer electrolytes and their development and parameters governing the ionic transportation in the polymer electrolytes. In addition, the reasons for choosing the materials and the application of the polymer in electrochemical device are discussed in this chapter. Chapter 3 presents the methodology of the sample preparation, sample characterization and electrochemical device fabrication. Chapters 4, 5 and 6 discuss the results obtained from all the characterization. On the other hand, Chapter 7 compares and discusses the results obtained from three different ionic liquid systems. Chapter 8 is the conclusion of the work. The future study is also mentioned in the last chapter.

CHAPTER 2

LITERATURE REVIEW

This chapter presents a review of related literature on polymer electrolytes. The first section discusses the development of the polymer electrolytes and reviews different types of polymer electrolytes. The second section reviews parameters governing the ionic conduction in the polymer electrolytes and covers the methods to improve the ionic conductivity of polymer electrolytes. The third section emphasizes the reasons for choosing PVA, CH_3COONH_4 and ionic liquids in this research. The final section highlights applications of the polymer electrolytes in electrochemical devices and the advantages of EDLCs over other electrochemical devices.

2.1 Types of Polymer Electrolytes

Polymer electrolytes are divided into few classes as shown below.

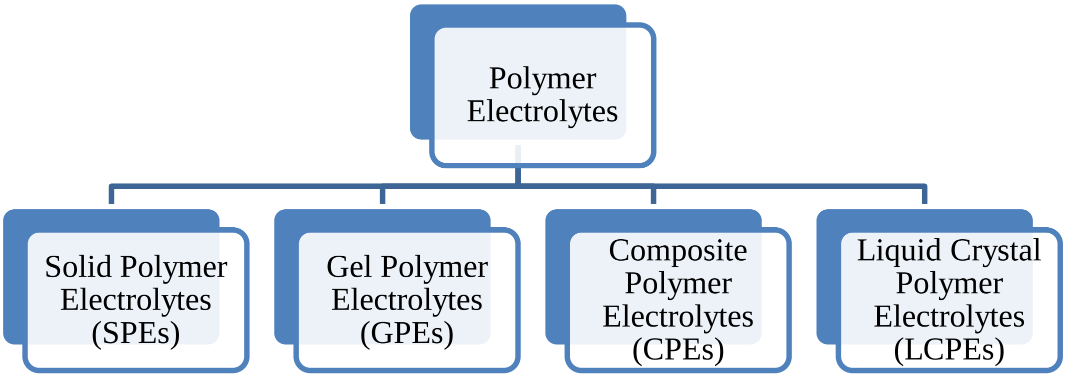

Figure 2.1: Four main classes of polymer electrolytes.

2.1.1 Solid Polymer Electrolytes

SPEs are developed to replace the conventional liquid electrolytes. Excellent safety performance is the main characteristic of SPEs because of its solvent free condition. With SPEs, lithium metal electrodes can be used in lithium ion batteries with good compatibility and low self–discharge. SPEs exhibit high elastic relaxation properties under stress and are easy to handle and process (Ibrahim *et al*., 2012). The superior mechanical integrity of SPEs and the high flexibility of polymer matrix allow the fabrication of all solid–state electrochemical cells (Gray, 1997). Electrochemical cells based on SPEs have excellent electrode–electrolyte interfacial contact over crystalline or glassy electrolytes–based cells. The contact can be maintained under stresses at all the times of charging and discharging processes (Gray, 1991; Gray, 1997). SPEs also do not build up the internal pressure which may cause the explosion during charge and discharge processes in the electrochemical cell (Liew *et al.*, 2013). In addition, Gray (1991) stated that the ionic transportation within the polymer electrolytes depends on the local relaxation processes in the polymer chains which may give the similar properties as liquid electrolytes. The donor atom (or known as solvating group) of polymer could form the covalent bonding with the cations in the salt for ion transport mechanism. The coordination occurs when positive charge on the cation interacts with the negative charge on the solvating group via electrostatic interactions. The ionic conduction in the polymer electrolytes arises from the ion dissociation from the coordination.

The first generation of SPEs was crystalline poly(ethylene oxide) (PEO)–based polymer electrolytes invented by Wright and his groups in year 1975 (Fenton *et al.*, 1973; Quartarone *et al.*, 1998). They reported the effect of alkali metal salts that are sodium and potassium salts when incorporated in PEO (Fenton *et al.*, 1973; Wright, 1975). Although PEO have good solvating properties, the ionic conductivity of PEO–based polymer electrolytes is still relatively low ($\sim 10^{-8}$–10^{-7} S cm^{-1}) due to its high crystallinity and its high ability to recrystallize (Fenton *et al.*, 1973; Wright, 1975). Numerous ways have been implemented to inhibit the recrystallization of the polymer complexes and/or reduce the degree of crystallinity in the polymer electrolytes, for example polymer modifications, polymer blending, utilization of semi–crystalline or amorphous polymer like poly(methyl methacrylate) (PMMA) and addition of additives like plasticizers and inorganic fillers.

The structural modifications onto the short chains of ethylene oxide in PEO polymer backbone such as cross–linking, random, block or comb polymerization, radical polymerization, cationic polymerization, epoxides copolymerization have been proposed to minimize the crystallization (Quartarone *et al*., 1998). The first attempt of cross–linking PEO with poly(dimethylsiloxane) (PDMS) was prepared by Bouridah *et al.* (1985). These copolymers are cross–linked by an aliphatic isocyanate (grafted PDMS). The ionic conductivity of ~10^{-5} S cm^{-1} was achieved upon addition of 10 wt.% of lithium perchlorate ($LiClO_4$) (Bouridah *et al*., 1985). Another crosslinking reaction of triol type of PEO and poly(propylene oxide) (PPO) was prepared by Watanabe *et al*. (1986). Based on the findings, the ionic conductivity of $LiClO_4$–doped polymer network is 5 times higher than that of PEO polymer electrolytes without cross–linked with PPO. Yuan *et al.* (2005) synthesized polyacrylonitrile–polyethylene oxide (PAN–PEO) copolymer. Higher ionic conductivity of copolymers was observed compared to previous literatures. The highest ambient temperature–ionic conductivity of polymer electrolytes based on this copolymer and $LiClO_4$ was 6.79×10^{-4} S cm^{-1} with an [EO]/[Li] ratio of about 10 (Yuan *et al.*, 2005). Although SPEs are safe to be used and provide high mechanical strength, the SPEs exhibit low ionic conductivity that delays application in the electrochemical device.

2.1.2 Gel Polymer Electrolytes (GPEs)

Since the ionic conductivity of SPEs is very low, the second generation of gel polymer electrolytes (GPEs) was developed with enhanced ionic conductivity. GPEs are known as gelionic solid polymer electrolytes or plasticized–polymer electrolytes (Ramesh *et al.*, 2012). GPEs are formed when the polymer host and doping salt are dissolved in polar and high dielectric constant organic solvents or plasticizer (Osinska *et al*., 2009; Rajendran *et al*., 2008). GPEs can also be considered as liquid electrolytes entrapped in a polymer. This immobilization of liquid electrolyte in a polymer matrix exhibit a unique characteristic compared to SPE (Han *et al*., 2002). The local relaxations in GPEs provide liquid–like degree of freedom which is comparable to those conventional liquid electrolytes at the atomic level (Ramesh *et al.*, 2012). Hence, GPEs possess both cohesive property of solids and the diffusive property of liquids. Carbonate ester such as propylene carbonate (PC), ethylene carbonate (EC), dibutyl phthalate (DBP), diethyl carbonate (DEC) and high dielectric constant solvent such as N,N–dimethyl formamide (DMF) and γ–butyrolactone are widely used as main components of GPE (Ramesh *et al.*, 2011a).

GPEs have many inherent properties, for instance low interfacial resistance, decreased reactivity towards the electrode materials, improved safety and exhibit better shape flexibility as well as significant increase in ionic conductivity with a small portion of plasticizers (Ahmad *et al.*, 2008; Pandey and Hashmi, 2009). Moreover, GPEs show better electrochemical properties with a wider operating temperature range in comparison to liquid electrolytes (Ahmad *et al.*, 2005; Stephan *et al.*, 2002). Other attractive advantages are leak proof construction, lighter, cheaper and easy fabrication into desired shape and size (Zhang *et al.*, 2011a).

The effect of plasticizers is observed greatly in the literature. The ionic conductivity of polymer electrolytes based on PEO–lithium trifluoromethanesulfonate ($LiCF_3SO_3$) is increased about three orders of magnitude from 7.13×10^{-7} S cm^{-1} to 6.03 $\times10^{-4}$ S cm^{-1} upon addition of dibutyl phthalate (DBP) (Sukeshini *et al.*, 1998). The plasticizer can help in dissociating the salt and increasing the carrier concentration. When poly(ethylene glycol) (PEG) was added into PEO–sodium metaphosphate ($NaPO_3$) complexes as plasticizer not only was ionic conductivity enhanced, but the cationic transport number in the polymer electrolytes also increased (Sukeshini *et al.*, 1998).

However, GPEs possess some shortcomings that are low mechanical strength compared to SPEs, slow evaporation of the organic solvent, low flash point, poor dimensional stability and reduction in thermal, electrical and electrochemical stabilities

(Kim *et al.*, 2006; Ramesh *et al.*, 2011a; Raghavan *et al.*, 2010). GPEs are less compatible with lithium metal anode in lithium batteries because of their poor interfacial stability (Pandey & Hashmi, 2009). GPEs also exhibit poor electrochemical performances due to their narrow working potential window range and high vapor pressure (Kim *et al.*, 2006; Ramesh *et al.*, 2011a; Raghavan *et al.*, 2010). All these disadvantages of GPEs initiate the invention of new generation of polymer electrolytes namely composite polymer electrolytes.

2.1.3 Composite Polymer Electrolytes (CPEs)

CPEs have received a lot of attention from researchers recently. CPEs are produced by dispersing small amount of organic or inorganic fillers into the polymer electrolytes (Osinska *et al*., 2009). CPEs containing nanometre grain size fillers are also known as nanocomposite polymer electrolytes (NCPEs). The fillers are usually added into GPEs to increase the physical and mechanical properties of polymer electrolytes. These CPEs offer some advantages such as good interfacial contact at electrode–electrolyte region, high flexibility, improved ion transport, high ionic conductivity and excellent thermodynamic stability towards lithium and other alkali metals (Gray, 1997). Superior interfacial properties towards lithium metal anode and electrochemical properties are also some features of CPEs (Stephan and Nahm, 2006). Addition of fillers increases the capacity of the fabricated lithium batteries as reported in Stephan and Nahm (2006). There are many examples of fillers that can be used in the polymer electrolyte preparation, for example manganese oxide (MnO_2), titania (TiO_2), zirconia (ZrO_2), fumed silica (SiO_2) and alumina (Al_2O_3).

Common fillers such as SiO_2 have been widely used in early years. Fan *et al.* (2003) reported that the addition of SiO_2 not only increased the ionic conductivity of PEO–based polymer electrolytes significantly, but also enhanced the mechanical properties of polymer electrolytes remarkably. They also compared the results obtained from unmodified SiO_2 with silane–modified SiO_2. Based on the findings, the polymer electrolytes containing silane–modified SiO_2 have much higher ionic conductivity than that of unmodified SiO_2. Special treatment on the conventional fillers can prevent the recrystallization of PEO–based polymer electrolytes and improve the ionic conductivity. Xi *et al*. (2005) prepared NCPEs based on PEO–$LiClO_4$ using solid acid sulphated–zirconia (SO_4^{2-}–ZrO_2, abbreviated as SZ) as filler. The ionic conductivity of these NCPEs was increased by two orders of magnitude in comparison to pristine PEO–$LiClO_4$ polymer electrolytes. Apart from that, there is an effect of the treatment on the fillers. The ionic conductivity of NCPEs with SZ (4.0×10^{-7} S cm^{-1}) is two times higher than untreated– NCPEs that is 1.5×10^{-7} S cm^{-1} to (Xi *et al*., 2005). New nano–sized organic–inorganic hybrid materials have been introduced. High surface area nano–scaled zinc aluminate ($ZnAl_2O_4$) with a mesoporous network was synthesized by Wang *et al*. (2009). The highest ionic conductivity of 2.23×10^{-6} S cm^{-1} was achieved at ambient temperature by adding 8 wt.% of $ZnAl_2O_4$ into PEO–$LiClO_4$. The fillers reduced the crystallinity of polymer membrane and increased the lithium ion transference number as reported in Wang *et al*. (2009).

2.1.4 Liquid Crystal Polymer Electrolytes (LCPEs)

Liquid crystal polymer electrolytes (LCPEs) are the newest type of polymer electrolytes discovered. LCPEs are the polymer electrolytes replacing the common polymers with liquid crystal polymers (LCPs) as host polymer. Ion transport coupled with segmental motions of the host polymers in common polymer electrolytes can achieve significant enhancement of ionic conductivity above glass transition temperature (T_g) only (Imrie *et al*., 2004). Mechanical stability of polymer electrolytes is greatly reduced when the T_g is decreased to sub–ambient temperature (Imrie &, Ingram 2000). So, a new material called LCP has been invented to solve these problems. LCP can exhibit high ionic conductivity in glassy and liquid crystal phases (Imrie *et al.*, 2004). For amorphous polymer complexes, the ionic motion is coupled to structural relaxations of the polymers. Therefore, the ionic mobility in the polymer complexes becomes very small at T_g. Therefore, the liquid crystalline behavior of LCPs can help in decoupling the ion mobility from the structural relaxations (McHattie *et al.*, 1998). Besides, LCPs have other advantages that result from a combination of anisotropic and excellent bulk properties with new possibilities for polymer processing (Park *et al.*, 2010).

LCPs are polymers consisting of mesogen (fundamental functional groups of liquid crystals that induce the structural order in crystal) in either their backbone or their side chain. The LCPs are divided into two main classes that are main chain–liquid crystal polymers (MCLCPs) and side chain–liquid crystal polymer (SCLCP) as shown below.

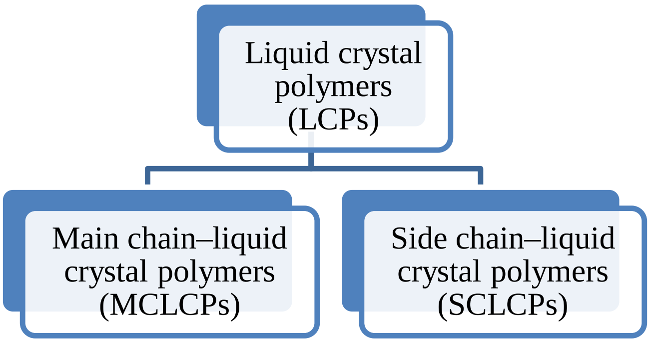

Figure 2.2: Two main types of liquid crystal polymers.

LCPs with mesogenic units located at the backbone are designated as main chain–liquid crystal polymers (MCLCPs). The mesomorphic (state of matters between conventional liquid and solid crystal) properties of MCLCPs depend on the chain flexibility and structure of the polymer. The incorporation of mesogenic units along an ionically conducting polymer backbone will give rise to main chain–liquid crystal polymer electrolytes (McHattie *et al.*, 1998). On the other hand, the side chain–liquid crystal polymer (SCLCP) is the name for the LCP that has mesogenic groups at the side chain. Polymer backbone, mesogenic units and a space which connects mesogenic units are the three main components needed in the SCLCPs preparation (Felipe, 2009). Side chain–

liquid crystal polymer electrolytes are produced when the ion coordinating cyclic macromolecule is inserted into mesogenes which are attached to the polymer backbones through flexible spacers (McHattie *et al.*, 1998). Several structural factors such as flexibility of polymer backbone, the distance between the side chains of polymer (that is repeating unit length) and spacer length determine the mesomorphic properties of SCLCPs. Since the molecular mobility of the polymeric backbone and the mesogenic groups are coupled through the flexible spacer in SCLCPs, thus the decoupling of ionic motions from structural relaxation is needed for the ionic transport in the polymer electrolytes. The degree of decoupling can be enhanced by increasing those structural factors as mentioned above. Decoupling also decreases the T_g of polymer electrolytes and hence promotes the ionic hopping mechanism in the polymer matrix.

Imrie and her research group have contributed a lot in the development of ionically conducting LCPEs (McHattie *et al.*, 1998; Imrie &, Ingram 2000; Imrie *et al.*, 2004). McHattie *et al.* (1998) synthesized a new mesogenic liquid crystalline side–chain polymers based on predominantly PEO backbone with mesogenic groups attached as pendants via flexible alkyl spacers. The liquid crystalline systems–based PEO–$LiClO_4$ exhibits higher ionic conductivity and different conductivity behavior compared to pristine PEO–$LiClO_4$ polymer complexes (McHattie *et al.*, 1998). Novel star branched amphiphilic liquid crystal copolymers based on PEO containing cyanobiphenyl mesogenic pendants (MAxLC) was synthesized using atom transfer radical polymerization (ATRP) by Tong *et al.* (2012). The ionic conductivity of polymer electrolytes had been increased significantly by inserting the mesogenic groups. They perceive that the mesogenes can provide efficient ion conducting pathway and suppress the crystallization of polymer which promotes the movement of polymer. The LCPEs have also been applied in electrochemical devices. Park *et al.* (2010) fabricated dye–sensitized solar cells (DSSCs) using a new series of SCLCPs. The maximum power conversion efficiency (PCE) of 4.11% was achieved using prepared LCPEs with better photovoltaic performances (Park *et al.*, 2010). So far, how the nature of the liquid crystalline region affects the ionic conductivity in the polymers electrolytes is not fully investigated and understood. A more extensive research needs to be done to make LCPEs a new highly ion conductive organic material for use in the electrochemical devices.

2.2 General Descriptions of Ionic Conduction Mechanism

2.2.1 Types of Ionic Conduction Mechanism

Diffusion refers to the movement of atoms, molecules or ions in a solid (Raghavan, 2004). Diffusion is a process in which uniformity of concentration of diffusing species under consideration is attained through its motion from a place to another place (Kudo & Fueki, 1990). The diffusion of mobile charge carriers is the main process in an electrolyte when an electric field is applied across the cell. The ions in an electrolyte are subjected to Brownian motion when there is no electric field and will migrate along the direction of electric field in the crystalline phase when a voltage is applied across the electrolyte (Kudo & Fueki, 1990). This phenomenon is known as ion conduction. However, the ions will have to overcome a potential barrier in order to diffuse, migrate or transport if they are being trapped in the lattice sites of crystalline phase (West, 1999). Even though the ions vibrate continuously in the lattice structure, they rarely have enough thermal energy to escape from the lattice site. Ionic conduction, migration, hopping or diffusion can occur if the ions able to overcome the barrier and move to adjacent lattice sites. There are two main possible mechanisms for ion diffusion in the polymer electrolytes i.e. vacancy mechanism and interstitial mechanism in an electrolyte. These mechanisms are sketched in Figures 2.3–2.5.

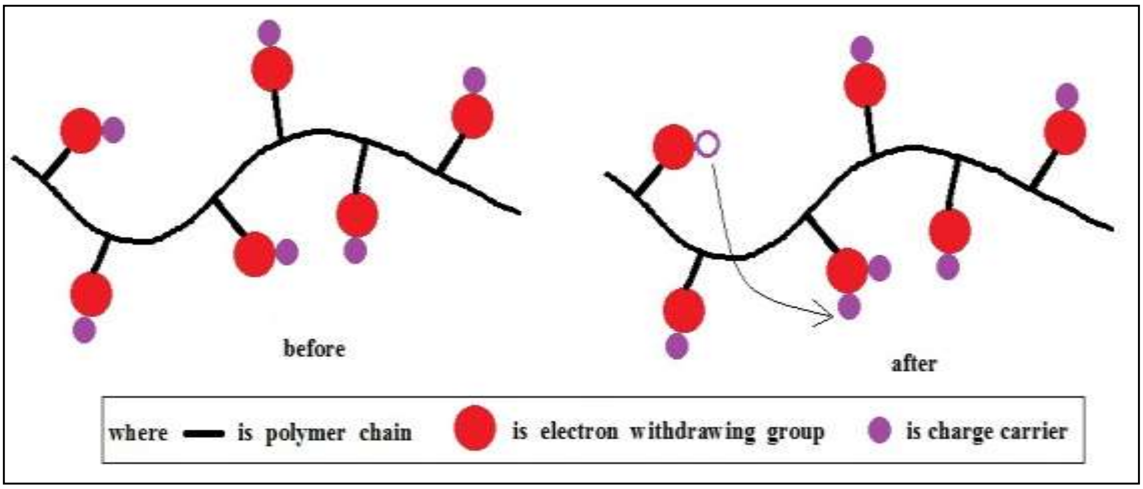

Figure 2.3: Schematic representation of ion diffusion before and after a vacancy mechanism (Souquet *et al*., 2010).

Vacancy mechanism is defined as the hopping mechanism of an ion from its normal position to an adjacent but empty site (Souquet *et al*., 2010). The ions require sufficient energy which arises from the thermal energy of ionic vibrations to break the coordination bonds and jump from a site to an adjacent empty site (Raghavan, 2004).

In contrast, the interstitial mechanism occurs when a mobile charge carrier migrates from one interstitial position to another as illustrated below (Raghavan, 2004; Smart and Moore, 2005, Souquet *et al*., 2010).

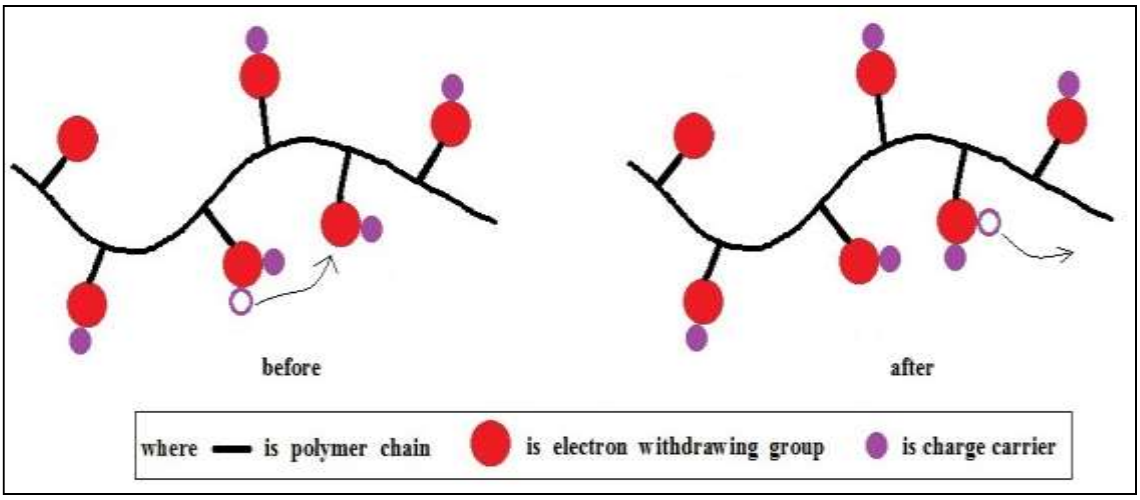

Figure 2.4: Schematic representation of ion diffusion before and after an interstitial mechanism (Souquet *et al*., 2010).

The interstitial diffusion is faster than vacancy diffusion because of weak bonding of the interstitials to the surrounding ions and high probability of an empty adjacent interstitial site for ions to jump during conduction (West, 1999).

There is another interstitial pair migration in the polymer electrolytes above T_g namely free volume mechanism. This is a cooperative mechanism of interstitial pair migration with polymer segment mobility.

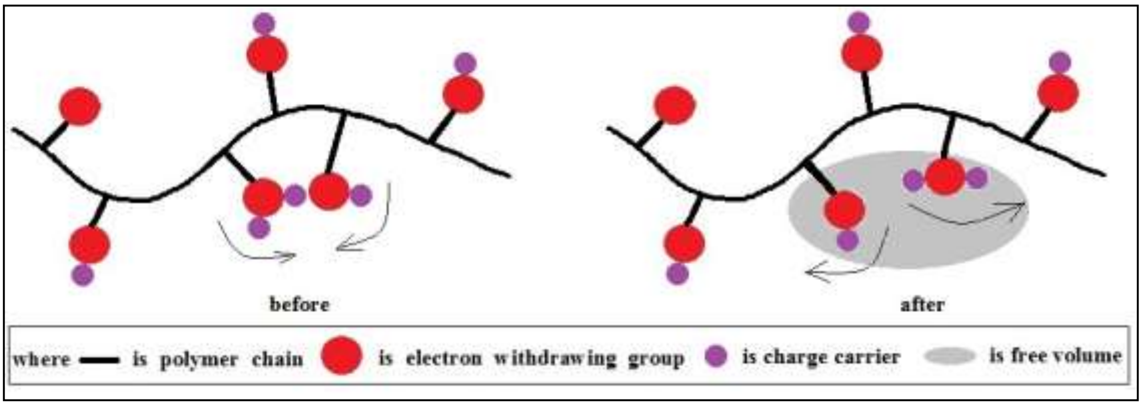

Figure 2.5: Schematic representation of ion diffusion before and after a free volume mechanism coupled with the chain movement (Souquet *et al.*, 2010).

A cage is formed by its nearest neighbours during the local movement of the polymer segments. The random density fluctuations or chain movement of polymer segments will produce the free volume in the polymer matrix. Therefore, the moving species can escape from the cage and jump to another cage when the random density fluctuations of polymer chains produce an adjoining cage large enough to allow the ion transport (Souquet *et al.*, 2010).

2.2.2 Basic Conditions to Generate the Ionic Conductivity

Ionic hopping process arises from the transportation of mobile charge carriers (or ions) which are dissociated from the polymer complexes. Five basic requirements must be fulfilled in order to create the ionic conduction mechanism in the polymer electrolytes. These basic conditions are:

(a) A large number of mobile ions to migrate

(b) A large number of vacant sites should be available and ready for the ionic hopping mechanism. This is a corollary of (a) because ions can only be mobile if there are empty sites available for them to occupy

(c) The empty and occupied sites should have similar potential energies with a low activation barrier (or known as activation energy) for jumping from one site to a neighboring empty site. It is useless to have many available vacant sites when the mobile ions cannot get into the space because of small sized vacant sites

(d) The structure should have a framework, preferably three–dimensional network, permeated by open pathway through which mobile ions may transport

(e) The framework of the structure should be highly polarizable (West, 1999)

2.2.3 Parameters that Govern the Ionic Conduction

The ionic conductivity of a polymer electrolyte is expressed as follows:

$$\sigma(T) = \sum_i n_i q_i \mu_i \qquad \text{(Equation 2.1)}$$

where n_i is the number of charge carriers of type i per unit volume, q_i is the charge of ions of type i, and μ_i is the ionic mobility of type i which is a measure of the drift velocity in a constant electric field (Gray, 1991; Gray, 1997; Smart and Moore, 2005). The ionic conductivity of polymer electrolytes is strongly dependent on the amount of free charge carriers and their mobility in the polymer electrolytes. Conductive polymer electrolytes must have following criteria:

i) more mobile charge carriers can be detached from coordination bond

ii) high mobility of the charge carriers transported in the polymer electrolytes

There are a few factors that govern these two criteria, for example degree of crystallinity, flexibility of polymer chains and dielectric constant of polymer electrolytes. Low degree of crystallinity (or high degree of amorphousness), low T_g, high ion mobility, high concentration of mobile ions and high dielectric constant of polymer with high flexible chains favor ionic conduction in the polymer electrolytes.

Crystallinity is a physical state of a solid material where the atom, molecules or ions are arranged in ordered and aligned arrangement, whereas amorphous is the state where the atom, molecules or ions are arranged in random and disordered arrangement as shown in figure below (Steven, 1999).

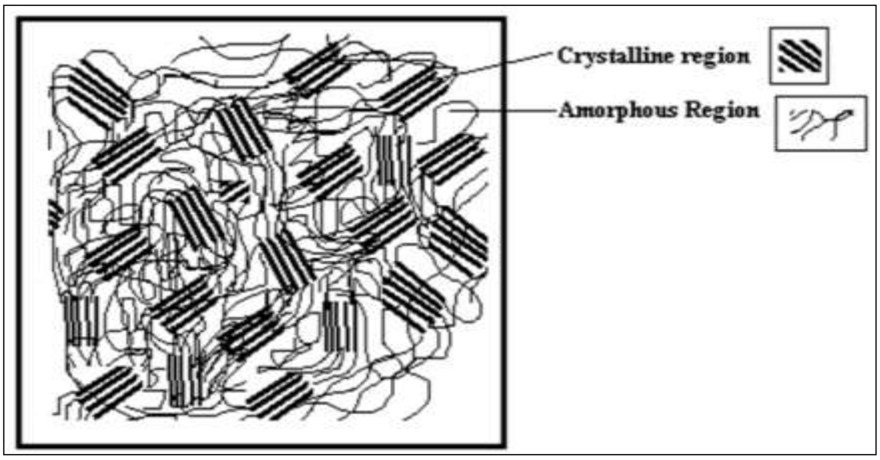

Figure 2.6: Schematic diagram of mixed amorphous and crystalline regions in semi–crystalline polymer structure.

Ions are difficult to be transported in the pure crystalline polymer electrolytes as the coordinative bonds among the molecules are packed orderly. Therefore, the ionic conduction is easier to occur if the polymer electrolytes have crystallographic defects. Therefore, the charge carriers can migrate at high rate in the amorphous regions of the polymer electrolytes. At the glass transition temperature, T_g the polymer electrolyte undergoes a transition from a hard like–glassy state to a soft and elastomeric rubbery state in the amorphous region of the polymer. Even though short range vibration and rotations are observed below T_g, the mobility of the ions are still restricted when the polymers are in the glassy state. Hence, the ion transportation is impeded in the polymer electrolytes below T_g. The glassy structure of polymer will be converted into rubbery state when the temperature is further heated. Above T_g, the rubbery state is associated with long range molecular motion. As a result, this transition increases the degree of rotational freedom and promotes the segmental movement among the atom, molecules or ions in the chains. The high dielectric constant of polymers favors ion separation and prevents the ion aggregates and ion clusters forming in the polymer electrolytes (Eliasson *et al*., 2000). Therefore, the high dielectric constant of polymer electrolytes could promote ion diffusion and improve the ion hopping mechanism. Flexibility of polymer chains is also an important parameter that governs the number density and mobility of the charge carriers. The solvating ions can be dissociated easily from the interactive bonds within the highly flexible polymer chains. As a result, this helps in increasing the ionic conduction in the polymer electrolytes.

2.3 Ways to Enhance the Ionic Conduction Mechanism

The low ionic conductivity of polymer electrolytes limits their application. Different approaches have been implemented to enhance the ionic conductivity of polymer electrolytes up to ~mS cm^{-1}. These ways are blending of two different polymers, modifications on the polymers, irradiation with gamma (γ) rays, mix salt system and addition of several additives, such as plasticizers, ionic liquids and fillers.

2.3.1 Polymer Modifications

Since crystallinity of a polymer can block the conducting pathway in electrolytes, thus the researchers have done some modifications onto the polymer to improve the degree of amorphousness. Efforts in this direction include the preparation of block copolymers, comb copolymers, graft copolymers and network polymers. Fish *et al*. (1988) reported that the polymer–salt complexes with more flexible chains and low glass transition temperature can facilitate the polymer segmental mobility which aids the ion transport through the polymer matrix. They have shown that polymer complexes of poly(methylsiloxane)s in which oligo(oxyethylene) side chains are anchored with $LiClO_4$ exhibit high ionic conductivity of 7×10^{-5} S cm^{-1} at room temperature and conductivity achieved above 10^{-4} S cm^{-1} at high temperatures (Fish *et al*., 1988).

Soo *et al*. (1999) have reported the synthesis and electrochemical characterization of poly(lauryl methacrylate)–*b*–poly[oligo(oxyethylene) methacrylate]–based block copolymer electrolytes in the rubbery state and these electrolytes showed higher ionic conductivity and better dimensional stability with a wide potential window up to 5V than those glassy block copolymer systems. The fabricated battery using this block polymer electrolyte exhibited high reversible capacity and good capacity retention (Soo *et al*., 1999). Another type of block copolymer electrolytes had been prepared by Guilherme *et al*. (2007). Block copolymer electrolytes comprising of polyethylene–*b*–poly(ethylene oxide) (PE–*b*–PEO) and $LiClO_4$ was investigated. This polymer electrolyte achieved the highest ionic conductivity of 3×10^{-5} S cm^{-1} at ambient temperature with addition of 15 wt.% of $LiClO_4$. The ionic conductivity reached ~10^{-3} S cm^{-1} at 100 °C. The block copolymerization also reduced the degree of crystallinity of polymer electrolytes.

Apart from that, a comb–shaped polymer was used as host polymer in the preparation of polymer electrolytes. Polysilane comb polymers, $[(CH_3CH_2OCH_2CH_2O(CH_2)_4)Si(CH_3)]_n$ incorporating ethoxyethoxybutane in the side chain of the polymer was synthesized by Lyons *et al*. (1996). The polymer electrolytes based on this comb polymer host and lithium triflate achieved a room temperature ionic conductivity of 1.2×10^{-7} S cm^{-1} at [Li]/[O]=0.25. Comb–branch copolymers was also synthesized by copolymerizing poly(ethylene oxide methoxy) acrylate with lithium 1,1,2–trifluorobutane sulfonate acrylate. These new fluorinated copolymers possess high ionic conductivity and low T_g (Cowie & Spence, 1999).

Comb–shaped polyethers have been prepared using poly(4–hydroxystyrene) (PHSt) as a multifunctional initiator through graft polymerization of ethylene oxide (EO) or a mixture of EO and propylene oxide (PO). Solid polymer electrolytes comprising of these polyethers and lithium triflate ($LiCF_3SO_3$) exhibited ionic conductivity of ~10^{-5} S cm^{-1} at room temperature. The grafting reaction greatly reduced the crystallinity of these polymer electrolytes having comb–shaped architectures (Jannasch, 2000). A novel series of graft copolymers containing graft chains of macromonomer poly(sodium styrenesulfonate) (macPSSNa) and polystyrene (PS) backbone were synthesized using a combination of stable free radical polymerization (SFRP) and emulsion polymerization by Ding *et al*. (2002). Although the graft polymer electrolytes showed lower water uptake, they gave remarkably good proton conductivity compared to the membranes prepared from random copolymers styrenesulfonic acid and styrene (PS–r–PSSA).

Network polymer based on poly[2–(2–methoxyethoxy)ethyl glycidyl ether] (PME2GE) was used as host polymer in random copolymer electrolytes containing $LiClO_4$ as dopant salt. This novel random copolymer system exhibited the maximum ionic conductivity of $\sim 10^{-4}$ S cm^{-1} at 40 °C with the optimum composition of EO/ME2GE=70/30 (Kono *et al.*, 1993). Network polymer electrolytes with hyperbranched ether side chains were also synthesized to achieve high ionic conducting polymer membranes. A monosubstituted–epoxide monomer, 2–(2–methoxyethoxy)ethyl glycidyl ether (MEEGE) was initially copolymerized with ethylene oxide (EO) by base–catalyzed anionic ring-opening polymerization using 2–(2–methoxyethoxy) ethanol. This copolymerization results in the formation of semiterechelic poly[ethylene oxide–co–2–(2–methoxyethoxy)ethyl glycidyl ether] [P(EO/MEEGE)] oligomers. After esterification of the oligomers with acrylic acid, polyether macromonomers were produced. Network polymer electrolytes were prepared by photo cross–linking the mixtures of the polyether macromonomer, lithium bis(trifluoromethylsulfonyl)imide (LiTFSI) salt and a photoinitiator. This network polymer electrolyte exhibited ionic conductivity of 1×10^{-4} S cm^{-1} at 30 °C and 1×10^{-3} S cm^{-1} at 80 °C (Nishimoto *et al.*, 1999). This polymer modification technique is not so effective to improve the ionic conductivity of polymer electrolytes as it does not increase the conductivity greatly.

2.3.2 Polymer Blending

Polymer blending is another approach to increase the ionic conductivity of polymer electrolytes. In polymer blending, two or more different polymers or copolymers are mixed physically without any covalent bonding. A new macromolecular material with special properties is produced. One of the materials in polymer blends is adopted to absorb the active transporting species in the electrolyte, whereas the second material is added to provide the mechanical support for electrolyte and sometimes it is substantially inert. Polymer blending offers several advantages, for instance ease of sample preparation and ease of controling the physical properties of polymer membrane within the definite compositional change (Rajendran *et al*., 2002). Polymer blending is also a cost effective way to prepare polymer electrolytes in comparison to polymer modifications as it does not require the polymerization process. The properties of polymer blends are dependent on the physical and chemical properties of the participating polymers and the state of the phase, whether homogenous or heterogeneous. The homogenous polymer blends or intermixing of the dissolved polymers will be produced if two or more different polymers are able to dissolve successfully in a common solvent due to the fast establishment of the thermodynamic equilibrium (Braun *et al*., 2005).

A variety of binary polymer electrolyte systems have been prepared and investigated, such as PMMA–PVC (Choi *et al*., 2001; Rajendran *et al*., 2000; Stephan *et al*., 2002), PVA–PMMA (Rajendran *et al*., 2004a), PMMA–poly(vinylidene fluoride) (PVdF) (Cui *et al*., 2008; Nicotera *et al*., 2006), poly(vinyl acetate) (PVAc)–PMMA (Baskaran *et al*., 2006a), PVAc–poly(vinylidene fluoride) (PVdF) (Baskaran *et al*., 2006b), PEO–PVdF (Yang *et al*., 2008), PVC–poly(ethyl methacrylate) (PEMA) (Han *et al*., 2002; Rajendran *et al*., 2008) and PVA–poly(styrene sulphonic acid) (PSA) (Kumar & Bhat, 2009). The blending between PMMA and poly (vinyl chloride) (PVC) is a common polymer blend used as polymer host in the development of polymer electrolytes. PMMA is a completely amorphous polymer with brittle properties. Therefore, PVC is introduced as a mechanical stiffener due to dipole–dipole interaction between hydrogen and the lone pair electrons of chlorine atom (Ramesh *et al*., 2013). The polymer electrolytes containing 70 wt.% of PMMA–30 wt.% of PVC polymer blends and 10 wt.% of LiTFSI reached the maximum ionic conductivity of 1.60×10^{-8} S cm^{-1} at room temperature. Above this ratio, phase separation was occurred onto the polymer electrolyte as reported in Ramesh *et al*. (2010). The globular agglomeration of PVC at high PVC loadings could block the ion transport in the polymer electrolytes.

Higher ionic conductivity of polymer electrolytes were obtained for other polymer blends compared to that of PMMA–PVC. Sivakumar *et al*. (2007) reported that the highest ionic conductivity of PMMA–PVdF blend gel polymer electrolyte with PVdF:PEMA ratio of 90:10 was 1.50×10^{-4} S cm^{-1}. The ionic conductivity of gel polymer electrolytes prepared using PVdF–PEMA blend was reduced at high PEMA content due to the increased crystalline phase in the PEMA domains. This conductive gel polymer electrolyte has good transport properties and superior interfacial stability with Li electrode (Sivakumar *et al.*, 2007). Novel hyperbranched polyether, poly(3–{2–[2–(2–hydroxyethoxy) ethoxy] ethoxy}methyl–3′–methyloxetane) (PHEMO) was blended with poly(vinylidene fluoride–hexafluoropropylene) (PVDF–HFP) as a host polymer in LiTFSI–based electrolytes by Wu *et al*. (2009). This novel polymer electrolyte showed a maximum ionic conductivity of 1.64×10^{-4} S cm^{-1} at 30 °C. This polymer electrolyte is a promising candidate as electrolyte in lithium ion batteries as it has wide electrochemical potential window up to 4.2 V vs. Li^+/Li and high decomposition temperature above 400 °C (Wu *et al.*, 2009). However, the ionic conductivity is still less than mS cm^{-1}. Researchers therefore have to propose another way to increase the ionic conductivity of polymer electrolytes significantly in replacing this polymer blending method.

2.3.3 Gamma irradiation

Exposing γ rays to the polymer electrolytes is a feasible way to improve the ionic conductivity. The ionizing radiation on polymeric materials could release the reactive intermediate products such as excited states, ions and free radicals (Rahaman *et al*., 2014). These free radicals produced from γ irradiation can affect the microstructure of the polymer chains through intermolecular cross–linking and/or main chain scission (Nanda *et al*., 2010; Sinha *et al*., 2008). The γ irradiation can alter the chemical, physical, structural, optical, mechanical and electrical properties of polymer complexes (Rahaman *et al*., 2014). This absorption of high energy can suppress the crystalline region, change the molecular weight distribution, increase the ionic conductivity and improve the mechanical strength of polymer electrolytes (Damle *et al*., 2008; Ghosal *et al*., 2013; Nanda *et al*., 2010).

PEO was initially cross–linked with $LiClO_4$ via γ radiation as reported by Song *et al*. (1997). The polymer blend electrolytes were further prepared by blending PVdF and cross–linked PEO and subjected to γ radiation to produce a simultaneous interpenetrating network (SIN). According to the authors, γ radiation induced SIN polymer electrolytes not only provide high mechanical modulus of 10^7 Pa, but also exhibit high room temperature ionic conductivity of more than 10^{-4} S cm^{-1} (Song *et al*., 1997). Another γ radiation work has been done by Tarafdar *et al*. (2010). They prepared polymer electrolytes based on γ radiated PEO–ammonium perchlorate (NH_4ClO_4) and found out that the ionic conductivity is increased greatly with γ radiation dose at 35 kGy. The enhancement of ionic conductivity is attributed to the decreased crystallinity of polymer electrolytes (Tarafdar *et al*., 2010). Gamma radiated PVdF–lithium bis(oxalato)borate (LiBOB) solid polymer electrolyte reached the highest room temperature conductivity of 3.05×10^{-4} S cm^{-1} which is 15% higher than the polymer electrolyte without any γ radiation (Rahaman *et al*., 2014). Gamma radiation is a potential way to improve the ionic conductivity. Nevertheless, the polymer electrolytes can be degraded at high γ radiation dose (Akiyama *et al*., 2010).

2.3.4 Mix Salt System

Mixing dual salts in the polymer electrolytes can enhance the ionic conductivity of polymer electrolytes because it may prevent the formation of aggregates and clusters which increases the mobility of ion carriers (Gray, 1997). In addition, this mix dual salt system can provide more mobile charge carriers for transport in the polymer electrolytes which in accordance with higher ionic conductivity in comparison to single salt system. Arof and Ramesh (2000) have prepared dual salt system–based polymer electrolytes that comprised poly(vinyl chloride) (PVC), $LiCF_3SO_3$ and lithium tetrafluoroborate ($LiBF_4$) as doping salts. The ionic conductivity is slightly increased in comparison to single salt system. The increase in conductivity is attributed to the increase in the mobility of charge carriers by avoiding the aggregation process. Gel polymer electrolytes comprising of PVdF/poly[(ethylene glycol) diacrylate] (PEDGA)/PMMA and salt mixtures of lithium hexafluorophosphate ($LiPF_6$)/$LiCF_3SO_3$ were prepared and investigated by Yang *et al.* (2006). The ionic conductivity of the mixed salt system–polymer electrolytes is 5 times higher than $LiCF_3SO_3$–based polymer electrolyte system. The polymer electrolytes containing 10 wt.% of $LiPF_6$ and 1 wt.% of $LiCF_3SO_3$ showed high ionic conductivity of 1.5 mS cm^{-1} and a stable electrochemical potential range (Yang *et al.*, 2006). However, there is a shortcoming of this technique. Solubility of dual salt in the same solvent is the major concern in this method. The researchers ought to ensure that the same solvent can be used to solubilize both salts.

2.3.5 Additives

Various types of additives can be used to increase the ionic conductivity, such as plasticizers, fillers, ionic liquids and liquid crystals.

2.3.5.1 Plasticizers

Plasticization is generally recognized as one of the effective and efficient methods available to boost up the ionic conductivity abruptly as it can decrease the degree of crystallinity of polymer electrolytes (Suthanthiraraj *et al.*, 2009). A plasticizer is a non–volatile and low molecular weight aprotic organic solvent which has a T_g in the vicinity of –50 °C (Ramesh *et al.*, 2012). There are many types of plasticizers used in plasticized–GPE, for example PC, EC, dimethyl carbonate (DMC), DEC, DMF, N,N–dimethylacetamide (DMAc), γ–butyrolactone, DBP, diocthyl adipate (DOA) and PEG (Ning *et al.*, 2009; Pradhan *et al.*, 2005; Suthanthiraraj *et al.*, 2009). The effect of plasticizers on the polymer electrolytes depends on the specific physical and chemical properties of the plasticizer, for example, viscosity, dielectric constant, the interaction between polymer and plasticizer, and the coordinative bond between ion and plasticizer (Rajendran and Sivakumar, 2008).

The incorporation of plasticizers into polymer electrolytes enhances the salt solvating power, increases the ion mobility and provides a better contact between polymer electrolytes and electrodes due to its sticky behavior (Ramesh and Arof, 2001; Rajendran *et al.*, 2004a). Plasticizers are also attractive additives because of their superior miscibility with polymer, high dielectric constant, improved processability and low viscosity (Ramesh and Chao, 2011). Addition of plasticizers is also a successful skill to enhance the ionic conductivity without reducing the thermal, electrochemical and dimensional stabilities (Ganesan *et al.*, 2008). It is important to know the roles of plasticizers in increasing the ionic conductivity of polymer electrolytes. The ionic conductivity of polymer electrolytes is expected to be increased by adding plasticizer via some important modifications such as significant changes in local structure, increment of amorphous fraction and changes in local electric field distribution in the polymer matrix.

The principal function of plasticizers is to lower the T_g of polymer electrolytes and hence reduce the modulus of polymer at the desired temperature. The plasticizer can exhibit the transition from the glassy state to rubbery region at progressively lower temperature. Besides, plasticizers reduce the viscosity of polymer system and facilitate the ionic transport within the polymer complexes. Moreover, plasticizers can help in weakening the coordinative interactions within the polymer chains and thus improve the flexibility of polymer chains in the polymer matrix which favors ionic migration (Ganesan *et al*., 2008). As a result, it promotes the formation of free volume in the polymer matrix and therefore enhances the long–range segmental motion of the polymer in the system when the polymer matrix is swollen in a plasticizer in this approach. In general, plasticizers have conjugated double bond. This double bond initializes the delocalization of electrons and improves the donor capacity of oxygen atom. Therefore, plasticizers can facilitate the binding of cations and dissociate the charge carriers from the interactive bonding easily. Hence, the ease of this detachment of the charge carriers increases the amount of mobile charge carriers and promotes the ionic hopping mechanism.

Three types of ester class plasticizers, that are dioctyl phthalate (DOP), DBP and dimethyl phthalate (DMP), were employed to examine their effect on ionic conductivity in the PEO–$LiClO_4$ polymer complex (Michael *et al*., 1997). Among all these plasticizers, DOP was found to be an excellent plasticizer in terms of thermal stability as proven in differential thermal analysis (DTA). The weight loss is decreased as the plasticizer concentration increased as shown in Michael's findings (Michael *et al*., 1997). Ali *et al*. (2007) studied the plasticized–polymer electrolytes composing PMMA as host polymer, propylene carbonate (PC) or ethylene carbonate (EC) as plasticizer and LiTf or $LiN(CF_3SO_2)_2$ as dopant salt. The ionic conductivity increases with the concentration of the plasticizer as expected. They also declared that the PC plasticized–polymer electrolytes exhibit higher ionic conductivity than the EC plasticized–polymer electrolytes (Ali *et al.*, 2007).

Rajendran *et al.* (2004a) also incorporated a few types of plasticizers in the polymer electrolytes containing PVA/PMMA–$LiBF_4$. The highest ionic conductivity of 1.29 mS cm^{-1} had been observed for EC complex because of the higher dielectric constant of EC (ε=85.1). A maximum electrical conductivity of 2.60×10^{-4} S cm^{-1} at 300 K has been observed for the electrolyte containing 30 wt.% of PEG as plasticizer. The ionic conductivity of this plasticized–polymer electrolyte has been increased by two orders of magnitude compared to the pure PEO–$NaClO_4$ system of 1.05×10^{-6} S cm^{-1}. This showed that the addition of plasticizer enhances the amorphous phase and reduces the energy barrier for ion transport. Eventually, it results in higher segmental motion of lithium ions (Kuila *et al.*, 2007). Hence, plasticizers can improve the ionic conductivity extensively, but, plasticization has some limitations, such as low safety performances, poor electrical, electrochemical, mechanical and thermal stabilities, slow evaporation and high vapor pressure. Other drawbacks are poor interfacial stability with lithium electrodes and narrow electrochemical window as well as low flash point (Pandey & Hashmi, 2009; Ramesh *et al.*, 2011a).

2.3.5.2 Ionic Liquids

A new attempt has been made to overcome these obstacles such as low safety performances, poor interfacial stability and poor electrochemical properties. In order to replace plasticizer, room temperature ionic liquids (RTILs) have been synthesized and developed in recent years. Ionic liquids (ILs) are non–volatile molten salts with a low melting temperature, T_m <100 °C (Pandey & Hashmi, 2009). ILs are designated as the molten salts which remain in their liquid state at room temperature (Quartarone and Mustarelli, 2011). ILs normally consist a bulky and asymmetric organic cation and a highly delocalized–charge inorganic anion. There are a variety of ionic liquids. Examples of organic cations are 1,3–dialkylimidazolium, 1,3–dialkylpyridinium, tetraalkylammonium, trialkylsulphonium, tetraalkylphosphonium, *N*–methyl–*N*–alkylpyrrolidinium, *N,N*–dialkylpyrrolidinium, *N*–alkylthiazolium, *N,N*–dialkyltriazolium, *N,N*–dialkyloxazolium, *N,N*–dialkylpyrazolium and guanidinium (Jain *et al.*, 2005; Ye *et al.*, 2013). On the other hand, the common inorganic anions such as acetate (CH_3COO^-), nitrate (NO_3^-), triflate (Tf^-), tetrafluoroborate (BF_4^-), bis(trifluoromethylsulfonyl imide) ($TFSI^-$), bis (perfluoroethyl sulfonyl) imide [$N(C_2F_5SO_2)^{2-}$], hexaflurophosphate (PF_6^-) and halides (Cl^-, Br^- and I^-) have widely been used in ionic liquids. The physical properties of ionic liquids such as melting point, dielectric constant, polarity, miscibility with water and other solvents, viscosity, density and hydrophobicity as well as dissolution ability depends on the cation–anion combination (Jain *et al.*, 2005; Vioux *et al.*, 2009).

ILs have emerged as promising candidates because of their unique and fascinating physicochemical properties. Ionic liquids have a number of beneficial properties, for example a wide electrochemical potential window (up to 6V), wide decomposition temperature range, negligible vapor pressure, non–toxic, non–volatile and non–flammable with environmental friendly feature (Cheng *et al.*, 2007; Patel *et al.*, 2011; Pandey & Hashmi, 2013; Ramesh *et al.*, 2011a). The properties of RTILs such as excellent chemical, thermal and electrochemical stabilities, high ionic conductivity due to high ion concentration, good oxidative stability and superior ion mobility as well as high cohesive energy density makes them promising candidates for use in PEs (Ye *et al.*, 2013). Besides, ILs have high ability to dissolve a wide range of organic, inorganic and organometallic compounds and exhibit excellent safety performance (Reiter *et al.*, 2006; Vioux *et al.*, 2009).

The strong plasticizing effect of ionic liquids can soften the polymer backbone and increase the flexibility of polymer chains. This initiates the transportation of mobile charge carriers within the polymer matrix and lead to higher ionic conductivity. Moreover, the low viscosity of ionic liquids decreases the crystalline region of the polymer matrix by disrupting the ordered arrangement of the polymeric backbone (Singh *et al.*, 2009). This provides more voids and free spaces for ion migration. As a result, it promotes the ionic mobility within the polymer system and hence enhances the ionic conductivity. The bulky cations paired with anions would lead to poor packing efficiencies and thus endorse the ion detachment of this ionic compound, resulting in higher ionic conductivity in the polymer electrolytes. Inclusion of ionic liquids produces sticky gel–like polymer electrolyte (GPE). Sticky gel polymer electrolytes are an advantage for designing of electrochemical devices since they can provide better contact between electrolyte and electrode (Reiter *et al.*, 2006). The immobilization of ionic liquids within polymer matrices makes it possible to take advantage of their unique properties in the solid state and thus minimizes some shortcomings related to shaping and risk of leakage.

The effect of adding ionic liquid onto polymer electrolytes had been widely studied and investigated by many researchers recently. Sirisopanaporn *et al*. had prepared freestanding, transparent and flexible gel polymer electrolytes by trapping N–n–butyl–N–ethylpyrrolidinium N,N–bis(trifluoromethane)sulfonimide–lithium N,N–bis(trifluoromethane) sulfonamide (Py_{24}TFSI–LiTFSI) ionic liquid solutions in poly(vinylidenefluoride–co–hexafluoropropylene) (PVdF–co–HFP) copolymer matrices. The resulting membranes exhibited high ionic conductivity at room temperature, from 0.34 to 0.94 mS cm^{-1}. These polymer electrolytes can be operated up to 110 °C without any degradation and any IL leakage within 4 months storage time (Sirisopanaporn *et al.*, 2009). A new proton conducting PVdF–co–HFP copolymer membrane composing 2,3–dimethyl–1–octylimidazolium trifluromethanesulfonylimide (DMOImTFSI) had been prepared. A maximum ionic conductivity of 2.74 mS cm^{-1} was achieved at 130 °C, along with good mechanical stability (Sekhon *et al*., 2006).

Ionic liquid was also added onto the biodegradable polymers to form biopolymer electrolytes. Biopolymer electrolytes containing corn starch, $LiPF_6$ and ionic liquids, 1–butyl–3–methylimidazolium hexafluorophosphate ($BmImPF_6$) or 1–butyl–3–methylimidazolium trifluoromethanesulfonate (BmImTf) were prepared using solution casting technique as reported in my published works (Ramesh *et al*., 2011b; Liew & Ramesh, 2013; Liew & Ramesh, 2014). Upon addition of ionic liquids in both systems, the ionic conductivity increased by three orders of magnitude. The highest room temperature ionic conductivity of 1.47×10^{-4} S cm^{-1} is achieved with addition of 50 wt.% of BmImTf (Ramesh *et al*., 2011b). Higher ionic conductivity was observed for Tf–based system where its maximum ionic conductivity is 3.21×10^{-4} S cm^{-1} (Liew & Ramesh, 2013). Ning and co–workers synthesized ionic liquid plasticized–corn starch films. The maximum conductance of $10^{-1.6}$ S cm^{-1} was achieved by introducing 30 wt.% of 1–ally–3–methylimidazolium chloride (AmImCl) (Ning *et al*., 2009). Among all the methods, doping of ionic liquids is a feasible way to improve the ionic conductivity greatly without degrading the polymer electrolytes

2.3.5.3 Fillers and Nano–fillers

Filler is an additive to improve the physical and mechanical properties of material. Incorporation of fillers into the polymer electrolytes could result the formation of composite polymer electrolytes (CPEs). On the other hand, the polymer electrolyte is assigned to nanocomposite polymer electrolytes (NCPEs) if nanometer–sized filler is dispersed into the polymer matrix. Nanotechnology has received an upsurge of interest recently. It is a new study to manipulate the materials on the nanoscale with dimension less than 100 nm. High surface area to volume ratio of nanoparticles becomes a driving force on the development of the nanotechnology in various research fields, especially in materials science. These nanoscale fillers also provide high activity and exhibit good chemical stability (Yang *et al*., 2010). Krawiec *et al*. (1995) found out that the particle size of filler is a vital parameter to govern the conductivity of the polymer electrolytes. He and his peers reported that the conductivity of nano–sized Al_2O_3 added polymer electrolytes was higher about an order of magnitude than that of micrometer–sized Al_2O_3. The small particle size of fillers can improve the homogeneity in the sample and its electrochemical properties (Krawiec *et al*., 1995). The higher conductivity of nanoscale filler compared to micro–sized filler is also attributed to the rapid formation of the space charge region between the grains (Mei *et al*., 2008).

Filler is generally divided into two main types, which are inorganic and organic. The examples of inorganic filler include biodegradable ceramics (e.g. calcium carbonate, calcium aluminates), fly ash, mica, clay, manganese oxide (MnO_2), cerium oxide (CeO_2), TiO_2, ZrO_2, SiO_2 and alumina (Al_2O_3), whereas the graphite fibre, aromatic polyamide and cellulosic rigid rods (whiskers) are the examples for organic filler (Samir *et al*., 2005). An upsurge of attention in the development of organic and inorganic fillers had led to a new invention that is the combination of organic and inorganic phases (or known as organic–inorganic hybrid) such as poly(cyclotri–phosphazene–co–4,40–sulfonyldiphenol) (PZS) microspheres (Zhang *et al*., 2010). Inorganic filler is classified into two main classes, viz. active and passive. Active filler is the material that involves in the ionic conduction process, such as lithium–nitrogen (Li_2N), lithium aluminate ($LiAlO_2$), lithium containing ceramics like lithium–alumina ($LiAl_2O_3$), titanium nitrides (TiN_x), titanium carbides (TiC_x) and titanium carbonitrides (TiC_xN_y) (Ishkov and Sagalakov, 2005). On the contrary, the passive filler does not contribute to the charge carrier concentration in transport mechanism (Stephan and Nahm, 2006; Giffin *et al*., 2012). Several types of inorganic inactive ceramic filler used in the polymer electrolyte preparation:

a) inert metal oxide (e.g. TiO_2, ZrO_2, Al_2O_3, MnO_2)
b) treated silica (SiO_2)
c) molecular sieves and zeolites (e.g. aluminosilicate molecular sieves and ordered mesoporous silica, OMS)
d) rare earth oxide (e.g. $SrBi_4Ti_4O_{15}$, $La_{0.55}Li_{0.35}TiO_3$ fibers)
e) ferroelectric materials (e.g. barium titanate, $BaTiO_3$)
f) solid superacid (e.g. sulphates and phosphates, including SO_4^{2-}/ZrO_2, SO_4^{2-}/Fe_2O_3, and SO_4^{2-}/TiO_2)
g) nano–clay (e.g. montmorillonite, MMT)
h) carbon (e.g. carbon nanotubes, CNTs)
i) heteropolyacid (e.g. silicotungstic acid (SiWA), phosphotungstic acid (PWA), molybdophosphoric acid, phosphomolibdicacid (PMoA)) (Jung *et al*., 2009; Noto *et al*., 2012; Zapata *et al*., 2012).

Filler can act as a mechanical stiffener. These fillers not only promote the ionic conduction in the polymer electrolytes, but also widen the electrochemical stability of polymer complex with enhanced membrane stability (Lue *et al*., 2008; Polu and Kumar, 2013; Zhang *et al*., 2010). Filler also possesses many advantages in the development of polymer electrolytes:

a) enhance interfacial stability between electrode and electrolyte (Krawiec *et al*., 1995)
b) reduce glass transition temperature (T_g) of polymer membrane (Kim *et al*., 2002; Saika *et al*., 2009)
c) increase cationic diffusivity by altering the transport properties (Samir *et al*., 2005)
d) improve the physical properties of polymer matrix (Hammami *et al*. 2013)

e) decrease the crystallinity (or increase the amorphous degree) of polymer electrolytes (Kim *et al*., 2002; Saika *et al*., 2009)
f) reduce the water retention of polymer electrolytes (Jian–hua *et al*., 2008)
g) enhance the thermal stability of polymer matrix (Kim *et al*., 2002; Saika *et al*., 2009)
h) improve the morphological properties of polymer electrolytes (Saika *et al*., 2009)
i) lower interfacial resistance (Krawiec *et al.*, 1995)
j) improve the long–term electrochemical stability of polymer electrolytes and electrochemical devices (Jian–hua *et al*., 2008)

Incorporation of nano–fillers also allows the amorphous polymer to maintain its liquid–like characteristics and hence produces fast ionic mobility at the microscopic level. This behavior not only improves the cell performances such as reduced capacity fading but also increases the electrochemical stability and long–term cycle life of these electrochemical devices (Raghavan *et al*., 2008; Yang *et al*., 2012).

Several literatures have reported that using CPEs or NCPEs. PEG–magnesium acetate [$Mg(CH_3COO)_2$] containing 10 wt.% of alumina achieved the maximum ionic conductivity of 3.45×10^{-6} S cm^{-1}. The fabricated battery showed the current density of 13.91 μA/cm^2, discharge capacity of 1.721 mA h, power density of 13.14 mW/kg and energy density of 1.84 W h/kg with an open circuit voltage (OCV) of 1.85 V (Polu and Kumar, 2013). Nanoscale TiO_2 also dispersed into porous membrane which comprised two copolymers, PVdF–co–HFP and poly (ethylene oxide–co–ethylene carbonate) (P(EO–co–EC)) as reported by Jeon *et al.* (2006). According to this study, the highest ionic conductivity of 5.1×10^{-5} S cm^{-1} was achieved at 25 °C. The ionic conductivity was slightly higher than the polymer electrolyte without addition of TiO_2 nanoparticles.

The effect of an amorphous SiO_2 nano–filler on ionic conductivity and crystallinity of PEO–based electrolyte has been investigated by Ketabi and Lian. The ionic conductivity of this polymer–ionic liquid electrolyte containing 1–ethyl–3–methylimidazolium hydrogensulfate ($EMIHSO_4$) and nano–sized SiO_2 reached 2.15 mS cm^{-1} at room temperature, which is more than 2–fold increase over the electrolyte without filler (Ketabi and Lian, 2013). A new type of nano–filler was used by Johan and Ting, namely nano–sized MnO_2. This filler was dispersed into PEO–$LiCF_3SO_3$–DBP polymer system. The optimum conductivity of this NCPE was 4.2×10^{-4} S cm^{-1} at room temperature with dispersion of 12 wt.% of MnO_2 (Johan & Ting, 2011). Addition of filler is an excellent method to improve the ionic conduction; however the extent of the enhancement is still restricted.

2.3.5.4 Liquid Crystals

Liquid crystal (LC)–embedded polymer electrolytes are the new class of solid polymer electrolytes. Room temperature liquid crystals are good candidates to replace the volatile liquid in the electrolytes as they form a mesophase with few desirable properties, such as high charge carrier mobility and high conductivity (Ahn *et al.*, 2012). These polymer electrolytes have widely been used for DSSC applications because LC alignment in the polymer electrolytes increases the photovoltaic performance in DSSCs. The LC molecules increase the ordering strength in the polymeric materials. Therefore, the aligned LC can provide a superior charge carriers pathway inside the polymer electrolytes (Kim *et al.*, 2010). Vijayakumar stated that the introductions of liquid crystals (LCs) in the polymer electrolyte can initialize the iodide exchange reaction and increase the chain mobility, thereby improving the ionic conductivity and short–circuit current density (J_{sc}) (Vijayakumar *et al.*, 2009). Few reports using liquid crystal (LC)–embedded polymer electrolytes in DSSCs had been studied. Kim et al. found out that the polymer electrolyte with an aligned LC increased the power conversion efficiency (PCE) about 25 %

compared to that of without LC alignment and 80 % compared to the conventional DSSCs (Kim *et al*., 2010).

A novel polymer electrolyte system composed of LC had been developed and applied in DSSCs (Ahn *et al*., 2012). The effect of adding E7 liquid crystal on PVdF–co–HFP based polymer electrolytes and DSSCs was elucidated briefly in this literature. The ionic conductivity of this gel polymer electrolyte was found to be 2.9 mS cm^{-1} at ambient temperature which is 37% higher than that of polymer gel electrolyte without E7. The results obtained from DSSCs fabricated using this conductive LC–embedded polymer electrolyte was comparable to those liquid electrolytes. The assembled DSSCs showed open circuit voltage (V_{oc}) at 0.72 V, J_{sc} of 14.62 mA/cm^2 and fill factor of 64.8% along with PCE of 6.82 % at 1 sun intensity (Ahn *et al*., 2012). DSSCs with configuration of SnO_2:F/TiO_2/N719 dye/ liquid crystal–embedded polymer electrolyte/Pt was fabricated by Karim *et al*. (2010). The DSSC possessed PCE of 4.70 % at 1 sun which was much higher than that of the PAN–based polymer electrolyte. Similar to LCPEs, how the liquid crystals affect the ionic conduction in polymer complexes is not fully investigated. Perhaps, it can be a promising way to improve the ionic conductivity of polymer electrolytes in the future.

2.4 Reasons of Choosing the Materials

PVA–CH_3COONH_4 based polymer electrolytes were prepared in this present work. PVA was used as polymer to form the complexation, whereas CH_3COONH_4 was employed as salt to provide charge carriers in the polymer electrolytes. Three types of 1–butyl–3–methylimidazolium cations ($BmIm^+$)–based ionic liquids were further added into the polymer electrolytes to improve the ionic conductivity that are 1–butyl–3–methylimidazolium chloride (BmImCl), 1–butyl–3–methylimidazolium bromide (BmImBr) and 1–butyl–3–methylimidazolium iodide (BmImI).

2.4.1 Poly(vinyl alcohol) (PVA)

Biopolymer electrolytes using biodegradable polymer is of great interest to solve the environmental issue in recent years. Natural and synthetic biopolymers are two main groups of biodegradable polymers. Several renewable resource–based biopolymers are suitable to be used as host polymer in the polymer electrolytes, such as starch, cellulose, chitosan, carrageenan, pectin, chitin, lignocellulosic materials, hyaluronic acid, agarose, polylactides, polyhydroxyalkanoates (bacterial polyesters) and soy–based plastics (Ramesh *et al.*, 2011b). However, natural based polymers exhibit low mechanical integrity with brittle properties. Therefore, synthetic durable biopolymer, PVA was selected in this research. PVA is a synthetic biodegradable semi–crystalline polymer bearing with hydroxyl functional group as illustrated below:

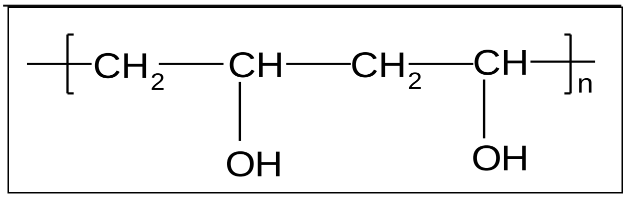

$$-\!\!\left[CH_2-\underset{OH}{\underset{|}{CH}}-CH_2-\underset{OH}{\underset{|}{CH}}\right]_n\!\!-$$

Figure 2.7: Chemical structure of PVA.

PVA is an attractive material with excellent tensile strength and high ability to form transparent film (Dasenbrock *et al.*, 1998; Liew *et al.*, 2014b). PVA has merits of being a host polymer due to its availability, good optical properties, cost effectiveness, non–toxicity, high hydrophilicity and excellent mechanical strength as well as high temperature resistance (Yang & Wu, 2009; Liew *et al.*, 2014a, Liew *et al.*, 2014b). PVA also possesses some inherent characteristics, viz. biocompatible, ease of preparation, high abrasion resistance and high flexibility with superior chemical and thermal stabilities (Qiao *et al.*, 2009; Liew *et al.*, 2014a; Liew *et al.*, 2014b; Lu *et al.*, 2009). Other reasons for choosing PVA as host polymer are greater extent of polar groups (hydroxyl group) and high chain flexibility which promotes the salt–solvation (Hirankumar *et al.*, 2004; Liew *et al.*, 2014a; Liew *et al.*, 2014b). High dielectric constant, excellent charge storage capacity and dopant–dependent electrical properties make PVA as a promising candidate in the development of electrochemical devices, especially EDLC and fuel cell applications (Hirankumar *et al*., 2005; Liew *et al*., 2014a; Liew *et al*., 2014b).

2.4.2 Ammonium Acetate

Ammonium salt is a good proton donor to polymer electrolytes (Hirankumar *et al*., 2005). Ammonium salts has widely been used in the proton conducting polymer electrolytes, for example CH_3COONH_4, NH_4ClO_4, ammonium thiocyanate (NH_4SCN), ammonium trifluoromethanesulfonate ($NH_4CF_3SO_3$), ammonium bisulfate (NH_4HSO_4), ammonium nitrate (NH_4NO_3), ammonium sulfate [$(NH_4)_2SO_4$], ammonium chloride (NH_4Cl), ammonium bromide (NH_4Br) and ammonium iodide (NH_4I) (Hema *et al*., 2009; Zhao *et al*., 2003). CH_3COONH_4 is an ammonium salt consisting of ammonium cation and acetate anion. The chemical structure of CH_3COONH_4 is depicted in the following figure.

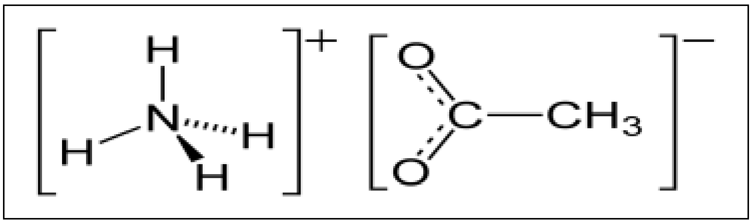

Figure 2.8: Chemical structure of CH_3COONH_4.

CH_3COONH_4 is chosen due to its strong plasticizing effect and hydrophilic properties as well as inexpensive. High solubility of CH_3COONH_4 in water is another reason as the solvent used to prepare the polymer electrolytes is distilled water. Besides, NH_4^+ is a cation with small radius of 1.4 Å (Damle *et al*., 2008). So, the small size of cations can be dissociated and transported in the polymer electrolytes easily. On the other hand, the acetate anion (CH_3COO^-) is preferred in solvation through hydrogen bonding in the polymer matrix (Liew *et al*., 2014b). Therefore, the separation of NH_4^+ is favored in the polymer electrolytes leading to rapid ion transport. Halide–based ammonium salts cannot be used in this present work to avoid the contribution of halide ions from salts into the ion conduction as the effect of the halides of ionic liquids onto the ionic conductivity is studied in this research.

2.4.3 Ionic Liquids

Three different halides–based ionic liquids are employed in this present work, namely BmImCl, BmImBr and BmImI. The chemical structure of these 1–butyl–3–methylimidazolium cations (BmIm$^+$)–based ionic liquids is exemplified as follows:

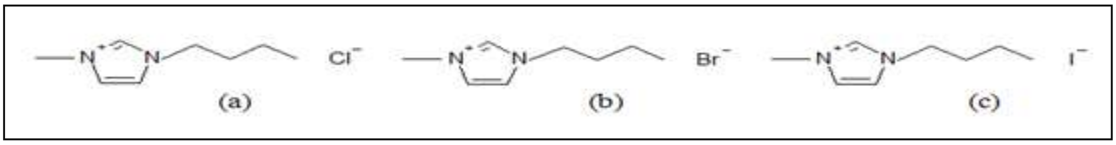

Figure 2.9: Chemical structure of ionic liquids.

The common BmIm$^+$ is an appealing cation because of its favorable properties and ease to gather abundant and useful information from literature (Kim *et al*., 2006). BmIm$^+$ can also be easily detached from the coordinative bonds with the counteranion in ionic liquids due to the bulky size which aids in ionic migration in the polymer electrolytes.

2.5 Supercapacitors

There is a wide range of applications of polymer electrolytes as mentioned in Introduction. However, we would like to focus on the supercapacitors fabrication in this project. Supercapacitor (or known as ultracapacitor or electrochemical capacitor) is energy storage–based electrochemical device as power source. The energy storage of a supercapacitor arises from the ion accumulation at the electrode–electrolyte interface of active materials through rapid and reversible adsorption and/or desorption of charges carriers (Frackowiak, 2007; Wu *et al*., 2013). Supercapacitors consist of one pair of electrodes and electrolyte. The electrode can be derived from many materials, such as carbon, metal oxide, conducting polymers and so on. On the other hand, the electrolyte can be liquid electrolyte, solid polymer electrolyte, gel polymer electrolyte or composite polymer electrolyte but must be conductive with high ionic mobility. The ion accessibility from electrolyte to the electrode becomes an important parameter to govern the capacitance of supercapacitors.

Supercapacitors are emerged as new type of electrochemical devices to replace lithium ion batteries and conventional electrolytic capacitors. Supercapacitors not only deliver higher power density than lithium ion secondary batteries but also exhibit higher energy density than conventional dielectric capacitors (Wu *et al*., 2013). Supercapacitors are subdivided into three main types, viz. pseudocapacitors, EDLCs and hybrid capacitors. EDLC is a great choice as an electrochemical device because of its long charge–discharge cycle lifetime (over 10^6 cycles), low cost, high power density (up to 10 kW kg^{-1}), high dynamic of charge propagation (short term pulse), fast energy storage, higher ability to be charged and discharged continuously without degrading, maintanance–free long life operation and short charging time (Choudhury *et al*., 2009; Endo *et al*., 2001; Frackowiak & Béguin, 2001; Pandey *et al*., 2010a; Yu *et al*., 2012).

2.5.1 Pseudocapacitors

Pseudocapacitors (also recognized as redox capacitors) are the capacitors involve fast Faradaic processes such as intercalation, under–potential deposition and redox reaction occurring at the surface of electrode at an appropriate applied potential (Choudhury *et al*. 2009). The active materials used as electrode in pseudocapacitors are electroactive conducting polymers [e.g. polypyrrole (PPy) and poly(thiophene) derivaties such as poly(3,4–ethylenedioxythiophene), PEDOT) and poly(aniline) (PANI)] and nobel metal oxide [e.g. ruthenium oxide (RuO_2), nickel (II) oxide (NiO), TiO_2, cobalt (II) dicobalt (III) oxide (Co_3O_4), tin dioxide (SnO_2), iridium (IV) oxide (IrO_2) and manganese (IV) oxide (MnO_2)] (Hashmi & Upadhyaya, 2002; Peng *et al*., 2008). Pseudocapacitors give rise to high capacitance value. But these capacitors bring some disadvantages such as shorter cycle life, poor electrochemical stability, relatively expensive due to high raw material cost and possess difficulty in processing which limits their practical applications (Shao *et al.*, 2012).

2.5.2 Electric Double Layer Capacitors (EDLCs)

On the contrary, EDLCs do not involve any electrochemical Faradic reaction over the potential range of operation. The basic principle of charge storage in these non–Faradaic capacitors is related to the formation of Helmholtz layer (or well–known as double layer) as a result of electrostatic charge accumulation between the electrode and electrolyte without any chemical reaction. In other words, the capacitive behavior of an EDLC is based on the ability to form an electrical double layer at the polarizable electrode–electrolyte interface which arises from the charge separation between the high specific area carbon–based electrodes and an organic electrolyte (Liew & Ramesh, 2014). Carbonaceous materials are the common electrode materials for an EDLC. These carbon–based materials are activated carbon powder, carbon black, carbon nanotubes (CNTs), graphite, carbon fibre and carbon aerogel (Hashmi *et al.*, 1997a). Carbon–based electrode offers several advantages, for instance well polarizable, excellent electrochemical properties due to its amphoteric behavior, environmental friendly, easy processability, easy accessibility of ions, high specific surface area, cost effective, chemically stable in different solution (from acidic to basic), long cycle life, maintenance–free, wide operating temperature with excellent performances (Fang & Binder, 2006; Frackowiak & Béguin, 2001; Wu *et al.*, 2013).

The materials used for the electrode preparation are activated carbon, CNTs and carbon black in this present work. Activated carbon (AC) is a predominant electrode material used in EDLCs because of its attractive properties. Large specific surface area (1000–2500m^2g^{-1}), high porosity and low cost are the advantages of AC (Frackowiak, 2007; Lei *et al.*, 2011). However, high microporosity (pore dimension: < 2nm) of activated carbon could limit the accessibility of charge carriers into the micropores of AC. It is because the bigger ion size serves as a hurdle for diffusion into the smaller pores (Frackowiak, 2007; Kumar *et al*., 2012). Therefore, carbon nanotubes (CNTs) which have mesoporous structure (pore size: 2–50nm) are introduced in this present work to increase ion absorption properties through its unique entanglement network onto the bigger pores of carbon with high electrolyte accessibility (An *et al*., 2002). CNTs also possess superb properties such as superior mechanical stability, excellent electrical properties, high dimensional ratios, low mass density, high charge–discharge capability and better chemical stability with well–defined hollow core shape (Peng *et al*., 2008; Portet *et al*., 2005; Wang *et al*., 2005). CNTs have been recognized as potential materials owing to their reduced mass density, low resistivity and narrow distribution of mesopores (or high mesoporosity), large specific surface area (100–1315 m^2g^{-1}), superior capability of charge transportation and as well as good absorption characteristic (Amitha *et al*., 2009; Emmenegger *et al*., 2003; Kim *et al*., 2012; Wang *et al*., 2005).

2.5.3 Hybrid Capacitors

Low specific capacitance of EDLC leads to the invention of hybrid capacitors which is the combinations of pseudocapacitor and EDLC to compromise both capacitors recently. There are many intensive approaches to hybridize the electrodes. The common way is to add the electrochemical active materials into the carbon–based electrode which produces composite hybrid capacitor (Deng *et al*., 2013). Asymmetric hybrid capacitor is another class of hybrid capacitors. This capacitor is comprised of a pseudo–capacitive metal oxide/hydroxide electrode and a capacitive carbon electrode such as activated carbon (AC)//$Ni(OH)_2$ and AC//MnO_2 (Jiang *et al*., 2013). Lithium insertion electrode with a capacitive carbon electrode like $Li_4Ti_5O_{12}$//AC is another brand new hybrid capacitor recently. However, the depletion of electrolyte in this hybrid capacitor has been identified as a major challenge (Jiang *et al.*, 2013). So, researchers come out with a brilliant idea which is the production of battery–like hybrid capacitor. The lithium cations (Li^+) will be intercalated to a cathode compound, such as $LiMn_2O_4$ as cathode, while activated carbon will be used as anode material (Jiang *et al.*, 2013).

In conclusion, we chose the method of inclusion of ionic liquids to improve the ionic conductivity of PVA–CH_3COONH_4 polymer complexes because of their environmental friendly feature and other superior characteristics. EDLCs were fabricated using the most conducting ionic liquid–added polymer electrolytes.

2.6 Summary

Methodologies of the preparation and characterization of polymer electrolytes will be discussed in the following chapter. Apart from that, the methods to prepare carbon–based electrodes and EDLCs fabrication as well as their electrochemical characterization will be discussed in following chapter.

CHAPTER 3

METHODOLOGY

This first section of this chapter reveals the materials used in this research. The second section explains the methodologies of sample preparation and characterization. The electrode preparation is further discussed in the following section. The last section talks about the EDLC fabrication and characterization.

3.1 Materials

Polymer–salt complexes containing PVA and CH_3COONH_4 were prepared in this work. Ionic liquids, BmImCl, BmImBr or BmImI were thus added to produce ionic liquid–added polymer electrolytes. PVA (Sigma–aldrich, USA, 99% hydrolyzed with molecular weight of 130000 g mol^{-1}) and CH_3COONH_4 (Sigma, Japan) were used as polymer and salt, respectively. BmImCl was obtained from Acros organic, USA, while BmImBr and BmImI were obtained from Merck, Germany were used as ionic liquids. All the materials were used as received.

3.2 Preparation of Ionic Liquid Added Poly(vinyl alcohol)–based Polymer Electrolytes

Ionic liquid added PVA–based polymer electrolytes were prepared by solution casting technique. PVA was initially dissolved in distilled water. An appropriate amount of CH_3COONH_4 was subsequently mixed in PVA solution. The weight ratio of PVA:CH_3COONH_4 was kept at 70:30. Different mass fraction of BmImCl, BmImBr or BmImI was then doped into the PVA–CH_3COONH_4 aqueous solution to prepare ionic liquid added polymer electrolytes. The resulting solution was stirred thoroughly and heated at 70 °C for a few hours. The solution was eventually cast in a glass Petri dish and dried in an oven at 60 °C to obtain a free–standing polymer electrolyte film. Tables 3.1, 3.2 and 3.3 show the weight proportion of PVA, CH_3COONH_4, BmImCl, BmImBr and BmImI added into the respective polymer electrolytes and the designations of the polymer complexes.

Table 3.1: The weight ratio of PVA, CH_3COONH_4 and BmImCl with their designations.

Designations of polymer electrolytes	Weight percent of materials (wt.%)		
	PVA	CH_3COONH_4	BmImCl
VH 0	70	30	–
CL 2	56	24	20
CL 5	35	15	50
CL 6	28	12	60
CL 7	21	9	70

Table 3.2: The weight ratio of PVA, CH_3COONH_4 and BmImBr with their designations.

Designations of polymer electrolytes	Weight percent of materials (wt.%)		
	PVA	CH_3COONH_4	BmImBr
VH 0	70	30	–
BR 2	56	24	20
BR 4	42	18	40
BR 6	28	12	60
BR 7	21	9	70

Table 3.3: The weight ratio of PVA, CH_3COONH_4 and BmImI with their designations.

Designations of polymer electrolytes	Weight percent of materials (wt.%)		
	PVA	CH_3COONH_4	BmImI
VH 0	70	30	–
I 3	49	21	30
I 4	42	18	40
I 7	21	9	70

The polymer electrolytes with addition of BmImCl, BmImBr and BmImI were designated as CL system, BR system and I system, respectively.

3.3 Characterization of Poly(vinyl alcohol)–based Polymer Electrolytes

Several characterizations had been done to study the thermal, electrical, structural and electrochemical properties of prepared polymer electrolytes. The thermal properties were analyzed using TGA and DSC studies; meanwhile the electrical characteristics were studied using EIS. ATR–FTIR and XRD were used to examine the structural properties of polymer electrolytes, whereas LSV was employed to scrutinize the electrochemical properties of polymer electrolytes.

3.3.1 Differential Scanning Calorimetry (DSC)

DSC is a quantitative study of thermal transitions of polymer matrix by heating polymer electrolytes and an inert reference under an inert gas atmosphere. DSC analysis was performed using the TA Instrument Universal Analyzer 200 which consists of a DSC Standard Cell FC as main unit and Universal V4.7A software. The whole analysis was analyzed in a nitrogen atmosphere at a flow rate of 60 mL min^{-1}. Samples weighing 3–5 mg were hermetically sealed in an aluminum Tzero pan. A tiny hole was punched on top of the pan to eliminate the water and moisture which are released in the heating process. In contrast, an empty aluminum pan was hermetically sealed as reference cell. The samples were heated from 25 °C to 105 °C at a heating rate of 10 °C min^{-1} to remove any trace amount of water and moisture as a preliminary step. The heating process was maintained at 105 °C for 5 minutes to ensure complete evaporation. After that, an equilibrium stage was achieved at 25 °C. The samples were thus heated from 25 °C to 200 °C and followed up with a rapid cooling process to –70 °C at the pre–set heating rate. The samples were eventually reheated to 230 °C at the same heating rate. Glass transition temperature (T_g) was evaluated using the final heating scan with the provided software.

3.3.2 Electrochemical Impedance Spectroscopy (EIS)

3.3.2.1 Ambient Temperature–Ionic Conductivity Study

EIS is a powerful analytical tool to characterize the electrical properties of polymer electrolytes and their interfaces. Freshly prepared samples were subjected to ac–impedance spectroscopy for ionic conductivity determination. A digital micrometer screw gauge was used to measure the thickness of the samples. The impedance of the polymer electrolytes was measured using the HIOKI 3532–50 LCR HiTESTER impedance analyzer over the frequency range between 50 Hz and 5 MHz at ambient temperature. The measurement was taken by sandwiching the polymer electrolyte between two stainless steel (SS) blocking electrodes at a signal level of 10 mV. The ionic conductivity of polymer electrolytes was measured using the equation below.

$$\sigma = \frac{l}{R_b A} \qquad \text{(Equation 3.1)}$$

where σ is the ionic conductivity of polymer electrolytes (S cm^{-1}), l is the thickness of polymer electrolytes, R_b is bulk resistance of polymer electrolytes which is determined from Nyquist plot obtained from EIS and A is the surface area of the electrodes.

3.3.2.2 Temperature Dependent–Ionic Conductivity Study

Similar to the procedure above, the freshly prepared samples were subjected to ac–impedance spectroscopy for ionic conductivity measurements. The measurement was taken from ambient temperature to 120 °C.

3.3.3 Thermogravimetric Analysis (TGA)

TGA was used to evaluate the thermal stability and thermal degradation of polymer electrolytes as a function of change in temperature under an inert gas atmosphere. TGA was carried out using a thermogravimetric analyzer, TA Instrument Universal Analyzer 2000 with Universal V4.7A software. Samples weighing 2–3 mg were placed into a 150 μL silica crucible. The samples were then heated from 25 °C to 600 °C at a heating rate of 50 °C min^{-1} in a nitrogen atmosphere with a flow rate of 60 mL min^{-1}.

3.3.4 Attenuated Total Reflectance–Fourier Transform Infrared (ATR–FTIR)

The main fundamental of ATR–FTIR in the polymer electrolytes is to determine structural information about macromolecules which is related to the vibrational modes of the molecules polymer. Themoscientific Nicolet iS10 FTIR Spectrometer (from USA) was employed to perform ATR–FTIR study which is equipped with an ATR internal reflection system. The FTIR spectra were recorded with a resolution of 1 cm^{-1} in transmittance mode over the wavenumber range from 4000 cm^{-1} and 650 cm^{-1} at room temperature. The FTIR spectra and peak deconvolution were scrutinized using OMNIC 8 software which is provided by Thermo Fischer Scientific Inc. The transmittance mode of FTIR spectra was initially converted into absorbance mode for peak deconvolution process. In order to deconvolute the FTIR spectra, baseline correction and curve fitting must be implemented. The FTIR curve was fitted with Gaussian–Lorentzian mixed mode.

3.3.5 X–ray Diffraction (XRD)

XRD was mainly used to determine the structural properties of polymer electrolytes especially the crystalline and amorphous region in the polymer. The x–ray patterns were recorded using BTX benchtop x–ray diffractor with Cu–K_{α} radiation (λ=1.54060 Å), over the range of 2θ=5–50° at ambient temperature. The characteristic peaks were analyzed and deconvoluted using origin software. The XRD patterns were fitted with Gaussian fitting mode. The degree of crystallinity (χ_c) of pure PVA and polymer electrolytes was determined using the following equation:

$$\chi_C = \frac{I_C}{I_T} \times 100\% \qquad \text{(Equation 3.2)}$$

where I_c and I_t are area under the crystalline peak and area under all the peaks, respectively.

3.3.6 Linear Sweep Voltammetry (LSV)

LSV was probed to study the electrochemical potential window of the polymer electrolytes which is important for cell fabrication. A CHI600D electrochemical analyzer was used to evaluate LSV responses of ionic liquid–free polymer electrolyte and the most conducting ionic liquid added polymer electrolyte from each system. These cells were analyzed at a scan rate of 10 mVs^{-1} by placing the polymer electrolyte between SS electrodes in the potential range of ±3V.

3.4 Electrode Preparation

Activated carbon–based EDLC electrodes were prepared by dip coating technique. The preparation of carbon slurry was prepared by mixing 80 wt.% activated carbon (Kuraray Chemical Co Ltd., Japan) of particle size between 5 and 20 µm, surface area between 1800 and 2000 $m^2 g^{-1}$, 5 wt.% carbon black (Super P), 5 wt.% multi–walled carbon nanotubes (CNTs) (Aldrich, USA) with outer diameter, O.D. between 7 and 15 nm and length, L ranging from 0.5 to 10 µm and 10 wt.% poly(vinylidene fluoride) (PVdF) binder (molecular weight of 534000 g mol^{-1} from Aldrich) and dissolving them in 1–methyl–2–pyrrolidone (Purity ≥ 99.5% from Merck, Germany). Activated carbon was initially treated with sodium hydroxide (NaOH) and sulfuric acid (H_2SO_4) to increase the porosity of carbon. This slurry was stirred thoroughly for several hours at ambient temperature. The carbon slurry was then dip coated on an aluminum mesh current collector. The coated electrodes were dried in an oven at 110 °C for drying purposes.

3.5 EDLC Fabrication

EDLC cell was constructed in the configuration of electrode/polymer electrolyte/electrode. The EDLC cell configuration was eventually placed in a cell kit for further electrochemical analyses. The cells using the ionic liquid–free polymer electrolyte is designated as type I supercapacitor, whereas the EDLC cell containing the most conducting ionic liquid–based polymer electrolyte from each system is assigned as type II supercapacitor.

3.6 EDLC Characterization

The fabricated EDLC cell was subsequently subjected to cyclic voltammetry (CV), low frequency EIS and galvanostatic charge–discharge (GCD) for further characterization.

3.6.1 Cyclic Voltammetry (CV)

The CV study of EDLC was investigated using CHI600D electrochemical analyzer. The cell was rested for 2 seconds prior to the measurement. The EDLC cell was then evaluated at 10 mVs^{-1} scan rate in the potential range between 0 and 1 V in intervals of 0.001 V. The specific capacitance (C_{sp}) of EDLC was computed using the equation as follows (Amitha *et al*., 2009; Arof *et al*., 2012; Liew *et al*., 2014b):

$$C_{sp} = \frac{i}{sm} \text{ (F g}^{-1}\text{)} \qquad \text{(Equation 3.3)}$$

$$C_{sp} = \frac{i}{sA} \text{ (F cm}^{-2}\text{)} \qquad \text{(Equation 3.4)}$$

where i is the average anodic–cathodic current (A), s is the potential scan rate (V s^{-1}), m refers to the average mass of active materials (including the binder and carbon black) and A represents surface area of the electrodes, that is 1 cm^{-2}. The average mass of electrode materials is around 0.01–0.02 g.

3.6.2 Electrochemical Impedance Spectroscopy (EIS)

The impedance of the EDLC was probed by a HIOKI 3522–50 LCR HiTESTER impedance analyzer at room temperature with a bias voltage of 10 mV. The EIS measurements were done in the frequency range from 10 mHz to 100 kHz. The capacitances, C were determined from the impedance data at a frequency of 10 mHz using the following equation (Mitra *et al*., 2001; Liew *et al*., 2014b):

$$C = -\frac{1}{\omega Z''} = -\frac{1}{2\pi f \times Z''} \qquad \text{(Equation 3.5)}$$

where ω is angular frequency, which is represented by $2\pi f$ and Z'' is the imaginary part of the complex impedance (Z). The specific capacitance of EDLC was calculated by dividing the capacitance with average weight of active materials. The average weight of electrode materials is 0.01–0.02 g. The EIS data was fitted using ZSimpWin software to find out the suitable equivalent circuit of EDLCs. Stimulation has been done to determine the value of each element in the fitted equivalent circuit using ZSimpWin software.

3.6.3 Galvanostatic Charge–Discharge Performances (GCD)

The charge–discharge study was carried out using a Neware battery cycler. EDLC was charged and discharged at current of 1 mA. EDLC was allowed to rest for 10 minutes before taking the measurements. The specific discharge capacitance (C_{sp}) was obtained from charge–discharge curves, according to the following relation (Amitha *et al*., 2009; Liew *et al*., 2014b):

$$C_{sp} = \frac{I}{m\left({dV}/{dt}\right)} \qquad \text{(Equation 3.6)}$$

where I is the applied current (A), m is the average mass of electrode materials (including the binder and carbon black), dV represents the potential change of a discharging process excluding the internal resistance drop occurring at the beginning of the cell discharge and dt is the time interval of discharging process. The dV/dt is determined from the slope of the discharge curve. The mass of the electrode used in this study is 0.01–0.02 g.

Energy density, E (W h kg^{-1}), power density, P (kW kg^{-1}) and Coulombic efficiency, η (%) were assessed using the equations below (Yu *et al*., 2012; Liew *et al*., 2014b):

$$E = \frac{C_{sp} \times (dV)^2}{2} \times \frac{1000}{3600} \qquad \text{(Equation 3.7)}$$

$$P = \frac{I \times dV}{2 \times m} \times 1000 \qquad \text{(Equation 3.8)}$$

$$\eta = \frac{t_d}{t_c} \times 100\% \qquad \text{(Equation 3.9)}$$

where t_d and t_c are the discharging and charging times, respectively.

3.7 Summary

Results obtained for the polymer electrolyte systems will be presented and discussed in the following chapters.

CHAPTER 4

RESULTS AND DISCUSSION OF CHLORIDE (CL) SYSTEM

This chapter reviews the effect of BmImCl onto the polymer electrolytes and EDLCs. The first section reports the ionic conductivity of ionic liquid–free polymer system. The second section discusses the results obtained from all characterization of polymer electrolytes. The electrochemical performances of fabricated EDLCs are enlightened in the last section.

4.1 Ambient Temperature–Ionic Conductivity Study of Ionic Liquid–free Polymer Electrolytes

The ionic conductivity of ionic liquid–free polymer electrolytes with respect to different concentration of CH_3COONH_4 is initially measured as a preliminary step to determine the mass ratio of PVA to CH_3COONH_4 to be used for ionic liquid–added polymer electrolytes in next step. Figure 4.1 shows the ionic conductivity of polymer electrolytes without addition of ionic liquids as a function of different mass fraction of CH_3COONH_4.

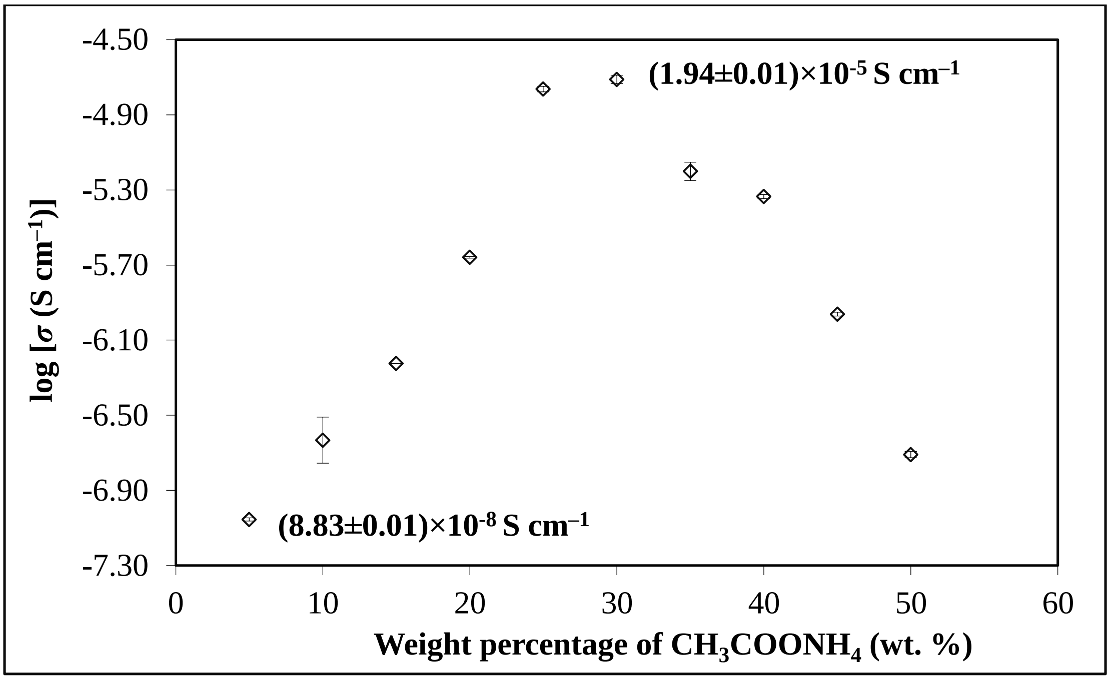

Figure 4.1: The ionic conductivity of ionic liquid–free polymer electrolytes versus the concentration of CH_3COONH_4.

The ionic conductivity of polymer electrolytes increases with the mass loadings of CH_3COONH_4 up to a maximum level. The ionic conductivity of polymer electrolytes is increased by three orders of magnitude from $(8.83\pm0.01)\times10^{-8}$ S cm^{-1} with addition of 5 wt.% of CH_3COONH_4 to $(1.94\pm0.01)\times10^{-5}$ S cm^{-1} upon addition of 30 wt.% of CH_3COONH_4. The ratio of PVA to CH_3COONH_4 is fixed as 70:30 for ionic liquid–added polymer electrolytes in all the systems.

The intense increase in ionic conductivity is probably due to the high salt concentration. Salt is basically a charge carrier’s provider. The NH_4^+ cations are dissociated from transient bonding with CH_3COO^- anions when the salt is dissolved in the polymeric solution. The mobile charge carriers are then migrated in the polymer electrolytes which lead to ionic conduction process. Therefore, the higher the concentration of the salt, the greater the number of mobile charge carriers. High salt concentration produces more mobile charge carriers and creates more ion transport in the polymer electrolytes which is correlated to high ionic conductivity. The plasticizing effect of doping salt is also an attributor. The plasticizing effect of salt softens the polymer backbone and favors the polymer segmental motion, thereby increasing the ionic migration in the polymer electrolytes. Above the optimum level, the ionic conductivity of polymer electrolytes is decreased. This is strongly related to the formation of ion aggregates as a result of excessive salt concentration. These ion aggregates block the ion conducting pathway and thus impede the ion migration in the polymer electrolytes. This results the decrease in ionic conductivity of polymer electrolytes.

4.2 Differential Scanning Calorimetry (DSC)

DSC is a vital analysis to determine the glass transition temperature (T_g) of the sample. This study signifies the phase transition of a polymer matrix in the amorphous region, from a hard glassy phase into a flexible and soft rubbery characteristic. DSC thermograms of pure PVA, VH 0, and ionic liquid–based polymer electrolytes are shown in Figure 4.2.

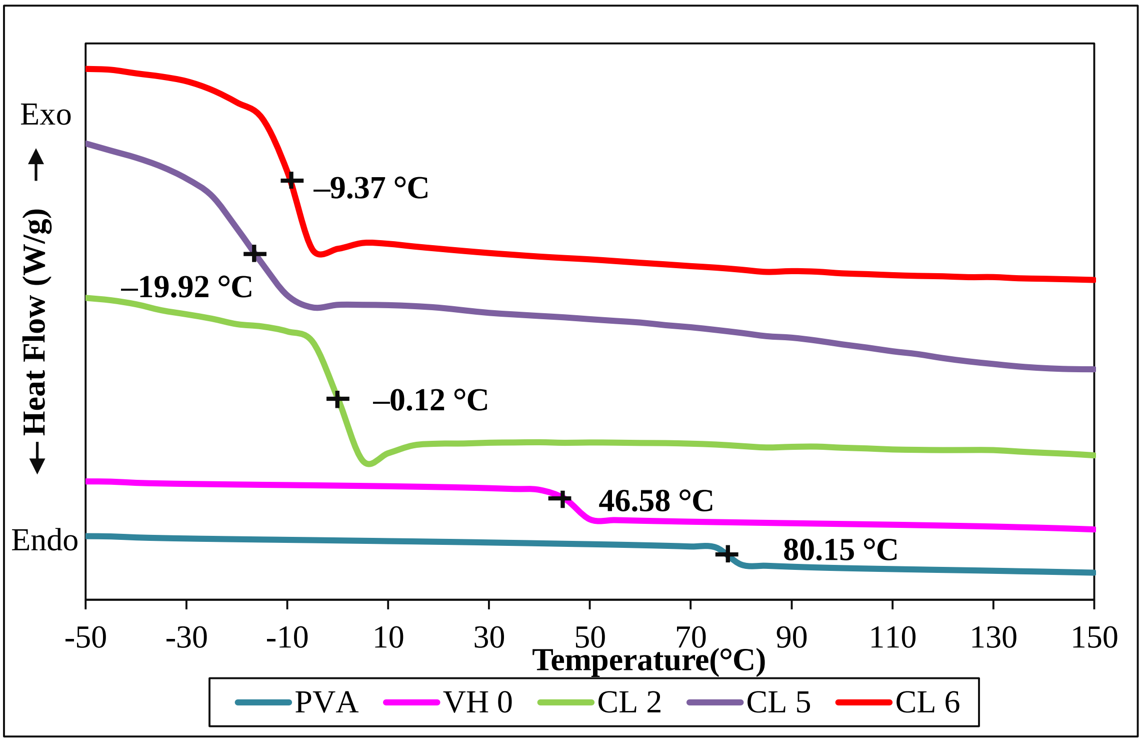

Figure 4.2: DSC thermograms of pure PVA, VH 0 and ionic liquid–added polymer electrolytes in CL system from –50 °C to 150 °C.

Ammonium acetate is a plasticizing salt as aforementioned in section 2.4.2. This can be proven in DSC curve profiles. Pristine PVA shows T_g of 80 °C. However, it is substantially reduced to around 47 °C when 30 wt% CH_3COONH_4 is complexed with 70 wt% of PVA. T_g of polymer membrane should be increased upon addition of dopant due to the partial coordination bonding in the complexation. Nevertheless, an oppose result is obtained. The significant decrease of T_g denotes that the plasticizing effect of the doping salt dominates the temporary interactive coordination. This plasticizing effect softens the polymer backbone and induces formation of flexible polymer backbone, resulting in higher polymer segmental mobility.

Sub–ambient temperature of T_g is attained by adding ionic liquid. These sub–ambient temperatures divulge the rubbery state of polymer electrolytes as the surrounding temperature is much higher than T_g. The molecules in the polymer matrix are allowed to undergo orientation and conformational changes in the rubbery phase. So, it can be concluded that the chain flexibility of polymer electrolytes containing ionic liquid is higher than the ionic liquid–free polymer complexes which induces higher segmental mobility of polymer chains. The abrupt decrease in T_g is assigned to the plasticizing effect of ionic liquid. Again, the plasticizing effect stimulates the flexibility of polymer backbone by softening the polymer matrix. As expected, the ammonium salt would form a complexation with the polymer chains. So, the charge carriers which are responsible for the ionic transportation tend to be dissociated from the native complexation owing to the flexible polymer chains. This favors the ionic transportation coupling with higher flexible polymer backbone.

In addition, T_g reduces with further inclusion of ionic liquid. The T_g exhibits downward shift from –0.12 °C to –19.92 °C corresponding to addition of 20 wt.% and 50 wt.% of BmImCl as portrayed in Figure 4.1. The plasticizing effect becomes more apparent with increasing mass fraction of ionic liquid. Therefore, the flexibility of polymer chain in CL 5 is higher than in CL 2. The ionic hopping mechanism is more favorable in CL 5 which leads to higher ionic conductivity. Nevertheless, different phenomenon is observed for CL 6. The T_g is enhanced to –9.37 °C by incorporating an additional 10 wt.% of BmImCl. The increase in T_g (instead of decrease) might be due to the formation of ion pairs and ion aggregates. Ion pairing and ion aggregation could obstruct the orientation of the molecules and hence constrain the flexibility of polymer chains. Therefore, the decoupling and migration of cations are hindered by the ion pairs and ion agglomerates.

4.3 Ambient Temperature–Ionic Conductivity Study

Figure 4.3 depicts the ionic conductivity of PVA–based polymer electrolytes at different mass fraction of BmImCl.

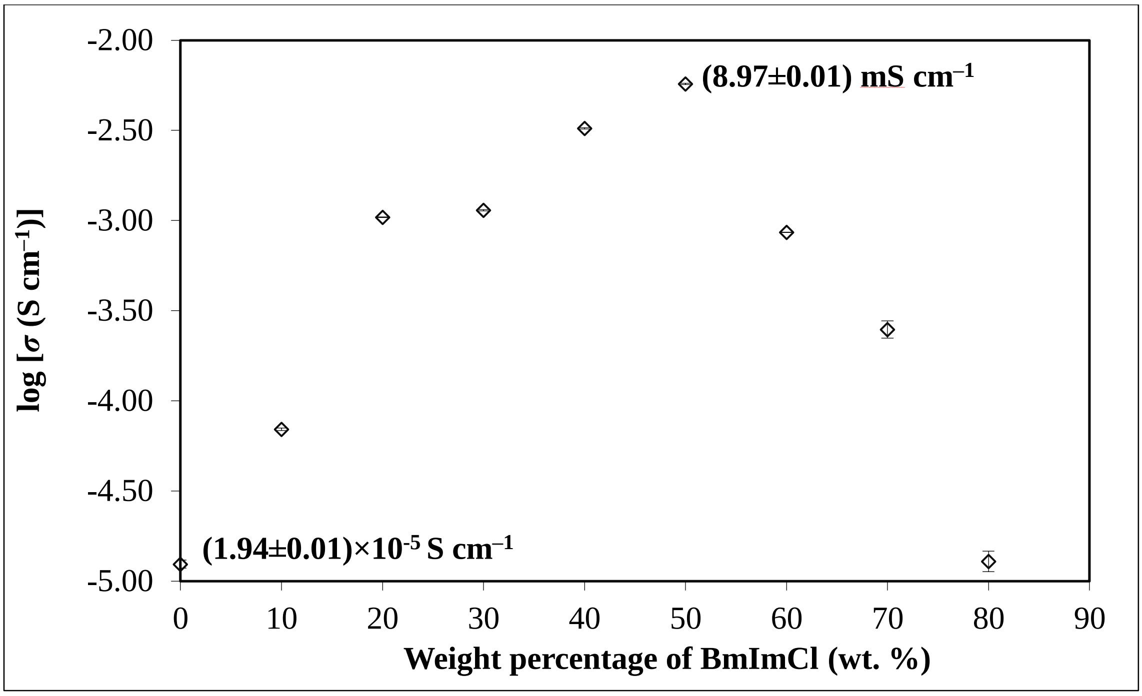

Figure 4.3: The ionic conductivity of proton conducting polymer electrolytes at different mass ratio of BmImCl.

Upon inclusion of ionic liquid, the ionic conductivity is increased. As expected, the ionic conductivity increases with mass loadings of ionic liquid, up to an optimum level. The ionic conductivity increases gradually when 10 wt.% of BmImCl is added into the polymer electrolyte. However, the ionic conductivity is found to be increased rapidly with doping of 20 wt.% of BmImCl. The highest ionic conductivity of (8.97±0.01) mS cm^{-1} corresponding to addition of 50 wt.% of BmImCl is observed. The amount and mobility of mobile charge carriers has reached the optimum level in this conductive polymer electrolyte. The ionic conductivity has been increased by two orders of magnitude in comparison to the polymer electrolyte without impregnation of ionic liquid. The abrupt increase in ionic conductivity is due to strong plasticizing effect of ionic liquid (Sekhon *et al.*, 2006; Ramesh *et al.*, 2011a; Ramesh *et al.*, 2011b). Strong plasticizing effect of ionic liquid aids to soften the polymer backbone and hence increases the flexibility of polymer chain. The proton can be transported easily within the polymer matrix with highly flexible polymer chains. Besides, higher flexibility of polymer chains improves the mobility of polymer segments and assists the ionic transport in the polymer complexes. Consequently, the ionic conductivity of ionic liquid–added polymer electrolyte is higher compared to the ionic liquid–free polymer electrolyte. Apart from that, ionic liquid can decrease the T_g of polymer electrolytes as proven in DSC findings in previous section. Moreover, ionic liquid increases the degree of amorphous of the polymer matrix. Ionic liquid could weaken the transient coordinative bonds among the molecules in the crystalline region and thus turn the polymer chains into flexible characteristic leading to higher amorphous degree of polymer complexes.

In addition, the mobility of charge carriers in amorphous region is faster than in crystalline region. High amorphous region of the polymer electrolyte can form rapid ion conduction process and result high ionic conductivity for ionic liquid–added polymer electrolyte due to the unordered arrangement of macromolecules in the amorphous region. The ionic liquids help in deteriorating the coordinative bonding between proton and the weakly bonded polar group in hydroxyl group of the polymer chains. Consequently, the protons are free to migrate from one site to another site. According to Kumar et al., the incorporation of ionic liquid can alter the electrical properties in different ways, for example bigger size of anion will dissociate the cations easily (Kumar *et al.*, 2011). In this present work, the bulky group of $BmIm^+$ also helps in improving the ionic conductivity by producing free volume for polymer segmental motion (Kumar *et al.*, 2011). Moreover, the physicochemistry of ionic liquid such as viscosity and dielectric constant also contributes to the increase in ionic conductivity. Lower viscosity of ionic liquid also enhances the polymer chain flexibility. Therefore, this flexible polymer backbone could interrupt the ion–polymer bonding and promote the ionic conducting process (Kumar *et al.*, 2011). In contrast, high dielectric permittivity of ionic liquid plays an important role to separate the ion pairs and/or ion aggregates with high self–dissociating properties. More mobile cations are consequently produced which leads to higher ionic conductivity (Kumar *et al.*, 2011).

In order to understand the principle in the proton–conducting polymer electrolytes, the proton hopping mechanism must be well studied. We propose a mechanism pertaining to transport of conducting ions for proton–conducting polymer electrolytes illustrated as follows. The ionic liquid: imidazolium cation ($BmIm^+$) and chloride (Cl^-) can be easily detached from the transient partial bonding due to the bulky size of the cation. Thus, the hydrogen at C2–position of the mobile $BmIm^+$ is initially de–protonated to form a stabilized carbene (Zhang *et al.*, 2011b; Canal *et al.*, 2006).

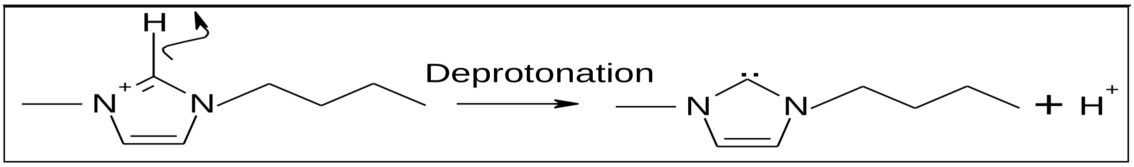

Figure 4.4: Deprotonation process of $BmIm^+$.

This carbene could then interact with the hydrogen in hydroxyl group of PVA and result carbocation in the imidazolium ring.

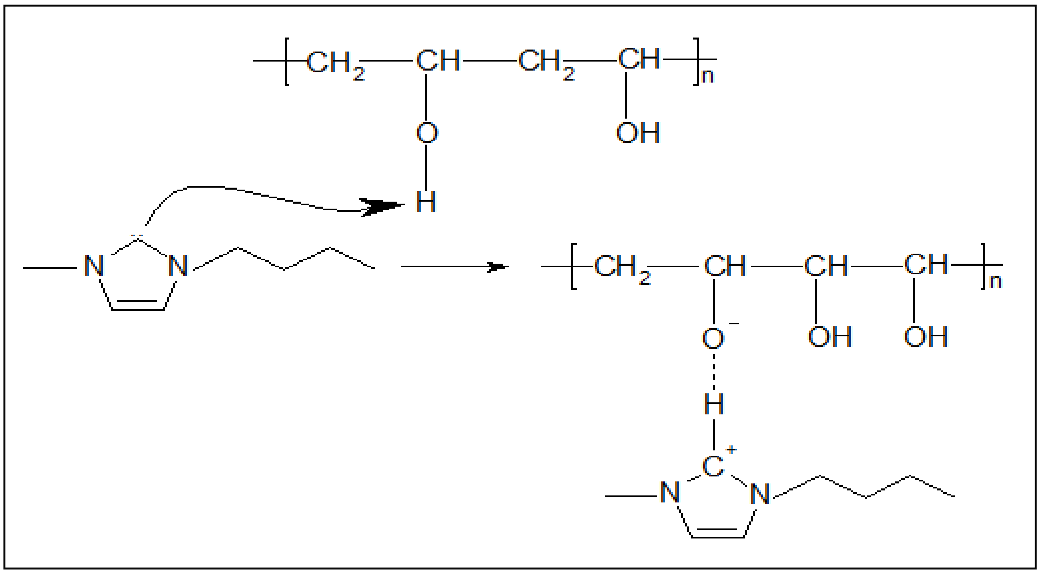

Figure 4.5: Formation of carbocation in the imidazolium ring $BmIm^+$.

This interaction leads to the partial hydrogen bonding between oxygen and hydrogen. In addition, the de–protonated hydrogen in this step can help in accelerating the proton conduction as it is in mobile state. When the hydrogen bonding is partially bonded, the dissociated chloride and acetate anions from ionic liquid and salt will prefer to interact with the carbocation and thus break the hydrogen bond between the imidazolium cations and side chain of PVA. After the disintegration of hydrogen bonding, the oxygen atom in the hydroxyl group of PVA turns into negatively charged or forms anions. Therefore, these electron deficient oxygen anions would accept the electron from proton from the loosely bounded ammonium cations or from imidazolium cations. Two possible side products could be formed in this segment, viz. 3–butyl–2–chloro–1–methyl–4,5–dihydro–1H–imidazole and 3–butyl–1–methyl–4,5–dihydro–1H–imidazole–2–carboxylic acid methyl ester, as shown in the mechanism below.

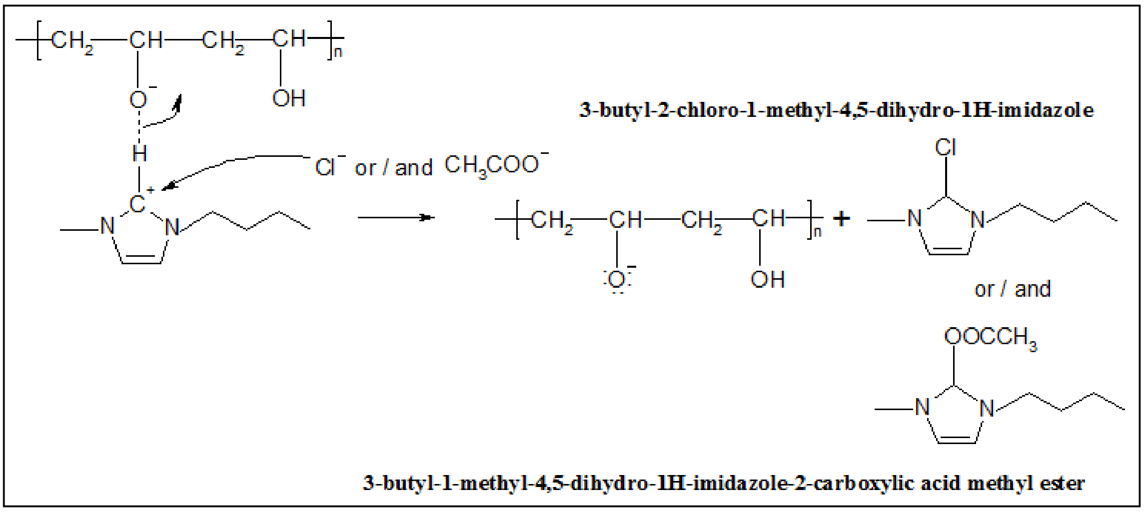

Figure 4.6: Formation of side products in the mechanism.

Beyond this step, there are two possibilities of proton conduction process. The proton transportation can be generated from the hydrogen in ammonium cations or the hydrogen in BmIm cations. The dissociated proton from loosely bonded ammonium cations of doping salt would then interact with this negatively charged oxygen and result the formation of hydroxyl group through hydrogen bonding. On the other hand, the detached chloride or/and acetate anions will abstract an electron from hydrogen. This hydrogen will thus leave the hydroxyl group and hence turn into anions. The adjacent hydrogen could interact with this oxygen and hence generate the proton transportation from site to another adjacent site.

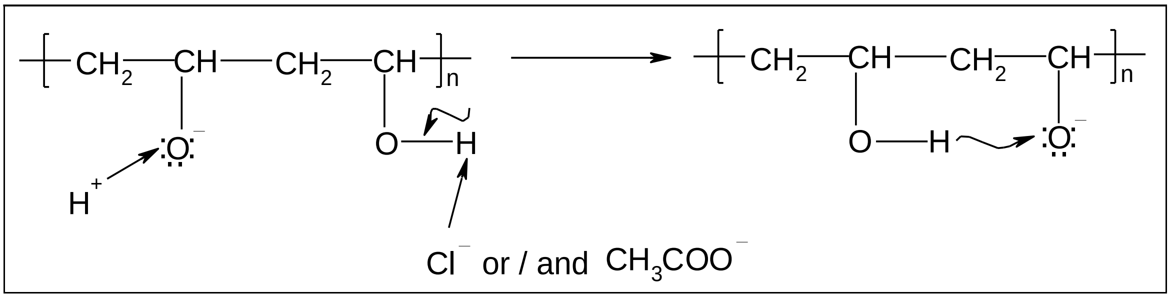

Figure 4.7: One of the possible proton conduction mechanisms.

Apart from that, we suggest that proton conduction can also take place at the BmIm cations. For this proton transport, BmIm cations could interact with the oxygen in PVA and form N–O bond temporarily. Similarly, the detached chloride or/and acetate anions will abstract an electron from hydrogen of another branched site and produce oxygen which appeared as anions. As next step, the electron from the hydrogen from C2–position in BmIm cations could be donated to this electron–deficient oxygen. In order to form a stable compound, the N–O bond must be broken down. Hence, this bond detachment could lead to the formation of carbene, which is an important chemical compound in weakening the transient coordination bond within the macromolecules. Eventually, the proton conduction mechanism is repeated with the formation of carbene. These two possible mechanisms will cause continuous ionic hopping mechanism in the polymer matrix.

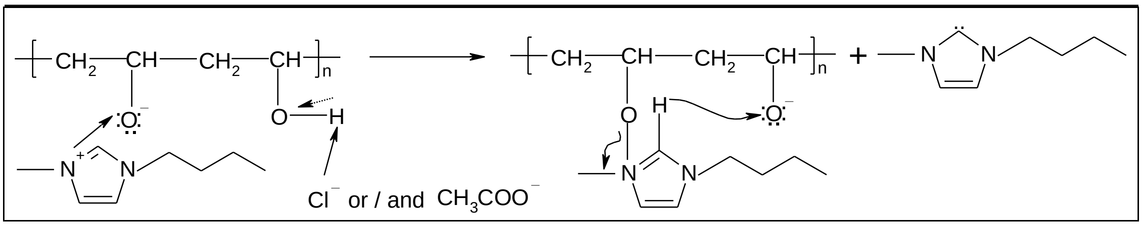

Figure 4.8: Another possible proton conduction mechanism.

Beyond adulteration of 50 wt.% of BmImCl, the ionic conductivity is found to be lower in value. This is ascribed to the agglomeration of ions. Excessive ions in the polymer electrolyte could form ion pairs and ion aggregates. These ion pairs and ion aggregates might block the conducting pathway and hinder the proton from transportation, leading to lower ionic conductivity. The amount of proton for conduction is also decreased in the presence of ion pairs and ion aggregates. At high concentration of ionic liquid, NH_4^+ cations could rather form ion pairs with other anions than provide proton for transportation due to excessive amount of anions. Similar observation goes to $BmIm^+$ cations. The cations could form ion neutral pairs with anions and thus turn the cations into immobile state at high mass loadings. These neutral ion pairs and ion aggregates could impede the conducting pathway and reduce the flexibility of polymer chains. The ionic conductivity of polymer electrolyte cannot be detected at 90 wt.% of BmImCl, because polymer electrolyte becomes mechanically unstable above adulteration of 80 wt.% of BmImCl.

4.4 Temperature Dependent–Ionic Conductivity Study

The temperature dependence plots are initially fitted with thermal activated–Arrhenius relationship to scrutinize the ion dynamic mechanism pertaining to ions. Figures 4.9 and 4.10 portray the ionic conductivity of ionic liquid–doped polymer electrolytes and ionic liquid free–polymer electrolyte in the temperature regime between ambient temperature and 120 °C, which are fitted with Arrhenius equation.

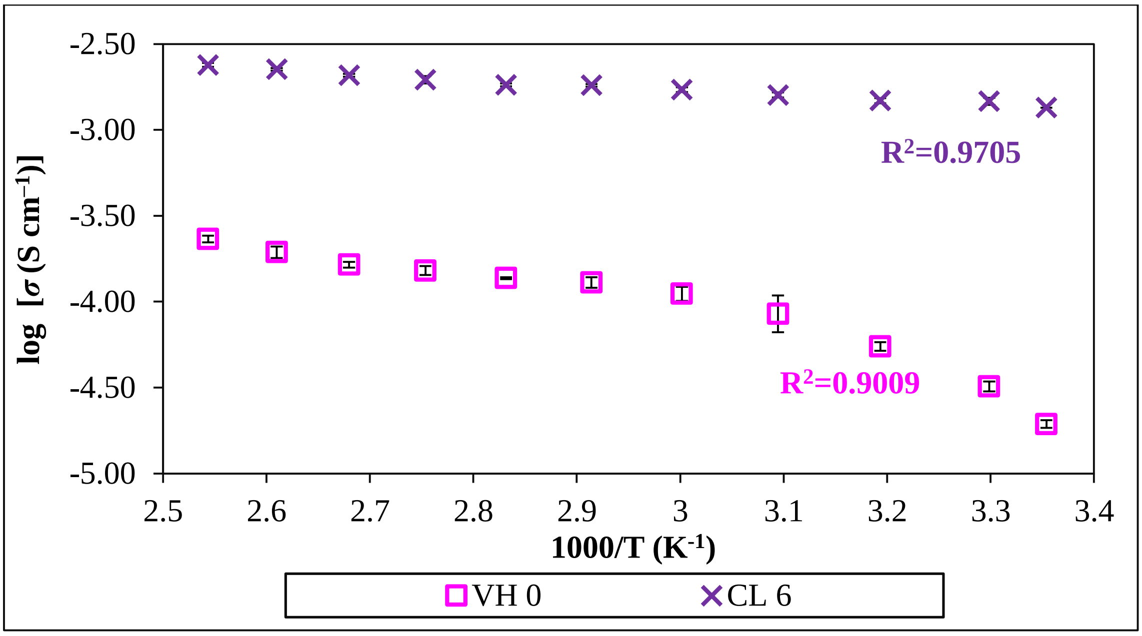

Figure 4.9: The Arrhenius plots of the ionic conductivity of VH 0 and CL 6 over a wide temperature range.

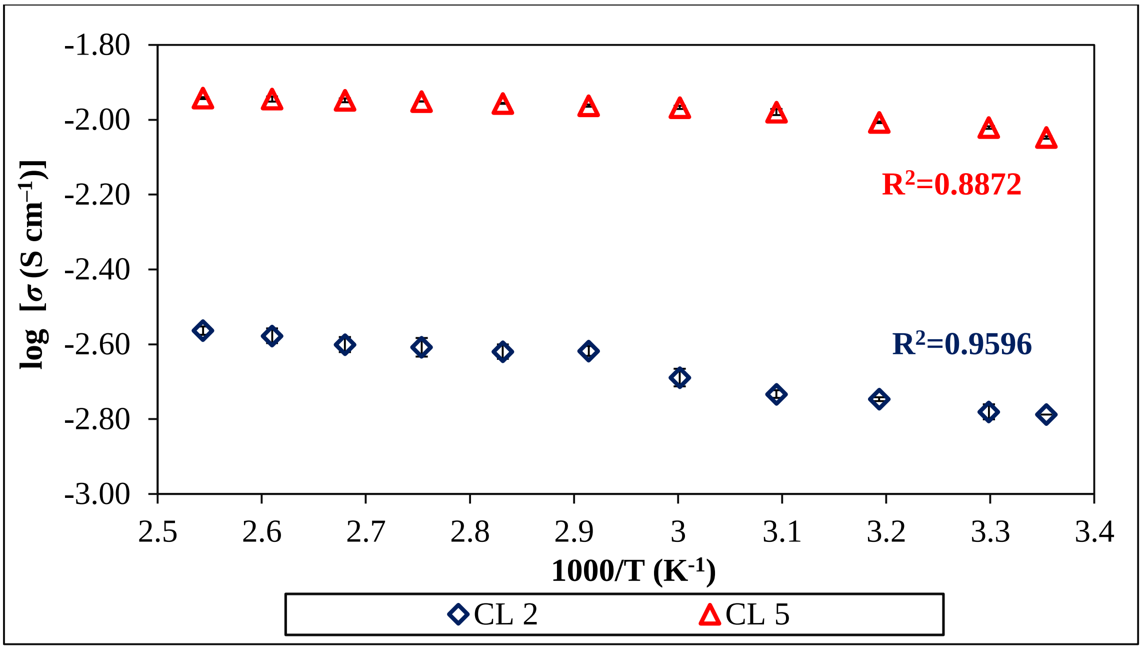

Figure 4.10: The Arrhenius plots of the ionic conductivity of CL 2 and CL 5 over a wide temperature range.

The Arrhenius formula based on thermally activated principle is expressed as follows:

$$\sigma = A\exp\left(\frac{-E_a}{kT}\right) \qquad \text{(Equation 4.1)}$$

where σ is the ionic conductivity (S cm^{-1}), A represent a constant which is proportional to amount of charge carriers (S cm^{-1}), E_a is defined as activation energy (eV), k is Boltzmann constant (8.6173×10^{-5} eV K^{-1}) and T stands for the absolute temperature (K). The highest ionic conductivity of $(1.14\pm0.01)\times10^{-2}$ S cm^{-1} has been achieved by adding 50 wt% of BmImCl at 120 °C. A moderate increase in ionic conductivity with a gradual increase in temperature is observed in both figures. This is principally due to the fast vibration modes of the molecules in the polymer membrane upon heating. Rapid vibration mode of the macromolecules promotes the bond rotation within the polymer matrix. The cations coupling with higher polymer segmental mobility can be detached from the coordination bond with the oxygen in PVA easily at elevated temperature. Therefore, ionic transportation is enhanced with increasing temperature. In addition, the amplitude of the molecular vibration increases with temperature. Therefore, the thermal vibration improves the decoupling rate of cation from transient coordination bonding with anion.

More cations can be transported within the polymer electrolytes with higher decoupling rate. Since the number of mobile cations which is responsible for ionic transportation is higher, thus more ionic conduction in the polymer electrolytes would be generated. So, as expected, higher ionic conductivity is attained in this study. Apart from that, the polymer membrane could be expanded due to higher amplitude of oscillation mode at elevated temperature. This thermal expansion creates free spaces for conduction mechanism. As a consequence, the charge carriers are decoupled and hence transported easily, contributing to increase in ionic conductivity with reciprocal of temperature.

Figures 4.9 and 4.10 illustrate positively curved plot for all the samples where its regression value is not close to unity (Seki *et al.*, 2005). So, the polymer electrolytes do not follow Arrhenius theory. In order to interpret the result, the plots are then fitted with VTF empirical formula as illustrated in Figure 4.11. Based on this volume–activated principle, the ionic conductivity is expressed as below:

$$\sigma = A_o T^{-\frac{1}{2}} \exp\left(\frac{-B}{T-T_o}\right) = A_o T^{-\frac{1}{2}} \exp\left(\frac{-E_a/k_B}{T-T_o}\right) \quad \text{(Equation 4.2)}$$

where A_o is pre–exponential constant proportional to the number of charge carriers, B represents a constant which is determined from the gradient of the plot (K^{-1}), E_a is pseudo–activation energy for conduction which is related to polymer segmental mobility (eV), k_B stands for Boltzmann constant, T represents the absolute temperature (K) and T_o is ideal vitreous transition temperature at which the polymer segments start to move (Galinski *et al.*, 2006). The T_o is also defined as the temperature at zero configuration entropy of polymer membrane and it is suggested to be 50 K below the glass transition temperature (T_g) (Jiang *et al.*, 2006; Marcilla *et al.*, 2006;). On the other hand, experimental T_g is determined from DSC measurement.

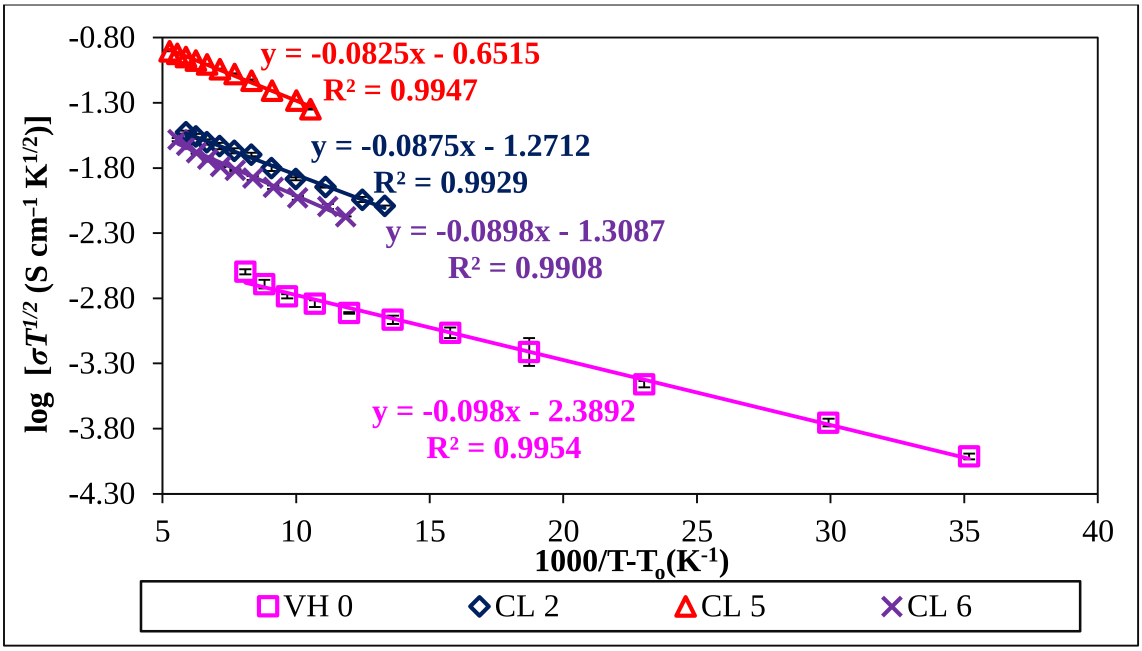

Figure 4.11: The temperature dependent–ionic conductivity of polymer electrolytes fitted with VTF relationship.

These non–linear variations reflect that all the polymer electrolytes exhibit Vogel–Tamman–Fulcher (VTF) theory which is associated with free volume model (Seki *et al.*, 2005; Hu *et al.*, 2004). All the plots are well–fitted with VTF rule where all the regression values are approximately to unity, as shown in Figure 4.11. Since all the regression lines approach to unity, therefore it can be concluded that these polymer electrolytes follow VTF behavior. VTF theory infers the cooperative process in the ionic conduction mechanism where the ionic hopping mechanism is coupled with higher polymer segmental mobility in an amorphous phase (Marcilla *et al.*, 2006). This principle states that the rise in temperature enhances the flexibility of polymer chains as a result of increase in thermal oscillation mode. Highly flexible polymer chains could promote the breaking down of the weak interaction between proton and polar group in the polymer. Therefore, the detachment of the proton will create more conducting sites for the ions to jump from an interstitial site to another adjacent equivalent site and eventually generate the ionic transportation. The movement of polymer segments is also improved at elevated temperature. High mobility of polymer segments in free volume mechanism (as shown in section 2.2.1) can improve the ion transport by creating more free volume of conducting pathways. Therefore, there are more spaces available for charge carriers to be diffused in the polymer electrolytes which produce more ion hopping mechanisms, reflecting high ionic conductivity at high temperature.

A non–linear least square technique is carried out to evaluate some output parameters (T_o, A_o, B and E_a) which are listed in Tables 4.1 and 4.2.

Table 4.1: The obtained parameters from each VTF plot with the experimental glass transition temperature from DSC thermogram in CL system.

Sample	Regression value, R^2	Glass transition temperature, T_g (K)	Ideal glass transition temperature, T_o (K)
VH 0	0.99	319.73	269.73
CL 2	0.99	273.03	223.03
CL 5	0.99	253.23	203.23
CL 6	0.99	263.78	213.78

Table 4.2: The obtained parameters from each VTF plot in CL system.

Sample	Log A_o	Pre–exponential constant, A_o (mS cm^{-1} K$^{1/2}$)	Gradient of the plot, B (K^{-1})	Pseudo–activation energy, E_a (meV)
VH 0	–2.3892	4.08×10^{-3}	0.0980	8.44
CL 2	–1.2712	5.35×10^{-2}	0.0875	7.54
CL 5	–0.6515	2.23×10^{-1}	0.0825	7.11
CL 6	–1.3087	4.91×10^{-2}	0.0898	7.74

T_o is determined by subtracting experimental T_g with 50 K, as aforesaid. A_o is pre–exponential constant proportional to the number of charge carriers, whereas B is correlated with the rate at which the viscosity of the sample changes with respect to the temperature (Pandey *et al.*, 2011). This rate is hence replaced with the ratio of E_a and k_b as displayed in equation 4.2. Among all the samples, CL 5 shows the highest conductivity value due to the maximum ion diffusion in the polymer electrolyte. This can be proven in the VTF plot by showing the highest value of A_o which is designated as pre–exponential constant proportional to the number of charge carriers. This indicates that there is plenty of charge carriers in the CL 5 compared to other ionic liquid–added polymer electrolytes. As expected, ionic liquid–free polymer electrolyte shows the lowest A_o value. Again, it is proven that the addition of ionic liquids can enhance the ionic conductivity by providing more free charge carriers for ion transport. E_a of each sample is subsequently calculated. As can be seen, the pseudo–activation energy is inversely proportional to the ionic conductivity. Among all the polymer electrolytes, CL 5 shows the highest ionic conductivity, but bears the lowest pseudo–activation energy in the system. This observation reveals that CL 5 manifests higher flexibility of polymer backbone coupled with increased segmental mobility within the polymer chains. Hence, CL 5 requires the lowest activation energy for the hopping process.

4.5 Thermogravimetric Analysis (TGA)

Figure 4.12 portrays thermogravimetric analysis for pure PVA, VH 0 and ionic liquid–added polymer electrolytes.

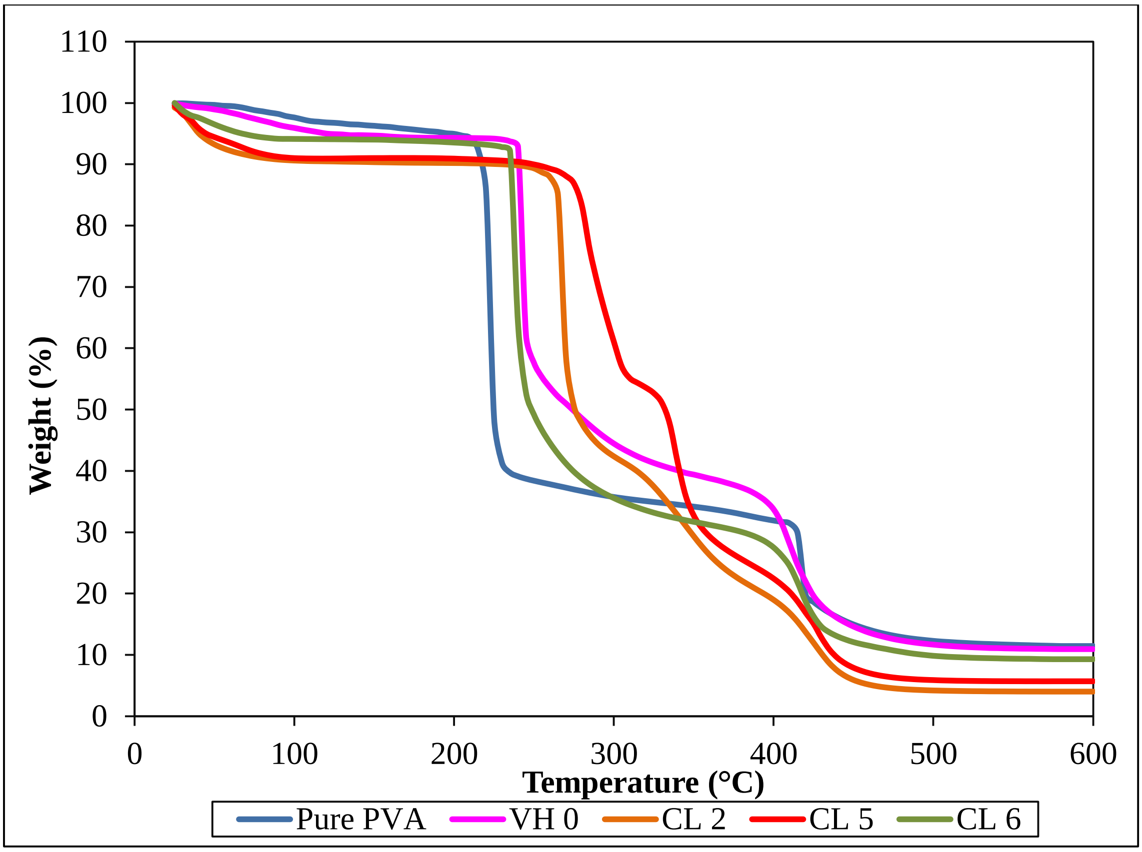

Figure 4.12: Thermogravimetric analysis of pure PVA, VH 0, CL 2, CL 5 and CL 6.

Pure PVA shows three major weight losses, as described in Yang *et al*. (2009). However, four thermal degradation steps are observed for salt and/or ionic liquid–added polymer electrolytes. The initial thermal degradation in the region of 25–125 °C is due to the dehydration of water or moisture as polymer is a hydroscopic compound (Sriupayo *et al*., 2005). The insignificant weight loss in this stage is also due to the elimination of impurities in the polymer electrolytes. Small weight losses of 5 %, 5 % and 6 % are observed for pure PVA, VH 0 and CL 6, respectively in this region. However, higher mass losses of 9 % have been observed for CL 2 and CL 5. Beyond this stage, the weight of all the samples remains the same until 200 °C. Upon the dehydration, ammonium acetate could be decomposed easily into acetamide, $CH_3C(O)NH_2$.

On the contrary, two PVA polymer chains might be cross–linked as a result of water removal. This elimination could lead to the formation of ether cross–linkages (Guirguis & Moselhey, 2012). Above 200 °C, an abrupt decrease in weight is observed for all the samples. Among all the samples, pristine PVA portrays the highest mass loss from 210 °C to 235 °C in this segment. Elimination of side chain in polymer backbone of PVA is the main attributor to this thermal degradation for pure PVA (Yang *et al*. 2009). Apart from formation of ether cross–linkages, the polymer backbone of PVA could start a rapid chain stripping on the polymer backbone upon heating and hence turn into conjugated double bonds, giving rise to formation of polyene, as illustrated as below (Guirguis & Moselhey, 2012):

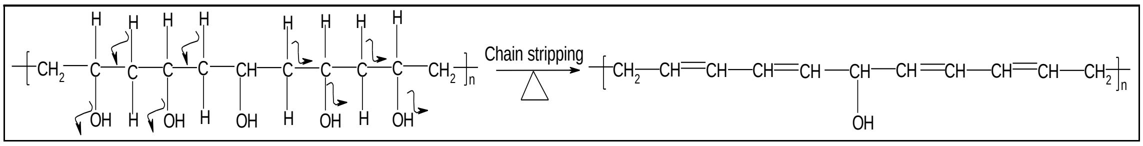

Figure 4.13: Chain stripping mechanism of PVA.

Upon addition of salt and ionic liquid, the mass loss in this stage is significantly decreased. Besides, the starting decomposition temperature in this stage is improved. These observations deduct the contribution from the complexation between salt and/or ionic liquid and PVA. This is because higher energy would be required to break the transient coordination bond in the complexation process. Weight losses of 32 %, 43 %, 33 % and 44 % corresponding to the temperature range of 240–245 °C, 245–285 °C, 250–305 °C, 235–245 °C are attained for VH 0, CL 2, CL 5 and CL 6, respectively. The contributor of this thermal decomposition stage is suggestive of the degradation of acetamide where its decomposition temperature is around 222 °C. The chain stripping mechanism is less favorable in VH 0 when the salt is complexed with PVA. In contrast, the carbene produced from ionic liquid interacts with the hydrogen from hydroxyl group in PVA and forms the coordination bond, as explained in section 4.2. Therefore, the chain stripping process might also be absent in the polymer electrolytes containing ionic liquid. Moreover, BmImCl starts to be degraded at 237 °C as reported by Lee *et al*. (2010). As a result, decomposition of BmImCl also causes the mass loss in this region. Hence, the weight loss of ionic liquid–based polymer electrolytes is found to be higher than VH 0 with this additional attributor. This is in good agreement with the result obtained where higher weight loss is obtained for those ionic liquid–plasticized polymer electrolytes. As can be seen, CL 5 depicts the highest decomposition temperature. This implies that the most conducting polymer electrolyte exhibits better thermal properties than other polymer complexes.

A consecutive enormous loss in weight is observed thereafter for all polymer electrolytes. However, pure PVA exemplifies insignificant mass loss of 8% from 235 °C until 410 °C. The weight loss of all polymer electrolytes remains in the regime of 20–30 %. VH 0 has weight loss of 20 %, starting from 245 °C until 375 °C, whereas CL 2 exhibits mass loss of 21 %, from 285 °C to 365 °C. Similarly, CL 6 also shows around 21% of weight loss in the temperature range of 245–350 °C. On the contrary, the weight loss of CL 5 is increased by 5%, which is around 26% whereby the degradation temperature starts from 305 °C to 355 °C. The thermal degradation in this phase arises from the chemical degradation processes. These chemical decomposition processes include the breakdown of ether cross–linkages and random chain scissoring between carbon–carbon bonds (Guirguis & Moselhey, 2012). Random bond scission yields two intermediate products and thus forms methyl–terminated allylic polyene in cis and trans ismoerisms via elimination process, as demonstrated below (Gilman *et al*., 2005).

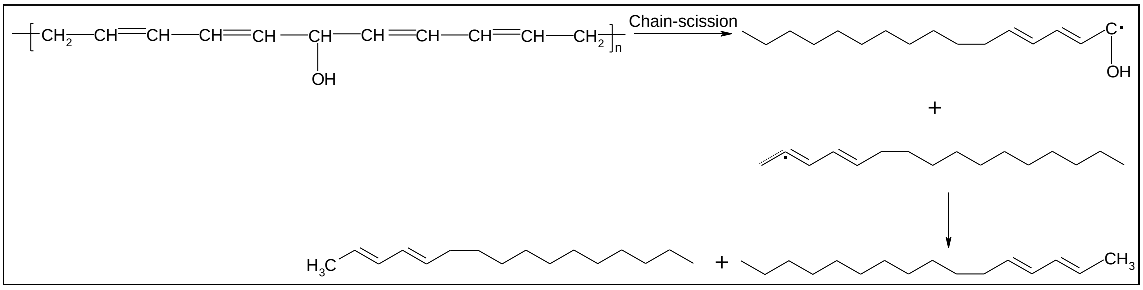

Figure 4.14: Chain scission mechanism of PVA.

Final weight loss is attained at elevated temperature. Pure PVA and VH 0 show 20 % and 26.8 % of weight losses, along with 12 % and 11 % of mass residues at 575 °C, respectively. Ionic liquid–added polymer electrolytes display lower mass loss in comparison to VH 0. CL 2 exhibits 21 % of weight loss from 365 °C to 570 °C with residual mass of 3 %, whereas CL 5 reveals higher mass loss, which is around 25 % with 6 % of residue in the temperature range of 355 °C–565 °C. CL 6 starts to loss its weight around 22 % with 9 % of residue from 350 °C to 575 °C. This final weight loss is connected to the breakdown of the polymer backbone (Yang *et al*. 2009). Upon further heating, the double bond of polyene would be broken down into single bond and eventually converted into aliphatic polymer chains at this stage (Gilman *et al*., 2005). Beyond this stage, the weight of samples remains unchanged. This observation infers the fully decomposition of the polymer matrix. Although the residual mass of ionic liquid–based polymer electrolytes is lesser, CL 5 is still a promising candidate as polymer electrolyte due to its higher first decomposition temperature.

4.6 Attenuated Total Reflectance–Fourier Transform Infrared (ATR–FTIR)

The FTIR results and the complexation between PVA and CH_3COONH_4 have been elucidated in the literature (Awadhia & Agrawal, 2007; Gedam & Bhoga, 2010; Hema *et al*., 2009; Hirankumar *et al*., 2004; Hirankumar *et al*., 2005; Lu *et al*., 2009; Pahune & Bharadwaj, 2011). Figure 4.15 depicts the ATR–FTIR spectra of pure PVA, ammonium acetate and VH 0. The assignment of each peak is listed in Table 4.3.

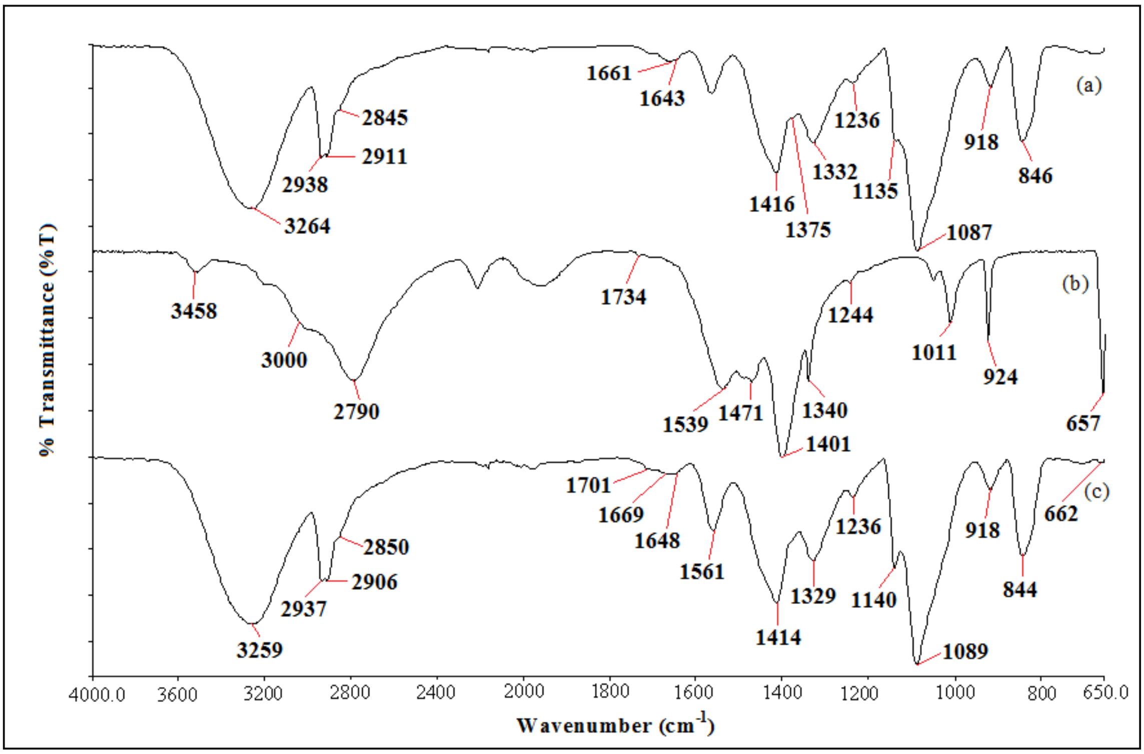

Figure 4.15: ATR–FTIR spectra of (a) pure PVA, (b) ammonium acetate and (c) VH 0.

Table 4.3: The assignments of the vibration modes of pure PVA, ammonium acetate and VH 0.

Descriptions of vibration modes	Wavenumber (cm^{-1})		
	Pure PVA	CH_3COONH_4	VH 0
C–H bending mode	–	657	662
Skeletal C–H rocking mode	846	–	844
O–H bending mode	918	–	918
Out–of–plane N–H bending	–	924	–
C–H wagging mode		1011	–
C–O stretching mode	1087	–	1089
C–C and C–O stretching mode of doubly H–bonded OH in crystalline region	1135	–	1140
C–O stretching mode	1236	1244	1236
CHOH bending mode, CH_3 in–plane deformation and C–H wagging mode	1332	–	1329
CH_3 bending mode	–	1340	–
CH_2 wagging mode	1375	–	–
N–H deformation and asymmetric CH_3 bending mode	–	1401	–
C–H deformation mode	1416	–	1414
N–H bending mode	–	1539, 1487–1471	1561
C–H stretching	1643	–	1648
–CONH– bonding mode	1661	–	1669
C=O stretching mode	–	1734	1701
C–H symmetric stretching mode of CH_2 group	2845, 2911, 2938	2790, 3000	2850, 2906, 2937
O–H stretching vibration mode of OH group	3264	–	3259
N–H stretching mode	–	3458	–

Five peaks of ammonium acetate are disappeared when it is mixed with PVA. These peaks are out–of–plane N–H bending at 924 cm^{-1}, C–H wagging mode at 1011 cm^{-1}, CH_3 bending mode at 1340 cm^{-1}, N–H deformation and asymmetric CH_3 bending mode at 1401 cm^{-1} and N–H stretching mode at 3458 cm^{-1} (Awadhia & Agrawal, 2007). The disappearance of these peaks establishes the salt complexation in the macromolecules. The shoulder peak at 1375 cm^{-1} which designated as CH_2 wagging mode of PVA is also missing when ammonium salt is added into PVA (Awadhia & Agrawal, 2007; Hema *et al*., 2009). All the peaks exhibit downward or upward shift, except O–H bending mode in PVA at 918 cm^{-1} and C–O stretching mode in PVA at 1236 cm^{-1} (Lu *et al*., 2009). The sharp peak at 657 cm^{-1} in Figure 4.15 (b) is designated as C–H bending mode. This peak is shifted to higher wavenumber of 662 cm^{-1}. Similarly, the weak peaks of C–H stretching and CONH bonding modes in PVA are shifted from 1643 cm^{-1} to 1648 cm^{-1} and from 1661 cm^{-1} to 1669 cm^{-1}, respectively (Awadhia & Agrawal, 2007; Sriupayo *et al*., 2005). The upward shifts reveal the interaction between ammonium acetate and PVA in the proton transportation within the polymer matrix. This suggests that acetate anion could abstract a proton from the hydroxyl group in PVA and then produce acetic acid. Meanwhile, the ammonium cations could form N–O bond with the oxygen in the hydroxyl group of PVA and induce to the formation of CONH bond, leading to proton conduction. Another proof has also been observed in C–O stretching mode and the combinations of C–C and C–O stretching mode which are located at 1087 cm^{-1} and 1135 cm^{-1}, respectively in Figure 4.15 (a) (Buraidah & Arof, 2011; Sriupayo *et al*., 2005). Upon the complexation with ammonium salt, these respective peaks shift to 1089 cm^{-1} and 1140 cm^{-1}.

Apart from that, some important peaks of PVA are shifted to lower wavenumbers with adulteration of ammonium salt. These shifting can be observed in skeletal C–H rocking and C–H deformation modes in PVA (Buraidah & Arof, 2011; Hema *et al*., 2009;

Lu *et al*., 2009; Sriupayo *et al*., 2005). The first peak shifts from 846 cm^{-1} to 844 cm^{-1}, whereas the latter peak has been shifted to 1414 cm^{-1} from its original location at 1416 cm^{-1}. The medium sharp peak at 1332 cm^{-1} is assigned as the combinations of CHOH bending mode, CH_3 in–plane deformation and C–H wagging mode in PVA and is shifted somewhat to 1329 cm^{-1} when ammonium salt is doped in the PVA solution (Awadhia & Agrawal, 2007). These changes in shift disclose the interaction between C–H bond of PVA and ammonium acetate and verify the complexation. Significant changes in peak location is also observed in C=O stretching mode of ammonium acetate which is placed at 1734 cm^{-1} in Figure 4.15 (b). When the salt is complexed with PVA, this weak peak is shifted to 1701 cm^{-1}. This downward shift reveals the interaction of C=O carbonyl group of ammonium salt with PVA and further confirms the complexation. This agrees well with the possible complexation that we suggest. The complexation between PVA and ammonium cations can also be confirmed in the range of 1600–1450 cm^{-1}. Double peaks at 1487 cm^{-1} and 1471 cm^{-1} with a new peak at 1539 cm^{-1} is attained in ammonium acetate spectrum. This band is assigned as N–H bending mode of ammonium cations. However, only one peak is observed at 1561 cm^{-1}. The disappearance of the double peak and upward shift divulge the interaction between N–H bond and PVA in the complexation. Moreover, a broad peak at 2790 cm^{-1} with a shoulder peak at 3000 cm^{-1} are denoted as C–H symmetric stretching mode of CH_2 group in ammonium acetate. The same vibration modes are also scrutinized for PVA by showing double peaks at 2911 cm^{-1} and 2938 cm^{-1} with a shoulder peak at 2845 cm^{-1} (Abdelrazek *et al*., 2010; Bhargav *et al*., 2007). The same pattern of spectra is obtained for VH 0 in this wavenumber regime. However, the location of the peaks has been shifted. The double peaks are located at 2906 cm^{-1} and 2937 cm^{-1}, whereas the shoulder peak is shifted to higher wavenumber that is around 2850 cm^{-1}. Again, these changes in shift disclose the interaction between C–H of PVA and ammonium salt and hence validate the complexation.

The PVA–CH_3COONH_4 based polymer electrolyte systems have been prepared and investigated in FTIR studies. The interactions between ionic liquid and ammonium acetate–doped polymer electrolyte are also analyzed and discussed in detail. Figure 4.16 depicts the ATR–FTIR spectra of VH 0, BmImCl, CL 2, CL 5 and CL 6.

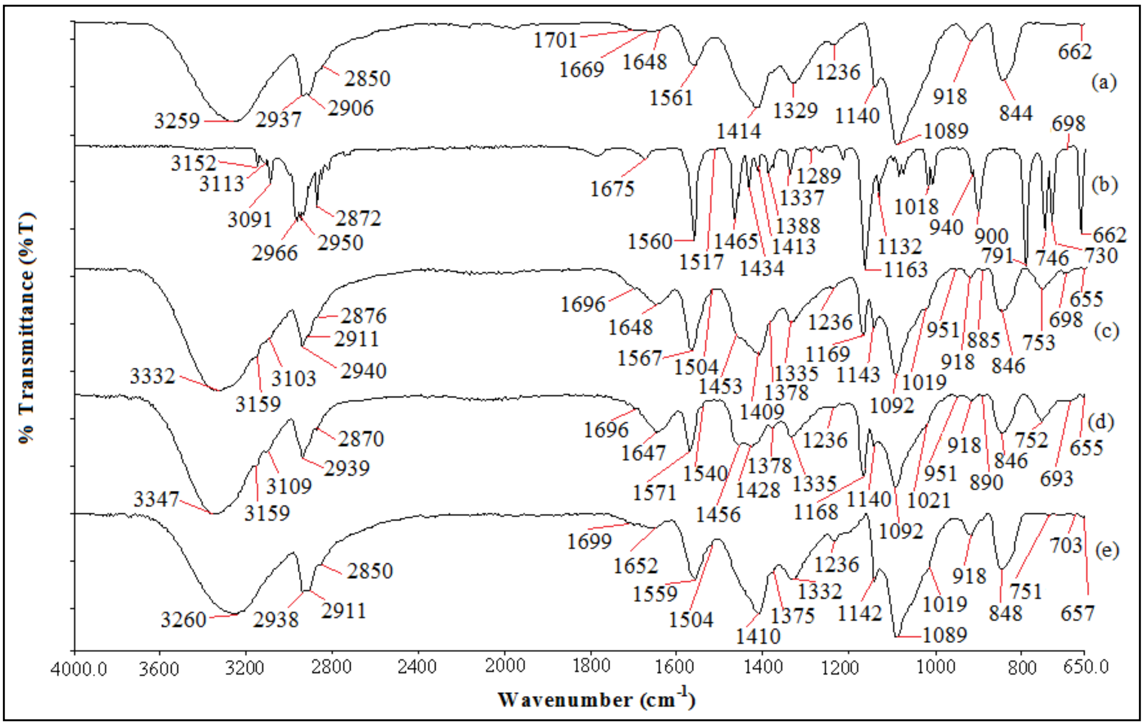

Figure 4.16: ATR–FTIR spectra of (a) VH 0, (b) BmImCl, (c) CL 2, (d) CL 5 and (e) CL 6.

On the other hand, the band assignment of the spectra is summarized in Table 4.4.

Table 4.4: The assignments of the vibration modes of BmImCl, VH 0, CL 2, CL 5 and CL 6.

Descriptions of vibration modes	Wavenumber (cm^{-1})				
	BmImCl	VH 0	CL 2	CL 5	CL 6
C–H bending mode of CH_3COONH_4	–	662	655	655	657
C–H vibration mode for cyclic BmIm$^+$	662, 698, 3113,3152	–	655, 698, 3103, 3159	655, 693, 3109, 3159	657, 703, –, –
Out–of–plane C–H bending mode of imidazolium ring	730	–	–	–	–
C–H bending mode for cyclic BmIm$^+$	746	–	753	752	751
C–Cl stretching mode	791	–	–	–	–
Skeletal C–H rocking mode of PVA	–	844	846	846	848
In–plane C–H bending mode of imidazolium ring	900	–	885	890	–
O–H bending mode of PVA	–	918	918	918	918
In–plane C–N–C bending mode	940	–	951	951	–
Out–of–plane C–H wagging mode in alkyl chain	1018	–	1019	1021	1019

Table 4.4, continued

Descriptions of vibration modes	**Wavenumber (cm^{-1})**				
	BmImCl	**VH 0**	**CL 2**	**CL 5**	**CL 6**
C–O stretching mode of PVA	–	1089	1092	1092	1089
C–H bending mode in methyl group	1132	–	–	–	–
C–C and C–O stretching modes of doubly H–bonded OH in crystalline region of PVA	–	1140	1143	1140	1142
CH$_3$–N stretching mode	1163	–	1169	1168	–
C–O stretching mode of PVA and CH$_3$COONH$_4$	–	1236	1236	1236	1236
C–N stretching mode of imidazolium ring	1289	–	–	–	–
CHOH bending mode, CH$_3$ in–plane deformation and C–H wagging mode of PVA	–	1329	–	–	–
CH$_2$ symmetric bending mode	1337	–	1335	1335	1332
CH$_3$ asymmetric stretching mode	1388	–	1378	1378	1375
C–H deformation mode of PVA and BmIm$^+$	1413	1414	1409	–	1410
CH$_3$ asymmetric bending mode	1434	–	–	1428	–
CH$_3$ symmetric bending mode	1465	–	1453	1456	–
C=C stretching mode	1517	–	1504	–	1504
C=N stretching mode	1560	–	–	1540	–
N–H bending mode of CH$_3$COONH$_4$	–	1561	1567	1571	1559
C–H stretching mode of PVA	–	1648	1648	1647	1652
–CONH– bonding mode of PVA	–	1669	–	–	–
C–C and C–N bending mode of imidazolium ring	1675	–	1696	1696	1699
C=O stretching mode of CH$_3$COONH$_4$	–	1701	–	–	–
C–H symmetric stretching mode in methyl group of alkyl chain	2872, 2950, 2966	2850, 2906, 2937	2876, 2911, 2940	2870, 2939	2850, 2911, 2938
=C–H stretching mode	3091	–	–	–	–
O–H stretching mode of OH group of PVA	–	3259	3332	3347	3260

The ATR–FTIR spectrum of CL 5 is investigated as it achieves the maximum ionic conducting as aforementioned in section 4.3. Upon adulteration of BmImCl, fifteen new peaks have been formed by comparing Figure 4.16(a) with (d). These peaks are C–H vibrational mode for cyclic BmIm$^+$ at 693 cm^{-1}, 3109 cm^{-1} and 3159 cm^{-1} (Jiang *et al.*, 2006), C–H bending mode for cyclic BmIm$^+$ at 752 cm^{-1} (Jiang *et al.*, 2006), in–plane C–H bending mode of imidazolium ring at 890 cm^{-1} (Shi & Deng, 2005), in–plane C–N–C bending mode at 951 cm^{-1} (Chowdhury & Thynell, 2006), out–of–plane C–H wagging mode in alkyl chain at 1019 cm^{-1} (Shi & Deng, 2005), CH_3–N stretching mode at 1168 cm^{-1} (Singh *et al*., 2010), CH_2 symmetric bending mode at 1335 cm^{-1} (Jiang *et al*., 2006), CH_3 asymmetric stretching mode at 1378 cm^{-1} (Jiang *et al*., 2006), CH_3 asymmetric bending mode at 1428 cm^{-1} and 1456 cm^{-1} (Singh *et al*., 2010), C=N stretching mode at 1540 cm^{-1} (Akai *et al*., 2010) and C–C and C–N bending modes of imidazolium ring at 1696 cm^{-1} (Jiang *et al*., 2006). Some characteristic peaks of VH 0 are disappeared with addition of BmImCl. Examples of these characteristic peaks are the combinations of CHOH bending mode, CH_3 in–plane deformation and C–H wagging mode at 1329 cm^{-1}, C–H deformation mode at 1414 cm^{-1} and C=O stretching mode at 1701 cm^{-1}.

Apart from that, the C–Cl stretching mode of BmImCl at 791 cm^{-1} is disappeared. This entails the chloride dissociation from BmIm cations. Therefore, the dissociated BmIm cations could form the carbene compound after the deprotonation process, as suggested in section 4.3. This idea is supported by the absences of out–of–plane C–H bending mode of imidazolium ring at 730 cm^{-1} (Chowdhury & Thynell, 2006), C–H bending mode in methyl group at 1132 cm^{-1} (Bazito *et al*., 2007), C–N stretching mode of imidazolium ring at 1289 cm^{-1} (Chowdhury & Thynell, 2006) and =C–H stretching mode at 3091 cm^{-1} (Chowdhury & Thynell, 2006). The proton conduction in ammonium salt–doped polymer electrolyte is based on the formation of CONH bond, as explained in section 4.3. However, the proton is migrated in a different way for polymer electrolytes containing BmImCl, as suggested in section 4.3. The CONH bonding mode of VH 0 is absent in all the ionic liquid–added polymer electrolytes and further verifies the proposed mechanism.

The C–H bending mode of VH 0 is shifted to lower wavenumber from 662 cm^{-1} to 655 cm^{-1} due to the overlapping of C–H vibration mode for cyclic $BmIm^+$. The C–H vibration mode for cyclic $BmIm^+$ at 698 cm^{-1} also exhibit downward shift to 693 cm^{-1} by comparing Figure 4.16 (a) with (d). The sharp peak at 844 cm^{-1} in Figure 4.16 (a) is designated as skeletal C–H rocking mode of PVA and shifted to 846 cm^{-1} with doping of ionic liquid. This peak not only exhibits the change in shift, but it also undergoes the change in peak intensity. The intensity of peak is gradually reduced from 11.28 % to 8.66 %, in transmittance mode, as demonstrated in Figure 4.17.

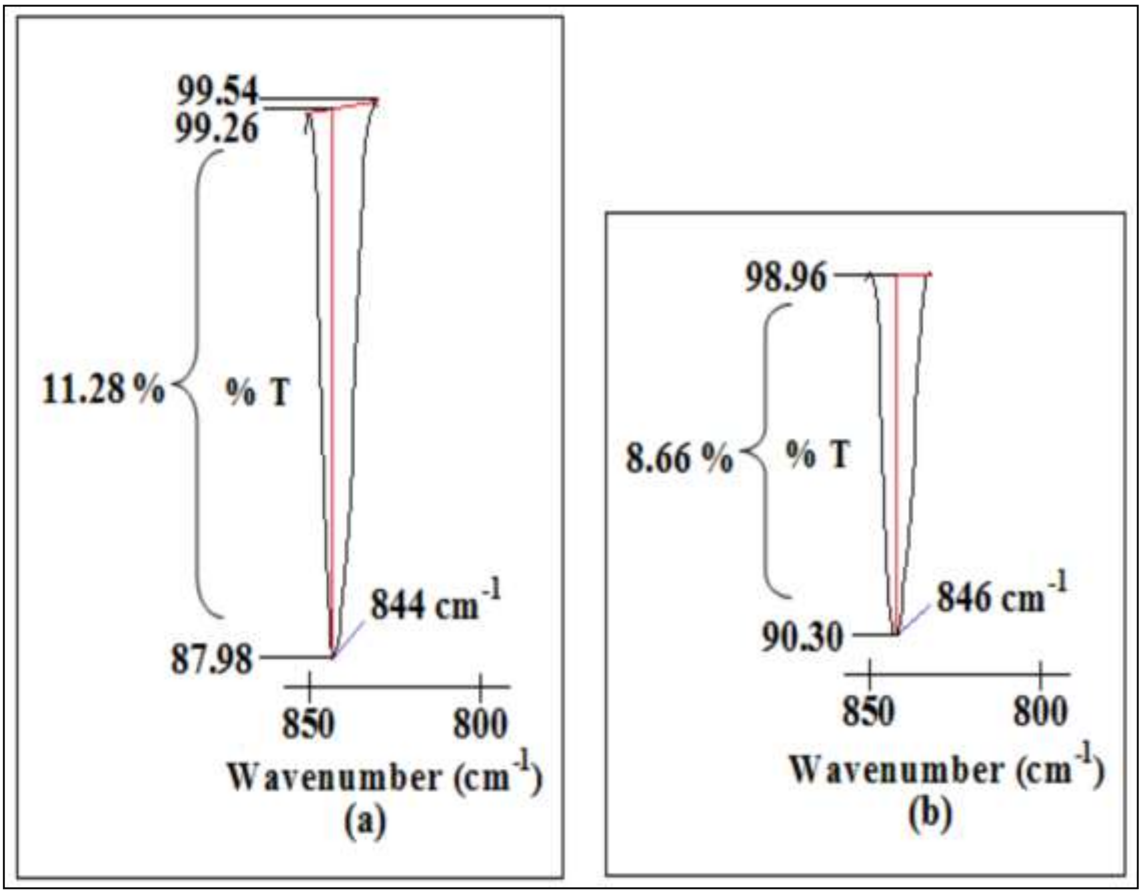

Figure 4.17: The change in peak intensity of skeletal C–H rocking mode of (a) VH 0 and (b) CL 5 in the wavenumber region of 850–800 cm^{-1}.

This phenomenon indicates the interaction between ionic liquid and polymer matrix. Another apparent proof to show the interaction between C–H bonding in imidazolium ring and VH 0 is also attained at the wavenumber of 890 cm^{-1}. A sharp peak with intensity of 19.12 % is observed in ionic liquid spectra; however it has been turned into a weak peak with intensity of 0.14 % in transmittance mode. Figure 4.16 (b) depicts a sharp peak at 900 cm^{-1} with a shoulder peak at 940 cm^{-1}. Upon addition of PVA and ammonium acetate, this band becomes two new peaks with an extremely low intensity at 918 cm^{-1} and 951 cm^{-1}. These two weak peaks are assigned as O–H bending mode and in–plane C–N–C bending mode at 918 cm^{-1} and 951 cm^{-1}, respectively, reflecting the formation of

NO bond as aforementioned in section 4.3 (Lu *et al.*, 2009). The intensity of first peak is also reduced from 3.35 % to 1.06 % in transmittance mode. A sharp peak is observed at 1089 cm^{-1} in the wavenumber range of 1100 cm^{-1} –1000 cm^{-1} for VH 0 and assigned as C–O stretching mode. But, it has been changed to a medium sharp peak at 1092 cm^{-1} with a shoulder peak at 1021 cm^{-1} when BmImCl is embedded into the polymer complex. This indicates the overlapping of out–of–plane C–H wagging mode in alkyl chain with polymer matrix and further deduces the interaction between C–O bond from polymer matrix and C–H functional group from ionic liquid. This result agrees well with our proposed mechanism in section 4.3 where the hydrogen from ionic liquid will be abstracted to the adjacent electron–deficient oxygen for the proton hopping mechanism. Even though the C–O stretching mode still remains unchanged at 1236 cm^{-1}, the intensity of the peak is relatively reduced upon impregnation of ionic liquid. The peak reduction entails that the proton conduction could be taken place at the C–O coordination bond when the ionic liquid is complexed with polymer backbone.

The sharp peak at 1163 cm^{-1} is designated as CH_3–N stretching mode, whereas the weak peak at 1388 cm^{-1} is associated with CH_3 asymmetric stretching mode. The first peak exhibits upward shift to 1168 cm^{-1} with reduced peak intensity of 31.11 %, from 44.11 % to 13 % in transmittance mode. On the contrary, the latter peak shifts to lower wavenumber to 1378 cm^{-1} where its intensity is gradually reduced from 3.17 % to 0.73 % in transmittance mode. The peak at 1414 cm^{-1} is designated as C–H deformation mode. However, the inclusion of 50 wt.% of ionic liquid induces to the formation double peaks at 1456 cm^{-1} and 1428 cm^{-1}, as shown in Figure 4.18.

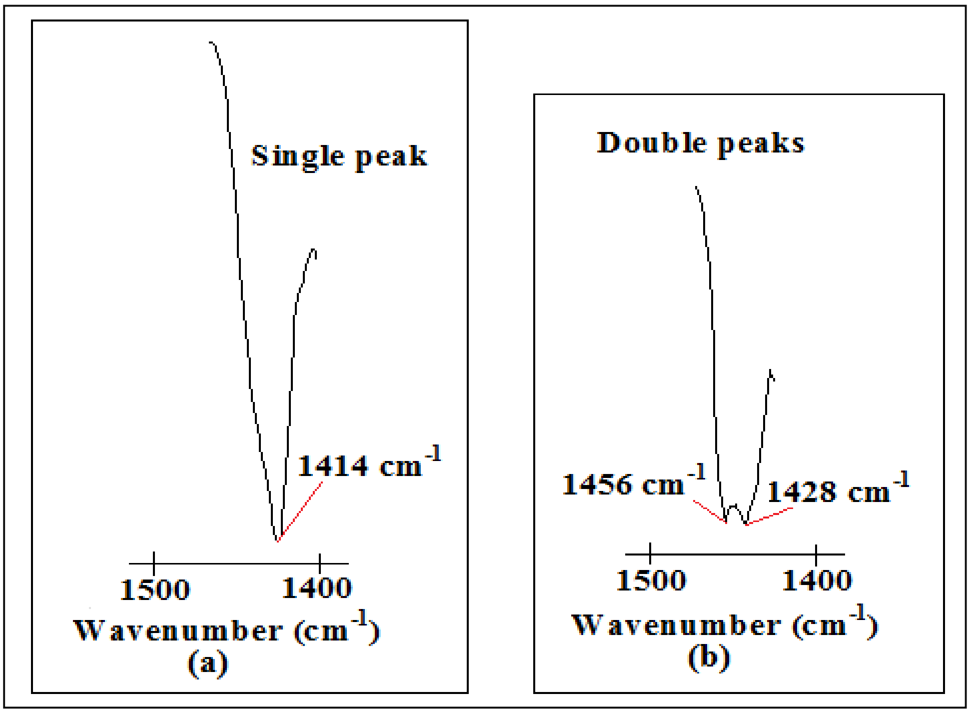

Figure 4.18: The change in shape of vibration modes of (a) VH 0 and (b) CL 5 in the wavenumber region of 1500–1400 cm^{-1}.

The change in shape is suggestive of the overlaps of C–H deformation mode at 1413 cm^{-1}, CH_3 asymmetric bending mode at 1434 cm^{-1} and CH_3 symmetric bending mode at 1465 cm^{-1}. This can be proven using the deconvolution method. The peaks are fitted and deconvoluted as illustrated in Figure 4.19.

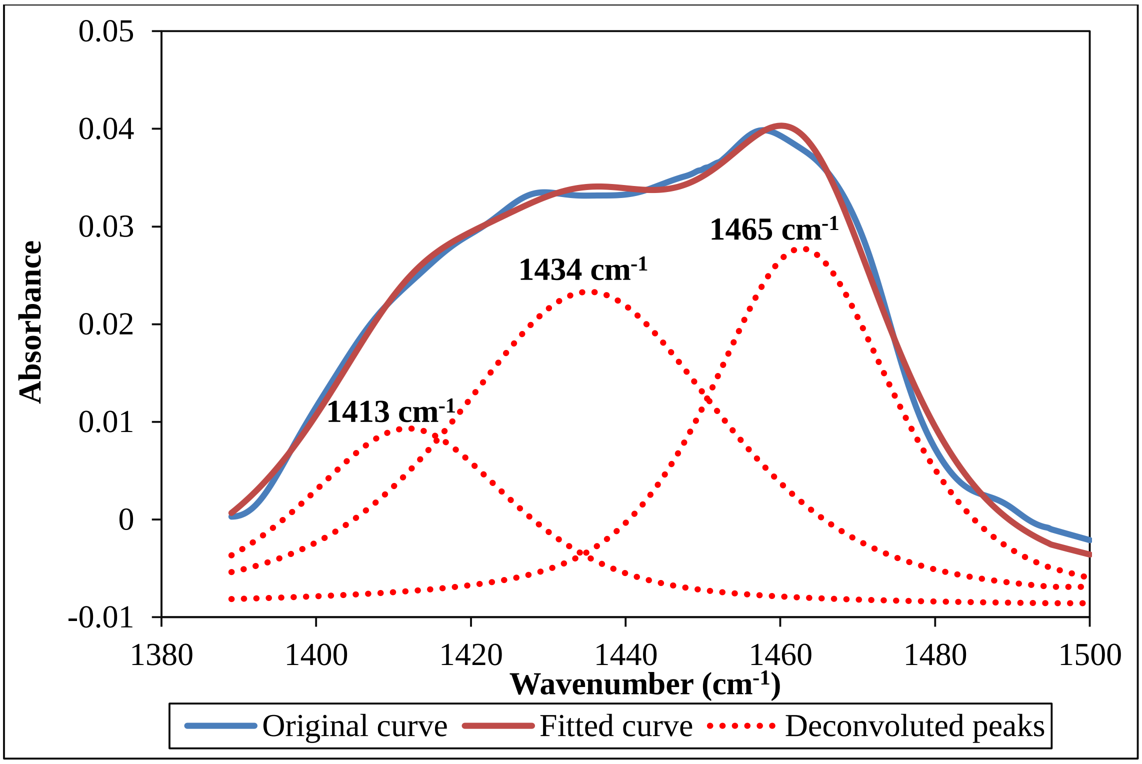

Figure 4.19: The original and fitted curves with the deconvoluted peaks of CL 5in the wavenumber region of 1500–1390 cm^{-1}.

Three deconvoluted peaks are obtained in this wavenumber range. This result is in good agreement with our suggestion. Again, this signifies the interaction of hydrogen from C–H bond with polymer membrane where the proton conduction can take place at. A medium sharp peak at 1561 cm^{-1} corresponding to N–H bending mode is attained in VH 0 spectra. Nevertheless, the peak has been developed into a sharp peak at 1571 with a shoulder peak at 1540 cm^{-1}. The intensity of the sharp peak is increased from 6.56 % to 10.01 % in transmittance mode. The overlapping of C=N stretching mode at 1560 cm^{-1} and C=C stretching mode from ionic liquid at 1517 cm^{-1} contributes to this changes of peak intensity, peak location and shape. This can be a sign of interaction between ionic liquid and VH 0. The weak peak analogous to C–H stretching mode at 1648 cm^{-1} is changed to a medium sharp peak at 1647 cm^{-1}. The intensity of this peak is increased from 0.43 % to 5.63 % in transmittance mode as observed in Figures 4.16 (a) and (d). This finding reveals the complexation between ionic liquid and macromolecules and verifies the proton conduction.

Another proof to show the proton conduction is also detected in the range of 3000–2800 cm^{-1}. Double peaks with a shoulder peak are appeared as a broad band within this region. This band is designated as C–H symmetric stretching mode in methyl group of alkyl chain. However, only a peak with a shoulder peak is observed at their respective wavenumber of 2939 cm^{-1} and 2870 cm^{-1} upon inclusion of BmImCl. Similar phenomenon is attained for the band within the range of 3400–3000 cm^{-1}. VH 0 illustrates a broad peak at 3259 cm^{-1} which is related to O–H stretching vibration mode of OH group in PVA. Two additional shoulder peaks are scrutinized at 3109 cm^{-1} and 3159 cm^{-1} in which the O–H stretching mode is shifted to 3347 cm^{-1} with adulteration of BmImCl. These newly formed shoulder peaks are known as C–H vibration mode for cyclic BmIm^{+} of ionic liquid. Therefore, these changes in shift and peak position can be indicative of interaction between C–H vibration mode of ionic liquid and O–H stretching mode of PVA which aids in the proton conduction.

Among all the samples, we found that the highest ionic conductivity is achieved by adding 50 wt.% of BmImCl as shown in Figure 4.3. One of the attributors in enhancing the ionic conductivity is correlated to lower crystalline region (or higher amorphous degree) in the polymer electrolytes. The vital feature can be proven in the ATR–FTIR spectra. C–C and C–O stretching modes of doubly H–bonded OH in crystalline region is located at 1140 cm^{-1} with its intensity of 5.57 % in Figure 4.16 (a). The intensity of this peak is gradually reduced to 3.97 % corresponding to CL 2 at 1143 cm^{-1} and 1.61 % at 1140 cm^{-1} for CL 5. Therefore, it can be concluded that CL 5 has the lowest crystalline region compared to VH 0 and CL 2. The intensity of this characteristic peak of CL 6 is increased to 6.42 % in comparison to VH 0, CL 2 and CL 5, as shown in Figure 4.16 (e). When the ionic liquid is added further, the crystalline phase of CL 6 becomes higher due to the ion pairing and ion aggregation as a result of excessive ion. The formation of ion pairs and ion aggregates can be further proven by the disappearance of some characteristic peaks in Figure 4.16 (e). These peaks are: in–plane C–H bending mode of imidazolium ring at 900 cm^{-1}, in–plane C–N–C bending mode at 940 cm^{-1}, CH_3–N stretching mode at 1163 cm^{-1}, CH_3 asymmetric bending mode at 1434 cm^{-1}, CH_3 symmetric bending mode at 1465 cm^{-1}, C=N stretching mode at 1560 cm^{-1}, and C–H vibration modes for cyclic BmIm^{+} at 3113 cm^{-1} and 3152 cm^{-1}. The changes in peak intensity, peak position and shape establish the complexation between ionic liquid and polymer matrix.

4.7 X–ray Diffraction (XRD)

Figure 4.20 portrays XRD diffractogram of PVA, CH_3COONH_4 and ionic liquid–free polymer electrolyte.

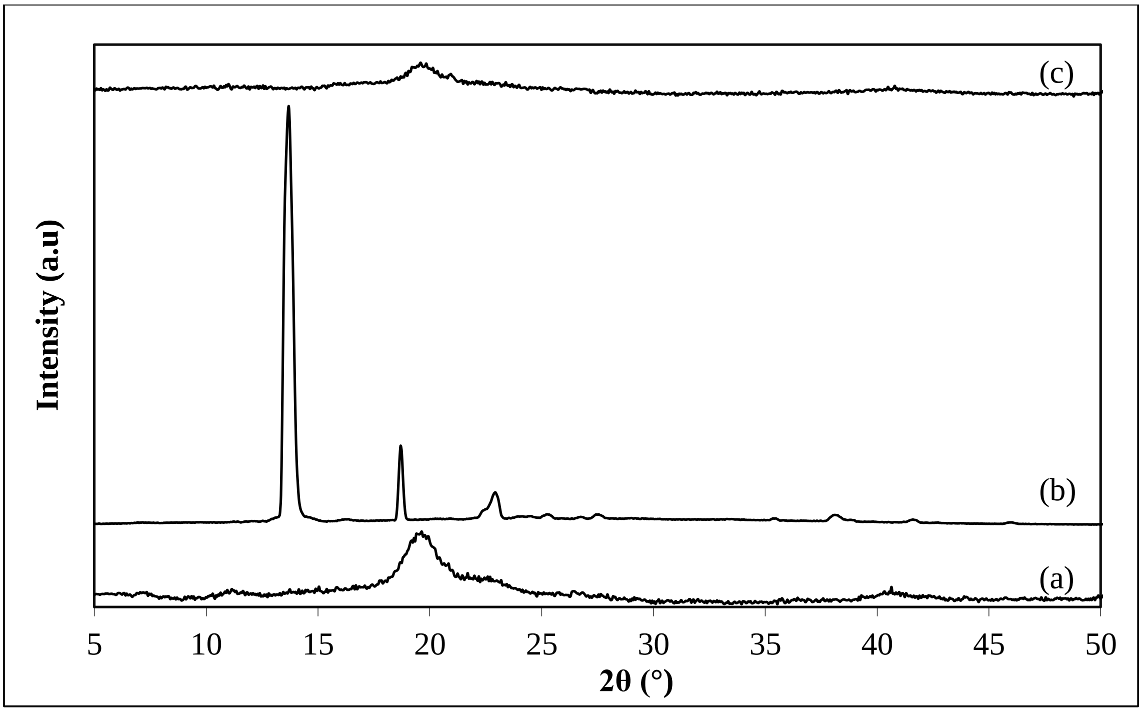

Figure 4.20: The XRD patterns of (a) pure PVA, (b) CH_3COONH_4 and (c) VH 0.

The XRD patterns of PVA had been widely studied. The diffractogram of PVA reveals two reflections peaks at the 2θ angles of 20° and 40° as mentioned in the previous findings (Hirankumar *et al.*, 2005; Yang *et al.*, 2008; Yang *et al.*, 2009). Rajendran and his group found that pure PVA has two diffraction peaks at 2θ=19.5° and 22.3° (Rajendran *et al.*, 2004b; Rajendran *et al.*, 2004c). All the peaks are observed in our XRD diffractogram that are an intense crystalline diffraction peak at the 2θ angles of 19.6°, a broad hump at the 2θ angles of 22.9° and a small peak at the 2θ angles of 40.6°. These peaks reveal the semi–crystalline feature of PVA. The crystalline peak at 2θ=19.6° corresponds to the (1 1 0) reflection (Hirankumar *et al.*, 2005, Selvasekarapandian *et al.*, 2005). Ammonium acetate exhibits few crystalline peaks at 2θ=13.7°, 18.7°, 22.9°, 25.2°, 26.5°, 27.5°, 35.4°, 37.9°, 41.6° and 46° as shown in Figure 4.20 (b). These crystalline peaks are disappeared in VH 0 when the salt is mixed with PVA. The disappearance of crystalline peaks of salts infers the complete dissolution of CH_3COONH_4 in PVA solution. All the peaks in PVA are observed in ionic liquid–free polymer electrolyte. However, these peaks possess lower intensity than in PVA. The crystalline sharp peak is located at 2θ=19.7°, whereas the hump is located at 2θ=22.7° with a small broad peak at 2θ=40.8°.

The importance of ionic liquid on the polymer electrolyte is also examined in XRD studies. The XRD patterns of VH 0, BmImCl and ionic liquid–added polymer electrolytes are depicted in Figure 4.21.

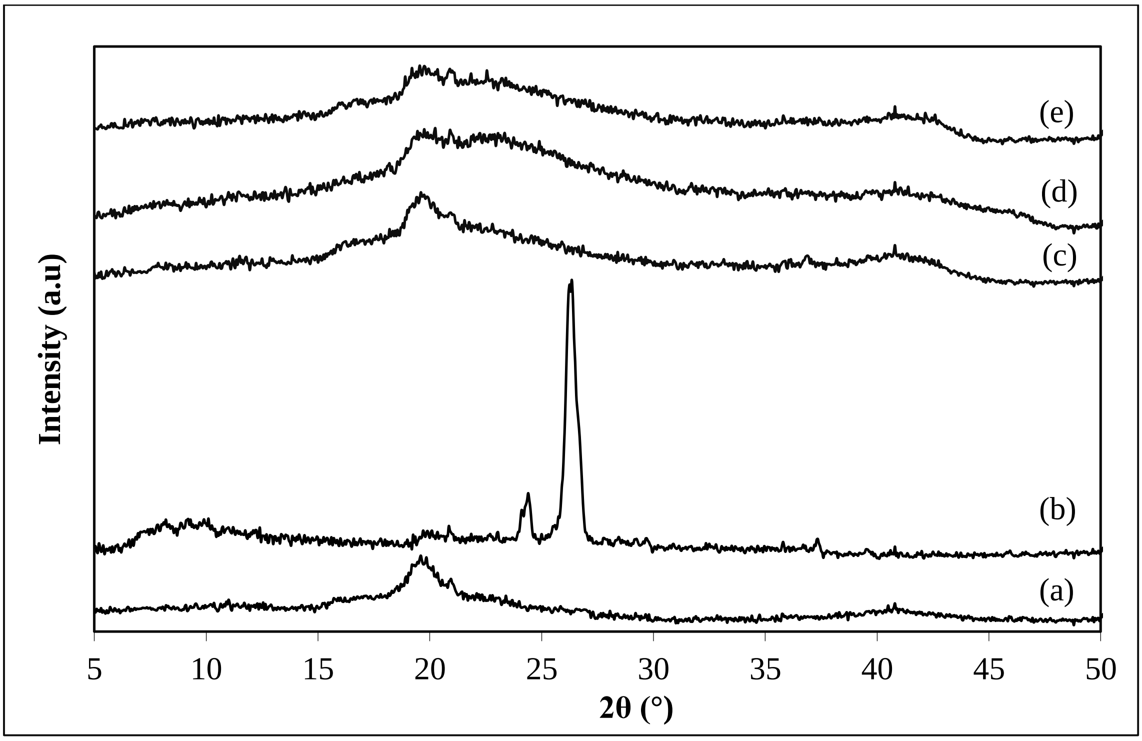

Figure 4.21: The XRD patterns of (a) VH 0, (b) BmImCl, (c) CL 2, (d) CL 5 and (e) CL 6.

BmImCl demonstrates few crystalline peaks at 24.1°, 24.4°, 26.2° and 26.4°. All these peaks are vanished in all ionic liquid–added polymer electrolytes. This is a good evocative of the complete dissolution of BmImCl in the polymeric solution. Upon inclusion of ionic liquid, two observations have been attained clearly by comparing Figure 4.21 (a) with (c)–(e). These observations are:

i) The intensity of crystalline peak at 2θ=19.7° of VH 0 becomes lesser

ii) The hump at 2θ=22.7° and the small peak at 2θ=40.8° of VH 0 become broader

CL 2 depicts a sharp crystalline peak at 2θ=19.7°, a hump at 2θ=22.0° and a broad peak at 2θ=40.8°. On the other hand, CL 5 and CL 6 manifest the sharp peak at the same 2θ degree of 19.7°. The peak at 2θ=22.7° is shifted to higher 2θ degree to 22.5° for CL 5, whereas it has been shifted to 22.6° for CL 6. In contrast, the small broad peak of CL 5 and CL 6 are located at 2θ=40° and 41.5°, respectively. The less intense of crystalline peak and broader amorphous peaks signify the reduced degree of crystallinity of polymer electrolytes which helps in promoting the ion transport in the electrolyte.

Deconvolution on XRD pattern of CL 5 is done to determine the area under the peaks using curve fitting method. Figure 4.22 confirms the presence of crystalline peak at 2θ=19.7° and amorphous peaks at 2θ=22.5° and 2θ=40° using deconvolution method.

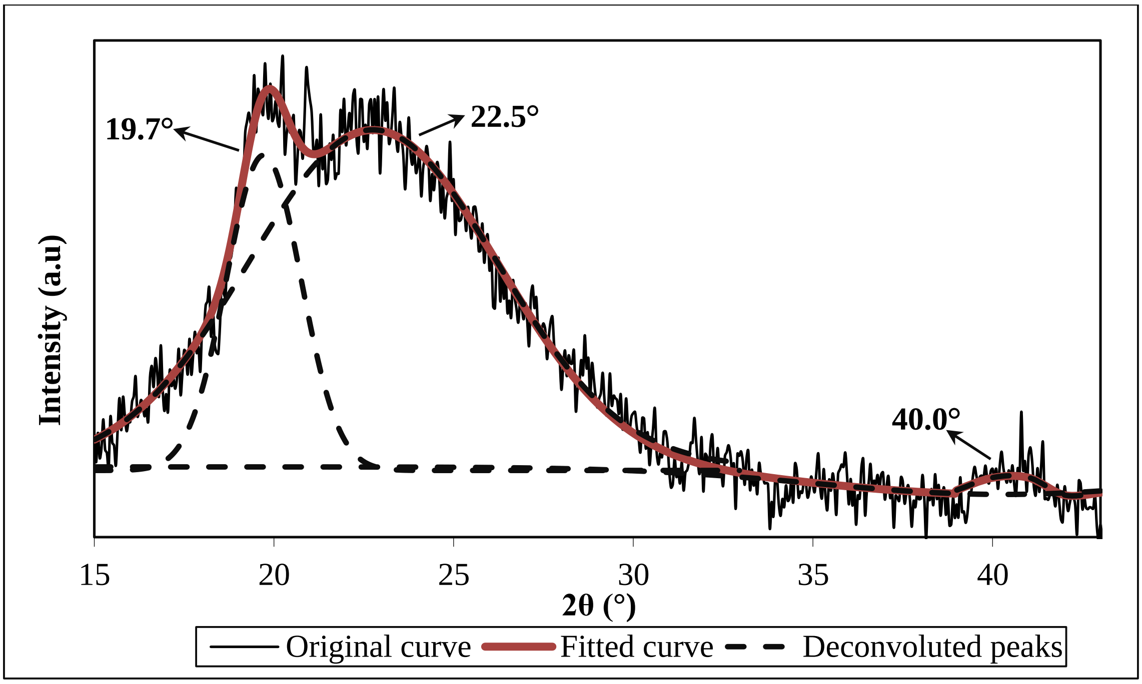

Figure 4.22: XRD pattern of CL 5 with fitted curve and deconvoluted peaks within the range of Bragg angle, 2θ of 15–43°.

The degree of crystallinity of polymer electrolytes is also calculated by dividing the area under the crystalline peak into total area of all the peaks. These relevant parameters obtained from the curve fitting process in XRD findings are summarized in Table 4.5.

Table 4.5: The relevant parameters obtained from the curve fitting in XRD findings in CL system.

Sample	Area under the curve of the crystalline peak, I_c	Total area under the curves of all the peaks, I_t	Percentage of crystallinity (χ_c) %
PVA	3979	4799	83
VH 0	1669	5366	31
CL 2	605	3008	20
CL 5	562	2977	19
CL 6	656	2841	23

PVA is a semi–crystalline compound with crystallinity of 83%. Interestingly, we found out that the addition of salt can reduce the degree of crystallinity substantially to 31%. It is proven that CH_3COONH_4 plays an important role to reduce the crystallinity of polymer electrolytes which causes conductive properties.

Moreover, addition of ionic liquids reduces the degree of crystallinity of polymer electrolytes from 31 % to 20 % which is corresponding to CL 2, 19 % for CL 5 and 23 % which is analogous to CL 6. It is a good proof to verify that the one of the reasons of high ionic conductivity in ionic liquid–added polymer electrolytes is due to high degree of amorphous region in the electrolytes. Low crystallinity or high amorphous degree of polymer electrolytes does not impede the ionic conductivity. The molecules in crystalline region are packed orderly; meanwhile the molecules in amorphous phase are arranged randomly. Therefore, the mobile charge carriers can be transported easily in amorphous region rather than in crystalline phase as amorphous region provides more empty spaces for hopping mechanism. Moreover, the charge carriers require larger energy to overcome the ordered arrangement in crystalline region for transportation. Therefore, high amorphous degree can contribute to high ionic conductivity as proven in this study.

4.8 Linear Sweep Voltammetry (LSV)

The maximum operational potential for charge or energy storage in EDLCs is checked by carrying out LSV study (Arof *et al.*, 2012). Figures 4.23 and 4.24 describe LSV responds of VH 0 and CL 5 polymer electrolytes, respectively.

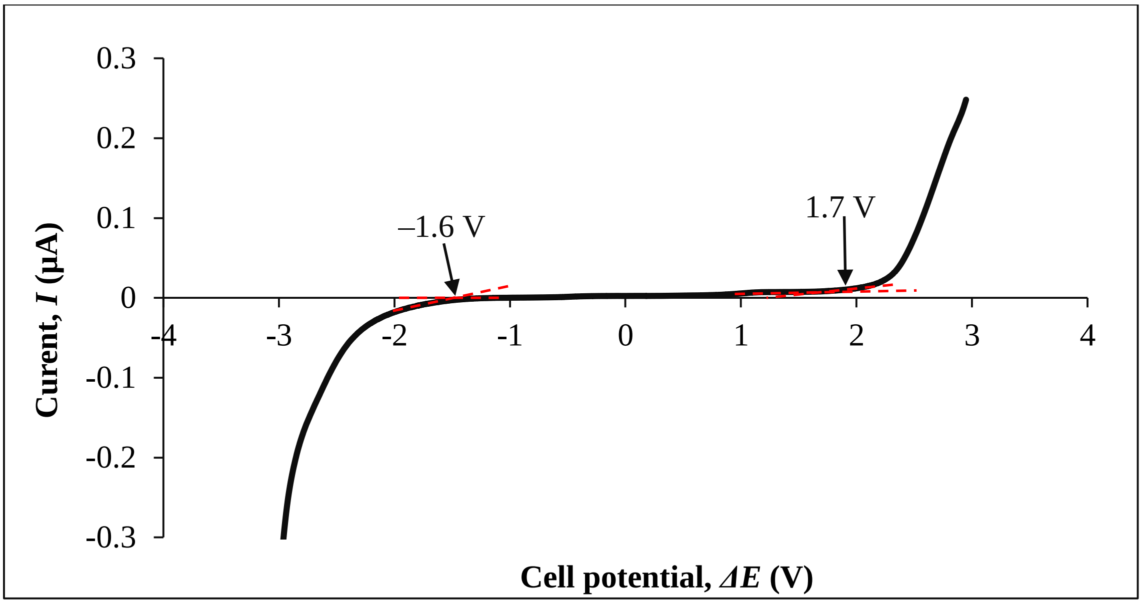

Figure 4.23: LSV response of VH 0.

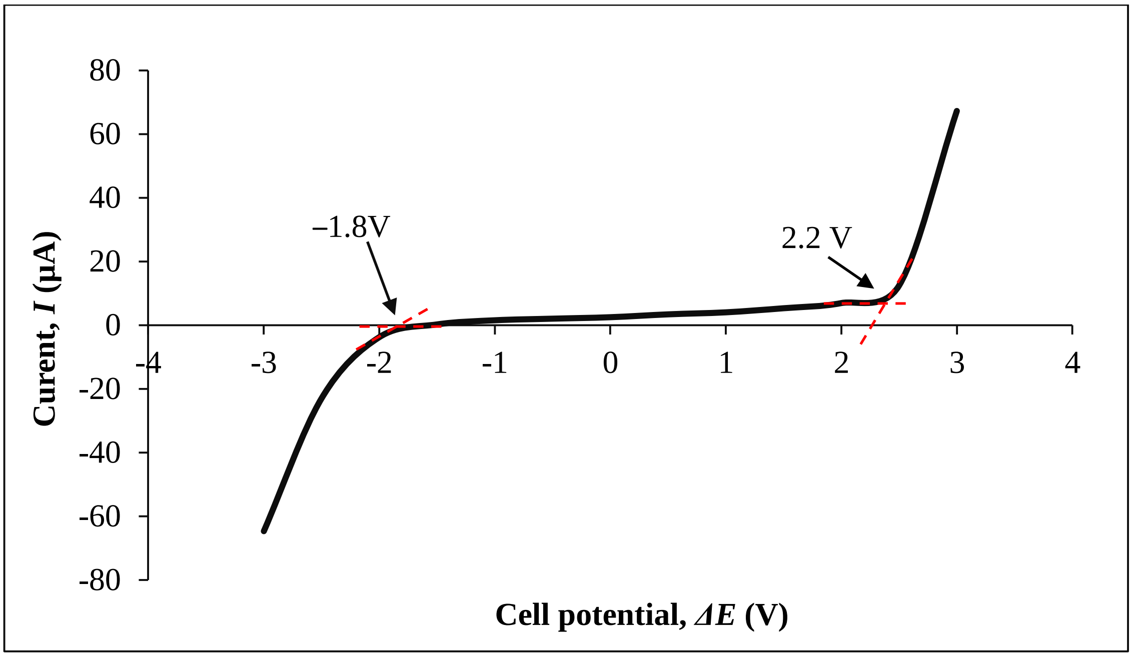

Figure 4.24: LSV response of CL 5.

VH 0 can be operated up to 3.3 V in the potential range between –1.6 V and 1.7 V, as shown in Figure 4.23. Upon inclusion of 50 wt.% of BmImCl into the polymer electrolyte, the electrochemical stability window is expanded to 4.0 V, where the cathodic and anodic potentials are detected at –1.8 V and 2.2 V, respectively. Therefore, it can be concluded that impregnation of ionic liquid can improve the electrochemical stability of polymer electrolyte. Apart from that, the operational current of CL 5 is higher than that of VH 0. This is mainly assigned to high ion concentration in ionic liquid and ion diffusion in the electrolyte. The rapid ion diffusion promotes the charge accumulation at the interface between electrolyte and blocking electrode. Therefore, more energy would be stored in this vicinity. More electrons will be left and transported from positive electrode to negative electrode when the ion absorption is increased. This is responsible for higher operational current in the CL 5 polymer membrane.

4.9 Cyclic Voltammetry (CV)

There are three different techniques to detect the capacity of the electrochemical devices viz. cyclic voltammetry, EIS and galvanostatic charge–discharge performance (Lewandowski & Swiderska, 2003). All these experiments will be analyzed and discussed in detail. In order to verify the capacitance of the fabricated EDLC cells, the results obtained from each experiment are compared. Figures 4.25 and 4.26 exemplify CV curves of type I and II cells, respectively.

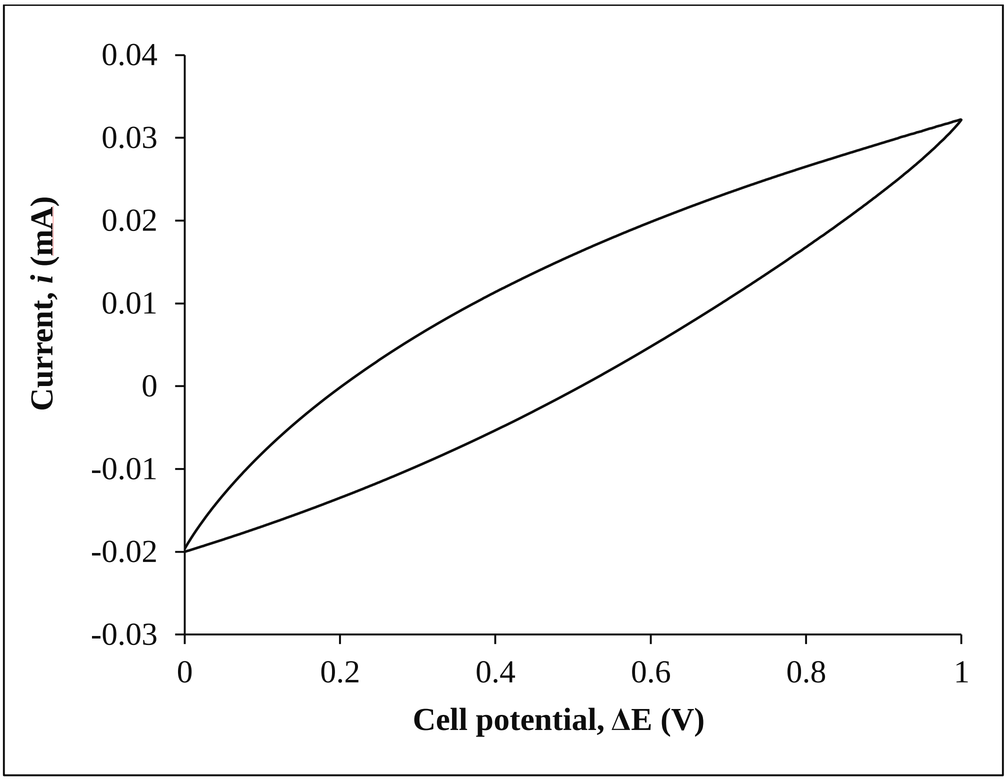

Figure 4.25: Cyclic voltammograms of type I EDLC containing PVA–CH_3COONH_4 polymer electrolyte.

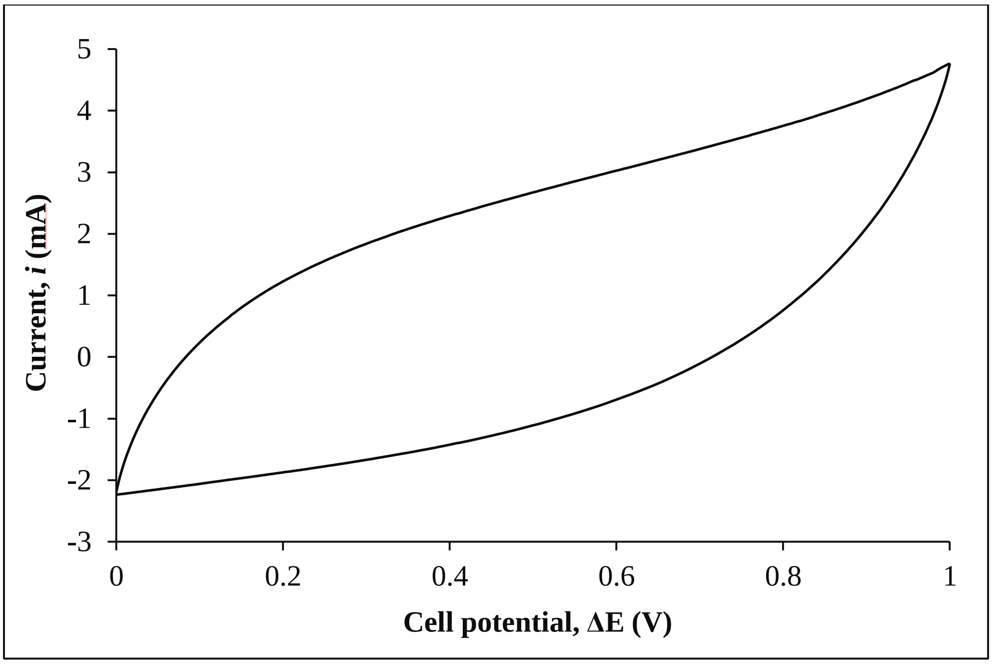

Figure 4.26: Cyclic voltammograms of type II EDLC containing PVA–CH_3COONH_4–BmImCl–polymer electrolyte.

Type I EDLC shows leaf–like shape of CV with specific capacitance of 0.14 F g^{-1} (or equivalent to 1.5 mF cm^{-2}), whereas type II cell illustrates a voltammogram approaching ideal box–like shape with specific capacitance value of 19.42 F g^{-1} (or equivalent to 0.2 F cm^{-2}) (Hashmi *et al.*, 1997b). This result is higher than some literatures. Pandey and his co–workers fabricated EDLC using ionic liquid–based poly(ethylene oxide) polymer electrolytes and multi–walled carbon nanotubes electrodes. The result is almost 10 times lower than our current work, which is 2.6–3 F g^{-1} (Pandey *et al.*, 2011). The EDLC using plasticized PVdF–co–HFP based polymer electrolyte and composite carbon electrodes was fabricated by Gu *et al.* (2000). The specific capacitance obtained from Gu *et al.* is slightly lower than our current work which is 13 F g^{-1}. Type I cell is deviated from the ideal rectangular shape due to the poor contact between electrode and electrolyte. So, the ions are very difficult to be absorbed onto the electrode surface with this low interfacial contact. The ill–defined rectangular shape in Figure 4.25 is also because of the low conductivity of polymer electrolyte (Choudhury *et al.*, 2009). However, when ionic liquid is added into the polymer matrix, sticky sample is produced due to the plasticizing effect of ionic liquid. Hence, the interfacial contact is improved with this sticky behavior leading to increase in energy storage in EDLC. The improvement of interfacial contact could then induce higher capacitive performance of EDLC.

In addition, the ionic conductivity is enhanced upon addition of ionic liquid which helps in improving the charge storage capacitive behavior. The capacitance of type I EDLC is extremely low compared with type II cell. The specific capacitance value is found to be increased about 13771 % with addition of ionic liquid into the polymer matrix. Apart from better interfacial contact, the increment of specific capacitance is attributed to the main feature of ionic liquid. As aforementioned in section 2.3.5.2, ionic liquid is comprised solely of ions. Consequently, higher ion concentration favors the ion migration within the polymer electrolyte and promotes the charge accumulation at the electrolyte–electrode boundary. Eventually, the formation of this electrical double layer increases the capability of energy storage in EDLC. No faradaic process is detected in the figure entailing no redox reaction in the EDLC. In addition, higher operational current also observed in this study. Based on the findings, inclusion of ionic liquid is a successful way to improve the capacitive feature of EDLC.

4.10 Electrochemical Impedance Spectroscopy (EIS)

EIS is a versatile method to assess the electrical behavior of the assembled cells. The information that we can obtain in EIS are:

i) Capacitance of the capacitor cells
ii) Resistances of the capacitor cells
iii) Warburg impedance, if any

Figures 4.27 and 4.28 illustrate the complex impedance plots of type I and type II EDLCs at ambient temperature.

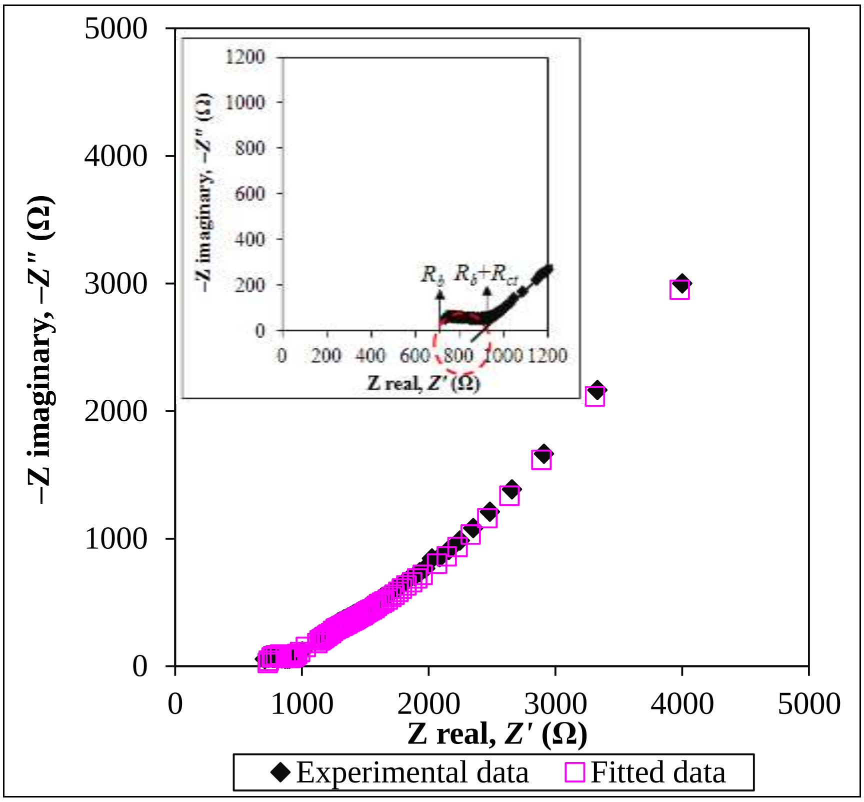

Figure 4.27: Nyquist impedance plot of EDLC containing PVA–CH_3COONH_4 polymer electrolyte at room temperature from 10 mHz to 100 kHz with close–up view of the plot in high frequency region (inset) and its fitted data in CL system.

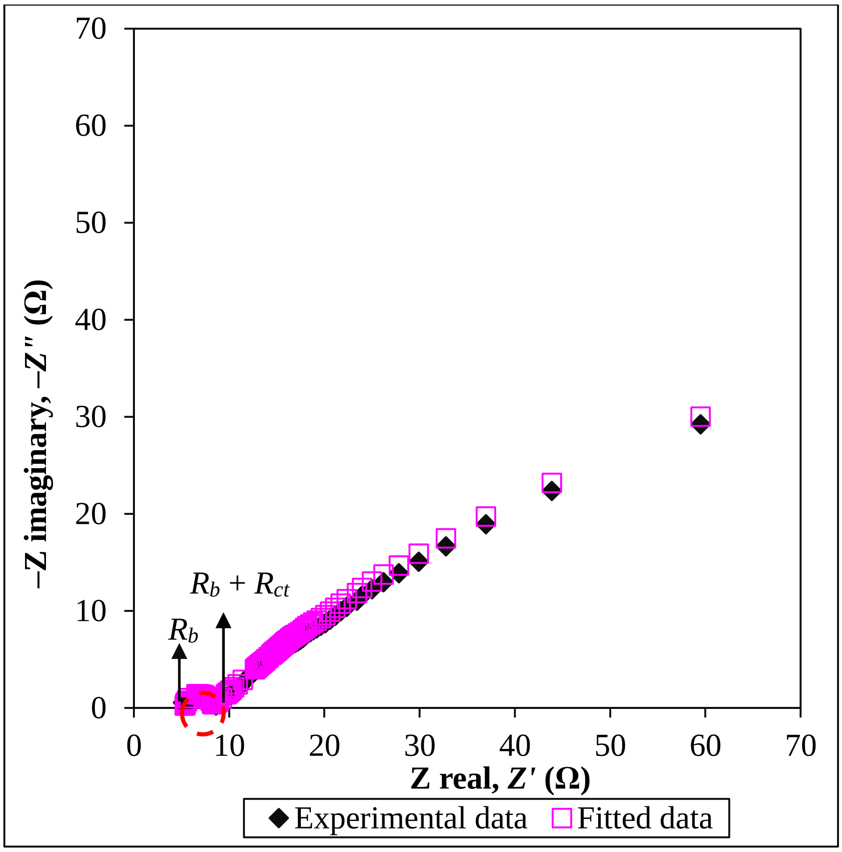

Figure 4.28: Nyquist impedance plot of type II EDLC at room temperature from 10 mHz to 100 kHz and its fitted data in CL system.

Both impedance responses illustrate a spike at low frequency range which is associated with a semicircle at high frequency region (Pandey *et al*., 2010b). The semicircular feature is not so clear in Figure 4.27, so the scale of the plot is enlarged and shown in inset of the figure. The Randles equivalent circuit of EDLC is propose as follows:

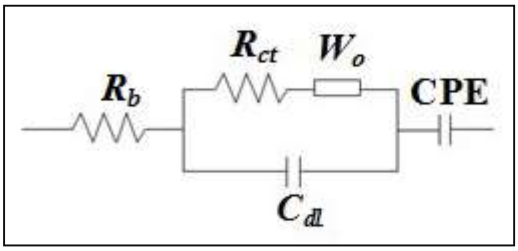

Figure 4.29: The proposed Randles equivalent circuit for EDLC.

The linearly rising pattern (or spike) in the impedance plot reveals the ion adsorption at the electrode–electrolyte boundary and hence indicates the capacitive behavior of EDLC. It can be seen that the experimental data is well–fitted and simulated using the proposed equivalent circuit in both impedance plots. This linear steep rising curve with the phase angle of ~45° indicates the presence of Warburg impedance (W_o) in the equivalent circuit as shown in Figure 4.29. The Warburg resistance is related to the ion diffusion into the porous carbon. This linearly rising pattern denotes the ion adsorption at the surface between carbon–based electrode and polymer electrolyte and leads to the electrical double layer formation. This pattern further proves the capacitive behavior of the EDLC which is represented by the constant phase element of capacitor (CPE) in the Randles equivalent circuit. We found that the impedance plots do not start at the origin point. This phenomenon is suggestive of the presence of a resistance and it is designated as bulk resistance (R_b) of EDLC as displayed in the equivalent circuit of the cell. This resistance is originated from the bulk resistance of polymer electrolyte, series resistance (R_s) of connector and internal resistance of electrode (R_i) for the ion diffusion as well as ohmic loss of the cell (Marcilla *et al*., 2006; Pandey *et al*., 2010b; Wang *et al*., 2014). The spike is then followed by a semicircle in the high frequency range. The semicircle consists of a capacitor and a resistor in parallel form as depicted in the equivalent circuit in Figure 4.29.

The capacitor is represented by the capacitance of double layer (C_{dl}). The C_{dl} comes from the formation of electrical double layer at electrode–electrolyte due to the ion accumulation between electrode and electrolyte when the ions are diffused in the electrolyte and adsorbed into the porous carbon electrode. The resistance is known as charge transfer resistance (R_{ct}) of ion transport from electrolyte to the porous carbon which is one of the bulk behaviors of electrode–electrolyte interface to form the ion adsorption (Wang *et al.*, 2014). This resistance of ion diffusion is the minimum energy required to form the electrical double layer at the electrode–electrolyte boundary. The mobile charge carriers must overcome this resistance in order to perform the ion diffusion and accumulation onto the pores of the carbon electrode. The R_b and R_{ct} are also determined using ZSimpWin software in this present work. The parameters of all the elements in the circuit obtained from the software are tabulated in Table 4.6.

Table 4.6: Simulation results of equivalent circuit elements in EDLCs from the fitted EIS data in CL system.

Element	Type I EDLC	Type II EDLC
Bulk resistance, R_b (Ω)	753	5.3
Double layer capacitance, C_{dl} (μF)	0.02	7.5
Charge transfer resistance, R_{ct} (Ω)	245	4.0
Warburg impedance, W_O ($S.s^5$)	1.3×10^{-3}	0.074
Constant phase element, CPE ($S.s^n$)	1.1×10^{-3}	0.071
Frequency power, n ($0<n<1$)	0.43	0.45

Type I cell displays high bulk resistance that is around 753 Ω, however, this resistance is significantly reduced to 5.3 Ω with doping of ionic liquid into polymer electrolyte for type II supercapacitor. Strong plasticizing effect of ionic liquid is an important contributor in decreasing the bulk resistance of polymer. The ionic mobility and transportation could be enhanced with this low bulk resistance, resulting in higher ionic conductivity. On the contrary, the charge transfer resistance is one of the bulk behaviors of electrode–electrolyte interface. It is defined as a resistance that the charge carriers required to overcome during the charge transfer process from the electrolyte to surface of electrode. It is noteworthy that the charge transfer resistance of type II EDLC is radically improved from 245 Ω to 4.0 Ω upon addition of ionic liquid into the polymer electrolyte. This observation indicates the effective role of ionic liquid in improving the interfacial contact between the electrode and electrolyte. Same explanation can also be applied on the higher value of C_{dl} and CPE elements of equivalent circuit in type II EDLC. The specific capacitance of the cells is then evaluated. As expected, the specific capacitance of type II cell is higher than type I cell. The specific capacitances of 0.13 Fg^{-1} and 18.76 Fg^{-1} are obtained for type I and type II EDLCs, respectively. The results are comparable with the CV findings. Again, the abrupt increase in specific capacitance of type II EDLC is suggestive of the high ion concentration and good adhesion of the electrolyte to electrode, as explained in previous study. Superior electrochemical properties in conjunction with excellent interfacial contact are observed in EDLC comprising of ionic liquid–based polymer electrolyte.

4.11 Galvanostatic Charge–Discharge Performances (GCD)

Galvanostatic charge–discharge experiment can also be done to inspect the electrochemical property of EDLC upon the charge and discharge processes and execute the cyclic durability test. The GCD result of type II supercapacitor is shown in Figure 4.30.

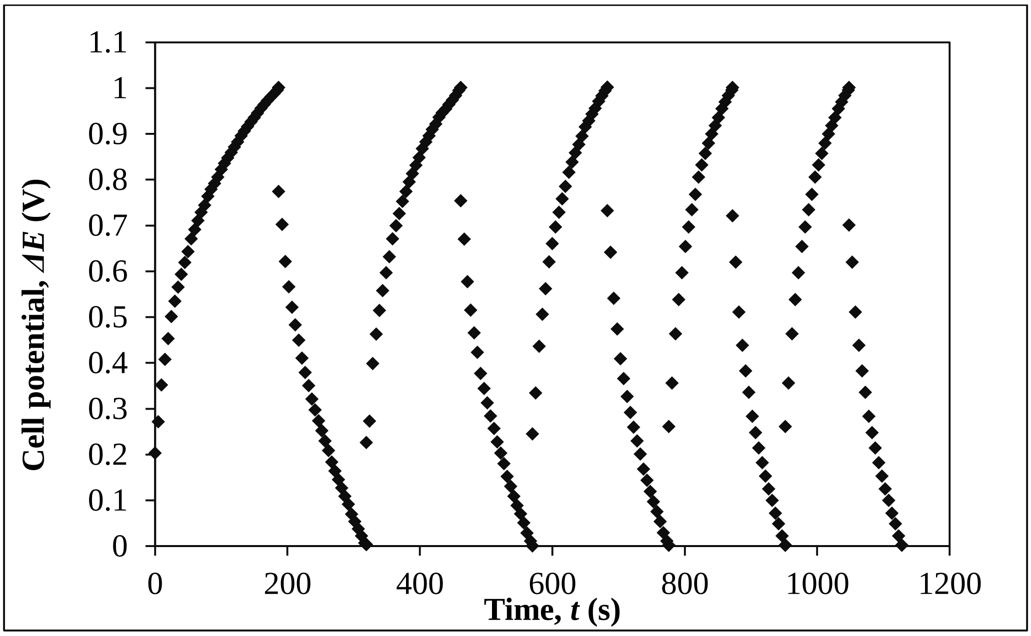

Figure 4.30: Galvanostatic charge–discharge performances of type II cell in CL system over first 5 cycles.

The symmetrical pattern of the charge and discharge behavior in Figure 4.30 implies the superior capacitive nature of EDLC (Amitha *et al*., 2009). As can be seen in Figure 4.30, the potential range of inclined part for charging is between 0.2 V to 1 V. The cell starts to be charged at 0.2 V instead of 0 V because of the internal resistance of the EDLC. Beyond charging process, it is followed with a cell discharge curve. The small drop in the initial part of discharge curve is assigned to the internal resistance of electrochemical capacitors. This ohmic loss arises from electrode and electrolyte, such as charge transfer resistance and bulk resistance of polymer electrolyte (Arof *et al*., 2012; Mitra *et al*., 2001). According to Pandey *et al*., the ohmic loss is also attributed to the depletion of polymer electrolyte (Pandey *et al*., 2010b). The ion migration and accumulation in the electrical double layer could reduce the amount of mobile charge carriers in the polymer membrane causing the depletion. The depletion of polymer electrolytes could increase the cell resistance. This phenomenon is supported by Figure 4.30. The internal resistance of the cell for both charging and discharging curves increase slightly with increasing cycle number. When the cycle number is increased, some ions are more preferred to be paired up rather than be transported into the electrolyte–electrode interface as a result of rapid charge accumulation in the region. This causes the depletion of polymer electrolyte and thereby rises up the internal resistance.

The principle of charging and discharging processes involving ion absorption and desorption is further described in Figure 4.31.

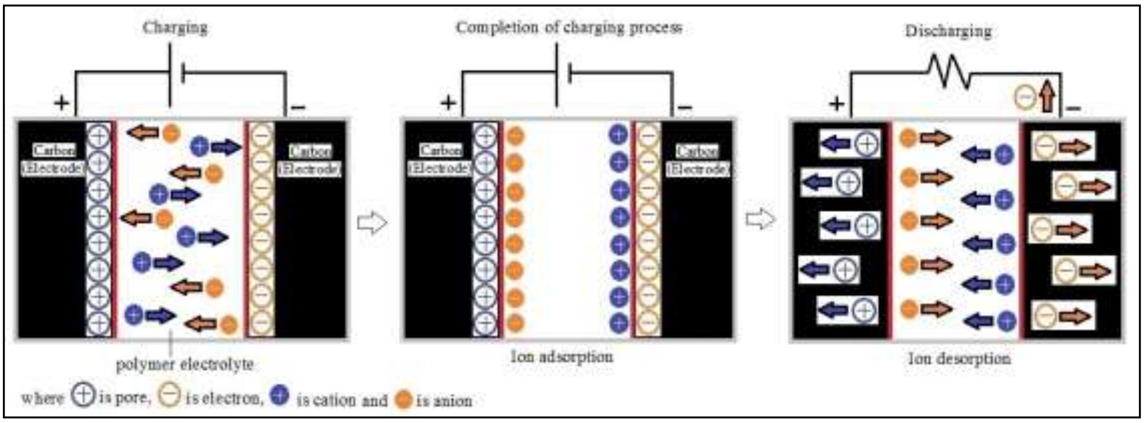

Figure 4.31: Schematic diagrams of charging and discharging processes for a typical EDLC.

When an external electric field is applied, the electrons would be given out and be transferred from positive electrode to negative electrode. The pores that the electrons leave from the activated carbon are considered as positively–charged. The anions from the polymer electrolyte (i.e. acetate anion, CH_3COO^- and chloride, Cl^- in this current project) could be drawn to this positively charged surface at the positive electrode through ion adsorption process when the voltage is applied across the cell. On the other hand, the hydrogen cations (H^+) in the polymer electrolyte are attracted to the negative electrode simultaneously. We suggest that 1–butyl–3–methylimidazolium cation ($BmIm^+$) is very hard to be attached to the electrode due to its bulky size with low ionic mobility. Therefore, only H^+ is available for the charge accumulation at the surface of negative electrode. The cations and anions are thus distributed relative to each other over the distance of the polymer matrix. Eventually, upon the completion of charging electricity process, the accumulation of the charge carriers at both electrodes will lead to the formation of electrical double layer and thereby create the energy storage in EDLC. Conversely, the ions will move away in the discharging process.

The cycle life test is a vital characterization to determine the stability of EDLC in terms of electrochemical performances after charging and discharging processes. Figure 4.32 represents the specific discharge capacitance and Coulombic efficiency of supercpacitor over 500 cycles.

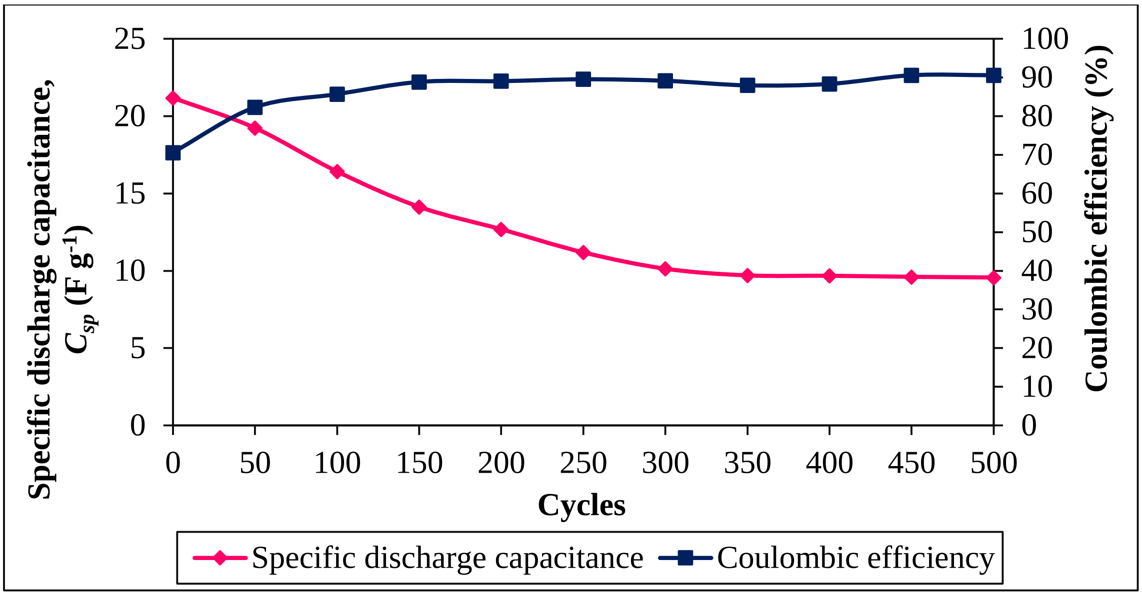

Figure 4.32: Specific capacitance and Coulombic efficiency of type II EDLC in CL system over 500 cycles.

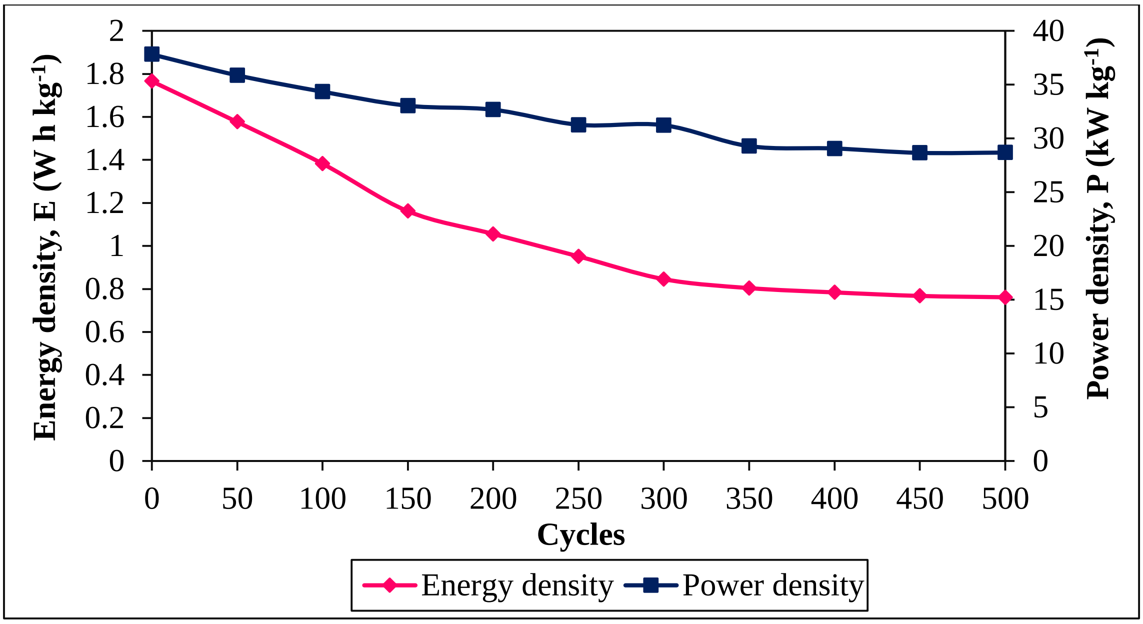

Figure 4.33: Energy density and power density of type II EDLC in CL system over 500 cycles.

The energy and power densities are thus calculated to check the electrochemical performances of EDLCs. The result obtained over 500 cycles is then plotted in Figure 4.33. The initial specific discharge capacitance of 21.19 Fg^{-1} with Coulombic efficiency of 71 % is observed for type II cell as shown in Figure 4.32. This capacitance value is similar with the result obtained in CV and EIS. However, the capacity of cell decreases with cycle number. The energy and power densities also possess the same pattern. The decreases in the electrochemical performance might be due to the depletion of polymer electrolyte. The amount of charge carriers within the polymer membrane is reduced with increasing cycle number. The internal resistance of cell is increased with cycle number as explained as aforesaid. So, the ions requires higher amount of energy to be transported towards the surface of electrode with higher internal resistance. These ions have to overcome this barrier in order to form the electrical double layer in the electrode–electrolyte region. As a result, the capacitive behavior is declined. The specific discharge capacitance is reduced abruptly to 9.56 F g^{-1} with 90 % of Coulombic efficiency upon charge and discharge for 500 cycles. On the other hand, the initial energy density is 1.76 W h kg^{-1}; however it has been reduced to 0.76 W h kg^{-1} in 500th cycles. A drop about 24 % is observed in power density of type II EDLC, from 37.83 kW kg^{-1} to 28.68 kW kg^{-1}, is also observed as shown in Figure 4.33. From both figures, we also observe that the specific capacitance, energy density and power density become almost constant above 400th cycles, suggesting that the ionic liquid–based polymer electrolyte is a best choice as separator in EDLC. The most conducting ionic liquid–based polymer electrolyte is also a promising candidate by maintaining its Coulombic efficiency above 90 % in 500 cycles of charging and discharging. According to the findings, CL 5 is very suitable to be applied in EDLC application as the electrochemical performance has been greatly improved.

4.12 Summary

In conclusion, addition of ionic liquid is a promising way to improve the ionic conductivity of polymer electrolytes and electrochemical properties of fabricated EDLC. The ionic conductivity of these polymer electrolytes is greatly increased with doping of BmImCl due to the strong plasticizing effect and high amorphous nature. The ionic conductivity also increases with mass fraction of ionic liquid, up to a maximum level, which corresponds to inclusion of 50 wt.% of BmImCl. Upon addition of 50 wt% of BmImCl, the highest ionic conductivity of (8.97±0.01) mS cm^{-1} and $(1.14\pm0.01)\times10^{-2}$ S cm^{-1} are achieved at ambient temperature and 120 °C, respectively. The samples obey non–Arrhenius VTF rule as convex upward curved profiles re shown in temperature dependence–ionic conductivity studies. This principle states that the ion transportation mechanism is coupled with highly flexible polymer chain which promotes the ion hopping process. Upon impregnation of BmImCl, the T_g of polymer electrolytes is lowered to sub–ambient value. The decrease in T_g helped in softening the polymer backbone. This most conductive BmImCl–based polymer membrane exhibits better thermal properties than other polymer electrolytes as it is stable up to 250 °C. The temperature of first thermal degradation stage is shifted to higher temperature with doping of salt and ionic liquid due to the complexation.

ATR–FTIR spectra show the interactions between PVA, ammonium acetate and BmImCl and further proved the complexation within the polymer electrolytes. XRD patterns reveal the semi–crystallinity behavior of polymer electrolytes. Among all the samples, the most conducting ionic liquid–added polymer electrolyte has the lowest percentage of crystallinity which is around 19 %, as shown in XRD study. This polymer electrolyte can also be charged up to 4 V, as illustrated in LSV study. Doping of ionic liquid into polymer electrolyte also increased the capacitive nature of assembled EDLC. The specific capacitance of 19.42 F g^{-1} is achieved with better electrochemical characteristic in cyclic voltammogram. The specific capacitance value obtained from impedance spectra (18.76 F g^{-1}) and galvanostatic charge–discharge test (21.19 Fg^{-1}) are also comparable with the result from CV study. Energy density of 1.76 W h kg^{-1} and power density of 37.83 W kg^{-1} are attained for EDLC based on ionic liquid–polymer electrolyte. The inclusion of ionic liquid not only improves the interfacial contact between electrode and electrolyte, but also increases the electrochemical properties of EDLC. Doping of ionic liquid into PVA–based polymer electrolyte is a good prospect for improving the electrochemical performance of an energy storage device.

CHAPTER 5

RESULTS AND DISCUSSION OF BROMIDE (BR) SYSTEM

This chapter reviews the effect of BmImBr onto the polymer electrolytes and EDLCs. The first section discusses the results obtained from all characterization of polymer electrolytes. The electrochemical performances of assembled EDLCs are discussed in the last section.

5.1 Differential Scanning Calorimetry (DSC)

Typical DSC thermograms of ionic liquid–doped polymer electrolytes are displayed in Figure 5.1.

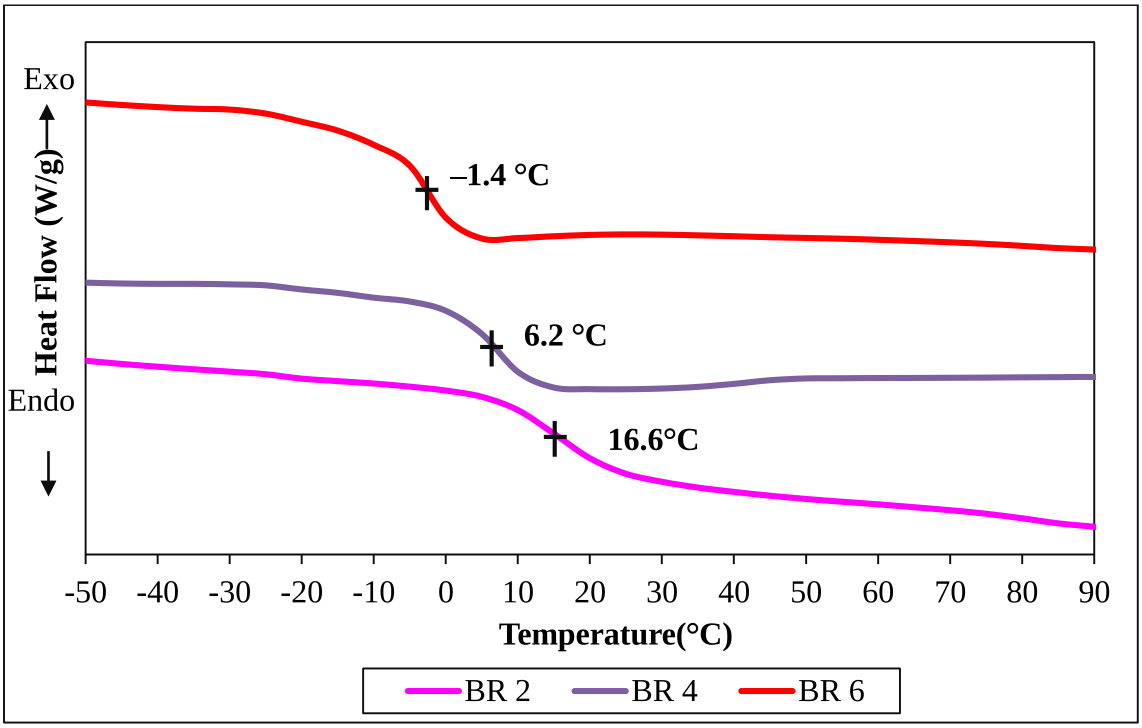

Figure 5.1: Glass transition temperature (T_g) of ionic liquid–added polymer electrolytes in BR system.

The T_g of pure PVA is around 80.2 °C. The T_g of the polymer membrane decreased to 46.6 °C with addition of salt as reported in section 4.2 (Liew *et al.*, 2014b). Similarly, upon doping with ionic liquid, T_g of polymer electrolyte decreased from 46.6 °C to 16.6 °C (BR 2) and 6.2 °C (BR 4), as illustrated in Figure 5.1. The T_g of polymer electrolyte is further reduced to sub–ambient temperature of –1.4 °C with increasing the mass loadings of ionic liquid. Low T_g infers high flexibility of the polymer chains. The reduction of T_g is primarily due to the strong plasticizing effect of ionic liquid. The plasticizing effect weakens the polymer chains and thus improves the flexibility of the polymer electrolytes by softening the polymer backbone. This feature helps in promoting the ionic transportation in the polymer electrolytes.

5.2 Ambient Temperature–Ionic Conductivity Study

Figure 5.2 portrays the ionic conductivity of polymer electrolytes with respect to different mass loadings of BmImBr.

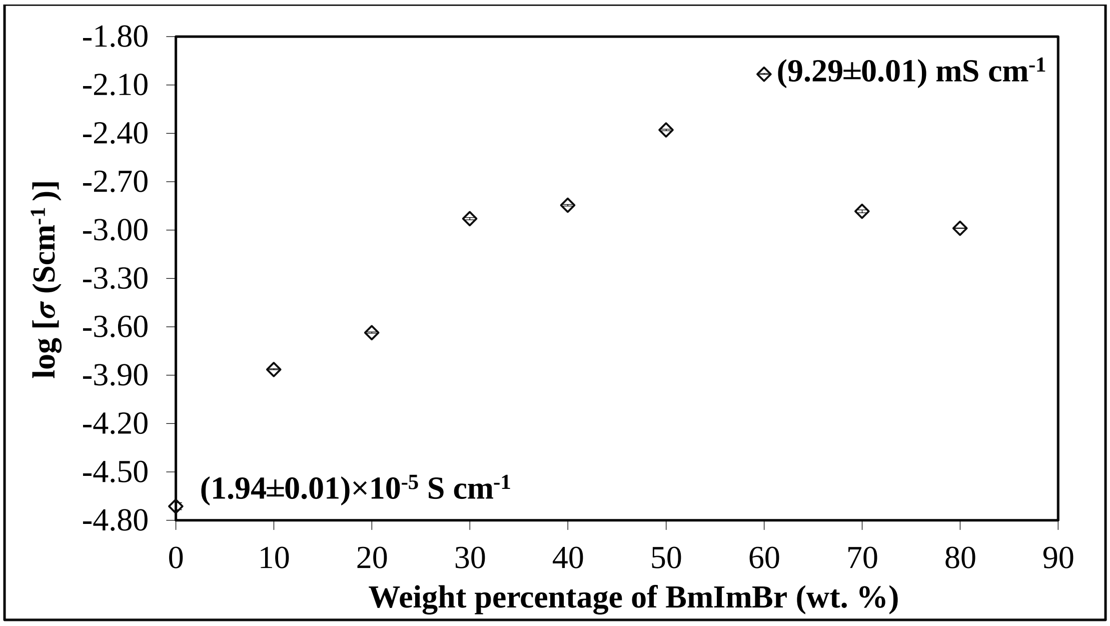

Figure 5.2: The ionic conductivity of polymer electrolytes with different weight fraction of BmImBr.

The ionic conductivity of polymer electrolytes increases with the concentration of ionic liquid, up to a maximum level after which conductivity decreases on further increase of IL concentration. The ionic conductivity of polymer–salt electrolyte has been enhanced by two orders of magnitude, from (1.94±0.01)×10^{-5} S cm^{-1} to (9.29±0.01) mS cm^{-1} with addition of 60 wt% of BmImBr (designated as BR 6). The increment of ionic conductivity is related to the strong plasticizing effect of ionic liquid. This effect not only softens the polymer backbone, but it also helps in producing sticky polymer electrolytes. The softening of polymer matrix could promote the dissociation of charge carriers (or ions) by weakening the coordinative bonds and hence lead to rapid ionic conduction. On the other hand, the sticky behavior of polymer membrane can provide better electrode–electrolyte contact. This feature is very vital in any fabrication of electrochemical device, especially in EDLC where its energy storage arises from the charge accumulation between electrode and electrolyte interface. The inherent physicochemical properties of ionic liquid, i.e. low viscosity and high dielectric constant can be the contributors for high ionic conductivity in the ionic liquid added polymer electrolytes (Kumar *et al.*, 2012). Low viscosity of ionic liquid could produce highly flexible polymer chains and thus improves the ionic mobility of the mobile charge carriers. In contrast, high dielectric constant can shield the cation–anion interaction in the polymer matrix and hence help in dissociating the cations from the attractive bonding with anions (Kumar *et al.*, 2012). As a result, high dielectric constant promotes charge carrier concentration.

The increased ionic conductivity of polymer electrolytes is also correlated to the crystallinity of polymer electrolytes. Addition of ionic liquid can reduce the crystallinity of polymer electrolytes. Large amorphous phase promotes the ionic transportation in the polymer electrolytes as the mobility of charge carriers in amorphous regions is higher than crystalline regions. Ionic liquid is also an additive to improve the amorphous region. We suggest that ionic liquid could break the coordination bonds among the molecules and hence disrupt the ordered chain structure. As a result, disordered arrangement of macromolecules with a random coil configuration is obtained. However, the polymer electrolytes become less conductive at high mass fraction of ionic liquid. Formations of ion pairs and ion aggregates contribute to this phenomenon. These ion pairs and ion aggregates would impede the ionic transportation within the polymer electrolytes. The mechanical stability of polymer electrolytes is extremely low above addition of 80 wt.% of BmImBr.

5.3 Temperature Dependent–Ionic Conductivity Study

Figures 5.3 and 5.4 depict the temperature dependent plot of ionic conductivity of ionic liquid–free polymer electrolyte and ionic liquid–added polymer electrolytes fitted with Arrhenius relationship ranging from room temperature until 120 °C.

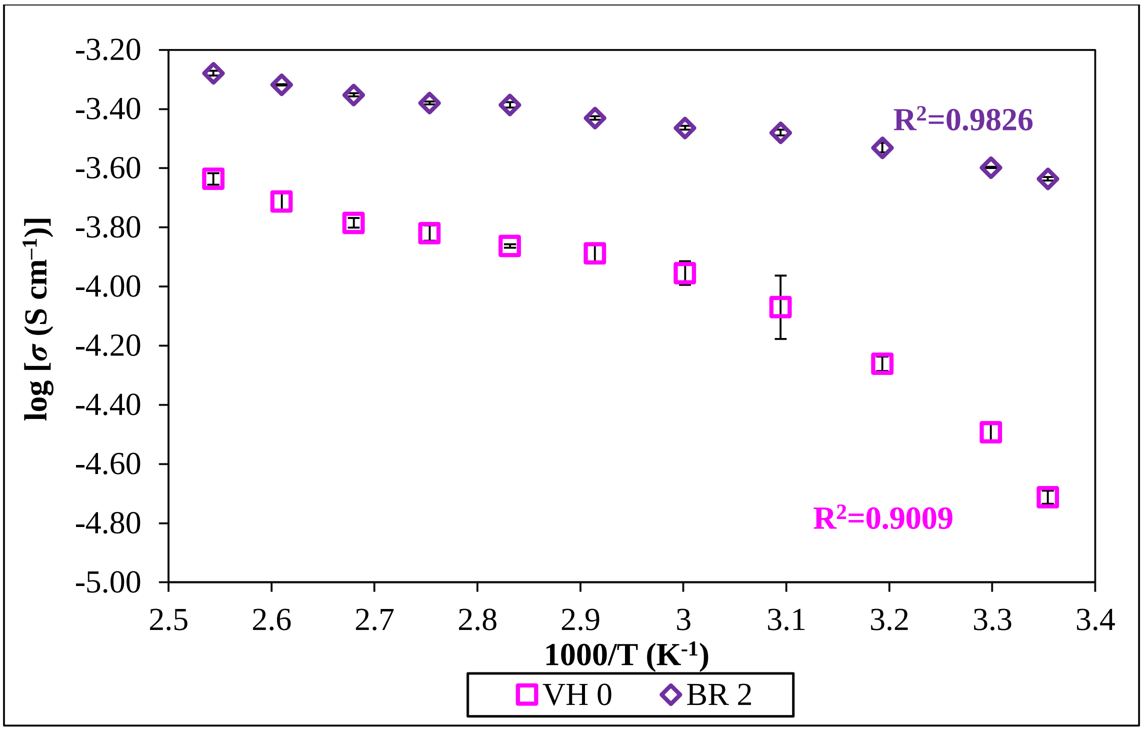

Figure 5.3: The temperature–dependent plot of VH 0 and BR 2 fitted with Arrhenius equation.

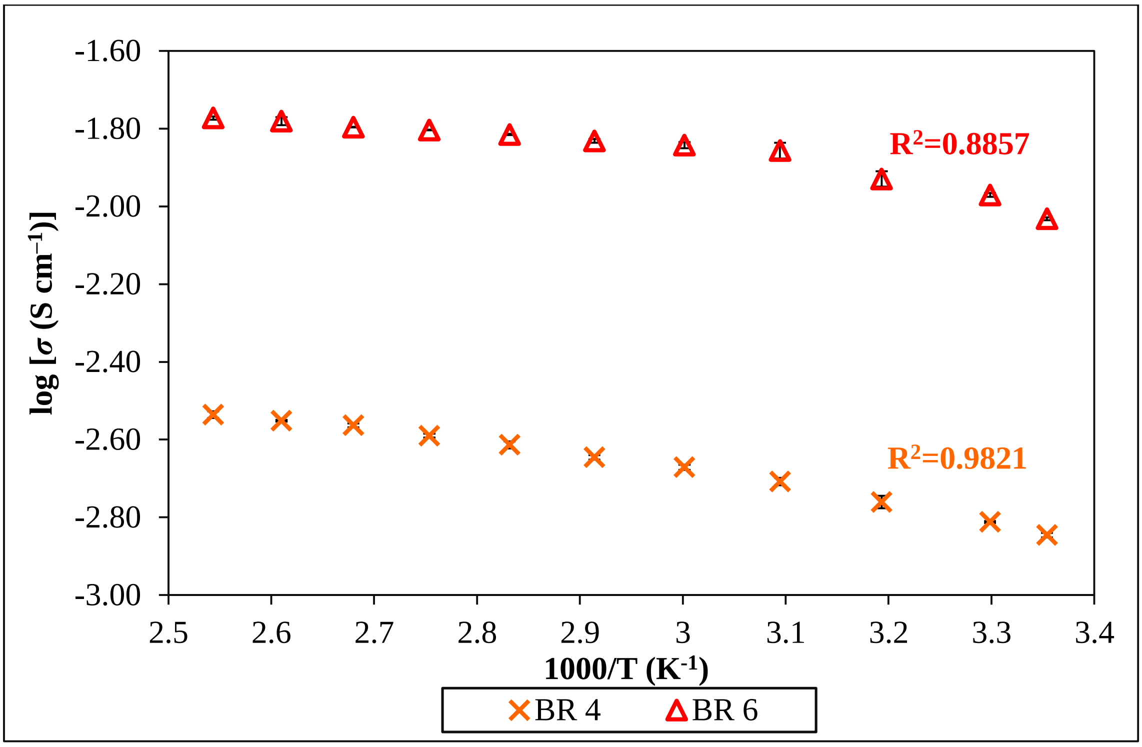

Figure 5.4: The temperature–dependent plot of BR 4 and BR 6 fitted with Arrhenius equation.

The curvature pattern of temperature plots is observed in both figures where the regression value of all the temperature dependent plots is deviated from unity. So, the Arrhenius theory cannot be applied in the ionic dynamics mechanism of these polymer electrolytes. Thus, the plots are fitted using free volume–based Vogel–Tamman–Fulcher (VTF) theory as illustrated in Figure 5.5.

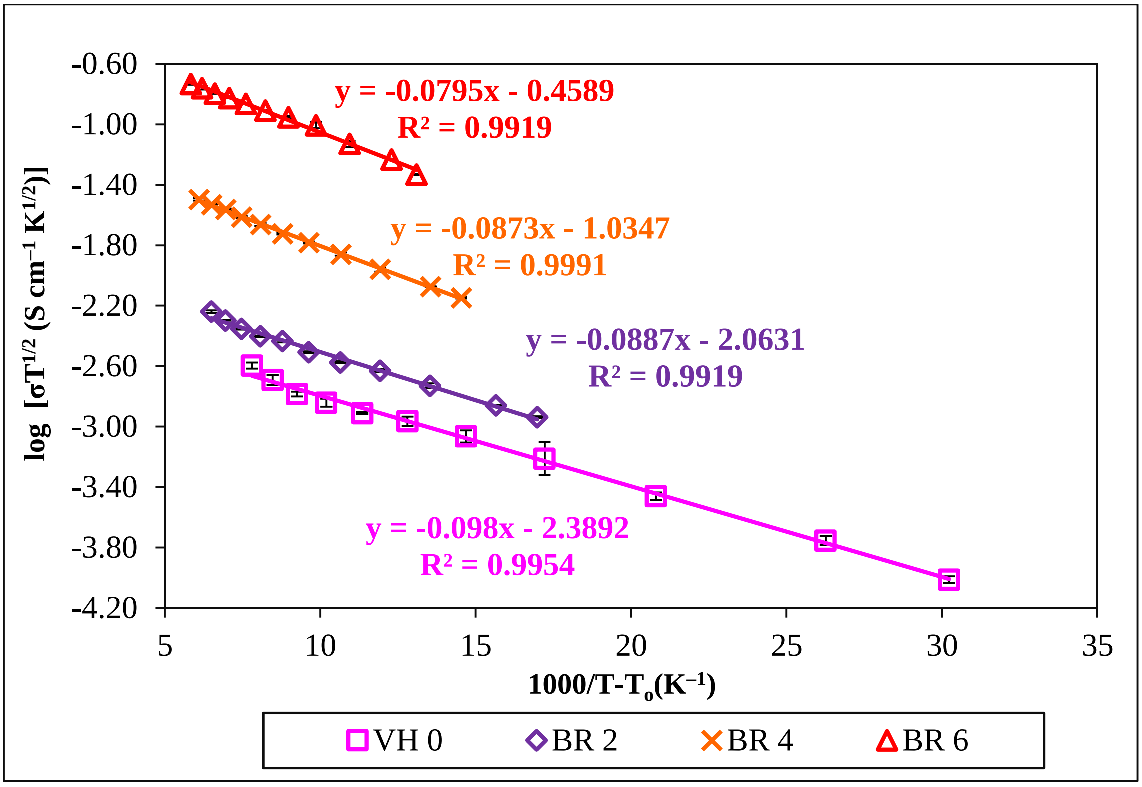

Figure 5.5: The VTF theory–based temperature–dependent plot of polymer electrolytes in BR system.

The highest ionic conductivity of (1.69±0.01)×10^{-2} S cm^{-1} is achieved at 120 °C. All the plots in Figure 5.5 demonstrate well–fitted pattern using the least squares method. So, the ion conduction mechanism obeys VTF empirical rule. The VTF theory implies that the ionic hopping mechanism is coupled with high segmental mobility in an amorphous phase. The ionic conductivity of polymer electrolytes increases with temperature as can be seen in the figure. The macromolecules would vibrate vigorously at elevated temperature. The rapid vibration of the molecules could increase the segmental mobility and create more free spaces for the ionic transportation. Therefore, the mobile ions can hop from one site to adjacent empty site of the highly flexible polymer chains.

All the parameters in VTF equation are determined from the plots. The results are summarized in Tables 5.1 and 5.2.

Table 5.1: The obtained parameters from each VTF plot with the experimental glass transition temperature from DSC thermogram in BR system.

Sample	Regression value, R^2	Glass transition temperature, T_g (K)	Ideal glass transition temperature, T_o (K)
VH 0	0.99	319.73	269.73
BR 2	0.99	289.25	239.25
BR 4	0.99	279.36	229.36
BR 6	0.99	271.77	221.77

Table 5.2: The obtained parameters from each VTF plot in BR system.

Sample	Log A_o	Pre–exponential constant, A_o (mS cm^{-1} K$^{1/2}$)	Gradient of the plot, B (K^{-1})	Pseudo–activation energy, E_a (meV)
VH 0	–2.3892	4.08×10^{-3}	0.0980	8.44
BR 2	–2.0631	8.65×10^{-3}	0.0887	7.64
BR 4	–1.0347	0.09	0.0873	7.52
BR 6	–0.4589	0.35	0.0795	6.85

The A_o proportional to the number of charge carriers increases with mass fraction of ionic liquid. This observation denotes that addition of ionic liquid can weaken the polymer backbone and dissociate the charge carriers. This effect becomes more obvious with increasing the weight percent of ionic liquid. We suggest that BR 6 achieves the highest ionic conductivity due to the largest amount of charge carriers compared to other ionic liquid–added polymer electrolytes. This is supported by A_o value obtained from the VTF plots. On the contrary, E_a is decreased as increases the weight ratio of ionic liquid. The decrement of E_a indicates that inclusion of ionic liquid reduces the energy required for the ion dissociation and bond reformation because of its strong plasticizing effect. The unique characteristic of ionic liquid can enhance the flexibility of polymer chains and hence decrease the energy barrier of charge carriers for ionic hopping mechanism.

5.4 Thermogravimetric Analysis (TGA)

Figure 5.6 describes the TGA curves of VH 0, BR 2, BR 4 and BR 6. The TGA curve of PVA is not explained in this section as it had been reported in our previous chapter.

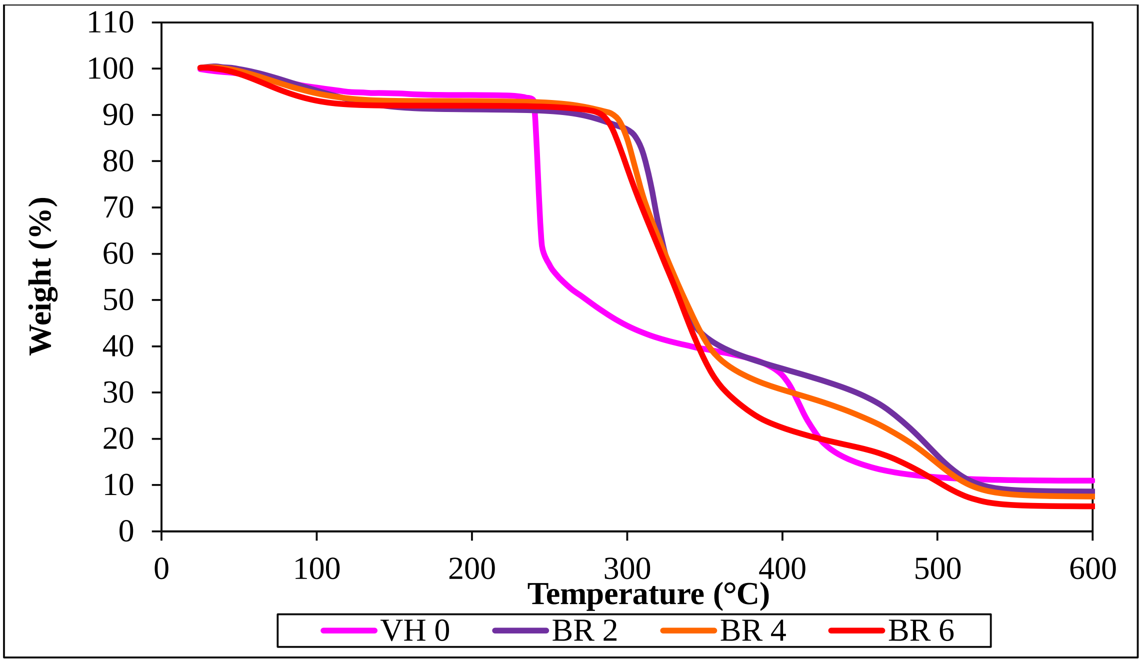

Figure 5.6: Thermogravimetric analysis of VH 0, BR 2, BR 4 and BR 6.

Four degradation steps are observed in all ionic liquid–added polymer electrolytes. The initial weight loss is assigned to the evaporation of water, elimination of trapped moisture and removal of impurities. VH 0, BR 2, BR 4 and BR 6 exhibit the respective mass losses of 5 %, 9 %, 7 % and 8% in the temperature range of 25–150 °C. The mass of polymer electrolytes remains stable above this dehydration stage until an abrupt drop in mass is observed subsequently. VH 0 and BR 2 start to decompose at 240 °C and 250 °C with mass losses of 32 % and 47 %, respectively. However, the degradation temperature range of BR 4 and BR 6 has been extended to 260–355 °C and 275–360 °C. The mass loss at this stage also increased to 54 % and 59 % for BR 4 and BR 6, respectively. This is attributed to the decomposition of PVA and ammonium acetate. Ether cross–linkages between the macromolecules could be formed as a result of water elimination. The chain stripping process on these cross–linkages can remove the side chain of PVA and induce weight loss at this stage, as shown in Figure 4.13. Besides, we suggest that the weight loss is attributed to the degradation of acetamide ($CH_3C(O)NH_2$), which is formed by the dehydration of ammonium acetate. Since Lee *et al*. reported that the decomposition temperature of BmImBr is 252 °C, we imply that the cause of this mass loss is due to the decomposition of BmImBr in the ionic liquid–added polymer electrolytes (Lee *et al*., 2010). This idea is supported by higher mass loss obtained in thermogram of ionic liquid–added polymer electrolytes than VH 0 and pure PVA. It is also noted that the degradation temperature of ionic liquid added polymer electrolytes is slightly higher than pure PVA and the ionic liquid–free polymer electrolyte. This is indicative of the complexation between PVA, ammonium acetate and BmImBr as higher energy is required to break these interactive bonds.

Beyond this mass loss, another two gradual drops in mass are observed. VH 0 displays around 20 % of mass loss from 245 °C until 375 °C, whereas BR 2 shows 11 % mass loss and its degradation temperature regime is between 345 and 420 °C. BR 4 and BR 6 have respective mass losses of 13 % and 12 % within the degradation temperature of 355 to 440 °C. The latter mass loss is the final weight loss before the samples have been fully decomposed. VH 0 and BR 2 start to lose 27 % and 25 % mass, along with 11 % and 8 % residual mass at 375 °C and 410 °C respectively. Upon further addition of ionic liquid, the mass loss in the final stage is improved. BR 4 exhibits around 19 % of mass loss with the remaining mass of 7 % at 440 °C. Mass loss of 14 % with 5 % of residue is observed for BR 6 at 435 °C. These two mass losses are strongly related to chemical degradation processes in the polymer chains such as random chain scissoring between carbon–carbon bonds and disruption of double bond in polyene of the polymer backbone (Liew *et al.*, 2014b). The mass of the polymer system remains stable above 550 °C. This finding infers the complete decomposition of the polymer membrane. BR 6 is a promising candidate as polymer electrolyte as it achieves the highest first degradation temperature.

5.5 Attenuated Total Reflectance–Fourier Transform Infrared (ATR–FTIR)

Figures 5.7 (a)–(e) depict the ATR–FTIR spectra of BmImBr, VH 0, BR 2, BR 4 and BR 6, respectively, whereas Table 5.3 summarizes the assignment of all vibration modes of VH 0, BR 2, BR 4 and BR 6. The spectrum of the most conducting ionic liquid–added polymer electrolyte (denoted as BR 6) is discussed in details.

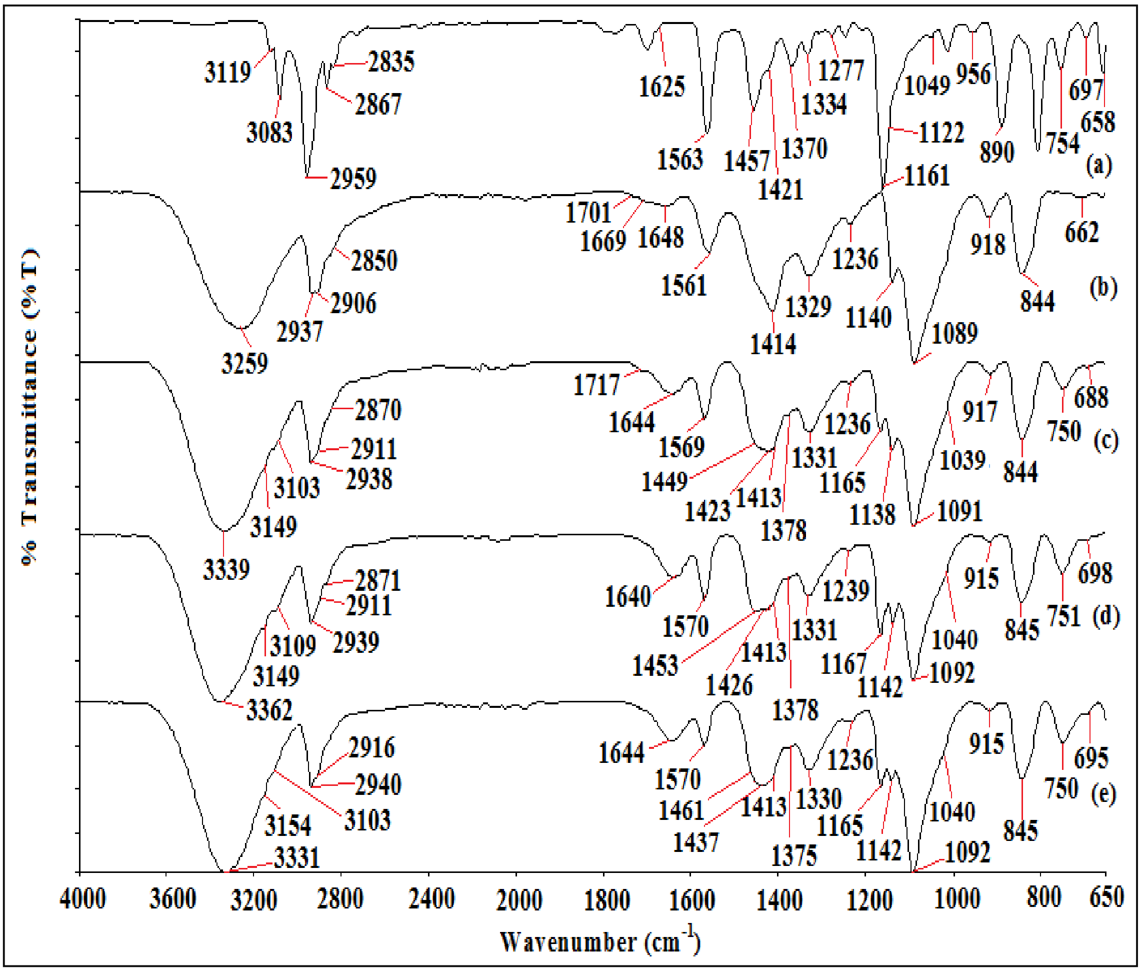

Figure 5.7: ATR–FTIR spectra of (a) BmImBr, (b) VH 0, (c) BR 2, (d) BR 4 and (e) BR 6.

Table 5.3: The assignments of vibration modes of VH 0, BR 2, BR 4 and BR 6.

Descriptions of vibration modes	**Wavenumber (cm^{-1})**				
	BmImBr	**VH 0**	**BR 2**	**BR 4**	**BR 6**
C–H bending mode of CH_3COONH_4	–	662	–	–	–
C–Br stretching mode	658	–	–	–	–
C–H vibrational mode for cyclic $BmIm^+$	697, 3119	–	688, 3149	698, 3149	695, 3154
C–H bending mode for cyclic $BmIm^+$	754	–	750	751	750
Skeletal C–H rocking mode of PVA	–	844	844	845	845
In–plane C–H bending mode of imidazolium ring	890	–	–	–	–
O–H bending mode of PVA	–	918	917	915	915
In–plane C–N–C bending mode	956	–	–	–	–
Out–of–plane C–H wagging mode in alkyl chain	1049	–	1039	1040	1040
C–O stretching mode of PVA	–	1089	1091	1092	1092
C–H bending mode in methyl group	1122	–	–	–	–
C–C and C–O stretching mode of doubly H–bonded OH in crystalline region of PVA	–	1140	1138	1142	1142

Table 5.3, continued

Descriptions of vibration modes	**Wavenumber (cm^{-1})**				
	BmImBr	**VH 0**	**BR 2**	**BR 4**	**BR 6**
CH_3–N stretching mode	1161	–	1165	1167	1165
C–O stretching mode of PVA and CH_3COONH_4	–	1236	1236	1239	1236
C–N stretching mode of imidazolium ring	1277	–	–	–	–
CHOH bending mode, CH_3 in–plane deformation and C–H wagging mode of PVA	–	1329	1331	1331	1330
CH_2 symmetric bending mode	1334	–	–	–	–
CH_3 asymmetric stretching mode	1370	–	1378	1378	1375
C–H deformation mode of PVA	–	1414	1413	1413	1413
CH_3 asymmetric bending mode	1421	–	1423	1426	1437
CH_3 symmetric bending mode	1457	–	1449	1453	1461
C=N stretching mode	1563	–	1569	1570	1570
N–H bending mode of CH_3COONH_4	–	1561	1569	1570	1570
C–H stretching mode of PVA	–	1648	1644	1640	1644
–CONH– bonding mode of CH_3COONH_4	–	1669	–	–	–
C–C and C–N bending mode of imidazolium ring	1625	–	–	–	–
C=O stretching mode of CH_3COONH_4	–	1701	1717	–	–
C–H symmetric stretching mode in methyl group of alkyl chain	2835 2867, 2959	2850, 2906, 2937	2870, 2911, 2938	2871, 2911, 2939	2916, 2940
=C–H stretching mode	3083	–	3103	3109	3103
O–H stretching vibration mode of OH group of PVA	–	3259	3339	3362	3331

There are new 10 peaks formed upon addition of BmImBr by comparing Figure 5.7 (b) with (e). These peaks are C–H vibrational mode for cyclic BmIm$^+$ at 695 cm^{-1} and 3154 cm^{-1}, C–H bending mode for cyclic BmIm$^+$ at 750 cm^{-1}, out–of–plane C–H wagging mode in alkyl chain of BmIm$^+$ at 1040 cm^{-1}, CH_3–N stretching mode of BmIm$^+$ at 1165 cm^{-1}, CH_3 asymmetric stretching mode of BmIm$^+$ at 1375 cm^{-1}, CH_3 asymmetric bending mode of BmIm$^+$ at 1437 cm^{-1}, CH_3 symmetric bending mode of BmIm$^+$ at 1461 cm^{-1}, C=N stretching mode of BmIm$^+$ at 1570 cm^{-1} and =C–H stretching mode of BmIm$^+$ at 3103 cm^{-1}. The formation of new peaks indicates that the ionic liquid has complexed with PVA–CH_3COONH_4 in the polymer membrane. On the other hand, some characteristic peaks of VH 0 are disappeared with adulteration of BmImBr. These peaks include weak peaks at 662 cm^{-1} and 2850 cm^{-1}. The former peak is ascribed to C–H bending mode of

CH_3COONH_4, whereas the latter peak is one of the C–H symmetric stretching modes in methyl group of alkyl chain of PVA. The disappearance of the peaks divulges the interaction between the C–H bond of the polymer backbone and ionic liquid which induces to proton hopping mechanism. The disappearance of CONH bonding mode of CH_3COONH_4 at 1669 cm^{-1} infers the salt dissociation into ammonium cations and acetate anions. In addition, the absence of the weak peak at 1701 cm^{-1} (which is designated as C=O stretching mode of CH_3COONH_4) indicate that carbonyl functional group also contributes to the proton transportation in the polymer complexes.

Similarly, some peaks are absent when we compare BR 6 spectrum with BmImBr spectrum. The absence of the medium sharp peak at 658 cm^{-1} denotes the dissociation of ionic liquid into $BmIm^+$ and Br^- as this peak is referred as C–Br stretching mode. The hydrogen at C2–position of mobile $BmIm^+$ is initially decoupled from the cations to form carbene as illustrated in Figure 4.4 (Liew *et al.*, 2014a). This deprotonation is supported by the absence of some characteristic peaks. These peaks are the strong peak at 890 cm^{-1} which is denoted as in–plane C–H bending mode of imidazolium ring, the shoulder peak at 1122 cm^{-1} which is named as C–H bending mode in methyl group of imidazolium ring, the weak peak at 1334 cm^{-1} which is entitled as CH_2 symmetric bending mode of imidazolium ring and shoulder peak at 2835 cm^{-1} which is referred as C–H symmetric stretching mode in methyl group of alkyl chain. In addition, this deprotonation could affect the C–N–C coordination bond in the imidazolium ring, for example the in–plane C–N–C bending mode which is located at 956 cm^{-1}, C–N stretching mode of imidazolium ring at 1277 cm^{-1} and C–C and C–N bending mode of imidazolium ring at 1625 cm^{-1}. All the characteristic peaks are missing when the BmImBr are incorporated into the polymer matrix.

Apart from that, some characteristic peaks undergo the changes in shape, changes in shift and changes in peak intensity. A sharp peak is observed at 1561 cm^{-1} and ascribed to skeletal N–H bending mode, as shown in Figure 5.8 (a). Upon addition of ionic liquid, this sharp peak not only shifts to higher wavenumber to 1570 cm^{-1}, but it also undergoes the change in intensity, that is from 6.56 % to 3.65 %, in transmittance mode, as depicted in Figure 5.8.

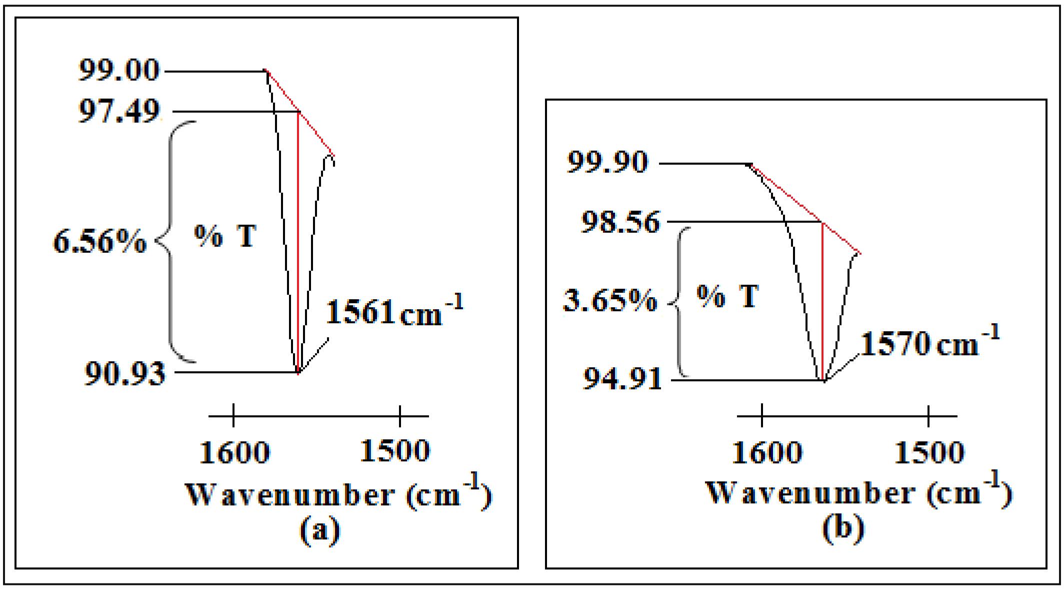

Figure 5.8: The change in peak intensity of skeletal N–H bending mode of (a) VH 0 and (b) BR 6 in the wavenumber region of 1600–1500 cm^{-1}.

The cause of upward shift is suggestive of the overlapping of C=N stretching mode of BmIm^{+} with skeletal N–H bending mode of ammonium acetate at 1563 cm^{-1}. The sharp peak at 844 cm^{-1} corresponding to skeletal C–H rocking mode also shifts to higher wavenumber to 845 cm^{-1}. However, this peak exhibits decrease in peak intensity from 11.28 % to 8.68 %, in transmittance mode. Similar observation has also been obtained at 1329 cm^{-1} with peak intensity of 4.67 % which is referred as the combinations of CHOH bending mode, CH_3 in–plane deformation and C–H wagging mode of polymer–salt complex. The intensity of this broad peak is reduced slightly to 3.72 % at 1330 cm^{-1} by adding ionic liquid into the polymer matrix. The decrease in peak intensity and upward shift reveal the interaction between PVA, CH_3COONH_4 and BmImBr and further indicate that the proton migration takes place at CHOH bonding of polymer backbone, as mentioned in our previous chapter. On the other hand, some characteristic peaks exhibit downward shift when we add ionic liquid into the polymer complexes. These peaks are

O–H bending mode of PVA at 918 cm^{-1} (to 915 cm^{-1}) and C–H stretching mode at 1648 cm^{-1} (to 1644 cm^{-1}). The former peak shows reduction from 3.35 % to 0.69 %, in term of intensity, whereas the latter peak illustrates increment from 0.43 % to 3.08 %. This signifies the proton hopping mechanism in the polymer matrix. Although the C–O stretching mode of polymer matrix remains unchanged at 1236 cm^{-1}, addition of ionic liquid reduces the peak intensity of this weak peak from 1.44 % to 0.62 %.

Moreover, changes in peak shape are observed on some vibration modes. Polymer electrolyte without addition of ionic liquid portrays a sharp peak at 1089 cm^{-1} and a shoulder peak at 1140 cm^{-1} in the wavenumber region between 1200 cm^{-1} and 1000 cm^{-1} in Figure 5.9 (a).

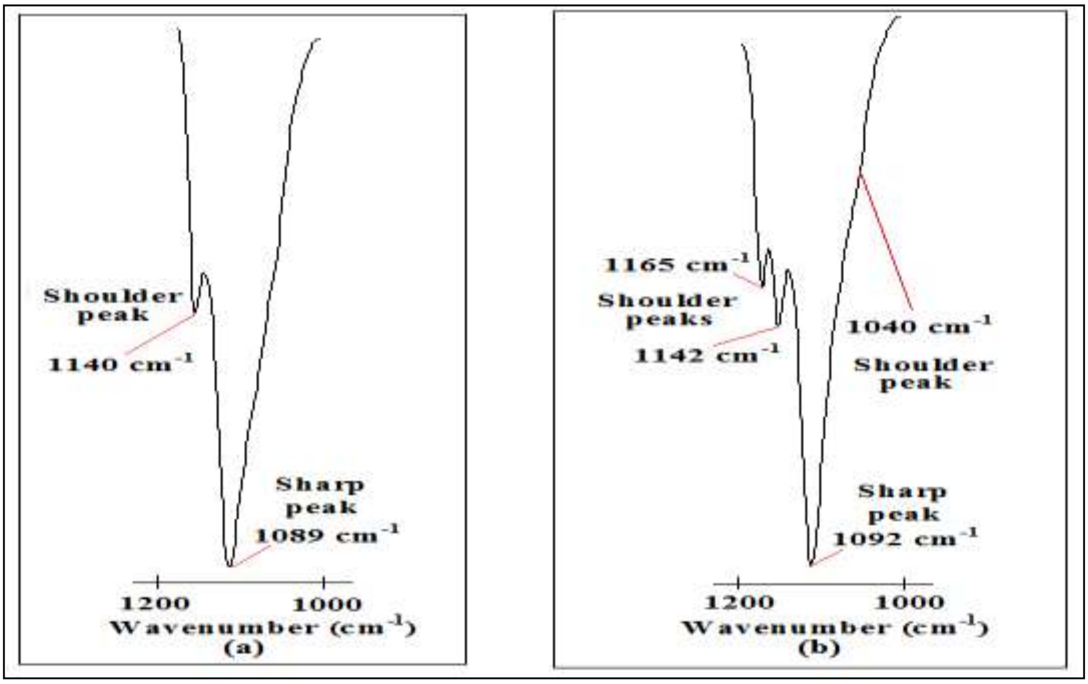

Figure 5.9: The change in peak shape of vibration modes of (a) VH 0 and (b) BR 6 in the wavenumber region between 1200 cm^{-1} and 1000 cm^{-1}.

Both of these peaks are related to the C–O stretching mode of PVA. The shoulder peak is referred as C–C and C–O stretching mode of doubly H–bonded OH in crystalline region. A sharp peak with three shoulder peaks are thus evolved in the wavenumber regime with incorporation of ionic liquid, as depicted in Figure 5.8 (b). Both sharp and shoulder peaks exhibit upward shift to 1092 cm^{-1} and 1142 cm^{-1}, respectively. However, the peak intensity of both peaks is reduced from 15.33 % to 12.28 % and from 5.57 % to 2.06 %, in transmittance mode, respectively. We propose that the new shoulder peak formed at 1040 cm^{-1} is out–of–plane C–H wagging mode in alkyl chain of BmIm^{+}, whereas the weak peak formed at 1165 cm^{-1} is CH_3–N stretching mode of BmIm^{+}. This idea can be proven using deconvolution technique. All the peaks in this region are fitted and deconvoluted as shown in Figure 5.10.

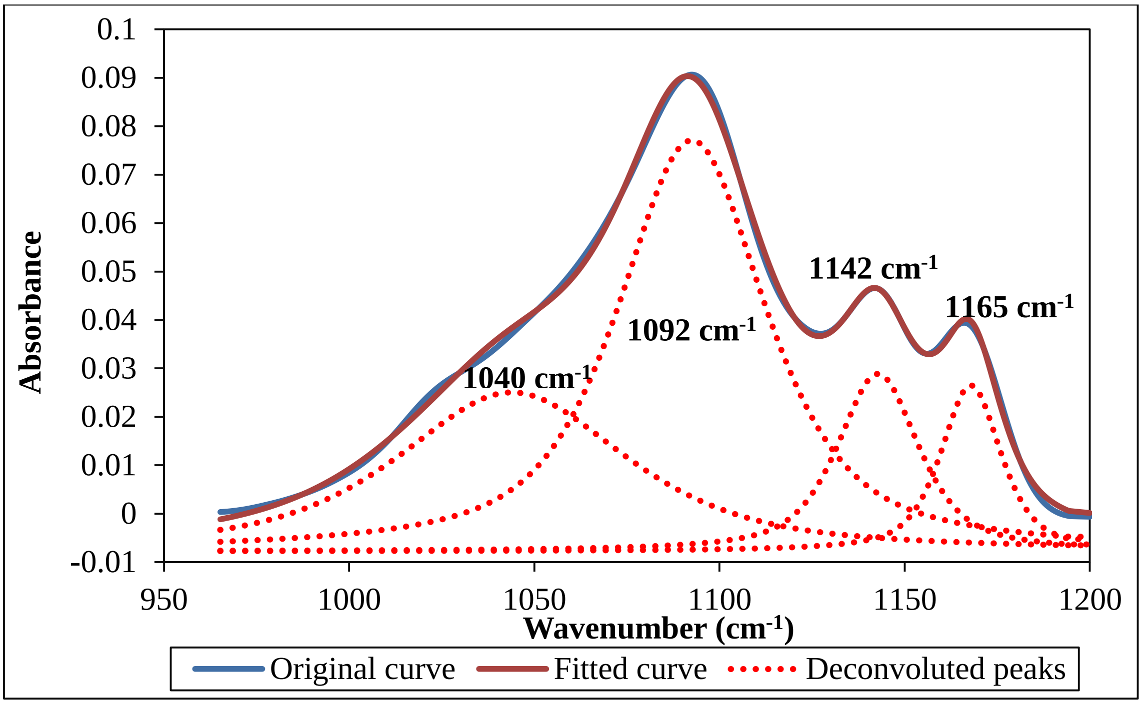

Figure 5.10: The original and fitted curves with the deconvoluted peaks of BR 6 in the wavenumber region between 1200 cm^{-1} and 960 cm^{-1}.

Four peaks have been attained with extreme low standard error of the curve fitting in Figure 5.10. The peak location from FTIR spectra is in good agreement with the peak position from deconvoluted peaks. The change in shape proves that the carbene formed after deprotonation of BmIm^{+} could interact with hydroxyl group of PVA. Therefore, the proton transportation takes place at the C–O functional group of the polymer matrix. An obvious change in shape is also observed in the range between 1500 cm^{-1} and 1350 cm^{-1}. We found out that the sharp peak corresponding to C–H deformation mode of PVA at 1414 cm^{-1} is turned into a broad band with a shoulder peak which is located at 1375 cm^{-1} by adding ionic liquid into PVA–CH_3COONH_4, as exemplified in Figure 5.11.

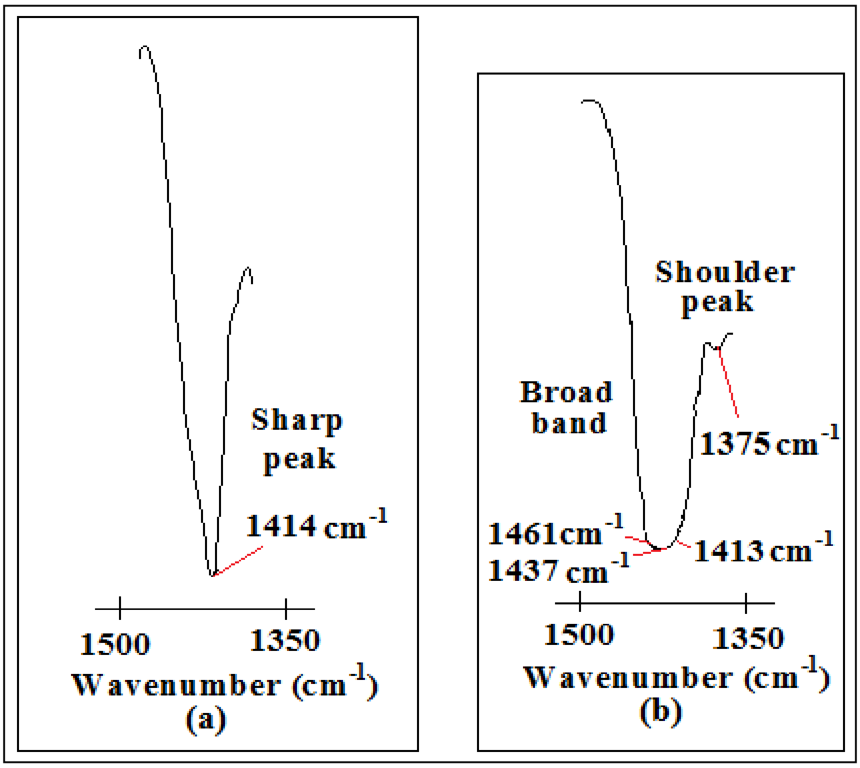

Figure 5.11: The change in peak shape of vibration modes of (a) BmImBr and (b) BR 6 in the wavenumber region between 1500 cm^{-1} and 1350 cm^{-1}.

Since a broad band is obtained, we couldn’t define the peak clearly due to the overlap of few peaks. Therefore, the deconvolution method is employed to detect each peak in the broad band. This broad band consists of three main peaks at 1413 cm^{-1}, 1437 cm^{-1} and 1461 cm^{-1}, as demonstrated in Figure 5.12.

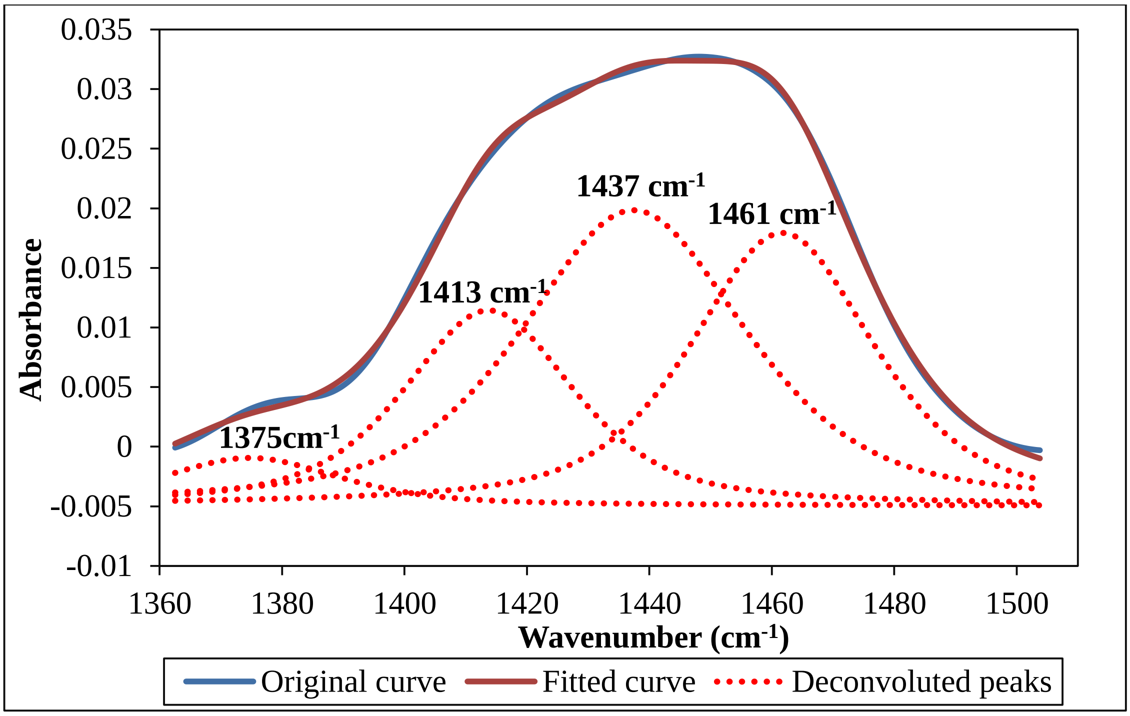

Figure 5.12: The original and fitted curves with the deconvoluted peaks of BR 6 in the wavenumber region between1500 cm^{-1} and 1360 cm^{-1}.

The shoulder peak at 1375 cm^{-1} belongs to CH_3 asymmetric stretching mode of $BmIm^+$, meanwhile the three peaks are C–H deformation mode of PVA–CH_3COONH_4 (at 1413 cm^{-1}), CH_3 asymmetric bending mode (at 1437 cm^{-1}) and CH_3 symmetric bending mode of $BmIm^+$ (at 1461 cm^{-1}). The overlapping of these peaks discloses the complexation between PVA, CH_3COONH_4 and BmImBr.

Change in shape is also observed at higher wavenumber. For example, the double peaks at 2906 cm^{-1} and 2937 cm^{-1} in the wavenumber between 2950 cm^{-1} and 2900 cm^{-1}. Both of these peaks are designated as C–H symmetric stretching mode in methyl group of alkyl chain of PVA. These double peaks are developed into a medium sharp peak at 2940 cm^{-1} and a shoulder peak at 2916 cm^{-1} upon addition of ionic liquid. The former peak shows a gradual increase in intensity from 2.02% to 2.92 %, meanwhile the latter peak illustrates an abrupt decrease in intensity from 1.22 % to 0.13 %. The overlapping of C–H symmetric stretching mode of PVA and $BmIm^+$ contributes to the changes in peak shape, changes in peak location and changes in peak intensity. VH 0 depicts a broad peak at 3259 cm^{-1} where its designation is O–H stretching vibration mode of OH group of PVA. This broad peak is shifted to higher wavenumber of 3331 cm^{-1} with two additional shoulder peaks at 3103 cm^{-1} and 3154 cm^{-1}. The shoulder peak at lower wavenumber is assigned to =C–H stretching mode of $BmIm^+$, whereas the shoulder peak at higher wavenumber is named as C–H vibrational mode for cyclic $BmIm^+$. The change in shape implies the interaction between $BmIm^+$ and hydroxyl group of PVA through the complexation. Based on the findings, we can conclude that the BmImBr has complexed with PVA and CH_3COONH_4.

The increase in ionic conductivity with the mass loadings of ionic liquid is due to the decrease of the crystallinity of the polymer matrix, as aforementioned in section 5.2. This idea can be supported by the FTIR result. The C–C and C–O stretching mode of doubly H–bonded OH in crystalline region is ought to focus in order to study the effect of degree of crystalline region in the polymer electrolytes. All the vibration modes of BR 6 can be found in the spectra of BR 2 and BR 4. Upon addition of 20 wt.% of BmImBr, the characteristic peak is shifted to lower wavenumber, that is from 1140 cm^{-1} to 1138 cm^{-1}. The peak moves upwards to 1142 cm^{-1} for BR 4 and BR 6. However, other trend is observed in term of peak intensity. The peak intensity is decreased rapidly with addition of ionic liquid and is further declined with increasing the concentration of ionic liquid. There is a significant drop from 5.57 % to 2.40 %, 2.22 % and 2.06 % for BR 2, BR 4 and BR 6, respectively. Since the extent of the peak divulges the degree of crystalline portion in the polymer electrolytes, so it can be concluded that BR 6 has the least crystallinity compared to others ionic liquid–added polymer electrolytes.

5.6 X–ray Diffraction (XRD)

Figure 5.13 portrays XRD diffractogram of BmImBr, ionic liquid–free polymer electrolyte and ionic liquid–added polymer electrolytes.

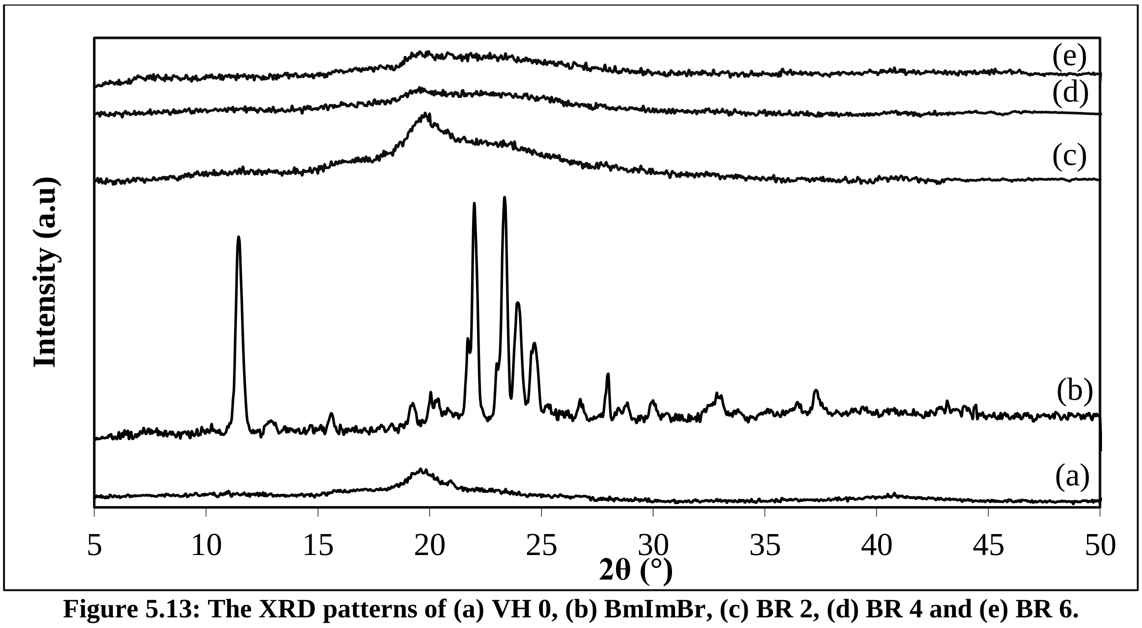

Figure 5.13: The XRD patterns of (a) VH 0, (b) BmImBr, (c) BR 2, (d) BR 4 and (e) BR 6.

A crystalline sharp peak is located at 2θ=19.7°, whereas a hump is located at 2θ=22.7° with a small broad peak at 2θ=40.8° as depicted in XRD pattern of VH 0. BmImBr shows nine crystalline peaks at the 2θ angles of 11.5°, 22°, 23.4°, 24°, 24.7°, 26.7°, 28°, 32.9°

and 37.3° in Figure 5.13 (b). Similarly, the characteristic peaks of ionic liquid are disappeared in all ionic liquid–added polymer electrolytes. Even though none of the characteristic peaks of ionic liquid is observed, but the characteristic peaks of PVA still exists in XRD patterns of all ionic liquid–added polymer electrolytes. The ionic liquid is fully dissolved in the polymer solution as the characteristic peaks of ionic liquid are absent.

BR 2 demonstrates a crystalline peak at 2θ=19.7° with a shoulder hump at 2θ=23.7° along with a weak peak at 2θ=40.9°. On the other hand, different peak shape is observed in the range of Bragg angle, 2θ from 19° to 30° when we increase the mass fraction of ionic liquid. Double peaks are observed instead of a sharp peak with a broad hump along with lower peak shifts at Bragg angle. BR 4 illustrates its first peak at 2θ=19.5° and second peak at 2θ=22.7°, whereas BR 6 depicts the peaks at 2θ=19.6° and 22.3°. The small peaks at around 2θ=40° are hardly be found in the XRD diffractogram because of the low peak intensity. Nevertheless, this small peak still exists in XRD patterns of BR 4 at 2θ=40.9° and BR 6 at 2θ=40.8°. Curve fitting and deconvolution methods are implemented to verify the peak formation. The proof showing there are only 3 peaks in BR 6 has been shown in Figure 5.14.

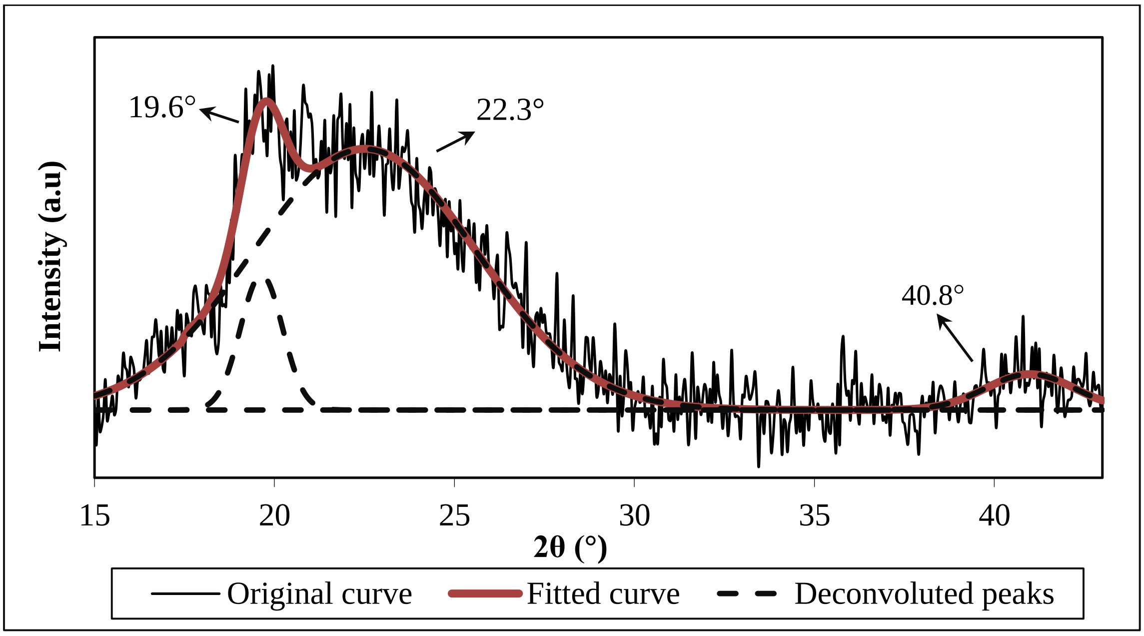

Figure 5.14: XRD pattern of BR 6 with fitted curve and deconvoluted peaks within the range of Bragg angle, 2θ of 15–43°.

The XRD pattern of BR 6 is well–fitted and deconvoluted using Gaussian mode as exemplified in Figure 5.14.

Crystallinity of polymer electrolytes is an important parameter to govern the ionic conductivity of polymer electrolytes as aforementioned in section 5.2. The degree of crystallinity of polymer electrolytes can be determined from XRD studies by calculating the area under the crystalline peak and area under the curves of all the peaks using deconvolution method. The relevant parameters are listed in Table 5.4.

Table 5.4: The relevant parameters obtained from the curve fitting in XRD findings in BR system.

Sample	Area under the curve of the crystalline peak, I_c	Total area under the curves of all the peaks, I_t	Percentage of crystallinity (χ_c) %
VH 0	1669	5366	31
BR 2	868	5895	15
BR 4	215	2349	9
BR 6	135	1610	8

The percentage of crystallinity of polymer salt complexes is 31 %. The crystallinity of polymer electrolytes is also decreased upon addition of ionic liquid. BR 2 manifests the crystallinity of 15 %, whereas BR 4 has the crystallinity of 9 %. Lower degree of crystallinity of BR 6 is observed in comparison to BR 2 and BR 4 that is only 8 %.

5.7 Linear Sweep Voltammetry (LSV)

The LSV curve of most conductive polymer electrolyte (assigned as BR 6) is shown in Figure 5.15.

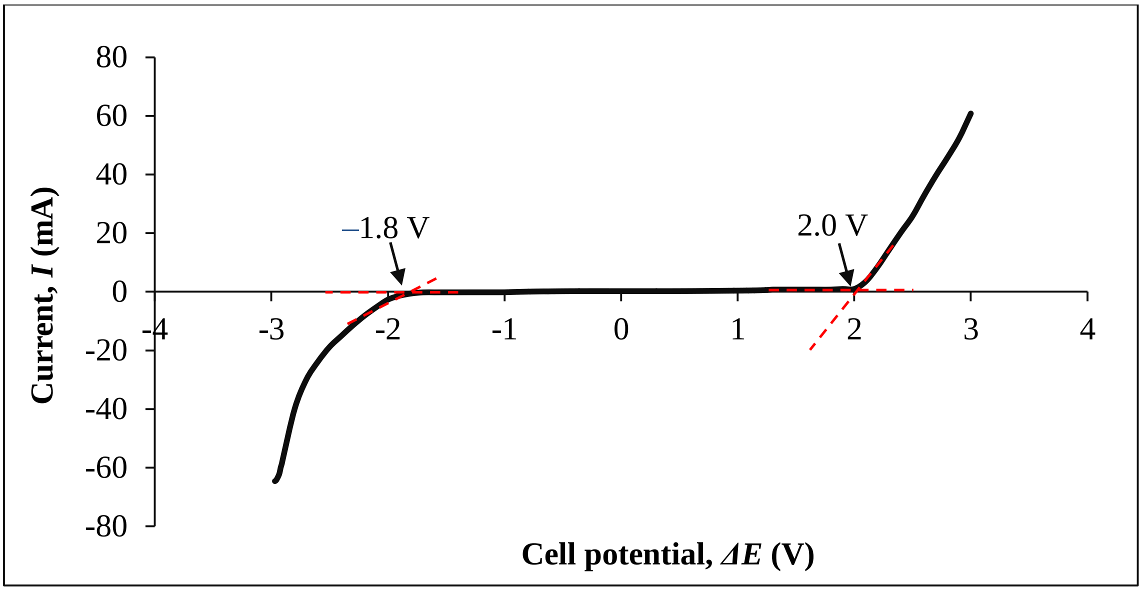

Figure 5.15: LSV response of BR 6.

The potential window range of VH 0 is around 3.3 V, starting from –1.6 V to 1.7 V, as demonstrated in Figure 4.23. However, the operational potential window of ionic liquid added polymer electrolyte is wider. The cell can be charged up to 3.8 V in the regime between –1.8 V and 2 V. This observation reveals that the ionic liquid doping can improve the electrochemical stability window of the polymer matrix.

5.8 Cyclic Voltammetry (CV)

Figure 5.16 depicts cyclic voltammetry of type II EDLC using the most conductive polymer electrolyte in BR system.

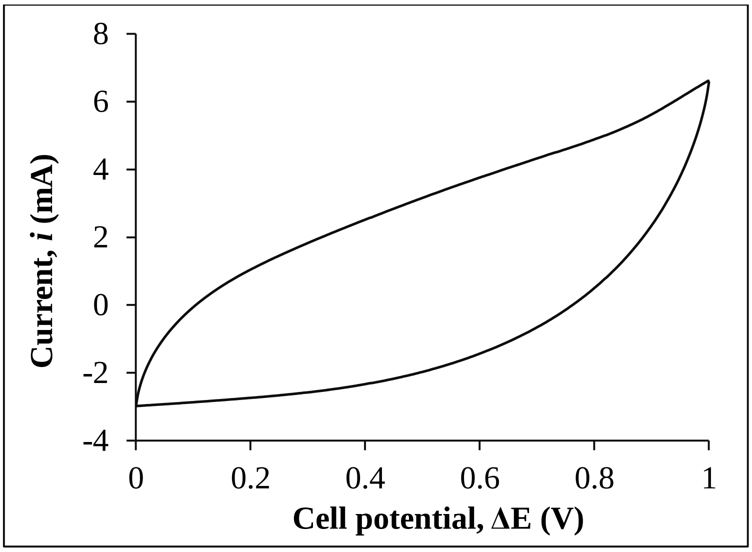

Figure 5.16: Cyclic voltammograms of type II EDLC containing PVA–CH_3COONH_4–BmImBr–polymer electrolyte.

Redox peak from a Faradic current is absent in both figures inferring the non–Faradic reaction in the EDLC. In other words, the energy storage of the EDLC is based on the ion absorption at the electrode–electrolyte interface without presence of any chemical reaction. Type I EDLC shows a leaf–like shape CV curve with specific capacitance of 0.14 Fg^{-1} (or equivalent to 1.5 mF cm^{-2}) in Figure 4.25. However, the specific capacitance of type II EDLC has been enhanced drastically upon inclusion of ionic liquid into the polymer electrolyte. The CV curve of type II EDLC demonstrates a voltammogram approaching ideal box–like shape with specific capacitance value of 21.89 F g^{-1} (or equivalent to 0.2650 Fcm^{-2}). This increment of around 15535 % in specific capacitance is owing to the high ionic conductivity of polymer electrolyte as a result of plasticizing effect and high ion content of ionic liquid, as mentioned in section 5.2.

For a conductive polymer electrolyte, the amount of mobile ions transporting within the medium could be higher with enhanced mobility. This theory explains why ionic liquid–added polymer electrolytes have higher specific capacitance. Therefore, more free ions are drifted from an electrode to another electrode and hence absorbed onto the carbon pores forming charge accumulation at the electrode–electrolyte region. This charge accumulation is well–known as electrical double layer. The energy could be stored when the voltage is applied across the circuit. Moreover, better electrode–electrolyte contact in the ionic liquid added polymer electrolyte is another reason causing higher capacitance in type II EDLC. These mobile ions require lower energy barrier to overcome the resistance of forming ion absorption at the interface when the contact between electrode and electrolyte is intimate. Consequently, the ions are more easily to be absorbed onto the carbon–based electrodes. This effect promotes the formation of electrical double layer and ultimately leads to increase in capacitive behavior of EDLC.

5.9 Electrochemical Impedance Spectroscopy (EIS)

Figure 5.17 illustrates the EIS impedance plot of EDLC containing the most conducting ionic liquid–added polymer electrolyte in BR system along with its Randle’s equivalent circuit. The simulation results using the proposed equivalent circuit are listed in Table 5.5.

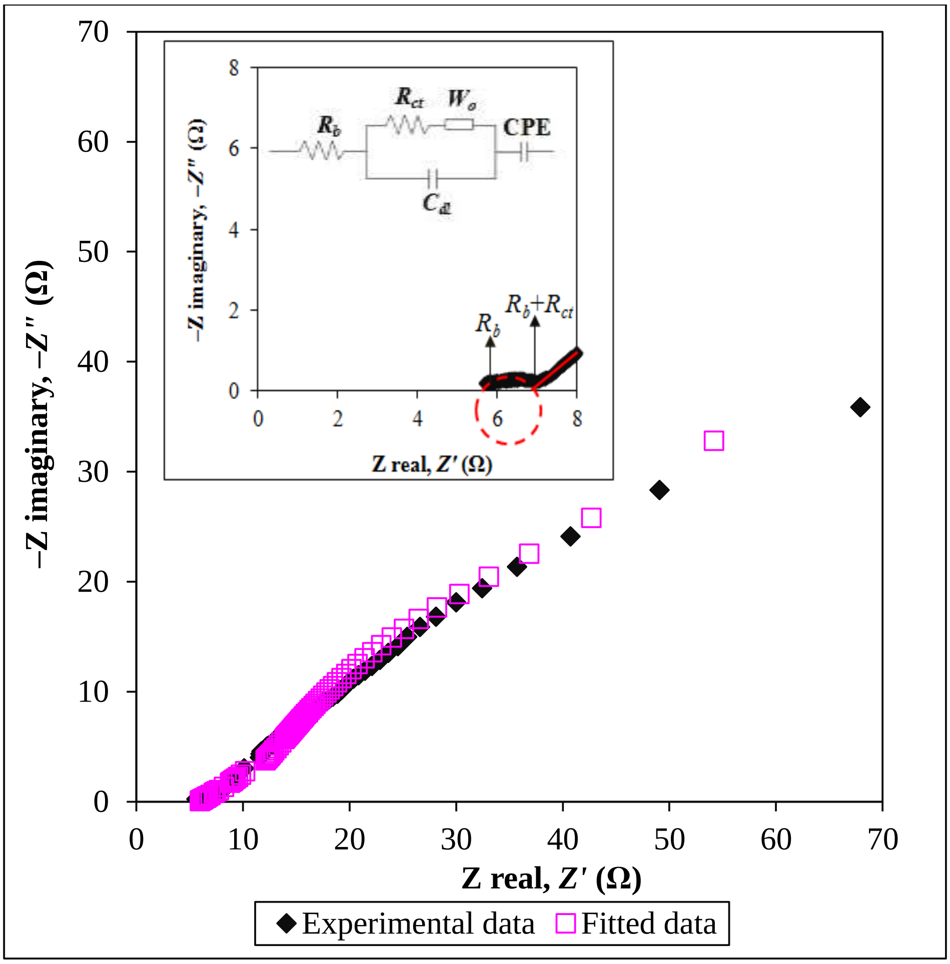

Figure 5.17: Nyquist impedance plot of type II EDLC containing the most conducting polymer electrolyte in BR system at room temperature from 10 mHz to 100 kHz with close–up view of the plot in high frequency region (inset) and its fitted data.

Table 5.5: Simulation results of equivalent circuit elements in EDLCs from the fitted EIS data in BR system.

Element	Type I EDLC	Type II EDLC
Bulk resistance, R_b (Ω)	753	5.5
Double layer capacitance, C_{dl} (μF)	0.02	29.6
Charge transfer resistance, R_{ct} (Ω)	245	1.6
Warburg impedance, W_O ($S.s^5$)	1.3×10^{-3}	0.06
Constant phase element, CPE ($S.s^n$)	1.1×10^{-3}	0.057
Frequency power, n ($0<n<1$)	0.43	0.45

The experimental data is well–fitted as can be seen in Figure 5.17. The R_b values obtained in type I and type II EDLCs are 753 Ω and 5.5 Ω, respectively. On the other hand, the respective R_{ct} values of type I and type II EDLCs are 245 Ω and 1.6 Ω. The resistance of type II EDLC is relatively lower than that of type I EDLC. Sticky behavior of the ionic liquid added polymer electrolyte is the main factor to lower the resistance in this phenomenon. This inherent property could provide excellent interfacial contact between electrode and electrolyte. The ions require lower energy to be transported within the polymer matrix when the polymer electrolyte possesses low resistance barrier. Rapid mass transport within the pores of porous activated carbon based electrode also decreases the charge transfer resistance. Again, we observe that the C_{dl} and CPE of type II EDLC have higher value than type I EDLC. These findings prove that addition of ionic liquid can improve the ion diffusion in the electrolyte and thus promote the ion adsorption at the electrode–electrolyte boundary.

The specific capacitance of type I EDLC obtained in EIS is around 0.13 F g^{-1}. However, the specific capacitance of type II EDLC has been increased abruptly to 21.63 F g^{-1} by doping ionic liquid into the polymer electrolyte. The result is in good agreement with CV findings. Conductive behavior of ionic liquid added polymer electrolyte is the main contributor for enhancing the capacitance of EDLC, as explained in previous section. The charge carriers can be dissociated easily from the polymer complex when ionic liquid is added into the matrix. Thus, the polymer backbone could turn into flexible chain. Therefore, the number of ions and ionic mobility are increased thereafter which leads to higher ion absorption onto the electrodes. Another reason of higher capacitance of type II EDLC is the sticky and adhesive properties of ionic liquid–added polymer electrolyte. Based on the result, it reflects the effect of addition of ionic liquid on the capacitive behavior of EDLC.

5.10 Galvanostatic Charge–Discharge Performances (GCD)

Figure 5.18 shows the galvanostatic charge–discharge performance of type II EDLC over 5 cycles of charging and discharging.

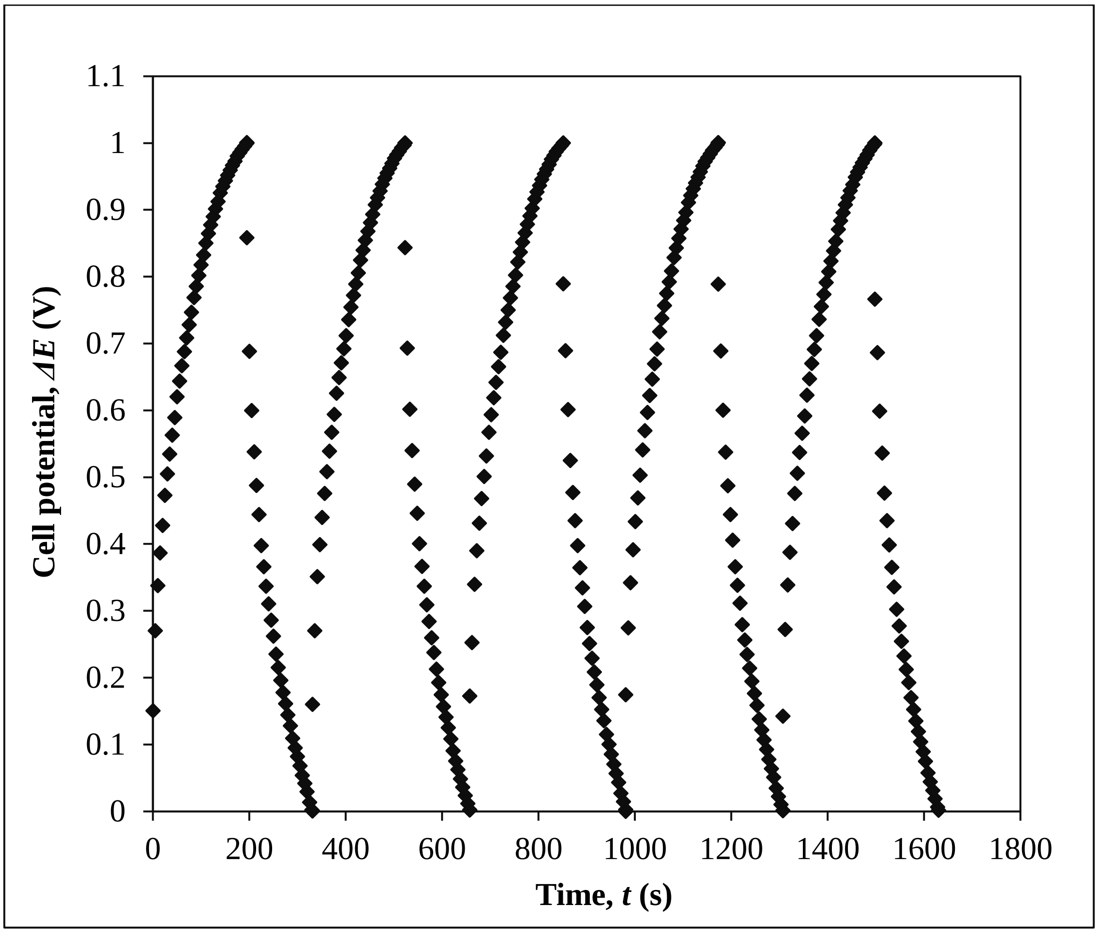

Figure 5.18: Galvanostatic charge–discharge performances of type II cell in BR system over first 5 cycles.

The starting cell potential of EDLC during charging process is 0.15 V instead 0 V, meanwhile the cell potential starts at 0.85 V instead of 1 V for discharging process. These phenomena are associated with the internal resistance of the cell. Factors that cause the ohmic loss of the EDLC are interfacial resistance between electrolyte and electrode, interfacial resistance between current collector and active material, and resistances of electrolyte, active materials and connector. It is noteworthy that the internal resistance of the cell increases somewhat with cycle number, as described in Figure 5.18. We suggest that the ions might form the neutral ion pairs due to the rapid charge adsorption onto the carbon at high cycle number. Therefore, the mobile charge carriers transported into the electrolyte–electrode interface become lesser and lead to the depletion of polymer electrolyte.

The specific discharge capacitance, Coulombic efficiency, energy density and power density of the electrochemical cell obtained in the first cycle are 21.38 Fg^{-1}, 70 %, 2.18 W h kg^{-1} and 41.27 kW kg^{-1} respectively. The specific discharge capacitance is similar with the results obtained in CV and EIS studies. The electrochemical stability of the EDLC is further analyzed by subjected the performance over 500 cycles. The long–term cyclability tests of type II EDLC are revealed in Figures 5.19 and 5.20.

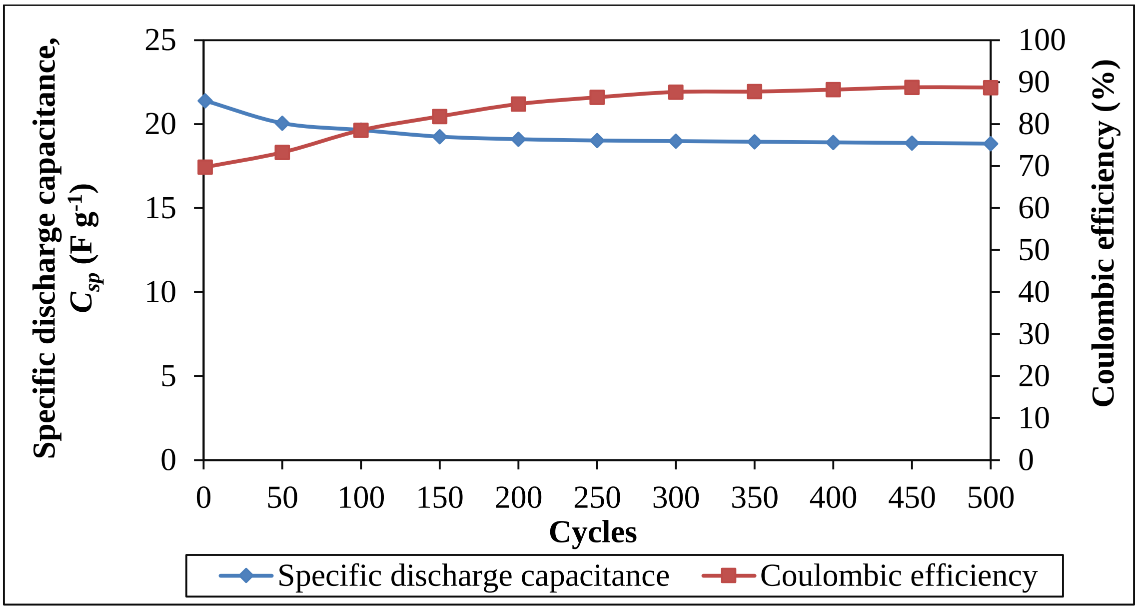

Figure 5.19: Specific capacitance and Coulombic efficiency of type II EDLC in BR system over 500 cycles.

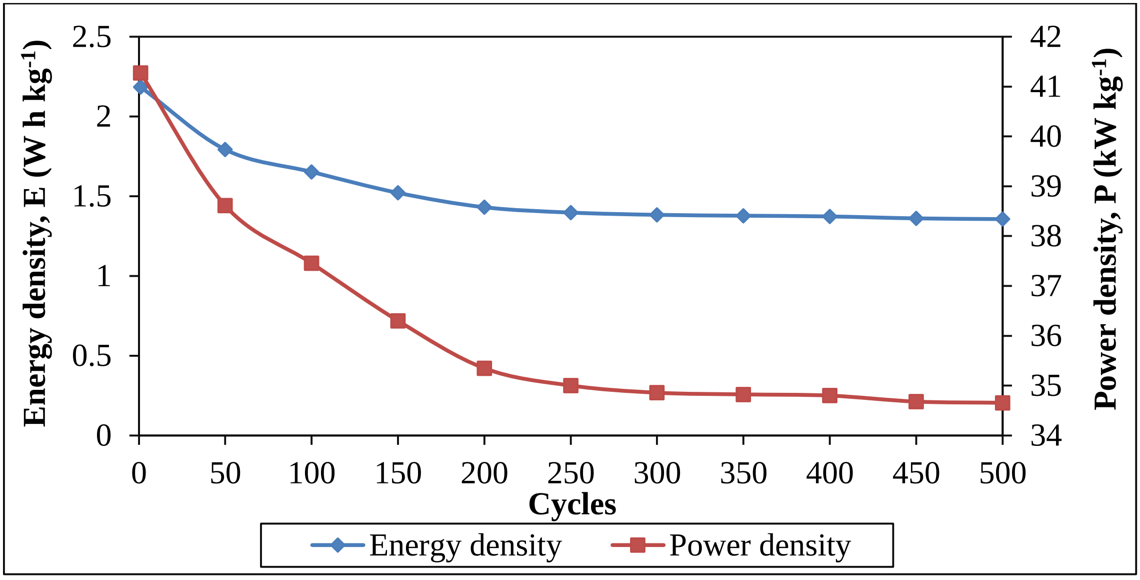

Figure 5.20: Energy density and power density of type II EDLC in BR system over 500 cycles.

The electrochemical properties of EDLC fade with increasing the cycle number of charging and discharging processes, as shown in both figures. There is a drastic drop in specific discharge capacitance, energy density and power density below 250 cycles of charging and discharging. Upon charging and discharging for 250th cycles, the specific discharge capacitance is reduced about 11 % to 19.02 F g^{-1}, meanwhile power density exhibits around 15 % of drop along with the value of 35 kW kg^{-1}. However, around 36 % of decrease in energy density is obtained, where its value is 1.40 W h kg^{-1}. The decrease in the electrochemical performances is suggestive of depletion of electrolyte. In addition, formation of neutral ion pairs is a possible contributor in decreasing the electrochemical stability. Mobile charge carriers which are available for transportation from an electrode to opposite electrode are reduced in the formation of ion pairs and ion aggregates. Therefore, the ion absorption onto the electrodes is reduced. In contrast, the Coulombic efficiency of the cell remains in the range of 70–89 % over 500 cycles. The cell remains almost stable above 250 charging and discharging cycles. The cell possesses specific discharge capacitance of 18.84 F g^{-1}, energy density of 1.36 W h kg^{-1} and power density of 34.66 kW kg^{-1} upon 500 cycles of charge and discharge processes. So, we can conclude that the prepared ionic liquid added polymer electrolyte is a promising candidate as a separator in the EDLC as it still can maintain its electrochemical stability over 500 cycles of charge and discharge processes.

5.11 Summary

BmImBr–added polymer electrolytes containing PVA and CH_3COONH_4 are prepared and characterized. The ionic conductivity of polymer electrolytes increases with mass fraction of ionic liquid and temperature. Inclusion of 60 wt.% of BmImBr increases the ionic conductivity of polymer electrolytes by two orders of magnitude, which is (5.94±0.01) $mScm^{-1}$ at ambient temperature. The ionic conductivity of polymer electrolyte reaches $(1.69\pm0.01)\times10^{-2}$ S cm^{-1} at 120 °C. The enhancement of ionic conductivity of polymer electrolytes is due to the increased amorphous degree of polymer matrix. This has been proven in XRD study by determining the crystallinity of polymer electrolytes. All the polymer electrolytes exhibit VTF theory which is associated with the free volume theory in temperature dependence study. Addition of BmImBr reduces the T_g and improves the electrochemical potential window of polymer electrolytes. BmImBr–added polymer electrolytes show better thermal stability in comparison to BmImBr–free polymer electrolyte. The complexation between PVA, CH_3COONH_4 and BmImBr are verified through the changes in peak shape, peak location and peak intensity. Some characteristic peaks of polymer electrolytes are also disappeared upon addition of ionic liquid. This reveals the interactions between PVA, CH_3COONH_4 and BmImBr to form the polymer complexes.

The specific capacitance of the constructed EDLCs can also be increased by 15535 % with adulteration of ionic liquid. The specific capacitance of 21.89 F g^{-1} was obtained for EDLC containing the most conducting polymer electrolyte as shown in CV curve. The result is in a good agreement with EIS (21.63 F g^{-1}) and charge–discharge studies (21.38 F g^{-1}). The fabricated EDLC shows energy density of 2.18 W h kg^{-1} and power density of 41.27 kW kg^{-1} along with Coulombic efficiency of 70 %. The electrochemical stability was also examined over 500 cycles. The fabricated EDLC remains stable after charge and discharge for 250 cycles. Ionic liquid–added polymer electrolyte is a potential candidate as an electrolyte in EDLC as it has excellent electrochemical properties.

CHAPTER 6

RESULTS AND DISCUSSION OF IODIDE (I) SYSTEM

This chapter highlights the effect of BmImI onto the polymer electrolytes and EDLCs. The first section discusses the results obtained from all characterization of ionic liquid–added polymer electrolytes, whereas the last section enlightens the electrochemical performances of fabricated EDLCs.

6.1 Differential Scanning Calorimetry (DSC)

Figure 6.1 demonstrates the T_g obtained in the DSC curves.

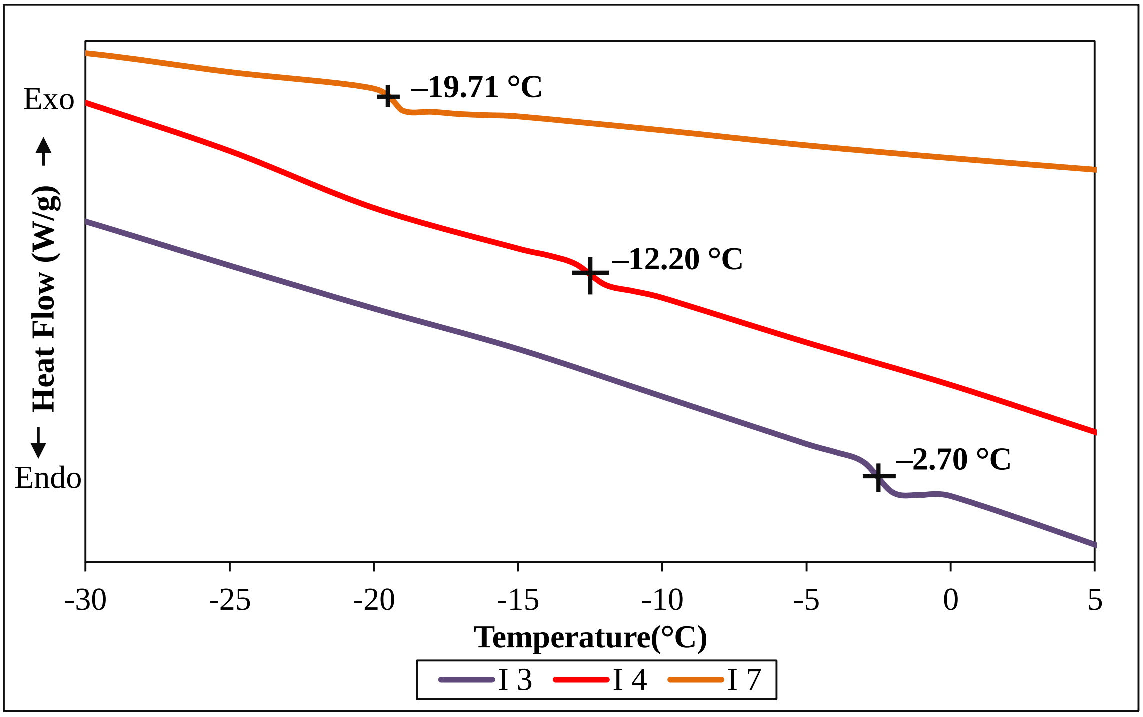

Figure 6.1: Glass transition temperature (T_g) of polymer electrolytes in I system.

The T_g of ionic liquid–free polymer electrolyte is around 46.58 °C, as reported in section 4.2. The T_g of ionic liquid–added polymer electrolytes is decreased to sub–ambient temperature with addition of ionic liquid. This finding deducts that addition of ionic liquid weakens the interaction in the polymer complexes and thus softens the polymer backbone. As a result, this can produce flexible polymer chains and eventually promote the ionic transportation which in accordance with high ionic conductivity. This theory can also be applied into the observation at which the T_g of polymer electrolytes decreases as the mass fraction of ionic liquid is increased.

6.2 Ambient Temperature–Ionic Conductivity Study

Figure 6.2 depicts the ionic conductivity of polymer electrolytes with different mass ratio of BmImI.

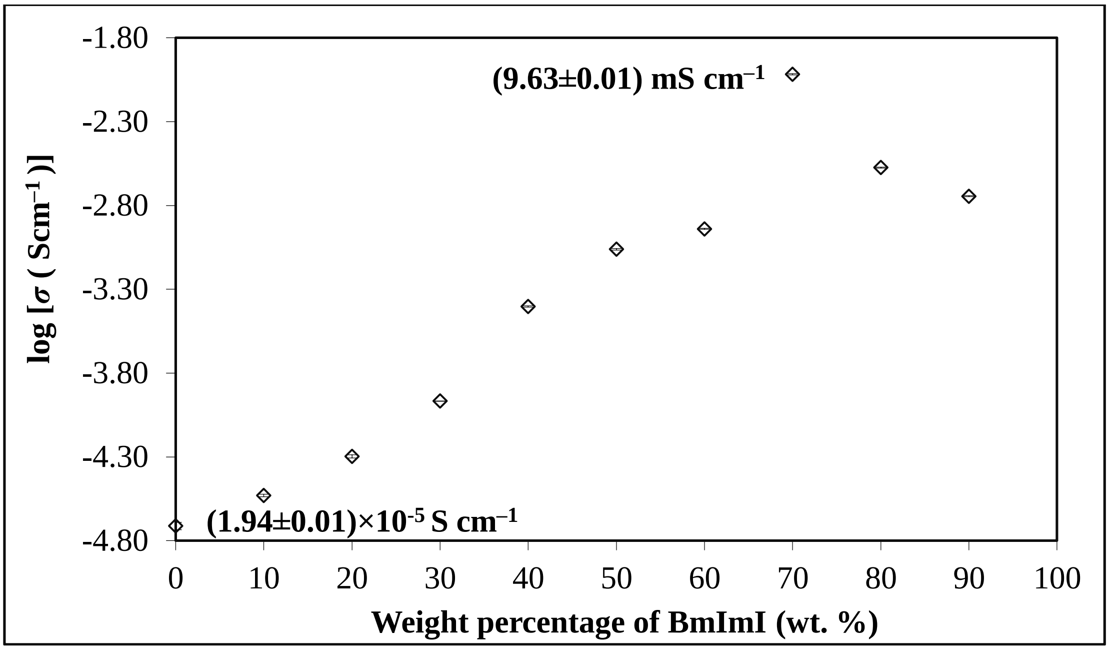

Figure 6.2: The ionic conductivity of polymer electrolyte with respect to the mass fraction of BmImI.

The ionic conductivity of polymer electrolytes increases gradually with mass ratio of BmImI, from 10wt.% to 60wt.%. However, there is an abrupt increase in ionic conductivity at the mass fraction of 70 wt.% where the highest conductivity of (9.63±0.01) mS cm^{-1} is achieved at room temperature. The ionic conductivity of this polymer electrolyte is increased more than two orders of magnitude compared to the ionic liquid–free polymer electrolyte. This is strongly related to the plasticizing effect of ionic liquid. This effect could soften the polymer backbone and hence enhance the flexibility of polymer chains which promotes the ionic transportation in the polymer matrix. The plasticizing effect can boost the mobility of the charge carriers and hence promote the ion dissociation in the polymer complexes. So, this conducting polymer electrolyte could have higher mobility of charge carriers and more mobile charge carriers in comparison to other polymer electrolytes.

The increase of ionic conductivity with the ionic liquid concentration is also due to the decreased T_g which is correlated to the flexibility of polymer chains. The transition from glassy state of the amorphous region to the rubbery state is occurred at low temperature. Therefore, the interaction between the coordination bonds becomes weaker upon addition of ionic liquid. As a result, the polymer chains are very flexible at low temperature. The charge carriers can be detached easily from the interactive bonding. These mobilized charge carriers are transported from one site to another adjacent vacant site for hopping mechanism. Incorporation of ionic liquid also reduces the crystallinity of polymer electrolytes. Beyond addition of 70 wt.% of BmImI, the ionic conductivity is decreased due to the formation of ion aggregates which blocks the ion transport in the electrolyte.

6.3 Temperature Dependent–Ionic Conductivity Study

Figures 6.3 and 6.4 depict the Arrhenius–based temperature dependent–ionic conductivity plots of polymer electrolytes in I system.

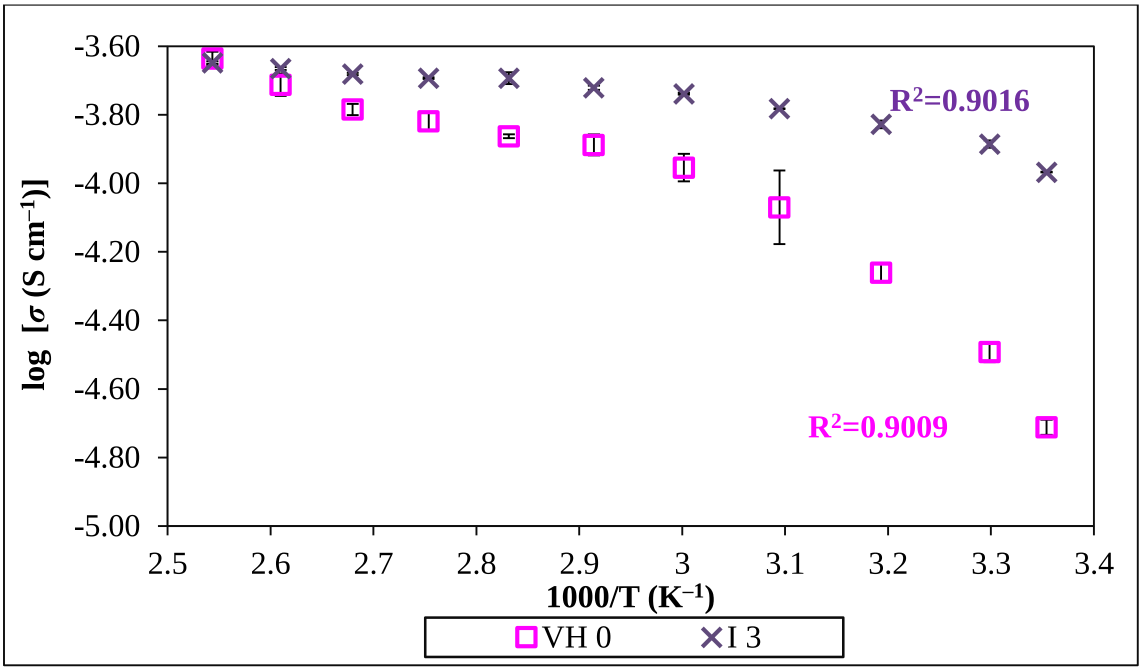

Figure 6.3: The temperature–dependent plot of VH 0 and I 3 fitted with Arrhenius equation.

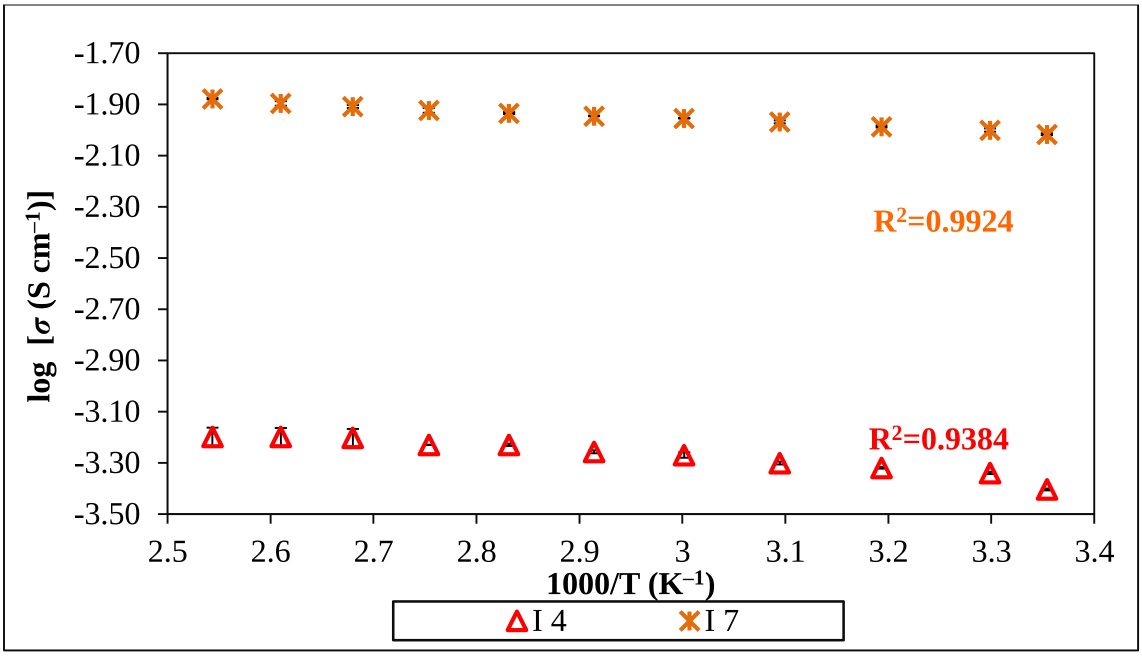

Figure 6.4: The temperature–dependent plot of I 4 and I 7 fitted with Arrhenius equation.

The ionic conductivity of polymer electrolytes increases with temperature as expected, owing to rapid thermal oscillation modes of the macromolecules. These fast vibrational modes could help in ion decoupling from the polymer matrix at high temperature and hence produce more mobile charge carriers transporting from a vacant site to another adjacent vacant site which in accordance with higher ionic conductivity. However, as can be seen in Figures 6.3 and 6.4, the regression value of all the plots is deviated from unity. So, the plots are thus fitted with volume activated–Vogel–Tamman–Fulcher (VTF) theory using non–linear least square technique as shown in Figure 6.5.

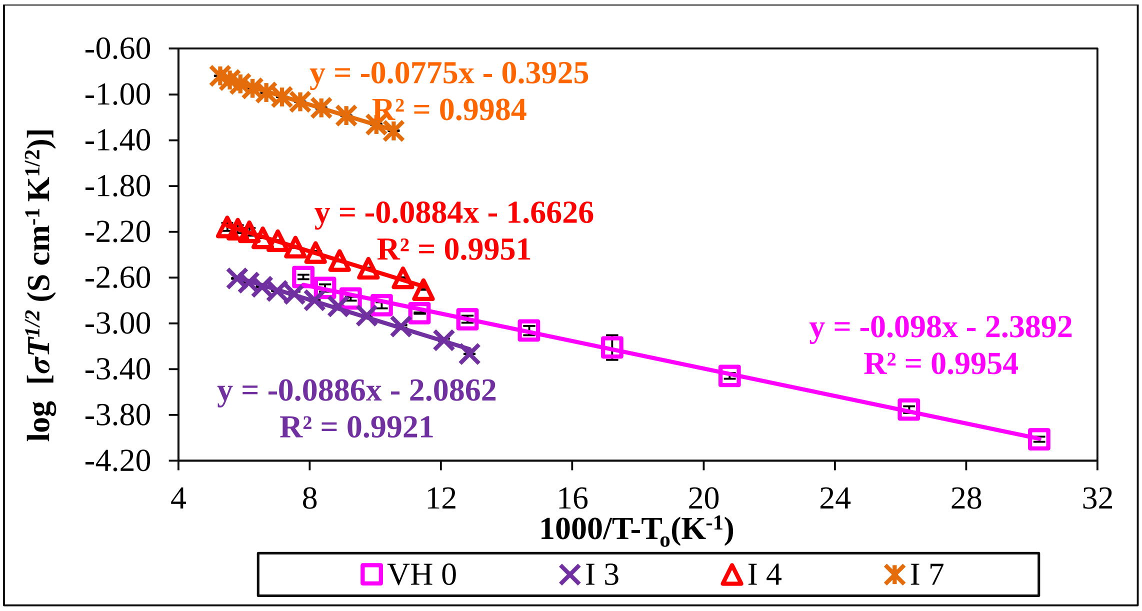

Figure 6.5: The VTF theory–based temperature–dependent plot of polymer electrolytes in I system.

All the relevant parameters are evaluated and listed in Tables 6.1 and 6.2.

Table 6.1: The obtained parameters from each VTF plot with the experimental glass transition temperature from DSC thermogram in I system.

Sample	Regression value, R^2	Glass transition temperature, T_g (K)	Ideal glass transition temperature, T_o (K)
VH 0	0.99	319.73	269.73
I 3	0.99	270.45	220.45
I 4	0.99	260.95	210.95
I 7	0.99	253.44	203.44

Table 6.2: The obtained parameters from each VTF plot in I system.

Sample	Log A_o	Pre–exponential constant, A_o (mS cm^{-1} K$^{1/2}$)	Gradient of the plot, B (K^{-1})	Pseudo–activation energy, E_a (meV)
VH 0	–2.3892	4.08×10^{-3}	0.0980	8.44
I 3	–2.0862	8.20×10^{-3}	0.0886	7.64
I 4	–1.6626	21.75×10^{-3}	0.0884	7.62
I 7	–0.3925	0.41	0.0775	6.68

It is noticeable that the regression value of all the plots approaches to unity. So, VTF theory is applied to describe the ion conduction mechanism in the polymer electrolytes. The VTF relationship reveals the coupling effect of ionic hopping process with high segmental mobility in an amorphous phase based on free volume theory. High mobility of polymer segments provides more spaces for charge carriers to hop from a site to another vacant site at elevated temperature. The conduction is finally generated through the process above.

The A_o and E_a parameters are discussed further in this present work. The E_a is defined as the minimum energy that the charge carriers used for the ion transportation. The higher the ionic conductivity of polymer electrolytes, the lower value is the E_a. This is in a good agreement with the observation in Table 6.2. The E_a is reduced with addition of ionic liquid and it is further decreased with increasing the concentration of ionic liquid. An important feature is also attained in Table 6.2. The A_o shows opposite trend in comparison to E_a. Since A_o is a pre–exponential constant directly proportional to the number of charge carriers, so we can conclude that the number of charge carrier is increased upon addition of ionic liquid and it is further increased as increases the mass fraction of ionic liquid. We suggest that it is related to the flexibility of polymer chains.

The strong plasticizing effect of ionic liquid not only increases the flexibility of polymer membrane but also promotes the ion dissociation from the coordination bond. The highly flexible polymer chains could reduce the resistance for the ions to be migrated from an interstitial site to another adjacent equivalent site. Hence, the number of charge carriers will be increased with reduced minimum energy when the polymer chains are flexible. We deduce that I 7 has the highest ionic conductivity and highest A_o with the lowest E_a compared to all ionic liquid–added polymer electrolytes.

6.4 Thermogravimetric Analysis (TGA)

Thermogravimetric curves of ionic liquid–free polymer electrolyte and ionic liquid–added polymer electrolytes are demonstrated in Figure 6.6.

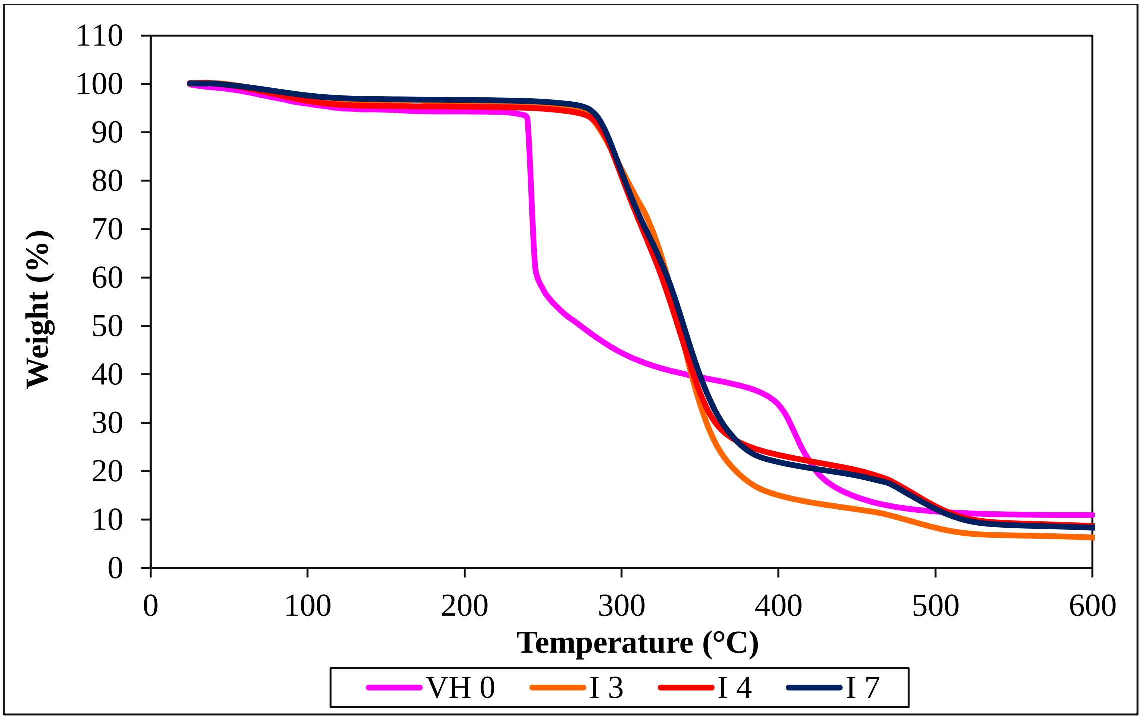

Figure 6.6: Thermogravimetric analysis of ionic liquid–free polymer electrolyte and ionic liquid–added polymer electrolytes in I system.

Four decomposition steps are observed in all TGA curves. All the polymer electrolytes depict an insignificant mass loss in the temperature regime between 25 °C and 150 °C. VH 0, I 3, I 4 and I 7 show 5 %, 3 %, 4 % and 3 % of mass losses in this stage, respectively. Dehydration of water and/or moisture and removal of impurities contribute to this initial mass loss. Then, the mass of polymer electrolytes remains stable up to 240 °C for VH 0, 260 °C for I 3, 268 °C for I 4 and 270 °C for I 7. VH 0 shows around 32 % of mass loss in this region. This major mass loss is due to the decomposition of PVA and CH_3COONH_4. The ether cross–linkages could be formed due to the elimination of water as proposed in our previous work (Liew *et al*., 2014a). Thus, these cross–linkages perform the chain stripping process to remove the side chain of PVA and hence cause the mass loss in this step, forming polyene compound. Apart from that, it is suggestive of degradation of acetamide ($CH_3C(O)NH_2$) which is the product formed upon the water dehydration (Liew *et al*., 2014a). Abrupt increase in mass loss has been observed in ionic liquid–added polymer electrolytes. I 3, I 4 and I 7 illustrate their respective mass losses of 73 %, 66 % and 72 % in the temperature ranges of 260–366 °C, 268–366 °C and 270–381 °C. An additional contributor for this mass loss is also proven where the onset decomposition temperature of BmImI is around 240 °C as reported in Lee *et al*. (2010). We found that the decomposition temperature of ionic liquid–added polymer electrolytes is higher than that of ionic liquid–free polymer electrolyte. This phenomenon is correlated to the coordination bond strength in the polymer complexes between PVA, CH_3COONH_4 and BmImI. Higher energy is needed to break these interactions when the ionic liquid is added into the polymer matrix.

Beyond this mass loss, the curves exhibit two gradual mass losses. VH 0 has mass loss of 20 %, starting from 245 °C until 375 °C, whereas I 3 illustrates mass loss of 11 %, starting from 366 °C until 468 °C. Lower mass loss has been obtained for I 4 and I 7. I 4 and I 7 exhibit the drop in mass of 9 % (whereby the degradation temperature starts from 366 °C to 464 °C) and 7 % (whereby the decomposition temperature starts from 381°C to 470 °C), respectively. The decomposition in this stage arises from the chemical decomposition processes of PVA including the breakdown of ether cross–linkages and random chain scissoring between carbon–carbon bonds (Guirguis & Moselhey, 2010). This mass loss is then followed up by a moderate mass loss. VH 0 and I 3 demonstrate

27 % and 5 % of weight losses, along with 11 % and 6 % of mass residues at 375 °C and 580 °C, respectively. I 4 and I 7 start to lose mass of 10 % and 9 %, along with 8 % residual masses at 464 °C and 470 °C respectively. Yang and his coworkers state that this drop in mass is ascribed to breakdown of the polymer backbone at which the double bond in polyene will be converted into aliphatic chains (Yang *et al.*, 2009). Above 550 °C, the mass of polymer electrolytes remains constant and this reveals the complete decomposition process of polymer electrolytes. I 7 exhibits better thermal stability as it can withstand higher first decomposition temperature compared to VH 0, I 3 and I 4.

6.5 Attenuated Total Reflectance–Fourier Transform Infrared (ATR–FTIR)

Figures 6.7 (a)–(e) portray the ATR–FTIR spectra of BmImI, ionic liquid–free polymer electrolyte and ionic liquid–added polymer electrolytes, whereas Table 6.3 summarizes the assignments of all the characteristic peaks in these samples.

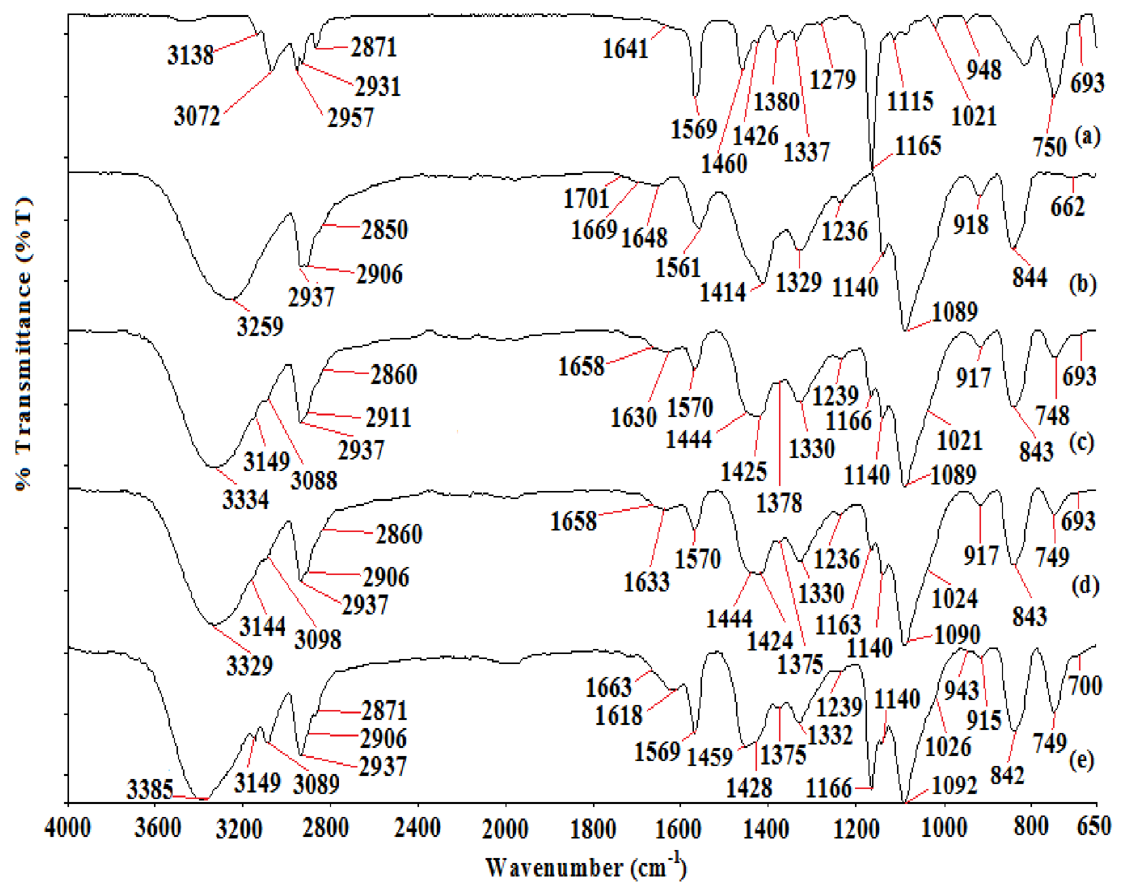

Figure 6.7: ATR–FTIR spectra of (a) BmImI, (b) VH 0, (c) I 3, (d) I 4 and (e) I 7.

Table 6.3: The assignments of vibration modes of BmImI, VH 0, I 3, I 4 and I 7.

Descriptions of vibration modes	**Wavenumber (cm^{-1})**				
	BmImI	**VH 0**	**I 3**	**I 4**	**I 7**
C–H bending mode of CH_3COONH_4	–	662	–	–	–
C–H vibration mode for cyclic $BmIm^+$	693, 3138	–	693, 3149	693, 3144	700, 3149
C–H bending mode for cyclic $BmIm^+$	750	–	748	749	749
Skeletal C–H rocking mode of PVA	–	844	843	843	842
O–H bending mode of PVA	–	918	917	917	915
In–plane C–N–C bending mode	948	–	–	–	943
Out–of–plane C–H wagging mode in alkyl chain	1021	–	1021	1024	1026
C–O stretching mode of PVA	–	1089	1089	1090	1091
C–H bending mode in methyl group	1115	–	–	–	–
C–C and C–O stretching modes of doubly H–bonded OH in crystalline region of PVA	–	1140	1140	1140	1140
CH_3–N stretching mode	1165	–	1166	1163	1166
C–O stretching mode of PVA and CH_3COONH_4	–	1236	1239	1236	1239
C–N stretching mode of imidazolium ring	1279	–	–	–	–
CHOH bending mode, CH_3 in–plane deformation and C–H wagging mode of PVA	–	1329	1330	1330	1332
CH_2 symmetric bending mode	1337	–	1330	1330	1332
CH_3 asymmetric stretching mode	1380	–	1378	1375	1375
C–H deformation mode of PVA	–	1414	–	–	–
CH_3 asymmetric bending mode	1426	–	1425	1424	1428
CH_3 symmetric bending mode	1460	–	1444	1444	1459
C=N stretching mode	1569	–	1570	1570	1569
N–H bending mode of CH_3COONH_4	–	1561	1570	1570	1569
C–H stretching mode of PVA	–	1648	1630	1633	1618
–CONH– bonding mode of CH_3COONH_4	–	1669	–	–	–
C–C and C–N bending mode of imidazolium ring	1641	–	1658	1658	1663
C=O stretching mode of CH_3COONH_4	–	1701	–	–	–
C–H symmetric stretching mode in methyl group of alkyl chain	2871, 2931, 2957	2850, 2906, 2937	2860, 2911, 2937	2860, 2906, 2937	2871, 2906, 2937
=C–H stretching mode	3072	–	3088	3098	3089
O–H stretching mode of OH group of PVA	–	3259	3334	3329	3385

An important feature has been observed in Figure 6.7 (e) compared to (b) that is new peak formation. These peaks are C–H vibration mode for cyclic $BmIm^+$ at 700 cm^{-1} and 3149 cm^{-1}, C–H bending mode for cyclic $BmIm^+$ at 749 cm^{-1}, in–plane C–N–C bending mode of $BmIm^+$ at 943 cm^{-1}, out–of–plane C–H wagging mode in alkyl chain of $BmIm^+$ at 1026 cm^{-1}, CH_3–N stretching mode of $BmIm^+$ at 1166 cm^{-1}, CH_2 symmetric bending mode of $BmIm^+$ at 1332 cm^{-1}, CH_3 asymmetric stretching mode of $BmIm^+$ at 1375 cm^{-1}, CH_3 asymmetric bending mode of $BmIm^+$ at 1428 cm^{-1}, CH_3 symmetric bending mode of $BmIm^+$ at 1459 cm^{-1}, C–C and C–N bending mode of imidazolium ring at 1663 cm^{-1} and =C–H stretching mode of $BmIm^+$ at 3089 cm^{-1}. The formation of these twelve peaks denotes that ionic liquid has complexed with PVA–CH_3COONH_4 polymer matrix. On the contrary, some characteristic peaks are disappeared when we incorporate ionic liquid into VH 0, for example, C–H bending mode of CH_3COONH_4 at 662 cm^{-1}, C–H deformation mode of PVA at 1414 cm^{-1}, –CONH– bonding mode of CH_3COONH_4 at 1669 cm^{-1} and C=O stretching mode of CH_3COONH_4 at 1701 cm^{-1}. The disappearance of these peaks reflects the interaction between PVA, CH_3COONH_4 and BmImI, especially the salt dissociation. The absence of C–H bending mode and –CONH– bonding mode of CH_3COONH_4 proves that the salt has been dissociated to NH_4^+ and CH_3COO^-.

Pure BmImI illustrates two weak peaks at 1115 cm^{-1} and 1279 cm^{-1} as shown in Figure 6.7 (a). The former peak is designated as C–H bending mode in methyl group, whereas the latter peak is assigned to C–N stretching mode of imidazolium ring. The disappearance of these peaks verifies the deprotonation of $BmIm^+$ as proposed in section 4.4. Apart from that, some characteristic peaks demonstrate the changes in intensity, changes in position and changes in shape. All the characteristic peaks reveal the change in peak location, except the shoulder peak at 1140 cm^{-1}, shoulder peak at 2906 cm^{-1} and medium sharp peak at 2937 cm^{-1}. The former peak is assigned to C–C and C–O stretching modes of doubly H–bonded OH in crystalline region of PVA, whereas the latter two peaks are ascribed to C–H symmetric stretching mode in methyl group of alkyl chain of PVA. Although these peaks remain unchanged, these peaks exhibit the changes in peak intensity and further imply the complexation between PVA, CH_3COONH_4 and BmImI. The abrupt decrease in peak intensity from 5.57 % to 1.21 % at 1140 cm^{-1} indicates that the high ionic conductivity of I 7 is related to the crystallinity of the polymer electrolytes as proposed in section 6.2. On the other hand, an abrupt increase in peak intensity from 2.02 % to 8.02 % is observed at 2937 cm^{-1}. We suggest that the significant increase in peak intensity is due to the overlap of C–H symmetric stretching mode in methyl group of alkyl chain of PVA with C–H symmetric stretching mode of BmIm^{+} and hence induce to more intense peak.

VH 0 portrays a sharp peak at 844 cm^{-1} with intensity of 11.28 % in transmittance mode as illustrated in Figure 6.8 (a).

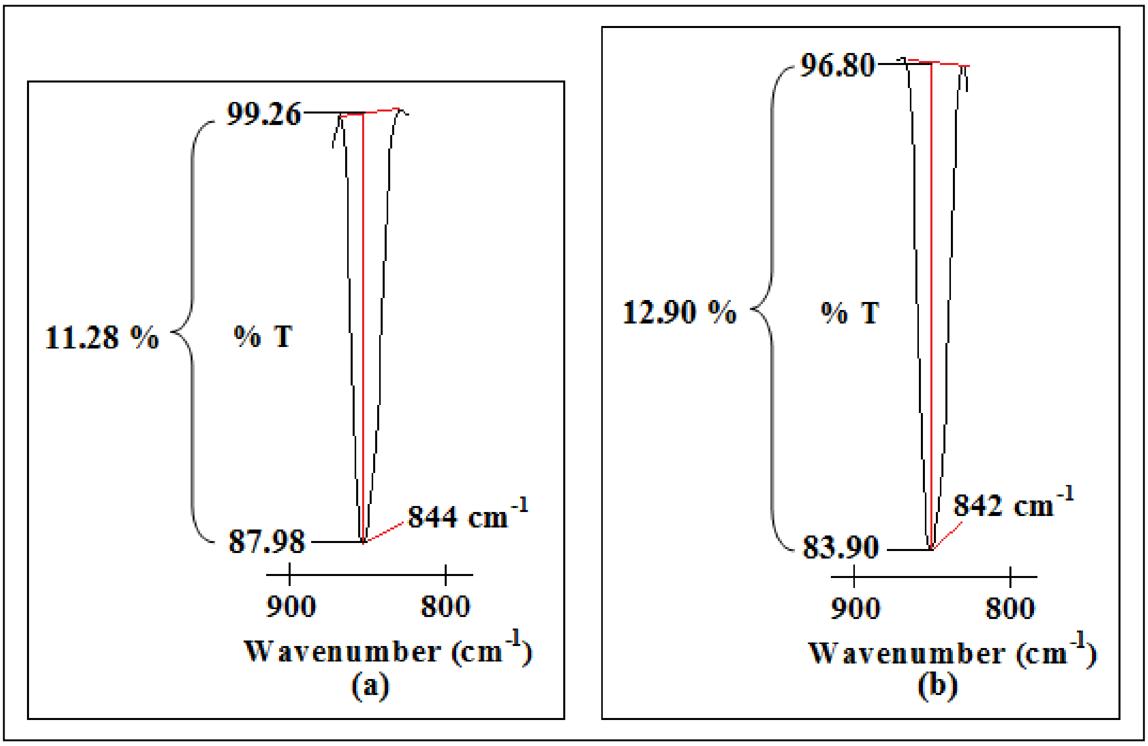

Figure 6.8: The change in peak intensity of skeletal C–H rocking mode of (a) VH 0 and (b) I 7 in the wavenumber region between 900 cm^{-1} and 800 cm^{-1}.

The assignment of this peak is skeletal C–H rocking mode of PVA. However, upon addition of 70 wt.% of BmImI, this sharp peak is shifted to lower wavenumber of 842 cm^{-1} with a slight increased intensity of 12.90 % in transmittance mode, as illustrated in Figure 6.8 (b). Similarly, the weak peak at 1648 cm^{-1} in Figure 6.7 (b) is designated as C–H stretching mode of PVA. Addition of ionic liquid causes the significant downward peak shifting to 1618 cm^{-1}. However, this characteristic peak shows an increase in peak intensity from 0.43 % to 1.29 % in transmittance mode. Opposite result is obtained for C–O stretching modes of PVA and CH_3COONH_4 which is located at 1236 cm^{-1} in the ionic liquid–free polymer electrolyte spectrum. This weak peak exhibits upward shift to 1239 cm^{-1} by adding ionic liquid. On the other hand, the peak displays the decrement of peak intensity that is from 1.44 % to 0.56 % in transmittance mode. This observation implies the interaction between PVA, CH_3COONH_4 and BmImI and further deduct that the proton hopping mechanism might take place at C–O interactive bond. In addition, O–H bending mode of PVA for I 7 depicts less intense peak with lower wavenumber compared to that of VH 0. This weak peak is shifted from 918 cm^{-1} to 915 cm^{-1} corresponding to 3.35 % and 1.29 %, in term of peak intensity with addition of ionic liquid. Similar observation is also attained at 3385 cm^{-1} which is referred as O–H stretching mode of OH group in Figure 6.7 (e). This broad peak is originated from 3259 cm^{-1} as shown in VH 0 spectrum. A small change in peak intensity is also observed in this broad peak, which is from 15.44 % to 15.41 % in transmittance mode corresponding to VH 0 and I 7.

The interaction between PVA, CH_3COONH_4 and BmImI can also be proven through the changes in peak intensity and the shifting of some coordination bonds. VH 0 spectrum exemplifies a medium sharp peak at 1329 cm^{-1} with intensity of 4.67 % in transmittance mode. This peak is shifted to higher wavenumber that is 1332 cm^{-1} along with its intensity of 4.29 % in transmittance mode. The upward shift is suggestive of the overlap of this characteristic peak with CH_2 symmetric bending mode of $BmIm^+$ because there is a weak peak obtained at 1337 cm^{-1} as shown in Figure 6.7 (a). A medium sharp peak bearing with 6.56 % intensity in term of transmittance mode is obtained at 1561 cm^{-1} in Figure 6.7 (b). This peak is designated as N–H bending mode of CH_3COONH_4. Upon addition of ionic liquid, the intensity of this peak is increased about 2.69 % and shifted to higher wavenumber position to 1569 cm^{-1}. The increment of peak intensity and upward shift confirm the overlapping between N–H bending mode of CH_3COONH_4 and C=N stretching mode of $BmIm^+$.

An obvious change in shape has been observed in the wavenumber range between 1200 cm^{-1} and 1000 cm^{-1}. There is only a sharp peak at 1089 cm^{-1} with intensity of 15.33 % (in transmittance mode) as shown in Figure 6.7 (b) within the wavenumber regime of 1100–1000 cm^{-1}. However, this sharp peak has been changed to less intense sharp peak with intensity of 14.49 %, in transmittance mode at 1092 cm^{-1} with a shoulder peak at 1026 cm^{-1} in that region. This additional shoulder peak is suggestive of out–of–plane C–H wagging mode in alkyl chain as the weak peak is present at 1021 cm^{-1} in Figure 6.7 (a). On the contrary, change in peak shape is also obtained in the wavenumber range of 1200–1100 cm^{-1}, as illustrated in Figure 6.9.

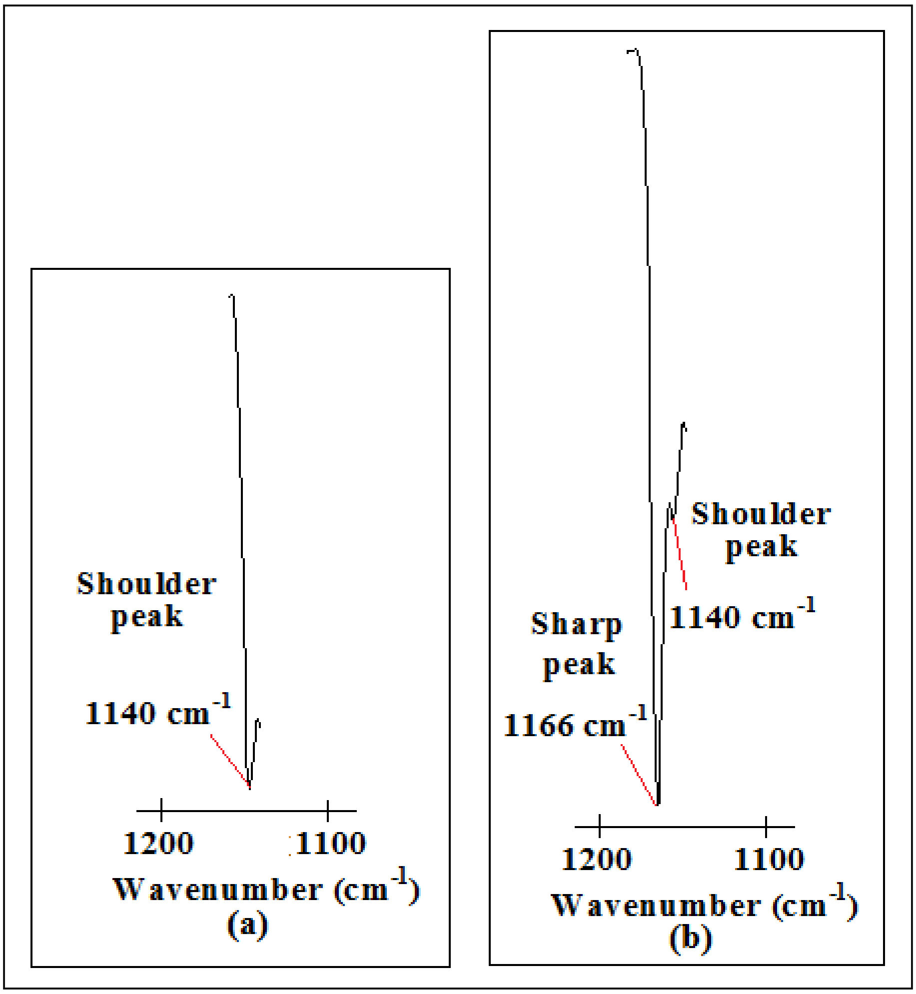

Figure 6.9: The change in peak shape of vibration modes of (a) VH 0 and (b) I 7 in the wavenumber region between 1200 cm^{-1} and 1100 cm^{-1}.

There is only a shoulder peak appeared at 1140 cm^{-1} as shown in Figure 6.9 (a). However, this peak turns into a sharp peak at 1166 cm^{-1} with a shoulder peak at 1140 cm^{-1}. The sharp peak is ascribed to CH_3–N stretching mode of BmIm$^+$ as an intense peak is attained at 1165 cm^{-1} in pure BmImI spectrum. This idea is supported by the deconvolution method. We found out that there are only two peaks in that region, as depicted in Figure 6.10.

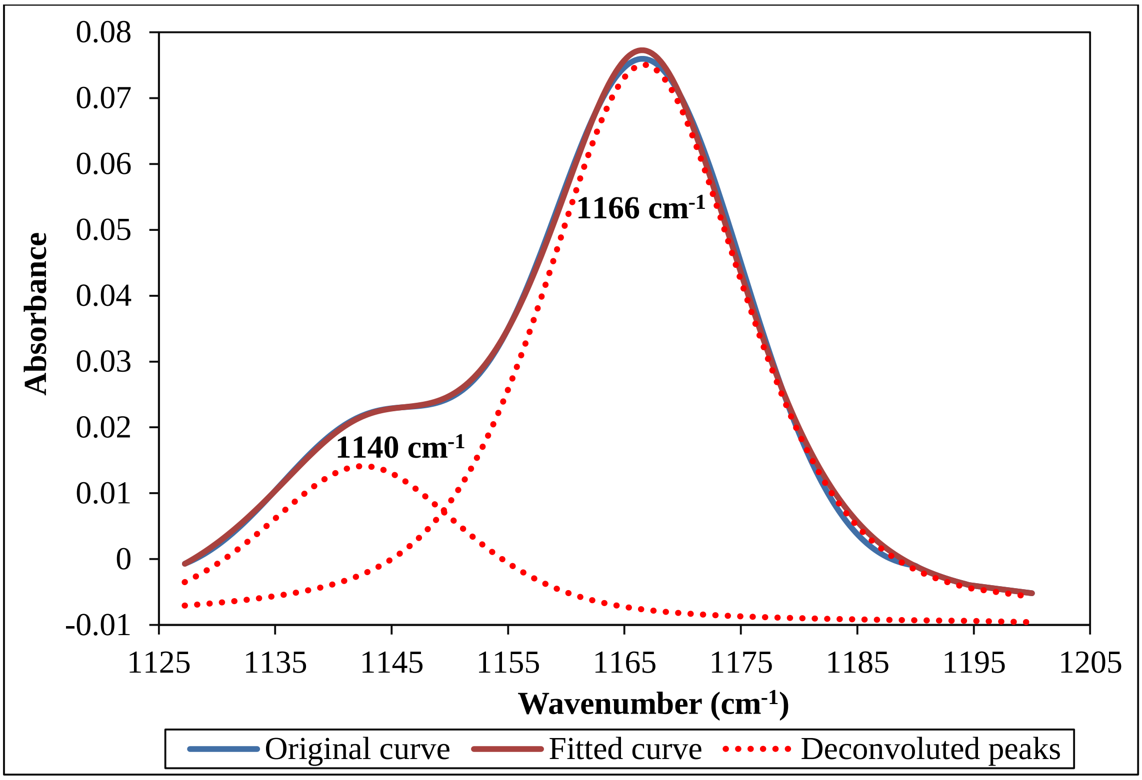

Figure 6.10: The original and fitted curves with the deconvoluted peaks in the wavenumber region between 1200 cm^{-1} and 1125 cm^{-1}.

The deconvoluted peaks lie on the same location in the spectrum. Therefore, the shoulder peak with shorter peak intensity is referred as C–C and C–O stretching modes of doubly H–bonded OH in crystalline region of PVA, whereas the sharp peak is CH_3–N stretching mode of BmIm$^+$. Similar observation is attained for the broad band which is assigned as O–H stretching mode of OH group of PVA at 3259 cm^{-1}. This broad band has been turned into a broad band with two shoulder peaks. These additional two shoulder peaks are =C–H stretching mode of BmIm$^+$ at 3089 cm^{-1} and C–H vibration mode for cyclic BmIm$^+$ at 3149 cm^{-1}. This phenomenon reflects the interaction of the C–H coordination bond towards the O–H stretching mode of the polymer chains.

Another obvious change in shape is also detected in the region from 2950 cm^{-1} to 2800 cm^{-1}, as demonstrated in Figure 6.11.

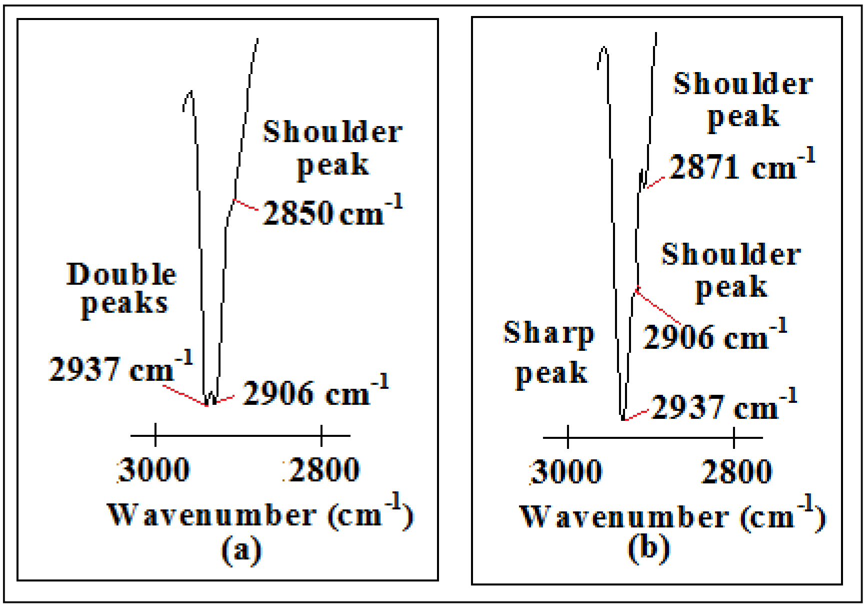

Figure 6.11: The change in peak shape of vibration modes of (a) VH 0 and (b) I 7 in the wavenumber region between 3000 cm^{-1} and 2800 cm^{-1}.

Double peaks at 2906 cm^{-1} and 2937 cm^{-1} with a shoulder peak at 2850 cm^{-1} are appeared in VH 0 spectrum. Upon addition of ionic liquid, the shoulder peak is still present but it is located at higher wavenumber which is 2871 cm^{-1}. The overlapping of both C–H symmetric stretching modes in methyl group of alkyl chain from PVA and BmIm^{+} of VH 0 also contributes to upward shift of the shoulder peak at 2850 cm^{-1}. However, the double peaks have been changed to a sharp peak at 2937 cm^{-1} with a shoulder peak at 2906 cm^{-1} for I 7. Both of these peaks are ascribed to C–H symmetric stretching mode in methyl group of alkyl chain. The change in peak shape is related to the overlapping of both C–H symmetric stretching modes of PVA and BmIm^{+}. Deconvolution is employed to confirm the presence of these peaks. Three well–fitted deconvoluted peaks are observed in Figure 6.12.

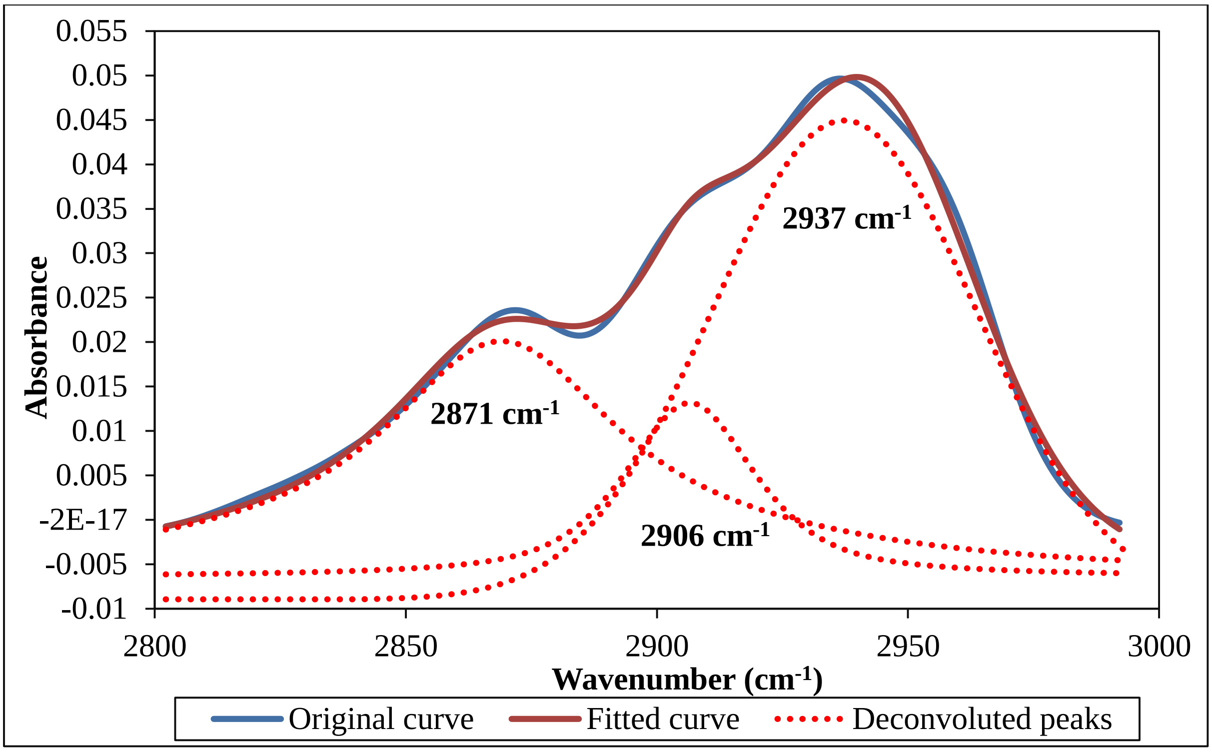

Figure 6.12: The original and fitted curves with the deconvoluted peaks in the wavenumber region between 3000 cm^{-1} and 2800 cm^{-1}.

These deconvoluted peaks are in a good agreement with the peak assignment in the spectrum.

The spectra of I 3 and I 4 are displayed in Figures 6.7 (c) and (d), respectively. All the characteristic peaks in I 7 can also be found in these two samples, except the in–plane C–N–C bending mode of $BmIm^+$ at 943 cm^{-1}. Reduced crystallinity can be one of the attributor of the increase in ionic conductivity with increasing the mass loadings of ionic liquids as aforementioned in section 6.2. This theory can be proven in FTIR study. The C–C and C–O stretching modes of doubly H–bonded OH in crystalline region of PVA is further investigated. We take note that the peak intensity of this peak decreases as increases the mass fraction of ionic liquids, from 5.57 % to 4.28 %, 4.15% and 1.21 % corresponding to VH 0, I 3, I 4 and I 7, in transmittance mode. Based on these findings, three ideas can be proven as stated below:

i) the crystallinity is reduced upon addition of ionic liquid

ii) the crystallinity decreases with increasing the mass loadings of ionic liquid

iii) I 7 has the lowest crystalline region compared to all the polymer electrolytes

6.6 X–ray Diffraction (XRD)

Figure 6.13 portrays the comparison of XRD pattern of ionic liquid–free polymer electrolytes and ionic liquid–embedded polymer electrolytes.

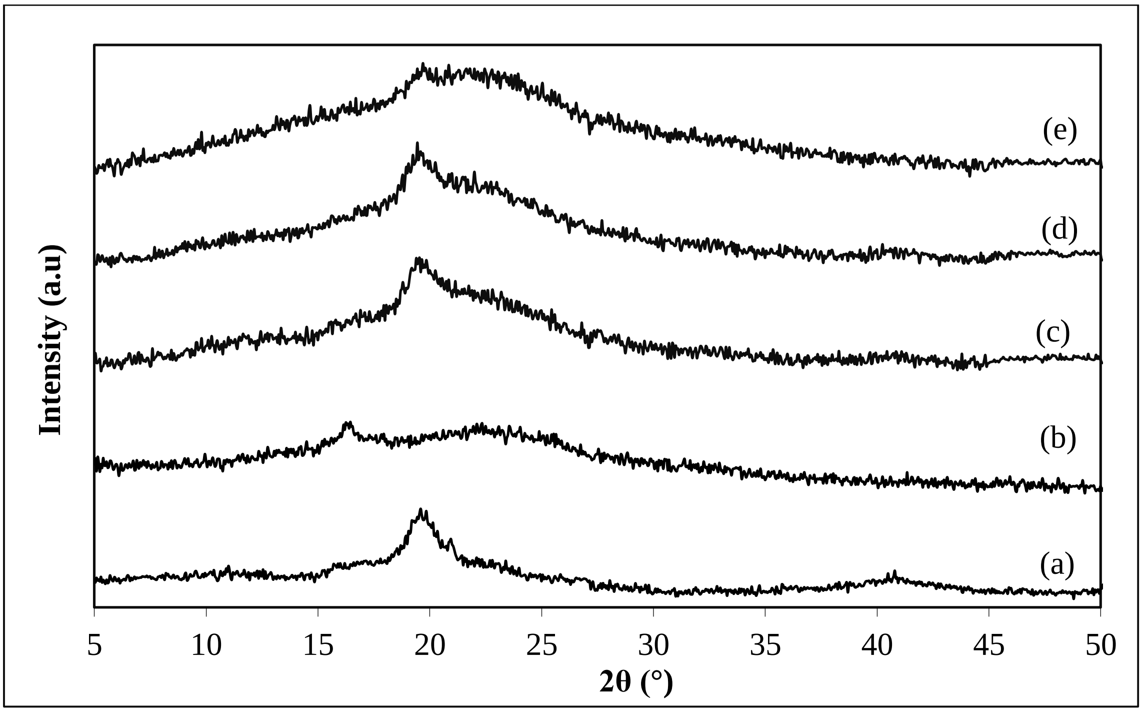

Figure 6.13: The XRD patterns of (a) VH 0, (b) BmImI, (c) I 3, (d) I 4 and (e) I 7.

VH 0 shows a crystalline peak at 19.7° and an amorphous hump at 22.5° along with a small broad peak at 40.8°. A sharp peak at 16.3° and a broad hump at 24° are observed in BmImI diffractogram. The peaks belonging to BmImI are not found in the XRD patterns of ionic liquid–embedded polymer electrolytes inferring the complete dissolution of BmImI in the polymer electrolytes. Upon addition of 30 wt.% and 40 wt.% of BmImI, I 3 and I 4 possess similar XRD patterns as VH 0. I 3 and I 4 illustrate the respective crystalline peak at 2θ=19.6° and 19.4°, whereas these samples exhibit the respective amorphous hump at 2θ=21.1° and 21.3°. On the contrary, the small broad peaks of I 3 and I 4 are located at higher 2θ degree of 44° and 47°, respectively in comparison to VH 0. However, this peak is absent in I 7 diffractogram, meanwhile the two peaks at lower 2θ degree are still existing in XRD pattern of I 7. The first crystalline peak is located at 19.6°, whereas the latter amorphous peak is placed at 22.1°. The presence of these peaks is further verified in deconvolution findings as shown below.

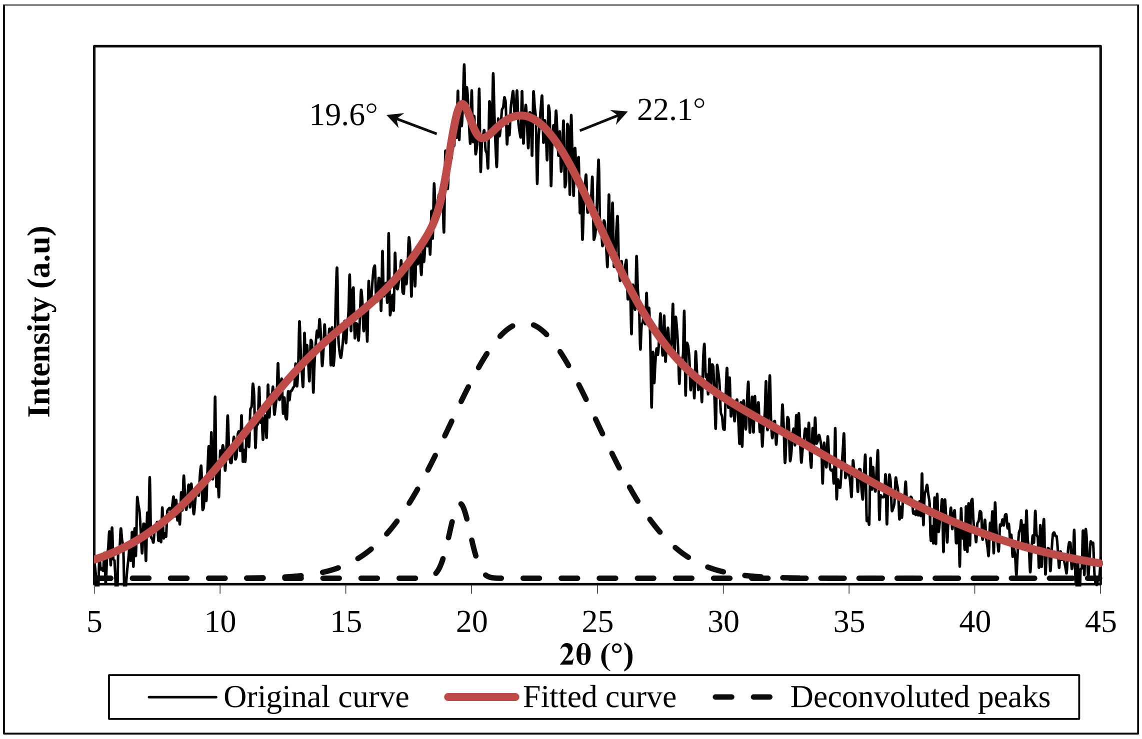

Figure 6.14: XRD pattern of I 7 with fitted curve and deconvoluted peaks within the range of Bragg angle, 2θ of 5–45°.

There are only two peaks present in the 2θ degree range in Figure 6.14. The peak at 2θ degree of 19.6° is assigned to the (1 1 0) reflection (Hirankumar *et al.*, 2005, Selvasekarapandian *et al.*, 2005). The intensity of the peaks is further elucidated using deconvolution technique to calculate the degree of crystallinity.

Table 6.4 shows the area under the crystalline peak, total area under the curves of all the peaks and percentage of crystallinity that we can obtain from the curve fitting through the deconvolution method.

Table 6.4: The relevant parameters obtained from the curve fitting in XRD findings in I system.

Sample	Area under the curve of the crystalline peak, I_c	Total area under the curves of all the peaks, I_t	Percentage of crystallinity (χ_c) %
VH 0	1669	5366	31
I 3	211	3325	6.4
I 4	212	3410	6.2
I 7	65	2964	2

We postulate that one of the contributors for enhancing the ionic conductivity with addition of ionic liquid is due to the reduced degree of crystallinity of polymer electrolytes. The XRD result obtained can prove this idea. The percentage of crystallinity of polymer electrolytes is reduced significantly from 31 % for ionic liquid–free polymer electrolyte, to 6.4 % for I 3, 6.2 % for I 4 and 2 % for I 7. So, it can be concluded that the amorphous nature of polymer electrolytes increases with the ionic liquid mass loadings and the most conducting polymer electrolyte has the lowest percentage of crystallinity.

6.7 Linear Sweep Voltammetry (LSV)

Figure 6.15 portray the potential window of I 7.

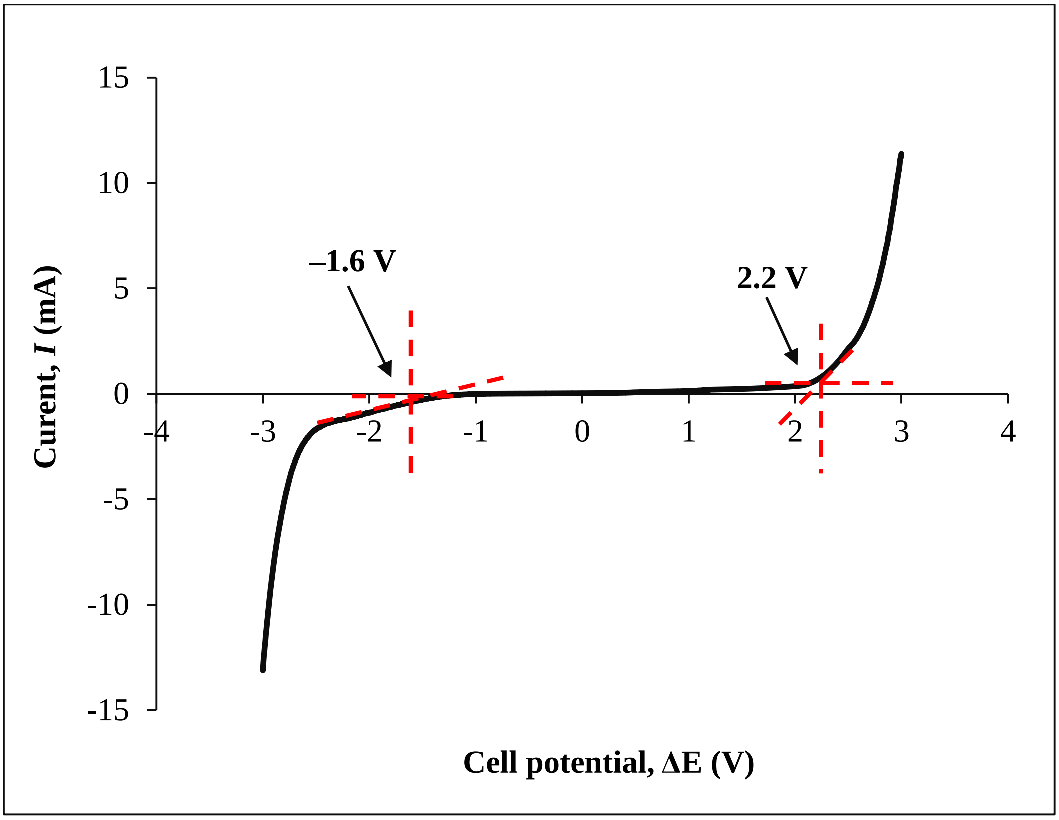

Figure 6.15: LSV response of I 7.

The LSV of VH 0 is 3.3 V, where the cathodic and anodic potentials are detected at –1.6 V and 1.7 V as shown in Figure 4.23. Upon addition of BmImI, the operational potential range is expanded to 3.8 V, ranging from –1.6 V and 2.2 V. This finding infers that ionic liquid can enhance the electrochemical stability of polymer electrolytes. Moreover, the operational current of the ionic liquid–free polymer electrolyte is much lower than the ionic liquid–embedded polymer electrolyte. We predict that it is related to the number of charge carriers. The number of charge carriers of ionic liquid–free polymer electrolyte is extremely lower than that of ionic liquid–added polymer electrolyte. So, ion adsorption at the interface between blocking electrode and ionic liquid–free polymer electrolyte is lesser than ionic liquid–embedded polymer electrolyte as the ion transportation is less favorable. Therefore, the energy storage in this vicinity requires lesser electrons to generate the current compared to ionic liquid–added polymer electrolyte.

6.8 Cyclic Voltammetry (CV)

Figure 6.16 portrays CV curve of EDLC using the most conducting polymer electrolyte in iodide system.

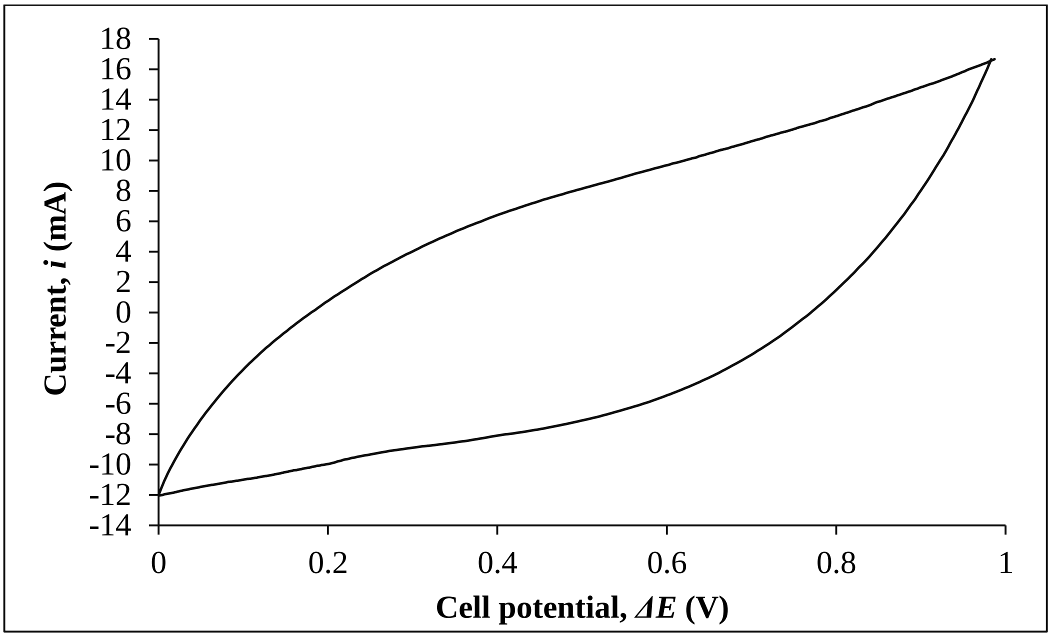

Figure 6.16: Cyclic voltammograms of type II EDLC containing PVA–CH_3COONH_4–BmImI–polymer electrolyte.

The CV of EDLC containing ionic liquid–free polymer electrolyte displays a leaf–like shape with specific capacitance of 0.14 F g^{-1} or equivalent to 0.0015 Fcm^{-2}, as shown in Figure 4.25. The CV curve has been changed significantly to the almost ideal box–like shape upon addition of ionic liquid into the polymer electrolyte. Upon addition of ionic liquid into the polymer electrolytes, the specific capacitance of EDLC is increased about 40457 % to 52.78 F g^{-1} (or equivalent to 0.81 Fcm^{-2}). The abrupt increase of capacitance in type II EDLC is probably due to high ionic conductivity of polymer electrolyte. There would be more mobile charge carriers with high mobility transported in the high conductive polymer matrix. As a result, more mobile ions are diffused into the pores of porous electrode and accumulated at the electrode–electrolyte boundary. This can promote the double layer formation and thereby increase the capability of energy storage in EDLC. In addition, ionic liquid can alter the physical properties of polymer electrolytes. Addition of ionic liquid into polymer electrolyte produces sticky behavior due to strong plasticizing effect of ionic liquid. The adhesive characteristic improves the interfacial contact between electrode and electrolyte and hence eases the ion adsorption onto the electrode interface which in accordance with high capacitance.

The absence of pseudocapacitive hump (or known as redox peak) in charge and discharge processes of Figure 6.16 denotes no Faradic chemical reaction in the cell. The capacitance value obtained from this current work is relatively higher than the previous literature. Sun and Yuan fabricated hybrid capacitors using PVA–sodium poly (acrylate) (PAAS)–potassium hydroxide (KOH) alkaline polymer electrolytes and nickel hydroxide ($Ni(OH)_2$)/activated carbon (AC) composite positive electrodes (Sun & Yuan, 2009). This hybrid capacitor has the specific capacitance of 29.8 F g^{-1}. Interestingly, the specific capacitance of EDLC obtained in this work is much higher than this hybrid capacitor. It can be concluded that EDLC using the most conducting polymer electrolyte is a promising candidate to be applied as one of the power sources.

6.9 Electrochemical impedance spectroscopy (EIS)

Low frequency–based EIS is another tool to determine the electrical properties of EDLC and its capacitance. Figure 6.17 shows the Nyquist impedance plot of type II EDLC in the frequency range of 10 mHz–100 kHz at ambient temperature with the proposed equivalent circuit of the capacitor cell in the inset of figure.

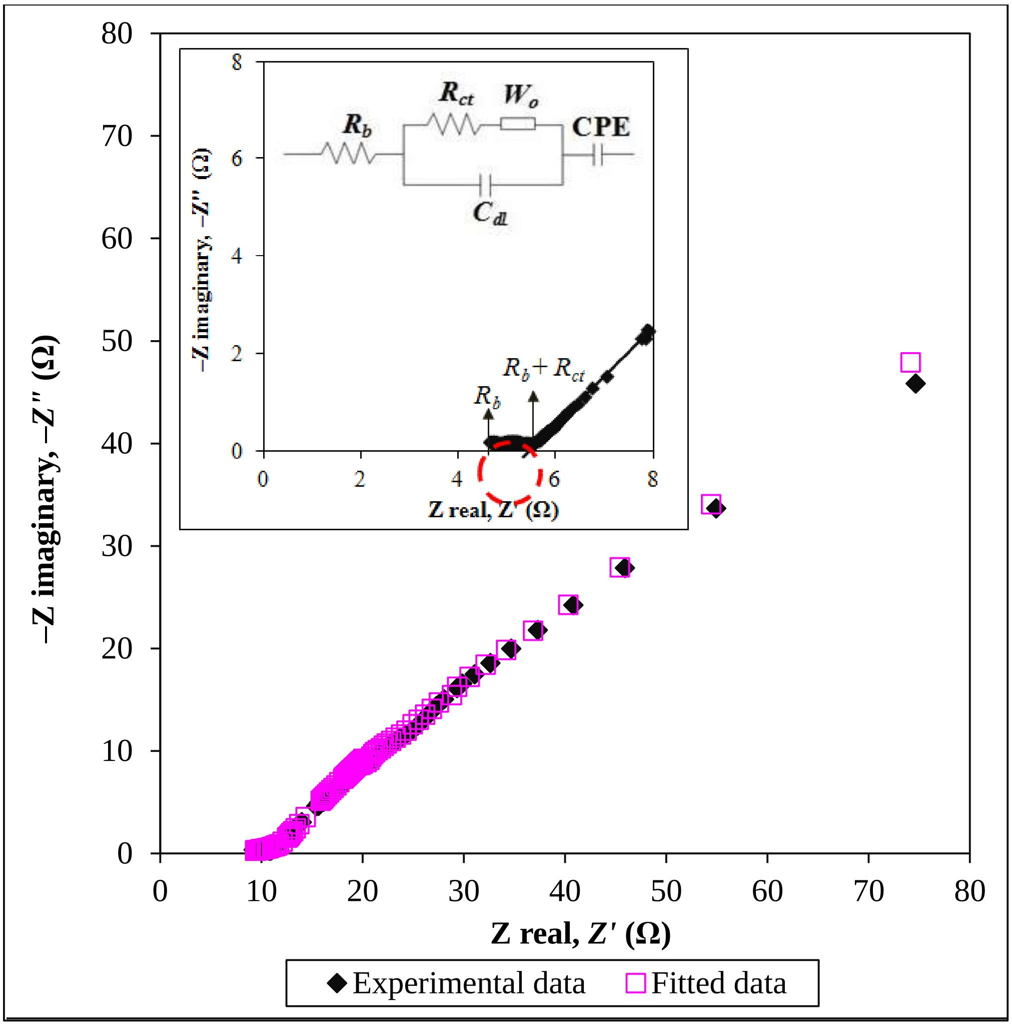

Figure 6.17: Nyquist impedance plot of type II EDLC containing the most conducting polymer electrolyte in I system at room temperature from 10 mHz to 100 kHz with close–up view of the plot in high frequency region (inset) and its fitted data.

The experimental data is fitted and stimulated using the proposed equivalent circuit (shown in inset of figures). It can be seen that the experimental data is well–fitted and simulated using the proposed equivalent circuit in the impedance plot. The simulation findings of all the elements in the equivalent circuit are summarized in Table 6.5.

Table 6.5: Simulation results of equivalent circuit elements in EDLCs from the fitted EIS data.

Element	Type II EDLC
Bulk resistance, R_b (Ω)	4.6
Double layer capacitance, C_{dl} (µF)	19.2
Charge transfer resistance, R_{ct} (Ω)	0.8
Warburg impedance, W_O ($S.s^5$)	0.06
Constant phase element, CPE ($S.s^n$)	0.05
Frequency power, n ($0<n<1$)	0.48

The R_b and R_{ct} are determined in this present work through stimulation method. Type I EDLC shows the R_b of 753 Ω and R_{ct} of 245 Ω as discussed in section 4.10. However, both of these resistances have been decreased drastically in type II EDLC. The R_b and R_{ct} of type II EDLC are only 4.6 Ω and 0.8 Ω, respectively. The steep reduction of resistances is basically due to the flexibility of polymer chains owing to the strong plasticizing effect and good adhesion property of the ionic liquid–added polymer electrolyte. Highly flexible polymer chain can reduce the breakdown of the charge carriers from the complexation and thus improve the ion mobility in the polymer matrix. So, the bulk resistance of polymer electrolyte is decreased drastically. On the contrary, the sticky behavior of polymer electrolyte provides a good interfacial contact between electrode and electrolyte and hence reduces the interfacial resistance. So, the ions possess low resistance barrier to be diffused into the electrolyte and adsorbed onto the carbon electrodes.

The specific capacitances of type I and type II EDLCs are found to be 0.13 F g^{-1} and 53.38 F g^{-1}, respectively. The specific capacitance obtained in this study is almost the same as the findings in CV responds. As expected, the specific capacitance of type II EDLC is much larger than type I EDLC. This is attributed to the high ionic conductivity of ionic liquid–added polymer electrolytes. The amount of charge carriers is greatly boosted upon inclusion of ionic liquid into the polymer electrolyte. Apart from that, the mobility of ions is improved with adulteration of ionic liquid. These two factors could enhance the ion transportation in the polymer electrolytes and promote the ion accumulation at the electrode–electrolyte interface. We also take note that the value of C_{dl} and CPE of type II EDLC are relatively higher than type I EDLC. This denotes the rapid ion diffusion in the polymer electrolyte and ion adsorption towards the interface between electrode and electrolyte.

6.10 Galvanostatic Charge–Discharge Performances (GCD)

Figure 6.18 describes the GCD curve of type II EDLC over first five charging and discharging cycles at room temperature.

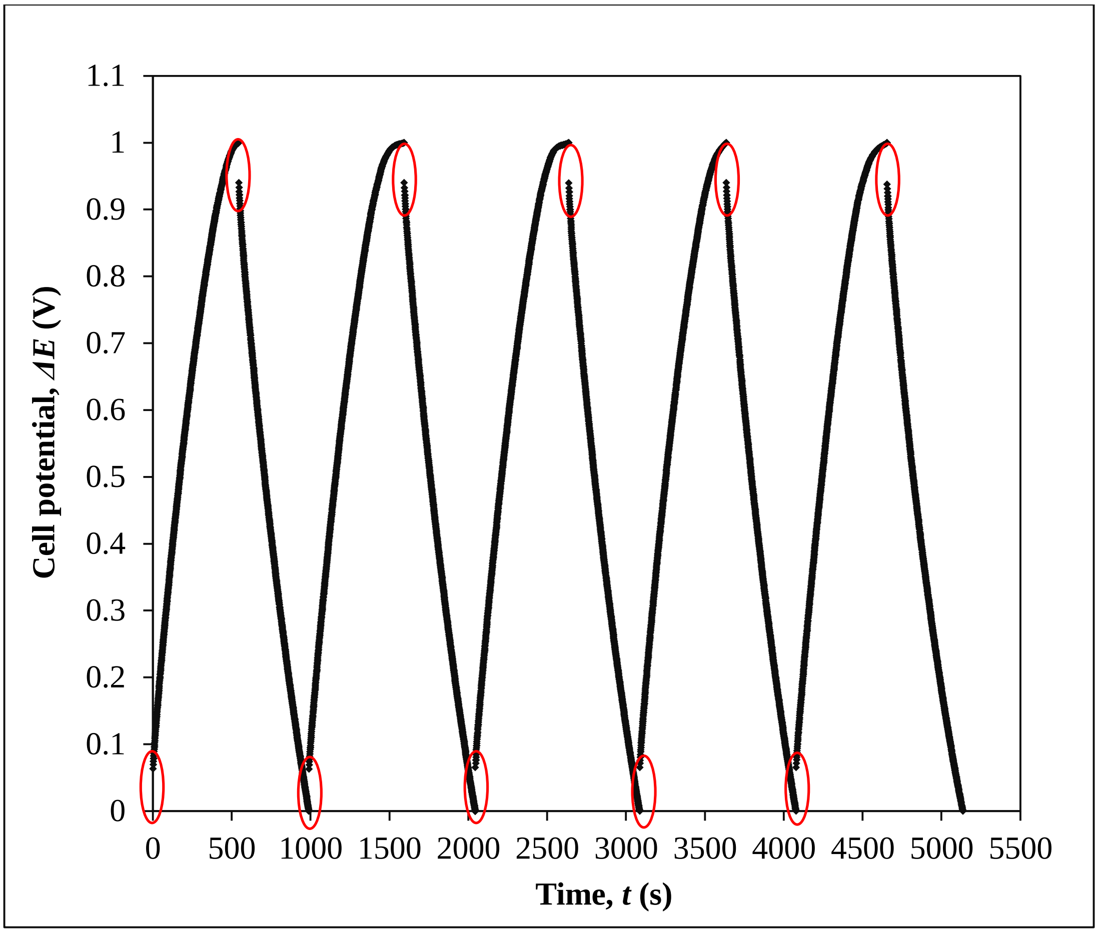

Figure 6.18: Galvanostatic charge–discharge performances of type II cell in I system over first 5 cycles.

The almost perfect symmetrical pattern of these five cycles implies the excellent capacitive performance of EDLC. The EDLC is supposed to be charged from 0 V to 1 V and discharged from 1 V to 0 V. However, it is noteworthy that the starting cell charge and discharge potentials are slightly deviated as highlighted in Figure 6.18. This observation is strongly related to the ohmic loss of the cell. This internal resistance arises from resistances of active materials and connector and bulk resistance of polymer electrolyte. The interfacial resistances between electrolyte and electrode and between current collector and active material can be the contributor to create this internal resistance. The assembled type II EDLC shows the specific capacitance of 56.16 F g^{-1}, energy density of 6.92 W h kg^{-1} and power density of 50.25 kW kg^{-1}, along with its Coulombic efficiency of 82 % for first cycle of charge and discharge processes. We take note that the specific capacitance obtained in this study is in good agreement with CV and EIS studies.

Cycle life test is also carried out to determine the ability of the cell at high charging and discharging cycles. Figures 6.19 illustrates the specific capacitance of type II EDLC and its Coulombic efficiency over 500 cycles of charging and discharging processes, meanwhile Figure 6.20 portrays the energy and power densities of the capacitor cells within 500 cycles of charging and discharging processes.

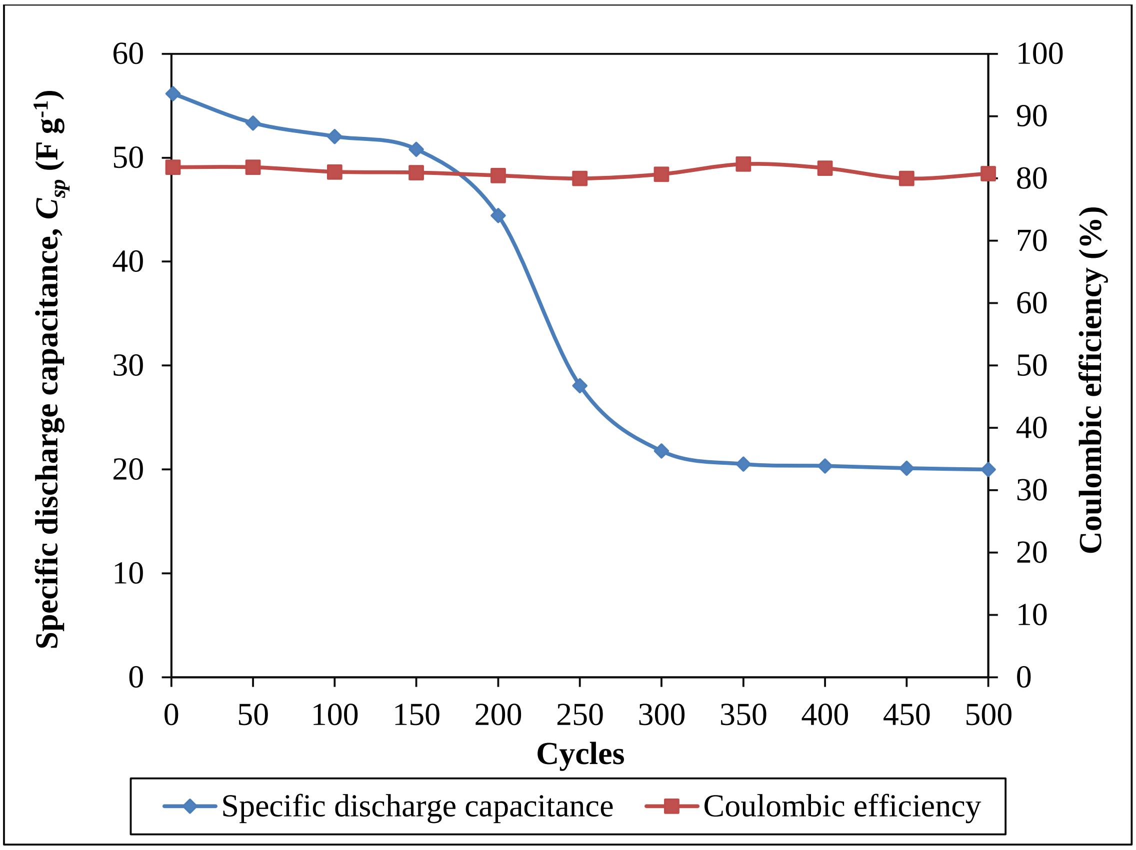

Figure 6.19: Specific capacitance and Coulombic efficiency of type II EDLC in I system over 500 cycles.

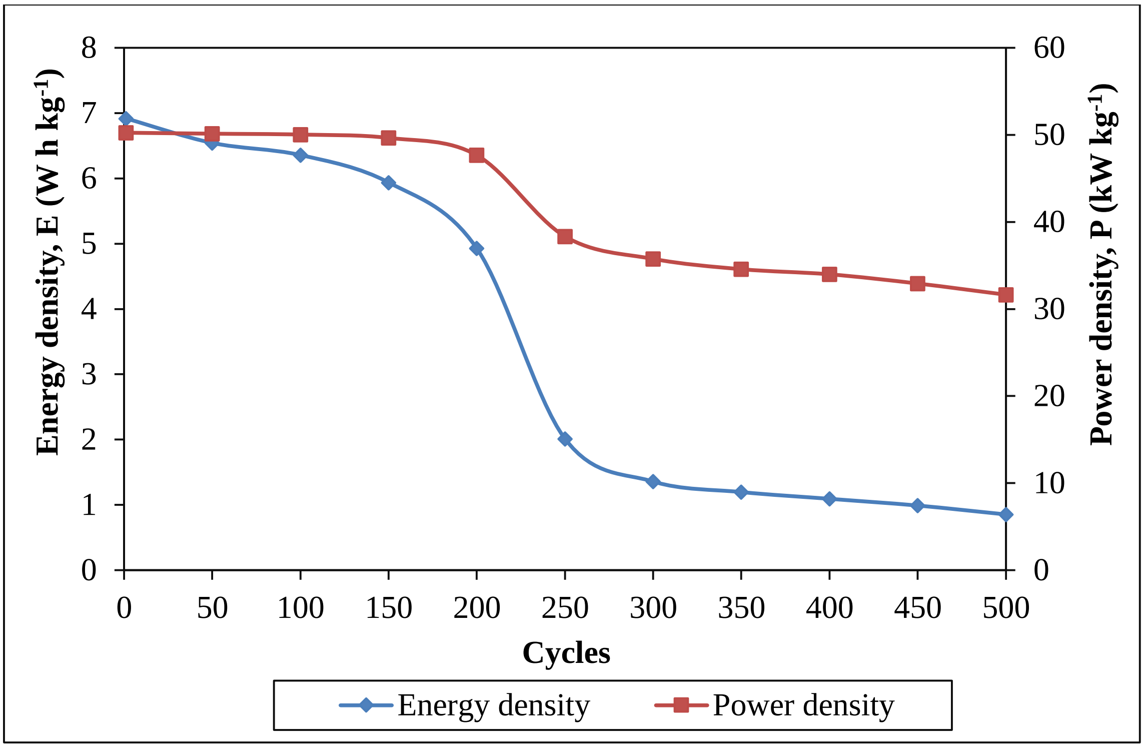

Figure 6.20: Energy density and power density of type II EDLC in I system over 500 cycles.

It is great to see that the Coulombic efficiency of the EDLC can maintain above 80 % over 500 cycles. Similar observation has been attained in specific capacitance, energy density and power density of the cell. These parameters drop gradually from first cycle to 200th cycles. However, these electrochemical properties of the capacitor cell decrease radically in the cycle range from 200th cycles to 300th cycles. However, these values almost remain unchanged above 300th cycles. These results infer that the electrochemical stability of EDLC becomes more stable upon 300th cycles of charging and discharging processes. The reduction in these electrochemical properties is mainly due to the depletion of electrolyte. So, the mobile charge carriers are getting lesser with increasing the cycle number. In addition, another reason for causing the reduction of these electrochemical properties could be the formation of ion aggregates. The mobile ions are more prefer to be paired up or aggregated after the rapid charge and discharge processes. So, these ion pairs can block the ionic migration in the polymer electrolyte and thus affect the ion diffusion into the pores of carbon which reduces the formation of ion adsorption at the electrode–electrolyte interface. Therefore, the specific capacitance, energy density and power density of EDLC decrease with increasing the cycle number. Upon charging and discharging for 500 cycles, the specific capacitance of EDLC reveals 64 % of reduction from 56.16 Fg^{-1} to 20 Fg^{-1}. In contrast, the energy density and power density of the cell demonstrate the decreases of 88 % and 37 % from 6.92 W h kg^{-1} to 0.85 W h kg^{-1} and from 50.25 kW kg^{-1} to 31.64 kW kg^{-1}, respectively. Although the decreases of these properties have been observed, however, this type II EDLC is still a promising candidate to be applied in electrochemical device as it can achieve high specific capacitance, energy density and power density compared to other studies. Several attempts can be employed in the future to achieve better electrochemical stability of EDLC.

6.11 Summary

PVA–CH_3COONH_4–BmImI electrolytes are prepared using solution casting technique in this chapter. The ionic conductivity of polymer electrolytes increases with the mass fraction of BmImI. The highest ionic conductivity of (9.63±0.01) mS cm^{-1} is achieved at ambient temperature with addition of 70 wt.% of BmImI. The ionic conductivity of polymer electrolytes increases with temperature and further infers the free volume theory for the ion transportation process. Addition of ionic liquid not only improves the ionic conductivity of polymer electrolyte, but also reduces the T_g and crystallinity of the polymer matrix as proven in DSC and XRD studies. Among all the samples, this most conducting polymer electrolyte shows the lowest T_g of 19.71 °C and percentage of crystallinity of 2 %, respectively. The complexation between PVA, CH_3COONH_4 and BmImI is established and proven in FTIR study. Addition of ionic liquid not only improves the thermal stability of the most conducting ionic liquid–added polymer electrolyte, but also enhances its electrochemical stability window which can be charged up to 3.8 V.

Incorporation of ionic liquid also improves the electrochemical properties significantly. The EDLC using the most conducting polymer electrolyte exhibits the specific capacitance of 52.78 Fg^{-1} which is much higher than that of ionic liquid–free polymer electrolyte. This indicates that ionic liquid can improve the electrochemical properties of the capacitor cell. The specific capacitance obtained in CV is comparable with the results obtained in EIS and GCD studies. The Coulombic efficiency of EDLC maintains above 80 % throughout 500 cycles of charge and discharge processes. PVA–CH_3COONH_4–BmImI electrolyte is a promising material to be used in EDLC fabrication as it can achieve high specific capacitance, energy density and power density with excellent Coulombic efficiency.

CHAPTER 7

RESULTS AND DISCUSSION OF COMPARISONS OF THREE DIFFERENT SYSTEMS

This chapter presents the comparisons of the three different systems, i.e. CL system, BR system and I system. The findings of the most conducting polymer electrolyte in each system are used and compared. This chapter also explains why I system has the highest ionic conductivity among all these systems and further implies the effect of the counteranion of ionic liquid in the ionic hopping mechanism.

7.1 Ambient Temperature–Ionic Conductivity Study

Figure 7.1 shows the room temperature–ionic conductivity of the most conducting polymer electrolyte in CL system, BR system and I system.

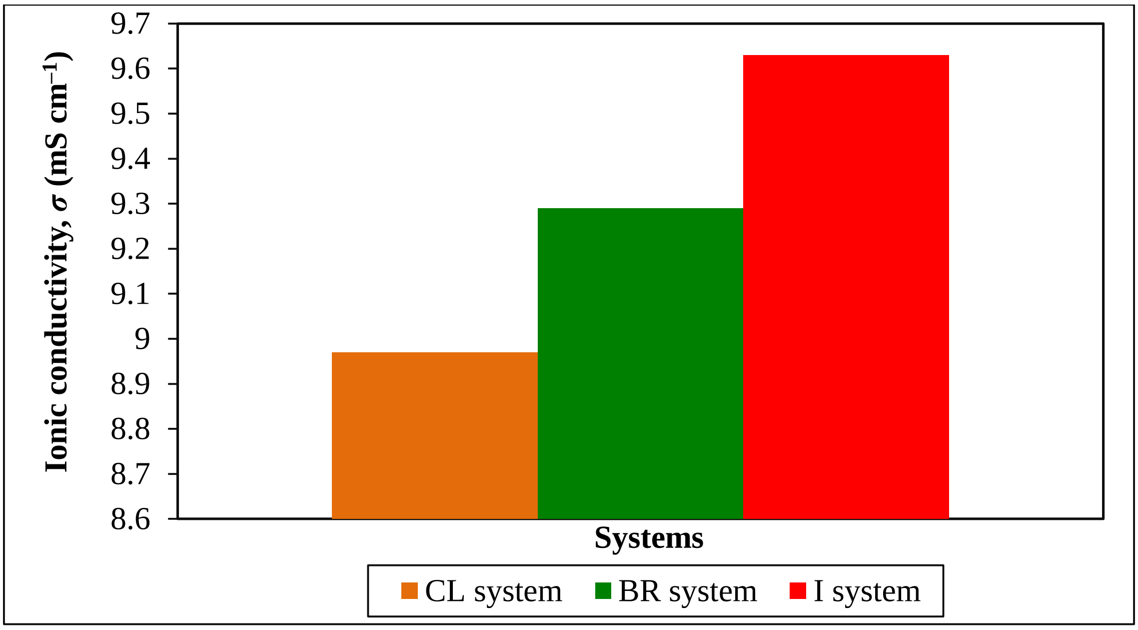

Figure 7.1: The ionic conductivity of the most conducting polymer electrolyte in each system at ambient temperature.

CL system achieves the highest ionic conductivity of 8.97 mS cm^{-1} with addition of 50 wt.% of BmImCl. On the other hand, BR system illustrates a maximum ionic conductivity of 9.29 mS cm^{-1} by doping 60 wt.% of BmImBr, whereas I system depicts the ionic conductivity of 9.63 mS cm^{-1} with addition of 70 wt.% of BmImI. The highest ionic conductivity of I system is suggestive of the highest amorphous region with flexible polymer backbone and rapid ion diffusion due to the highest mobile charge carriers in the polymer electrolytes with the lowest activation energy.

7.2 X–ray Diffraction (XRD)

One of the contributors that cause the highest ionic conductivity is high amorphous nature as mentioned in previous section. Figure 7.2 illustrates typical XRD patterns of all the systems.

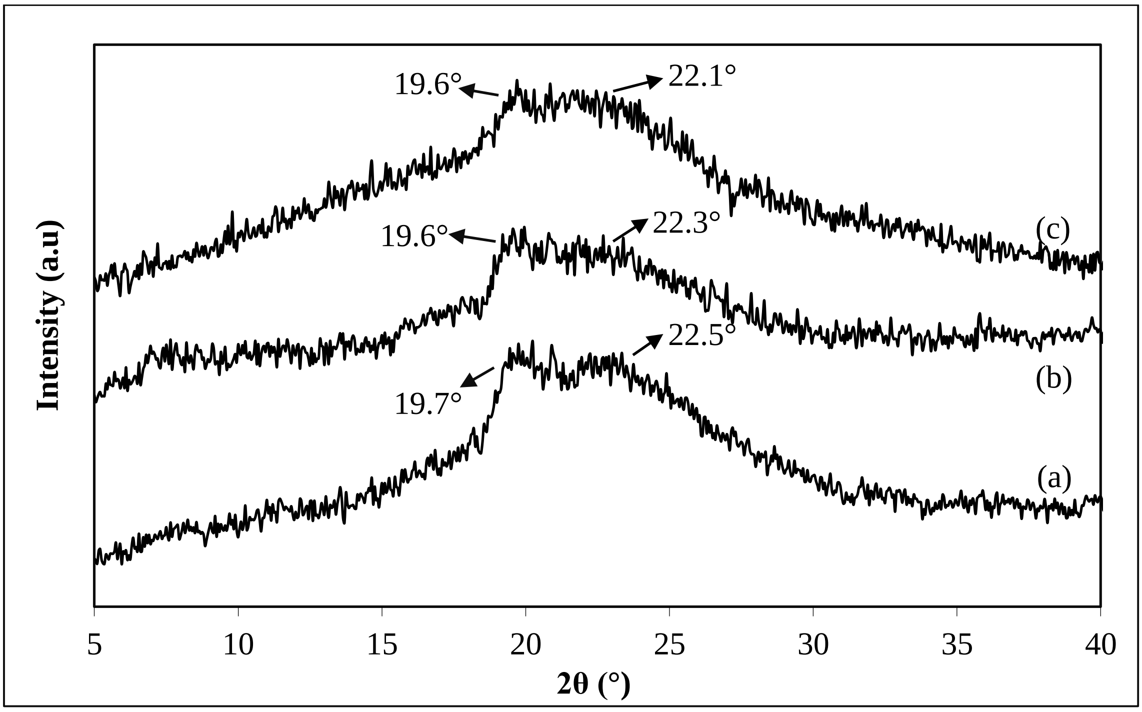

Figure 7.2: XRD patterns of the most conducting polymer electrolyte of (a) CL system, (b) BR system and (c) I system.

Similar XRD pattern is observed in all systems. Two peaks are observed in the 2θ degree range of 5–40°. A crystalline peak is observed at 2θ≈19°, whereas an amorphous hump is observed at 2θ≈22°. The most conductive polymer electrolyte in CL system exemplifies a crystalline peak at 2θ≈19.7° and an amorphous peak at 2θ≈22.5°. All these peaks manifest downward shift to lower 2θ degree in BR system and I system. The crystalline peak is shifted to 2θ≈19.6° for both BR and I systems. On the contrary, the hump is shifted to 2θ≈22.3° and 22.1° for BR system and I system, respectively. It is noticeable that the intensity of the crystalline peak is decreased across the system, from

CL system, to BR system and I system. This denotes that the degree of crystallinity of polymer electrolytes decreases in this order: CL system> BR system> I system. The percentages of crystallinity of CL, BR and I systems are depicted and compared in Figure 7.3.

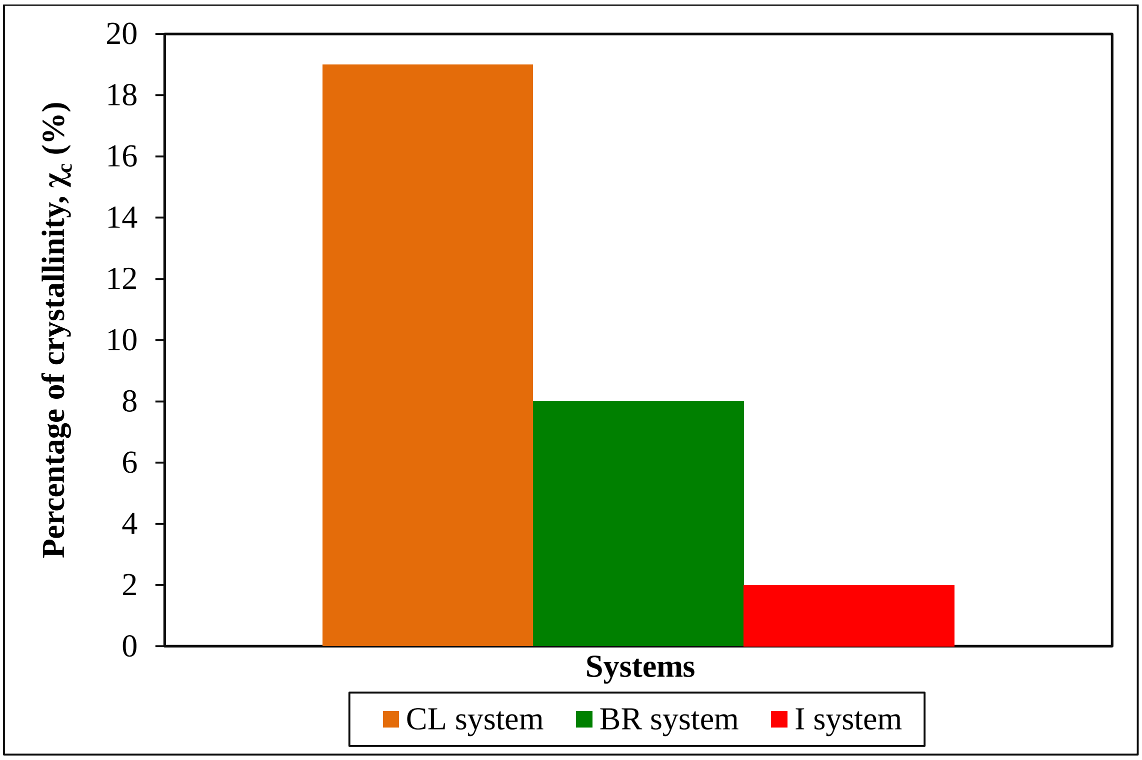

Figure 7.3: The percentage of crystallinity of the most conducting polymer electrolyte of each system.

CL system illustrates around 19 % of crystallinity. However, the degree of crystallinity is decreased abruptly to 8 % for BR system and 2 % for I system as shown in figure above. High degree of amorphous region can enhance the mobility of charge carriers in the polymer membrane as the mobility in amorphous phase is higher than in crystalline region. Since the amorphous is originated from the unordered arrangement of macromolecules, thus the charge carriers are more easily to be dissociated from the coordinative bonds. Amorphous region in the polymer electrolytes also provides more free spaces for ions to transport in the polymer electrolytes. Therefore, the mobile charge carriers can be migrated easily at high concentration of amorphous phase in the polymer matrix.

7.3 Temperature Dependent–Ionic Conductivity Studies

Other reasons of higher ionic conductivity obtained in I system compared to other two systems are more mobile ions and low E_a. This can be proven in temperature dependent–ionic conductivity study. The temperature–dependence plots in all systems obey VTF rule which is associated with free volume theory. According to Equation 4.2, A_o is pre–exponential constant proportional to the number of charge carriers. Therefore, this parameter has been determined to prove the quantity of mobile charge carriers can help in ionic conduction. Figure 7.4 shows A_o determined from the VTF plot in the three different systems.

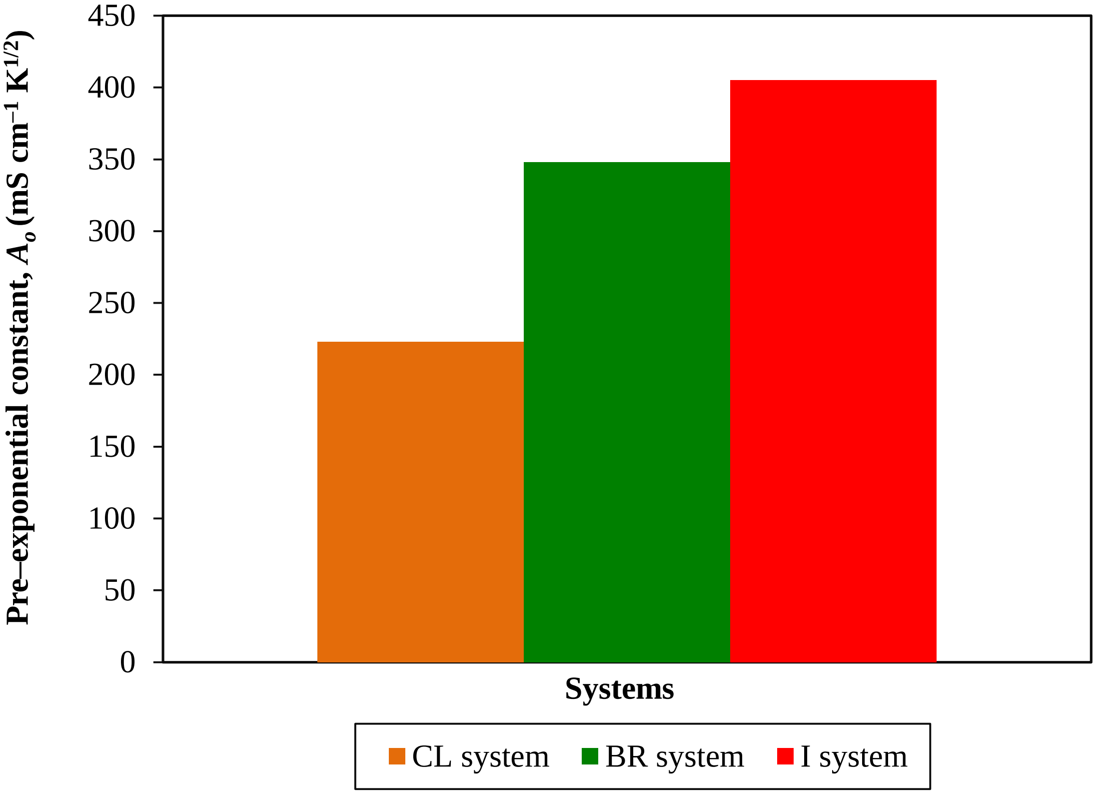

Figure 7.4: The pre–exponential constant, A_o of the most conducting polymer electrolyte of each system.

As expected, I system shows the highest value of A_o among all the systems. This implies that I system has the most number of free ions for conduction which leads to high ionic conductivity. This observation is strongly related to flexibility of polymer chains. High ionic conductivity of polymer electrolytes is usually coupled with low E_a. This normal trend is also observed. The pseudo–activation energy, E_a of the most conducting polymer electrolyte in all system is displayed in Figure 7.5.

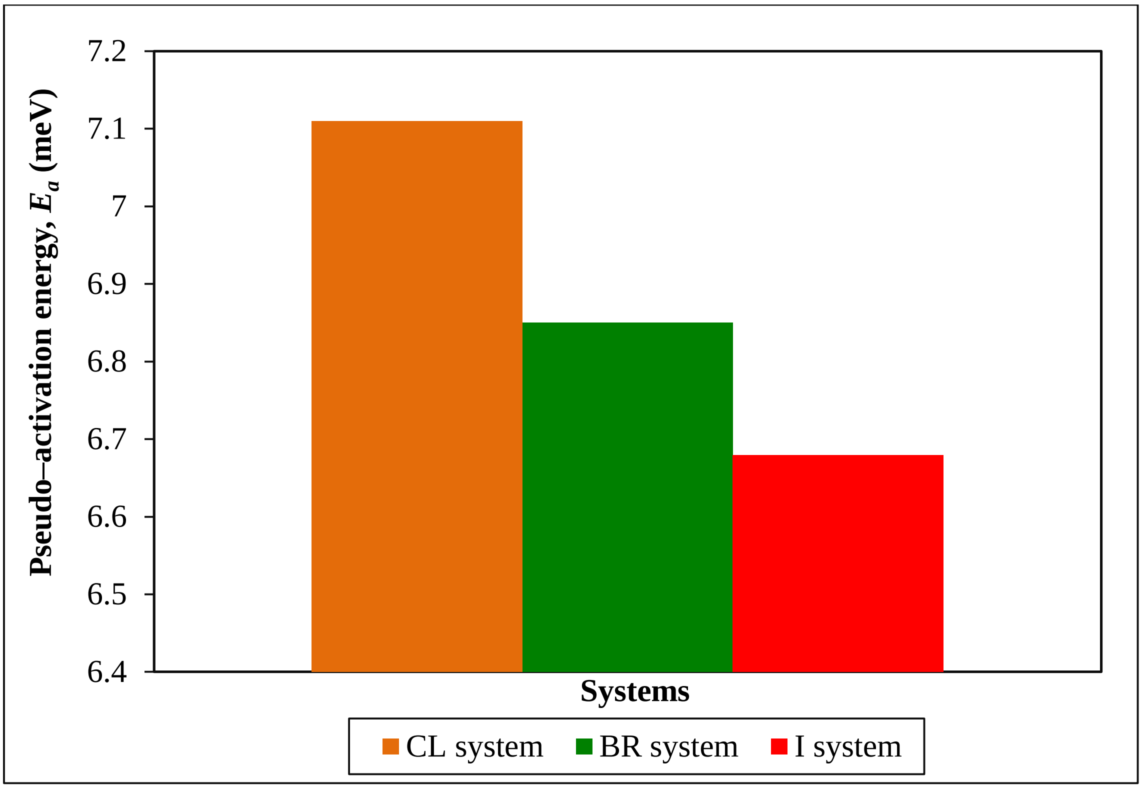

Figure 7.5: The pseudo–activation energy, E_a of the most conducting polymer electrolyte of each system.

CL, BR and I systems show the E_a of 7.11 meV, 6.85 meV and 6.68 meV, respectively. So, these results support that the charge carriers in I system needs the lowest energy for migration. Therefore, rapid ion transportation in the electrolytes can be formed with this low resistance.

7.4 Effect of halide anions

In order to investigate the effect of halide anions onto the polymer electrolytes, the concentration of ionic liquid in the polymer electrolytes must be fixed to make sure the quantity of all the materials are the same in all the polymer electrolytes. The concentration of 70 wt.% ionic liquid is chosen as I system had achieved the highest ionic conductivity at this concentration. The temperature dependence plots of the polymer electrolyte in all systems with mass loadings of 70 wt.% ionic liquids is envisaged in

Figure 7.6. On the other hand, the parameters obtained from the VTF equation are tabulated in Tables 7.1 and 7.2.

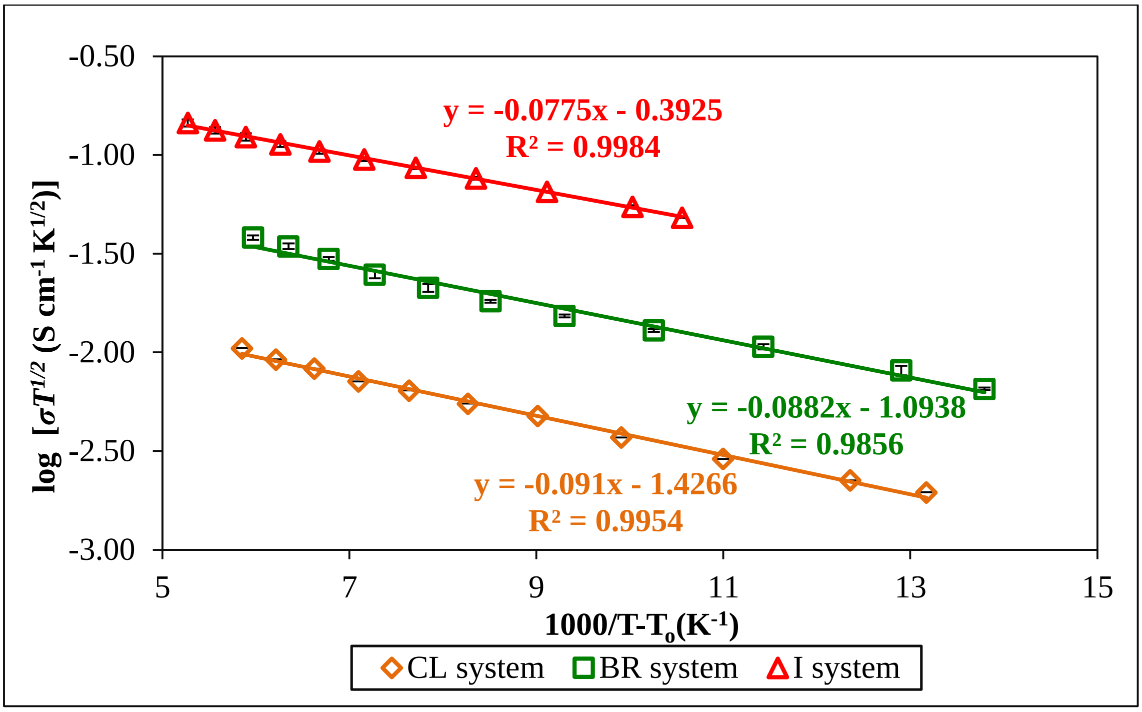

Figure 7.6: The VTF–based temperature dependent–ionic conductivity of polymer electrolytes at concentration of 70wt.% of ionic liquid.

Table 7.1: The obtained parameters from each VTF plot with the experimental glass transition temperature from DSC thermogram in all systems at concentration of 70wt.% of ionic liquid.

Sample	**Regression value, R^2**	**Glass transition temperature, T_g (K)**	**Ideal glass transition temperature, T_o (K)**
CL system	0.99	272.23	222.23
BR system	0.99	275.65	225.65
I system	0.99	253.44	203.44

Table 7.2: The obtained parameters from each VTF plot in all systems at concentration of 70wt.% of ionic liquid.

Sample	**Log A_o**	**Pre–exponential constant, A_o (mS cm^{-1} K$^{1/2}$)**	**Gradient of the plot, B (K^{-1})**	**Pseudo–activation energy, E_a (meV)**
CL system	–1.4266	3.74×10^{-2}	0.0910	7.84
BR system	–1.0938	8.06×10^{-2}	0.0882	7.60
I system	–0.3925	0.41	0.0775	6.68

From the findings above, there are two main observations are attained:

i) The A_o increases in the order of CL system< BR system< I system

ii) The E_a decreases in the order of CL system> BR system> I system

Among all the systems, I system achieves the highest value of A_o and the lowest value of E_a at the same concentration of ionic liquid. This implies that the iodide (I^-) can improve the ionic conduction in the polymer electrolytes in comparison to chloride (Cl^-) and bromide (Br^-) as it has higher mobile charge carriers in the polymer electrolytes where A_o is directly proportional to number of charge carriers for transportation. We postulate that this observation is related to the size of the anions. The anions tend to increase in size down a group in the periodic table. The sizes of Cl^-, $Br^-$and I^- are 180 pm, 190 pm and 198 pm, respectively. The bigger size of the iodide could enhance the self–dissociating property. In other words, the iodide can be dissociated easily compared to the other two anions from the countercation in the ionic liquid due to its bulky size. So, more and more countercation in the ionic liquid can be detached easily from the transient bonding with anions. Therefore, the deprotonation of the countercation shown in Figure 4.4 can be formed rapidly. As a result, the carbene produced in the deprotonation process can assist the ion conduction mechanism. In addition, I system shows the lowest T_g in comparison to CL and BR system which indicates the highest flexibility of polymer chains in I system.

7.5 Cyclic Voltammetry (CV)

The comparison of electrochemical performance of EDLC containing the most conducting polymer electrolyte of each system is also scrutinized in this work as shown in Figure 7.7.

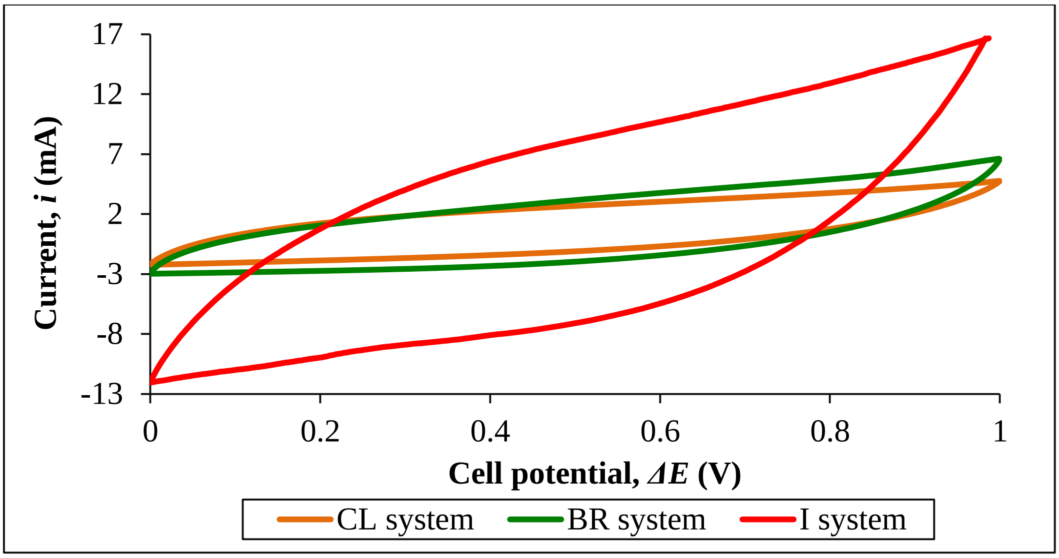

Figure 7.7: CV responses of the EDLCs comprising of the most conducting polymer electrolyte of each system.

No redox peaks observed in each CV curve of all the system. This result indicates that the capacitance of the prepared capacitors arises from formation of the double layer without any chemical reaction at the electrode–electrolyte boundary. As can be seen, EDLC using I system gives a better shape in CV curve compared to that of CL and BR systems. Another feature is also observed in Figure 7.7 that is the area under the CV curve of EDLCs increases in this order: CL system<BR system<I system. This observation gives rise to higher capacitance at which the area under the CV curve is bigger. The EDLCs containing the most conducting polymer electrolyte in CL and BR systems illustrate approximate specific capacitance that is 19.42 F g^{-1} and 21.89 F g^{-1}, respectively. In contrast, EDLC consisting of the most conducting polymer electrolyte in I system has the highest specific capacitance value which is double of the previous two systems, i.e. 52.78 F g^{-1}. EDLC comprising of I system is the most capacitive among all the systems. This is probably due to the higher ionic conductivity in I system as a result of more mobile charge carriers with high mobility. This can cause the rapid ion transport in the polymer electrolytes. These mobile ions are thus adsorbed onto the porous carbon electrode and formed the electric double layer easily. This rapid ion accumulation improves the capacitive properties of the EDLC.

7.6 Electrochemical impedance spectroscopy (EIS)

Figure 7.8 depicts the comparison of three impedance plots of EDLC containing the most conducting polymer electrolyte in CL system, BR system and I system.

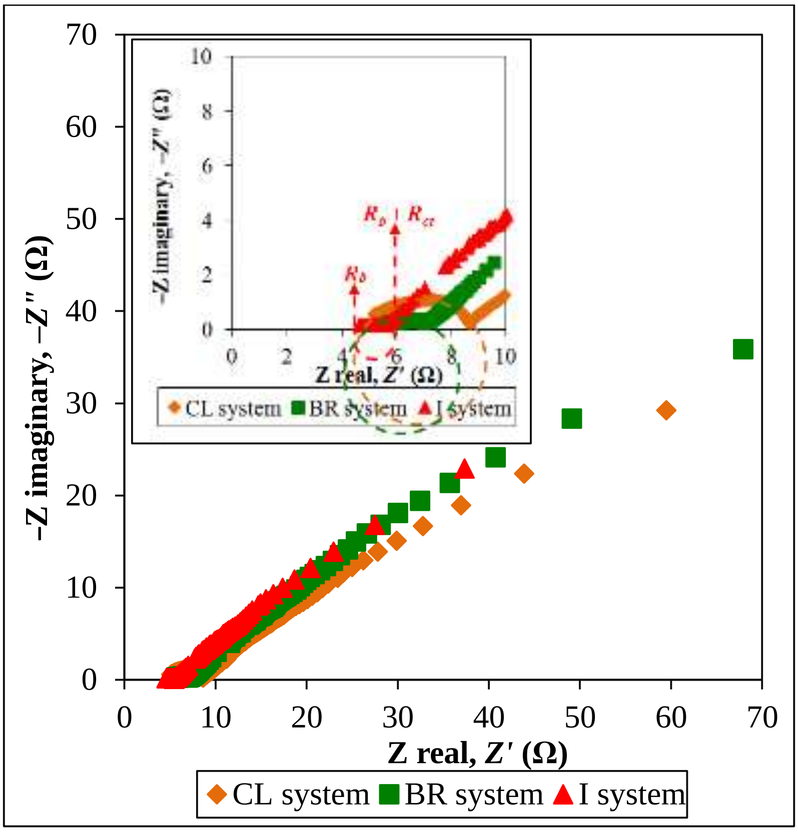

Figure 7.8: Nyquist impedance plots of EDLC containing the most conducting polymer electrolyte in each system at room temperature from 10 mHz to 100 kHz with close–up view of the plot in high frequency region (inset).

The R_b of these three systems is almost the same and falls in the range 5–5.5 Ω. However, R_{ct} is decreased across the system, from CL system (4 Ω), to BR system (1.6 Ω) and I system (0.8 Ω). Since EDLC assembled with I system has the lowest R_{ct}, so it can be concluded that I system favors the ion migration in the electrolyte and ion adsorption towards the porous carbon. Therefore, the specific capacitance of EDLC containing I system shows the highest value. This is in a good agreement with the EIS findings where EDLCs comprising of CL system, BR system and I system have the respective specific capacitance of 18.76 F g^{-1}, 21.63 F g^{-1} and 53.38 F g^{-1}. I system based–EDLC depicts the highest specific capacitance is due to the highest ionic conductivity of I system as shown in section 7.1.

7.7 Galvanostatic Charge–Discharge Performances (GCD)

Figure 7.9 portrays the first cycle charge–discharge curve of EDLCs assembled with the most conducting polymer electrolyte in all the systems.

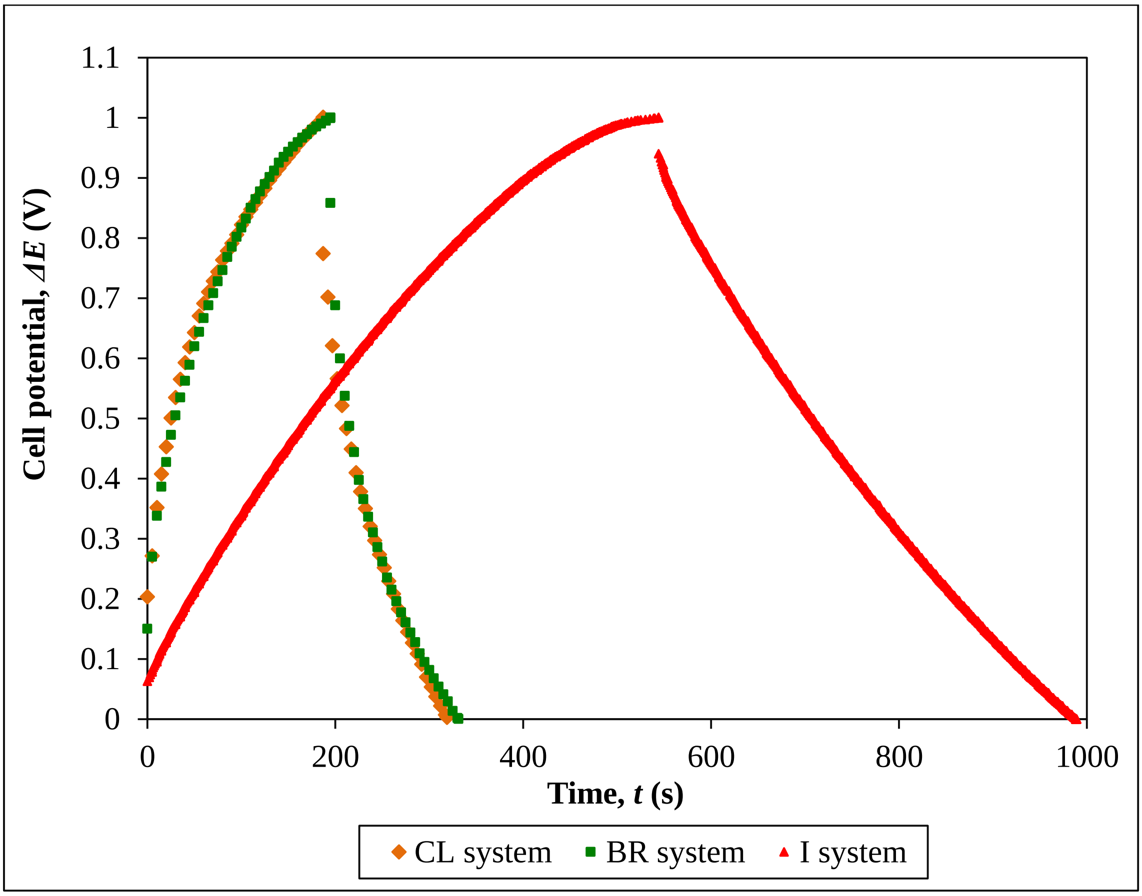

Figure 7.9: Galvanostatic charge–discharge performances of EDLCs with the most conducting polymer electrolyte in each system for first cycle.

It is obvious to see that the EDLC containing I system has symmetrical shape in charge and discharge process compared to that of other two systems. As a result, I system has higher Coulombic efficiency in comparison to CL and BR systems. Among all the systems, I system has the best electrochemical performance in the capacitor cell as it has the lowest internal resistance which is the initial drop in the discharging process. Moreover, EDLC containing I system exhibits higher specific capacitance than other two systems. The specific discharge capacitances of EDLC consisting of CL system, BR system and I system are 21.19 F g^{-1}, 21.39 F g^{-1} and 56.15 F g^{-1}, respectively. The highest ionic conductivity with rapid ion diffusion in I system is the main cause of the highest specific discharge capacitance of EDLC containing I system. High concentration of mobile ions with their high ionic mobility can lead to the rapid ion adsorption at the electrode–electrolyte interface.

7.8 Summary

BmImI–embedded polymer electrolyte is the most promising candidate as electrolyte in EDLC application compared to BmImCl and BmImBr systems as it achieves the highest ionic conductivity and capacitance. Besides, it has the lowest activation energy and degree of crystallinity which is around 2 % only. Better electrochemical properties of the EDLC fabricated using this iodide–based conductive electrolyte can also be observed in EDLC application in comparison to that of two systems. The EDLC comprising of this conductive polymer electrolyte has the lowest charge transfer resistance which assists the ion transport from the electrolyte to the porous carbon electrode. Apart from that, this system shows the lowest internal resistance for charging and discharging process compared to CL and BR systems with symmetrical pattern. Therefore, BmImI is a much favored material to be added into polymer matrix to improve the electrical, thermal and structural properties of polymer electrolytes as well as the electrochemical properties of EDLCs.

CHAPTER 8

CONCLUSION

PVA–CH_3COONH_4–ionic liquid electrolytes are prepared by solution casting technique. Several characterizations have been done to investigate the electrical, structural and thermal properties of polymer electrolytes as well as the electrochemical properties of prepared EDLCs. The effect of adding ionic liquid is investigated throughout the whole research. Ionic conductivity of polymer electrolytes increases with mass fraction of ionic liquid up to a maximum level. It is then followed by a decrease in ionic conductivity due to the formation of ion aggregates which blocks the ion conducting pathway. The increment of ionic conductivity of polymer electrolytes is suggestive of low T_g and low degree of crystallinity. The ionic conductivity of polymer electrolytes also increases with temperature. This study reveals that the polymer electrolytes obey VTF rule for conduction. This VTF theory infers the cooperative mechanism of ionic hopping mechanism with high segmental mobility.

Addition of ionic liquid reduces the T_g of polymer electrolytes greatly, improves the thermal stability of polymer electrolytes and widens the electrochemical potential window of polymer electrolytes. The complexation between PVA, CH_3COONH_4 and ionic liquids are further verified in FTIR studies. The impregnation of ionic liquid can also improve the electrochemical properties of EDLCs. The specific capacitance of EDLCs containing ionic liquid–embedded polymer electrolyte is much higher than that of ionic liquid–free polymer electrolyte due to high ionic conductivity. These capacitive EDLCs also possess excellent electrochemical performances as proven in EIS and GCD studies. Therefore, addition of ionic liquid onto the polymer electrolytes is a suitable way to improve the ionic conductivity of polymer electrolytes, increase the amorphous region of polymer matrix and enhance the electrochemical properties of EDLCs.

Three different polymer electrolyte systems comprising of BmImCl, BmImBr and BmImI have been prepared to determine the effect of counteranion of ionic liquid onto the ionic conduction mechanism. Among all the systems, I system achieves the highest ionic conductivity at ambient temperature due to the lowest activation energy and the lowest degree of crystallinity of polymer electrolyte. The EDLC assembled using I system–based polymer electrolyte exhibits better electrochemical performances than that of other two systems. The specific capacitance of I system–based EDLC has two folds higher value than EDLC containing CL and BR systems. The EDLC comprising of this conductive polymer electrolyte also manifests the lowest charge transfer resistance as shown in EIS plot. Moreover, this EDLC also exhibits the highest Coulombic efficiency, power density and energy density with the lowest internal resistance for charging and discharging process in comparison to EDLCs comprising of CL and BR systems as illustrated in GCD studies. Among these three ionic liquids, BmImI is the most promising candidate to be used as additive in the polymer electrolytes.

Since the capacitance of EDLC containing ionic liquid–added polymer electrolytes can be improved abruptly, thus I would like to employ these polymer electrolytes into the pseudocapacitor application for my further study. The electrode materials of the pseudocapacitor can be either metal oxides or conducting polymers. In addition, I would like to fabricate fuel cell as ammonium salt is used to provide proton charge carriers. Preparation of gel polymer electrolytes can be another future plan to improve the ionic conductivity and interfacial contact between electrode and electrolyte by replacing the water with dimethyl sulfoxide (DMSO) as solvent. Liquid crystal–embedded polymer electrolytes will be studied as liquid crystal is a new material in the development of polymer electrolytes. Perhaps, it can increase the ionic conduction in the polymer electrolytes.